SUSTAINABLE GROUND IMPROVEMENT METHOD USING RECYCLED PLASTIC PINS

by

MD NUR BASIT ZAMAN

DISSERTATION

Presented to the Faculty of the Graduate School of

The University of Texas at Arlington in Partial Fulfillment

of the requirements

for the Degree of

DOCTOR OF PHILOSOPHY

THE UNIVERSITY OF TEXAS AT ARLINGTON

May, 2019

ACKNOWLEDGEMENTS

I would like to express my sincere gratitude and appreciation to my supervising professor, Dr. Sahadat Hossain, for his constant support, guidance and encouragement throughout my graduate studies. Dr. Hossain has been an excellent mentor and shared his experience and knowledge with me, which provided me with the motivation I needed to complete my research work. His patience, constructive comments and valuable suggestions helped me to present myself as a better researcher. I consider myself lucky to get the opportunity to become a part of his research team.

I would like to specially acknowledge Dr. Nur Yazdani, Dr. Xinbao Yu, and Dr. Muhammad N. Huda for devoting their valuable time to serve as dissertation defense committee members and for their constructive comments.

Sincere thanks to the Texas Department of Transportation (TxDOT) for funding this research. I am grateful to the TxDOT officials, Nicasio Lozano and Boon Thian for their vision, guidance, constructive comments and continued encouragement.

Special thanks to my colleagues and friends for their cooperation and assistance throughout the research. Thanks to Dr. Sadik Khan, Dr. Sonia Samir, Dr. Asif Ahmed and Dr. Jobair Bin Alam for their guidance and support. I would like to thank Ahmed Khan, Anuja Sapkota, Prabesh Bandhari, Cory Rauss and Linkan Sarker for their continuous help during the field work, without them this work would have been much more difficult.

I wish to acknowledge my wife Fairuz Samiha Saeed for her constant cooperation, patience, sacrifice and unconditional support throughout my studies. I would like to thank my loving sister Tahnia Zaman for her support.

Finally, and most importantly, I would like to dedicate this research work and dissertation to my mother and father. Their unwavering trust, support, love and encouragement helped me to fulfill my dream to pursue a doctoral degree. Thanks to the almighty Allah for granting me with the strength and patience that I needed throughout my research work.

April 18, 2019

ABSTRACT

SUSTAINABLE GROUND IMPROVEMENT METHOD USING

RECYCLED PLASTIC PINS

Md Nur Basit Zaman

The University of Texas at Arlington, 2019

Supervising Professor: MD Sahadat Hossain

Failure of civil engineering infrastructures due to insufficient bearing and shearing capacity of the unsuitable foundation soil is a common problem in the area of North Texas which results in significant maintenance issues for the Texas Department of Transportation (TxDOT). The major concerns regarding construction over such foundation soil includes excessive total and differential settlement of footing resulting in bearing capacity failure and sliding failure of the Mechanically Stabilized Earth (MSE) retaining structure due to inadequate shear resistance. The most common technique followed by TxDOT to counter such problem is to remove and replace the existing soil with appropriate fill material. However, the excessive cost associated with the remove and replace method led to numerous research to develop sustainable alternative solution. A noble approach to improve the problematic soil could be the use of Recycled Plastic Pin (RPP). RPP is a lightweight material, produced from recycled plastics and other waste materials. It is more durable against chemical and biological degradation compared to other alternatives (e.g. concrete pile or timber pile). The current study summarizes the development of an alternative sustainable solution to the bearing capacity

failure by excessive settlement of the structures and sliding failure due to lack of sufficient shear resistant at the base of MSE wall.

RPPs provide with additional support to the structures (e.g. embankments) when driven into the weak foundation soil in addition to a layer of geogrid. Geogrid acts as load transfer device which ensures transfer of fill load to the RPP by soil arching effect. The RPP reinforcement in combination to geosynthetic helps to reduce both total and differential settlement of the structure by improving the weak foundation soil. Three identical 6ft. height embankment loading test sections of 15 ft. x 15 ft. were constructed in phase – I; one as control section (without any RPP) while the other two sections were instrumented with 10 ft. long RPP of 4 in. x 4 in. and 6 in. x 6 in. sizes respectively. Based on the field monitoring results, settlement for the control section was found to be about 2.01 inches, while due to the use of 4 in. x 4 in. and 6 in. x 6 in. RPP reinforcement, a reduction in settlement of about 60% and 70% compared to the control section was noticed respectively. As a part of phase –II construction and monitoring, one control section and one 4 in. x 4 in. RPP reinforced section was constructed, and the result was found to be in good agreement with the phase – I observation.

The study also endeavored to focus on increasing shear resistance of the base of MSE wall constructed on stiff foundation soil against sliding failure by utilizing RPP similar to a shear key. The research included construction of two identical MSE wall test sections of 24 ft. long and loaded with a backfill soil height of 4 ft.; one had a foundation reinforced with 10 ft. long 4 in. x 4 in. RPP at 3 ft. c/c spacing while the other section served as a control section. The performance monitoring result showed significant lateral movement for the control section (3.8 inches), while almost no movement was observed for the reinforced section. For further

evaluation, an increased backfill loading height of 5 ft. showed a lateral movement of 1.76 inches for the control section which was found to be reduced by about 80% (0.29 inches) for the RPP reinforced section.

The performance of the test sections was further evaluated in numerical modeling using finite element software PLAXIS 2D and a parametric study was conducted using the calibrated model to evaluate effect of RPP size, length and spacing for both cases. The parametric study indicated that the both vertical and lateral deformation decreases with larger RPP size and narrower RPP spacing. Based on the field monitoring results and FEM analysis, RPPs are expected to be an efficient and cost effective reinforcing material for ground improvement.

TABLE OF CONTENTS

LIST OF ILLUSTRATIONS

LIST OF TABLES

CHAPTER 1

INTRODUCTION

1.1 Background

Construction of civil engineering infrastructures for example, retaining structures, embankments for highways, roadways, dams, levees etc. is preferred in the sites having suitable foundation soil with good geotechnical characteristics. Better foundation soil ensures minimization of technical problems including compressibility and shear strength, and thus minimizes the cost associated with the construction of such infrastructures. However, rapid growth of civilization forced the use of weak unsuitable sub-grade soil for the construction and development of various transportation related projects (Rao, 2006). Failure of these structures, specially retaining structures poses significant threat to both the public and private sectors. When constructed on unsuitable soil, retaining wall causes bearing capacity and sliding failure, leading to failure of the structures supported by the wall; e.g. slopes, highway, roadways etc. Therefore, millions of dollars are spent every year for the maintenance and repair of U.S. roadways and highways. In addition, indirect cost considering the loss of revenue in relation to the use and access of facilities sometime exceeds the direct cost (Turner and Schuster, 1996; Khan, 2014).

Weak foundation soil exhibit poor strength and high compressibility (Nazir and Azzam, 2010). Major concerns associated with this soil type under large structural loads include bearing capacity failure, total as well as differential settlement of the footing, lateral pressure and instability. Structures (e.g. embankments, retaining walls etc.) constructed on such

foundation soil is prone to large deformations, resulting in construction delays as well as premature failure of infrastructures. According to a TxDOT (Texas Department of Transportation) memorandum (2013), for sites with problematic soils, sometimes a ground (foundation) improvement plan is more economical to allow the safe use of structure rather than changing the structure type. Ground improvement plan varies from simple remove and re-compact or replace of existing materials (e.g. crashed rock) to the complex, i.e, the use of geopiers, stone columns or geogrid reinforced pads. Also, particle packing (compaction) always increases density, with a resulting decrease in void ratio and reduces both immediate and long-term settlement (Bowles, 1988). The general and conventional approach to the construction of any highway or runway on weak sub-grade soil is remove and replacement method. However, the excessive material replacement cost causes the related administrations to evaluate alternative methods of construction on soils with low bearing capacity (Ozdemir, 2016). To support the load from the structures, installation of piles up to the bearing stratum below the unsuitable soil layer proved to be very effective (Barchard, 1999) and has been used for decades. In addition to piles, use of a thin layer of geosynthetics over the piles has the added benefit of enhancing the load transfer efficiency and minimizing total as well as differential settlement of the structure supported by the system (Reid and Buchanan, 1984, Han and Gabr, 2002).

In addition to the bearing capacity failure, sliding or shear capacity failure of the retaining structures, specially mechanically stabilized retaining walls (MSEWs) constructed on stiff soil is another major concern addressed by TxDOT. Most of the times, instead of a complete failure, a lateral shift at the base of the wall is noticed due to excessive lateral pressure generated from the backfill soil in the slope side of the wall. Which is mainly due to lack of

support resulted from insufficient shear resistance between the foundation and the base of the wall (Khan et al., 2014). The excessive lateral movement in some instances results in separation between wall and road approach embankment, which leads to significant distress on the pavement structure (Babu et al., 2016) and incur additional cost to the existing repair and maintenance cost. Typical recommended solution to restore structural integrity of the retaining structure consists of either wall anchors or helical tiebacks, which is really expensive. During the design and construction, incorporating a shear key almost completely restricts the sliding tendency of the wall and increases factor of safety against sliding significantly (Sarath et al., 2011). In case of MSE wall, there is no predefined shear key to incorporate additional shear resistance against sliding. Introducing a concrete shear key at the base of the MSE retaining structures can significantly improve the resistance against sliding and help restrict the sliding failures of such structures (Kim and Bilgin, 2011). However, incorporating concrete key at the base of the MSE wall is challenging.

The conventional techniques involved in improving the bearing capacity of the subgrade soil and shear resistance of the base of MSE wall might be either expensive in some instances or challenging to incorporate. Therefore, new, innovative, cost effective and sustainable solution to the improvement of bearing and shearing capacity of the unsuitable soil are being tested increasingly. One such method could be the use of recycled plastic pins (RPP).

In recent years Recycled Plastic Pin (RPP) has been used successfully in different projects within the north Texas region especially for the shallow slope stabilization work. As it is a sustainable and cost-effective solution, further investigations are required to use the recycled plastic pin in other geotechnical projects. The prime ingredient for the fabrication of

RPPs are mainly recycled plastics and other waste materials (Bowders et al., 2003; Chen et al., 2007). RPP is composed of 55% – 70% High Density Polyethylene (HDPE), 5% – 10% Low Density Polyethylene (LDPE), 2% – 10% Polystyrene (PS), 2% – 7% Polypropylene (PP), 1% – 5% Polyethylene-terephthalate (PET), and varying amounts (0% – 5%) of additives i.e. sawdust, fly ash etc. (Malcolm, 1995; Lampo and Nosker, 1997; Chen et al., 2007; Khan, 2014). According to Breslin et al. (1998), the modulus of elasticity for plastic pins may be significantly improved by the use of glass and wood fiber additives. RPP has considerable amount of compressive as well as flexural strength (Bowder et al., 2003); which can carry the load both axially and laterally. Therefore, RPP might be useful to reduce foundation settlement by improving bearing capacity of the soil and increase the sliding resistance of the MSE wall base.

The current study presents an innovative and sustainable solution for minimizing both foundation settlement due to the application of embankment loading and lateral movement of the base of the MSE retaining structures using Recycled Plastic Pin (RPP). RPP is a light weight material, which is less susceptible to both chemical and biological degradation. It is moisture resistant and requires almost zero maintenance; these characteristics can present it as an attractive alternative compared to other available structural solutions (Krishnaswamy and Francini, 2005). Apart from the structural benefits, the use of RPP reduces the volume of non-degradable wastes entering the waste stream and provides additional market for the recycled materials (Loehr et al. 2000).

1.2 Problem Statement

Structures e.g. MSE retaining walls and embankments underlain by unsuitable soil are known to be susceptible to bearing capacity and shear failure. Construction of highway embankments over weak foundation soil imposes significant stresses, resulting in problems including potential bearing failure, excessive settlement, and global or local instability (Liu et al., 2007; Chen et al., 2009). The failure is much more severe when differential settlement comes into the picture, which is pretty common for the cases associated with weak foundation soil (Han and Gabr, 2002). In addition, MSE retaining structures constructed on stiff soil, experience lateral movement away from the backfill due to lack of sufficient shear resistance between the base of the wall and the foundation soil. The lateral movement results in failure to the structure and the structures supported by the MSE wall. Complications associated with problematic soil are predominant in North Texas area due to the presence of high plastic clay which possess significant construction, repair and maintenance challenges to the Texas Department of Transportation (TxDOT).

The conventional bearing capacity improvement technique includes remove and replacement of existing soil, lime or cement stabilization, jet grouting, dynamic compaction, geopier, sand compaction pile, stone column, micropile, pile supported embankment etc. However, in most cases the conventional methods are expensive. The most common technique utilized by TxDOT is remove and replace method, which increases the cost of construction by millions of dollars. For MSE retaining structures subjected to lateral movement, the typical approach is the use of ground anchors, soil nails etc. (Christopher et al., 1990). Use of a shear key made of concrete can significantly improve the shear resistance which restricts the lateral

movement of the wall (Kim and Bilgin, 2007); however, the high cost of construction, limits the use of the concrete shear key.

An innovative, sustainable and cost effective solution to the bearing capacity and shear failure associated with unsuitable soil could be the use of Recycled Plastic Pins (RPPs). RPPs were found to provide significant lateral support to stabilize the sliding soil mass in the slope (Parra et al., 2003; Khan et al., 2015); which made RPP a potential candidate to be used as shear key for MSE retaining structures. In addition, RPP has considerable axial load carrying capacity. In combination with geosynthetics as load transfer device, RPPs might prove to be efficient in supporting structures, resulting in the reduction of total and differential settlement.

Previous studies showed an extensive and successful use of RPP in shallow slope stabilization. However, very few studies have been conducted to utilize it as an alternative to the improvement of bearing capacity of unsuitable foundation soil and shearing capacity of the base of MSE walls. Moreover, it is important to have a better understanding about the deformation and failure mechanism through graphical presentation using finite element (FE) program (Griffiths and Lane, 1999). Deformation analysis using elasto-plastic finite element modeling is a simple and robust method. To evaluate the influence of different parameters of RPP (e.g. length, spacing and size) in reducing settlement of foundation soil and restricting lateral movement of MSE wall base, FEM analysis can be effectively utilized.

1.3 Research Objectives

The overall objective of the current study was to establish a sustainable ground improvement method using Recycled Plastic Pin. Ground improvement include improvement

of bearing capacity of foundation soil and shearing capacity of MSE wall base. The specific objective of the study included:

- Site Investigation and selection for field scale study area.
- Development of preliminary design for Vertical and Lateral loaded sections.
- Field Installation of RPP.
- Instrumentation of control and RPP stabilized test sections.
- Performance monitoring of the test sections.
- Optimization and calibration of FEM analysis model using field performance monitoring results.
- Numerical study on different parameters of RPP for efficient and effective application.

1.4 Thesis Organizations

The thesis is divided into six chapters that can be summarized as follows:

Chapter 1 presents an introduction, the problem statement and overall objective of the research.

Chapter 2 presents the fundamental concepts of bearing capacity failure of foundation soil; and different types of failures of retaining structures while focusing on failure due to sliding of the base of MSE wall. In addition, a brief description of different methods used for improvement of bearing capacity of foundation soil and shearing capacity of MSE wall base is presented. An overview of previous studies to develop alternative methods to improve ground has been briefly discussed. This chapter also provides a brief review of the manufacturing process, physical and strength properties of recycled plastic pins for structural

application. Finally, few case studies on the application of RPP is presented to show the effectiveness of RPP in geotechnical application.

Chapter 3 describes the field investigation, laboratory testing and site selection followed by detailed field instrumentation program for the constructed test sections. This chapter also includes the reinforcement mechanism of RPP in improving the bearing capacity of weak soil and increasing shear resistance of the MSE wall base against sliding. Finally, field installation of RPP and construction of the test sections are briefly presented in this chapter.

Chapter 4 depicts the performance evaluation through analytical study and field monitoring of the instrumented test sections for both vertical and lateral loaded sections. The reinforced and unreinforced sections were monitored periodically and the performance monitoring results in comparison to the existing literature is presented in this chapter.

Chapter 5 demonstrated a numerical study on the performance of the RPP stabilized/reinforced test sections. A numerical study on different RPP parameters, e.g. length, size, and spacing of RPP, is also presented in this chapter.

Chapter 6 summarizes the major conclusions from the current research and provides with a few recommendation for future studies.

CHAPTER 2

LITERATURE REVIEW

2.1 Introduction

Failure of structures constructed over soil having insufficient bearing and shearing capacity is a common problem encountered by the civil engineers. In most of the cases, sites having problematic soil condition is not suitable for the construction of structures over it. Sometimes remove and replace of soil with proper fill material may be considered as the only option, even after being an expensive solution. However, a number of ground improvement methods are available to improve the bearing capacity of foundation soil and shearing resistance of the base of MSW retaining structures against sliding. This chapter presents comprehensive information collected from the related literature addressing the problem associated to the weak foundation soil and base sliding of the MSE wall and their conventional improvement techniques.

2.2 Improvement of Bearing Capacity

2.2.1 Background

Construction of highways and roadways over weak foundation soil is one of the most common problems faced by the civil/geotechnical engineers, in many parts of the world. The widely practiced and accepted approach to construct highway or roadway on such soil types is to remove and then replace the unsuitable soil with a stronger material such as crushed rock. However, the excessive replacement cost motivated the related administrations to develop and/or evaluate alternative methods of construction on weak foundation soils (Ozdemir, 2016).

It is important to have sufficient knowledge on the site soil condition before construction of any structures such as building, bridges, highway or dams. It is not always certain that the soil at the construction site will be suitable for supporting such structures. According to a TxDOT memorandum (2013), for sites with unsuitable foundation soils, it is sometimes more economical to provide a ground (foundation) improvement plan to accommodate the safe use of structure rather than changing the structure type. Ground improvement varies from simple remove and replace method to complex method, e.g. the use of stone columns, geopiers or geogrid reinforced pads.

An extremely large number of ground improvement methods have been used and/or reported in the literature; many of which have been patented. However, at an individual site one may use a combination of several methods to achieve the desired result. The main purpose is to obtain a significant increase in the bearing capacity of the soil, which can be achieved by modifying/improving the soil properties such as cohesion c, or density γ. Usually an increase in density (or unit weight) is accompanied by an increase in either c or both (assuming the soil is cohesive). According to Bowles (1988), Particle packing (compaction) always increases the density, with a resulting decrease in void ratio, and reduces long-term settlements. Particle packing in general increases the stress-strain modulus resulting in the reduction of any "immediate" settlements.

2.2.2 Weak Soil

Insufficient strength and excessive compressibility are the general characteristics for weak soils. Different climatic conditions are responsible for the consequential variation of the

physical as well as engineering properties (e.g. void ratio, strength, water content, permeability, grain size distribution and compressibility).

Pavement constructed on weak foundation soil bound to face problems during and/or after construction; e.g. sinking of the subbase or base layer into the subgrade soil, lateral and vertical deformation of the subbase or base layer etc., resulting in rutting of the pavement. These results in delay and disturbance to the traffic flow. Figure 2.1 shows some of the related problematic cases.

According to TxDOT designation (TEX-142-E), the consistency of a predominantly clay and/or silt is defined by its unconfined compressive strength (UCS) when tested in the laboratory under the natural moisture content in an undisturbed condition. Higher water content will result in lower strength and lower water content will yield higher strength. Consistency of soil based on unconfined compressive strength is shown in Table 2.1.

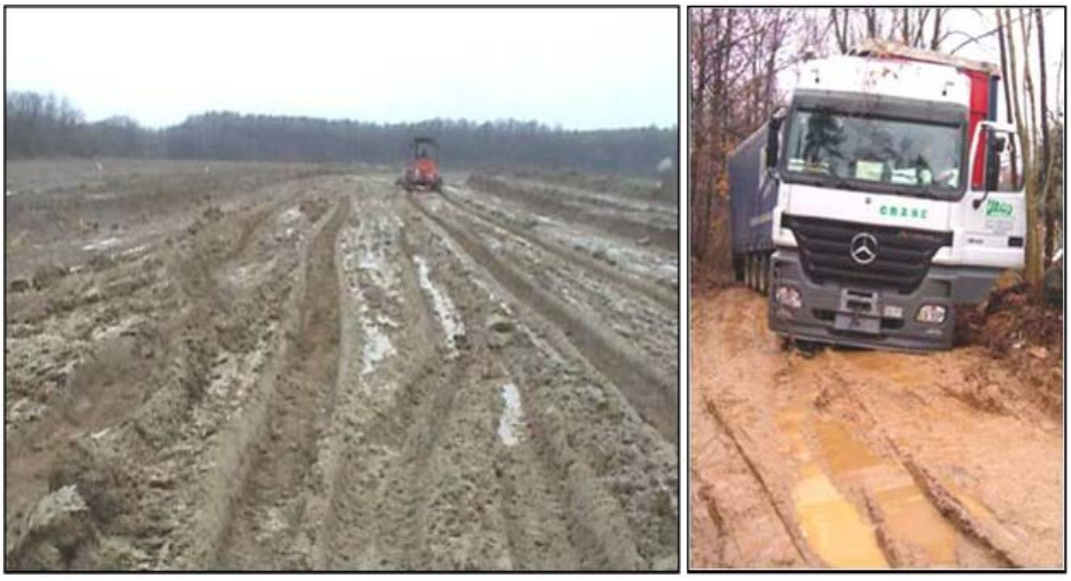

(a) (b)

Figure 2. 1 (a) Construction work on soft soil; (b) Truck sinking into a soft soil road.

Table 2. 1 Soil consistency based on UCS.

Unconfined Compressive Strength (tsf)	Consistency
Less than 0.25	Very Soft
0.25 to 0.50	Soft
0.50 to 1.0	Medium Stiff
1.0 to 2.0	Stiff
2.0 to 4.0	Very Stiff
Greater than 4	Hard

2.2.3 Bearing Capacity of Foundation

Ultimate bearing capacity of the foundation soil may be defined as the maximum load carrying capacity of a foundation before undergoing a large settlement (typically 1 inch settlement). Excessive settlement leads to failure of the structure supported by the underlying soil. Type of failure for a strip footing of width “B”, constructed on a dense sand or stiff cohesive soil is presented in Figure 2.2. There are three possible types of failure that might occur; they are known as, general shear failure (Figure 2.2a), local shear failure (Figure 2.2b) and punching shear failure (Figure 2.2c). General shear failure is pretty common, and it will occur in case of dense sand or stiff clay. If the soil type is medium dense or medium stiff clay, local shear failure may occur. Third type of failure, i.e. punching shear failure, will occur where the soil beneath the foundation is weak and foundation width is not enough to resist the punching force.

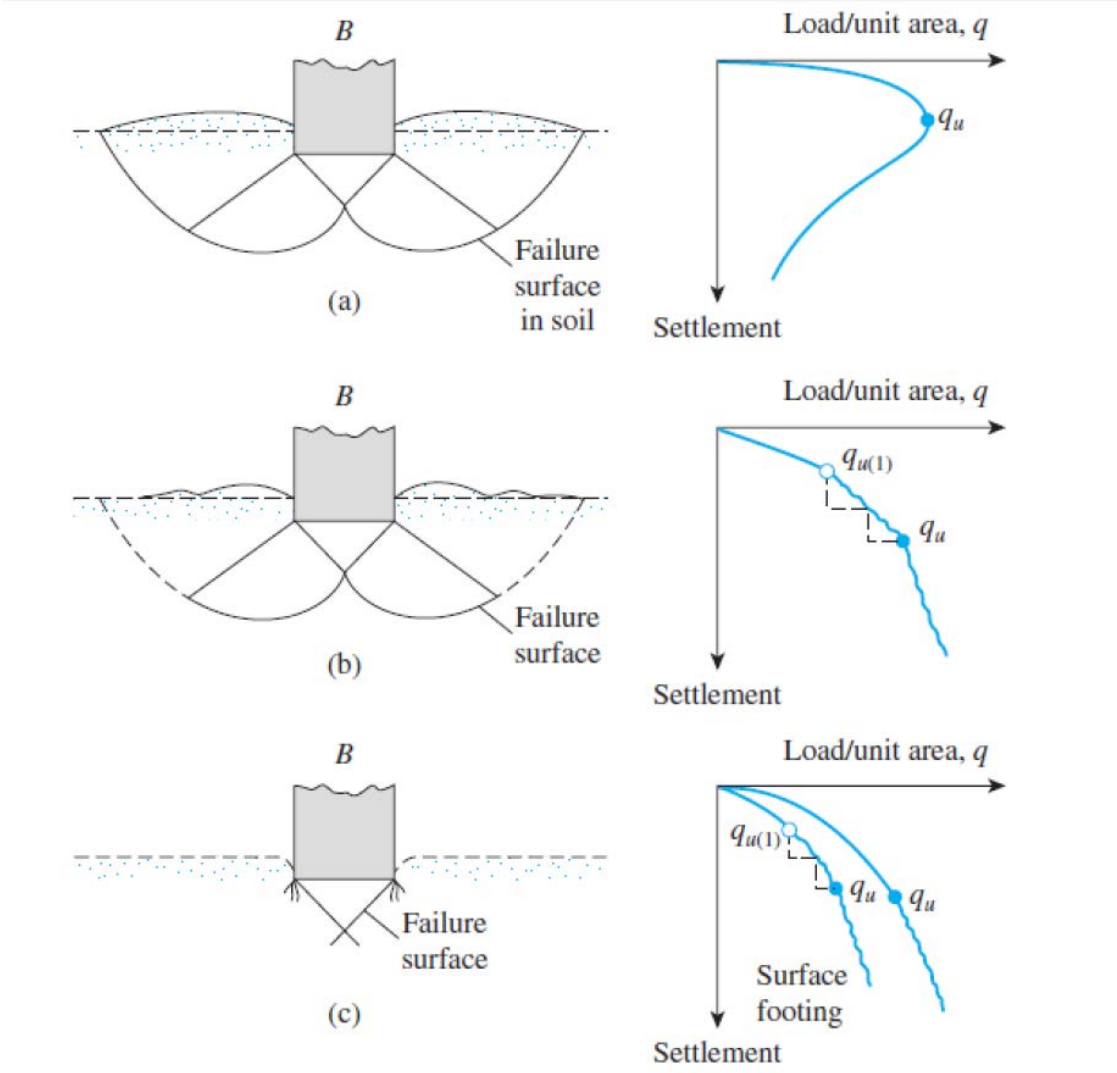

Figure 2. 2 Bearing capacity failure of soil: (a) general shear failure; (b) local shear failure; (c) punching shear failure (Das, 2011).

Terzaghi's solution for bearing capacity (based on drained strength parameter)

The ultimate bearing capacity of shallow foundations may be evaluated using a theory which was first presented by Terzaghi (1943). For a continuous, or strip foundation, Terzaghi suggested that, the failure surface in soil subjected to ultimate load may be assumed to be similar to the case presented in Figure 2.3a and all the forces acting on the soil is shown in Figure 2.3b.

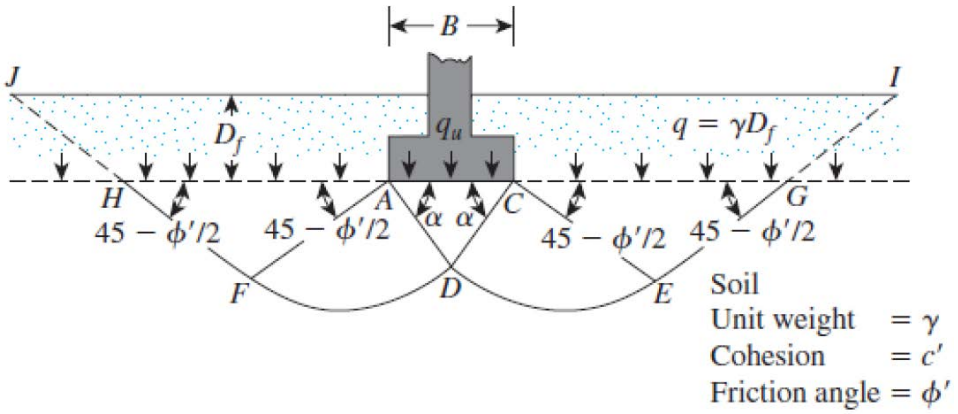

(a)

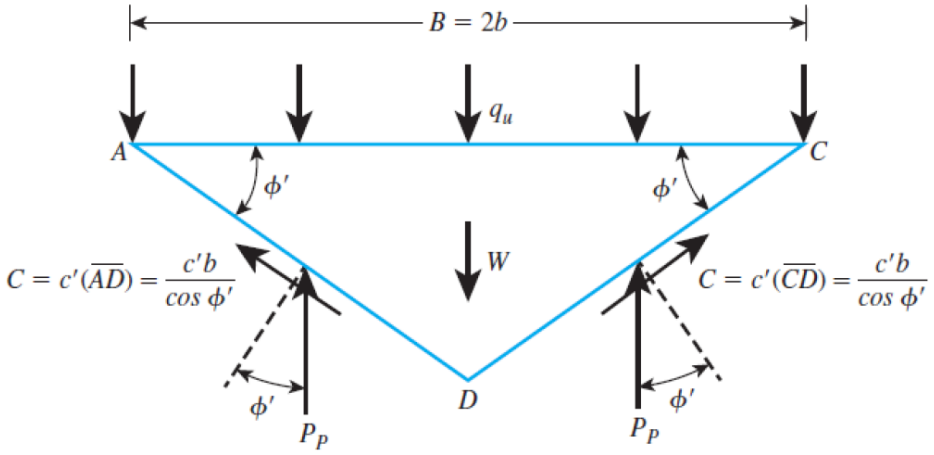

(b)

Figure 2. 3 (a) Ultimate bearing capacity for strip footing; (b) Free body diagram showing the force equilibrium (Das, 2011).

Terzaghi proposed the following equation to determine the ultimate bearing capacity for different foundations.

For strip footing:

$$q_u = c\ N_c + q\ N_q + \tfrac{1}{2}\ \gamma\ B\ N_\gamma \quad (2.1)$$

For square footing:

$$q_u = 1.3\ c\ N_c + q\ N_q + 0.4\ \gamma\ B\ N_\gamma \quad (2.2)$$

For circular footing:

$$q_u = 1.3\ c\ N_c + q\ N_q + 0.3\ \gamma\ B\ N_\gamma \quad (2.3)$$

Here,

c = drained cohesion of soil

N_c, N_q and N_γ are bearing capacity factors proposed by Terzaghi

B = width of footing/ diameter of footing.

Skempton's solution for undrained bearing capacity (based on undrained strength parameter)

Skempton modified Terzaghi's bearing capacity equation for the purpose of determining undrained bearing capacity of cohesive soil. He showed that the bearing capacity factor N_c in Terzaghi's equation tends to increase with depth for cohesive soil, and provided a modified factor N_{cu}. Therefore, Skempton's undrained bearing capacity factor (N_{cu}) has been used which depends on size and depth of the foundation. However, for square shape foundation placed at ground level, the value of N_{cu} will be equal to N_c. Skempton's equation is widely used for undrained clay soils:

$$q_u = s_u\ .\ N_{cu} + q_o \quad (2.4)$$

where,

N_{cu} = Skempton's bearing capacity factor = $N_c.\ s_c.\ d_c$

Where, s_c is a shape factor and d_c is a depth factor.

$N_q = 1$, $N_\gamma = 0$, $N_c = 5.14$

$s_c = 1 + 0.2\ (B/L)$ for $B \leq L$; $d_c = 1 + $ Ö $(0.053\ D/B)$ for $D/B < 4$

When the foundation is on ground surface, $q_o = 0$

Shape factor, $s_c = 1$; Depth factor, $d_c = 1$

For cohesive soil, it is assumed that the friction angle is zero, therefore, the undrained bearing capacity will be the multiplication of undrained shear strength and N_c and the simplified equation is as shown as follows.

$$q_u = 5.14\ s_u \text{ or } (2+\pi)\ s_u \quad (2.5)$$

2.2.3.1 Problems with Weak Foundation Soil

Sometimes the site soil condition is not suitable for construction of structures; therefore, field engineer needs to improve the bearing capacity by improving the soil strength parameters by means of reinforcement or other ground improvement methods. The major problems associated with weak subsoil encountered while constructing an embankment or any other type of structures over the soil are:

- Low shear strength
- Stability of embankment
- High compressibility and settlement of embankment

2.2.3.2 Drained and Undrained Shear Strength

In drained condition and under external loading, no change in pore water pressure is observed. In this condition, pore water drains out of the soil which results in volumetric strains in the soil. The shear strength in drained condition is called drained shear strength. On the other hand, if the pore water cannot escape from the soil matrix due to a much rapid load, the condition is termed as undrained condition and the corresponding shear strength for fine

grained soil is called undrained shear strength. During construction, excess pore water pressure is generated within the soil mass due to rapid load application. For the purpose of analysis, drained shear strength parameter should be used if the construction period is long enough to drain the excess water; however, in case of rapid construction, it is recommended to use undrained shear strength parameter. In general, the undrained condition is considered for a conservative design. In undrain condition, the lowest shear strength can be obtained; therefore, the most critical stability condition are considered to be at the end of construction, when loading is completed. The undrained shear strength is the critical shear strength found at the end of construction since no significant drainage has taken place and the stress state has not altered.

2.2.3.3 Methods of Measuring the Shear Strength

The shear strength of soil is a function of stresses that is applied to it and the manner in which they are applied. Knowledge about the shear strength is necessary to determine the bearing capacity of foundation soil, lateral pressure applied at the back of the facing of retaining structures, and the stability of slopes. There are several laboratory test available to determine the shear strength of cohesive soil, which are:

- Direct Shear Test
- Unconfined Compressive Strength Test
- Triaxial Compression Test

Direct Shear Test:

It is oldest and simplest testing method for the determination of shear strength of soil, which is widely accepted and inexpensive. The relatively thin sample thickness allows a rapid

drainage and fast dissipation of water during the test. However, it is possible to simulate undrained condition through the application of rapid shearing. When the shearing is really slow, it represents drained condition and the strength parameters obtained can be denoted as drained shear strength parameters.

For the direct shear test, the soil sample is kept within the shear box under saturated condition by filling it with water, followed by a shearing force at a constant rate of strain. The compressive load is varied for each test and the corresponding shear stress up and beyond the peak value is recorded and plotted against normal stress. The failure plane can be obtained by connecting the points plotted for each test. Residual stress can also be obtained after exceeding the peak value for larger deformation without any change in the peak. The shear strength of soil determined by direct shear test may be defined by the following equation;

$$S = C + \sigma \tan \varphi \tag{2.6}$$

where,

S = peak shear strength; σ = normal stress;

C = cohesion intercept; φ = angle of internal friction.

Unconfined Compressive Strength Test:

Unconfined compressive strength of the cohesive soil sample can be determined using this test method. The universal master loader capable of performing unconfined compression is used to determine soil sample strength. This is a type of unconsolidated undrained (UU or Q-type) test where the confining pressure on the soil sample equals to zero (atmospheric pressure).

The unconfined compressive strength found is the maximum deviator stress at failure, which may or may not intersect with the measured maximum applied force due to area correction. The value found is equal to the diameter of the Mohr's circle and the undrained shear strength (S_u) is considered as the maximum shear stress which can be expressed as;

$$S_u = ½ q_u \quad (2.7)$$

Triaxial Compression Test:

It is another type of laboratory test method for the determination of shear strength of soil which is relatively complex compared to other available shear strength test methods. Advantage of this test method is that, it can replicate the stress condition close to the field. Whenever a soil sample is extracted from the field, all surrounding forces (vertical and horizontal stresses) are removed; therefore, to replicate the field condition, tri-axial test can be used. For this test, the sample should have a cylindrical shape with a height to diameter ratio of 2 to 3 and is subjected to three dimensional loading. The confining pressure is applied by water pressure within the tri-axial cell, which is kept constant while deviator stress is applied to cause failure of the sample. Three types of tri-axial tests are present; which are:

- Unconsolidated undrained (UU) test
- Consolidated undrained (CU) test
- Consolidated drained (CD) test.

2.2.4 Stability Analysis

Stability analysis is required during the design period for every structures, e.g. embankments, to be constructed on weak foundation. It minimizes the risk of failure within

the weak layer which might result in catastrophic collapse. There are many factors present which are responsible for affecting soil behavior and the stability of the embankment. Therefore, to ensure safety, the following critical condition can be considered:

i) End of construction: This relates to the condition of stability developed during construction.
ii) Long term condition: This relates to the condition when the excess pore pressure developed during construction are fully dissipated.

The advantage of observational approach have been demonstrated in recent years. Usually the performance during and after construction is monitored. For large projects, it is particularly useful and advisable to construct tests sections of embankments.

2.2.5 Modes of Failure of Embankment Constructed Over Soft/Weak Soil

To mitigate the problems associated with failure of embankment, constructed over weak soil, it is very important to have a thorough idea on the modes of embankment failure. Embankments generally fail by one of the following mechanisms:

Bearing Capacity failure: Embankment might sink into the foundation soil or settle excessively which results in a total collapse if the bearing capacity of the soil is not enough to support the loading height of the embankment. The collapse height of embankment H_{max} can be determined by considering bearing capacity failure (Figure 2.4a).

Rotational Failure: If the embankment height is less than or equal to the collapse height H_{max}, rotational failure takes place. Failure occurs along circular arc passing through the foundation soil and the embankment (Figure 2.4b).

Sliding Failure: Due to the excess lateral pressure at the back of the slope portion, the slope portion ABC (as shown in Figure 2.4c) slides laterally as a rigid body. Failure occurs when $P_1 > P_2$.

Spreading Failure: Active pressure P_1' acting on the face A'B', as shown in Figure 2.4d, spreading failure occurs by sliding of soil wedge AB'C along B'C. Failure occur when $P_1' > P_2'$.

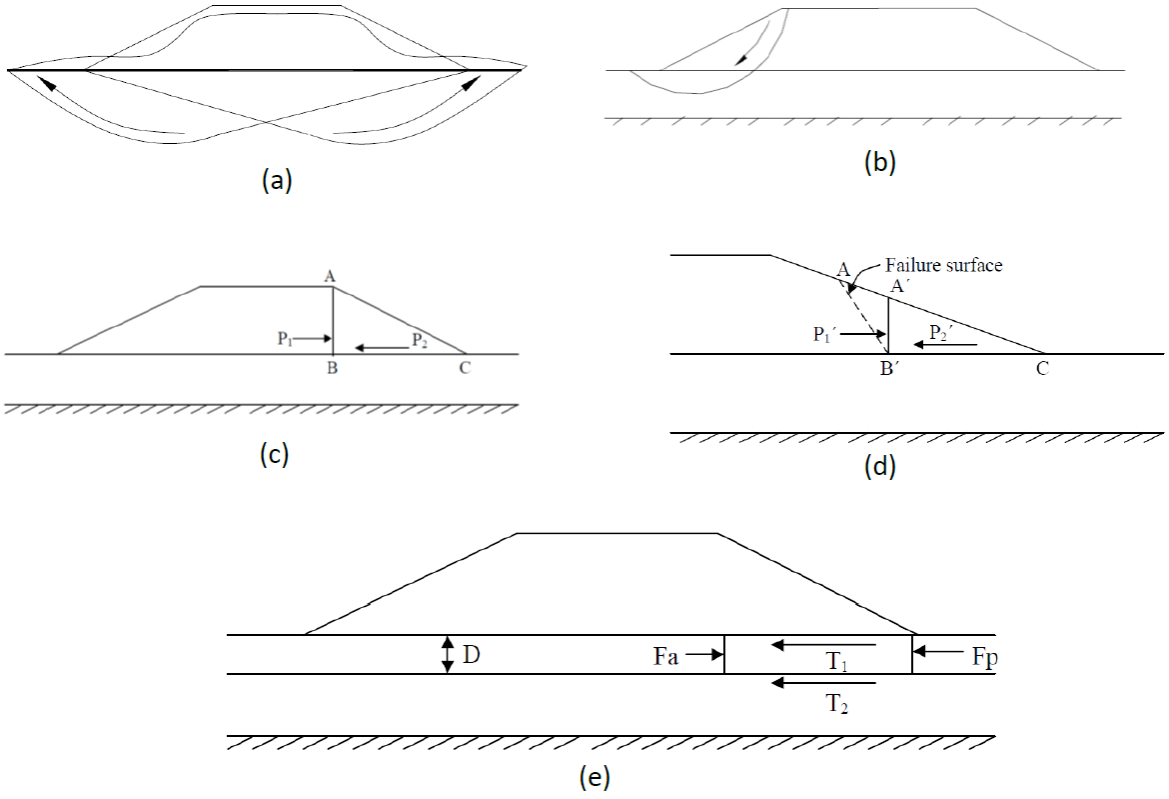

Figure 2. 4 (a) Bearing capacity failure; (b) rotational failure; (c) sliding failure; (d) spreading failure; (e) foundation soil squeezing failure.

Foundation Soil Squeezing Failure: If the foundation soil is composed of layered soft soils, there is possibility of presence of a layer with a much lower strength compared to other layers

resulting in formation of a preferential horizontal sliding plane. This mechanism of failure may be seen where stiff crest overlies a soft soil layer or where the soft soil layer is very thin. This type of failure takes place if total resisting force acting on the block is less than the disturbing force i.e. $F_p + T_1 + T_2 < F_a$ (Figure 2.4e).

Factor of Safety

The ratio between available shear strength and shear stress mobilized on the potential failure plane, in other words the ratio between the resisting force and driving force is termed as Factor of safety. In practice, for effective stress analysis, the factor of safety is taken to the order of 1.4. Much higher values are frequently employed with very soft soil to avoid excessive deformations.

2.2.6 Settlement of Foundation Soil

Foundation soil, when subjected to changes in applied stresses, experience volume change. The magnitude and rate of deformation depends on type of soil and the nature of applied loads. Terzaghi's theory of consolidation has provided the mechanism of the response of soil to applied loads. The soil parameters required for settlement prediction may be derived from consolidation test on undisturbed samples. When an embankment is constructed on soft clay, three components of settlements takes place; immediate settlement, consolidation settlement and secondary compression.

2.2.6.1 Immediate Settlement

Immediate settlement is commonly referred to as initial or undrained settlement which takes place on account of shear strains; it occurs instantaneously following the load application. If the clay is saturated, settlements take place at constant volume due to shear strains

underneath the loaded area. In case of embankment founded on soft clay, the immediate settlement is coterminous with the placement of the fill and as such, no further consequence.

2.2.6.2 Consolidation Settlement

The case of consolidation settlement arises due to the hydraulic gradient of excess pore pressure set-up by the applied load which causes water to be trapped within the soil matrix to drain out, resulting in stress transfer to the soil skeleton and at the same time compression of the soil mass. It is a time dependent process producing mainly volume change; however, shear deformations are also involved leading to further settlement. The classical Terzaghi's theory may be used to determine primary consolidation settlement in one dimension.

2.2.6.3 Secondary Compression

Secondary compression takes place essentially after complete dissipation of excess pore water pressures and at a practically constant effective stress. It is commonly referred to as drained creep. At present there is no general agreement stablished on how to separate consolidation into its primary and secondary components. Although both primary consolidation and secondary compression may progress concurrently, it is convenient to consider them in separate phases. It is required to have a thorough knowledge of the stress strain time relationship of the clay for near perfect estimation of the secondary compression.

2.2.7 Bearing Capacity Improvement Methods

Improvement of the soft soil bearing capacity has been one of the major concern for researchers over decades. Arenicz (1992) reported that, for soil reinforcement, ribbed strips are superior compared to the smooth strips to enhance soil shear strength. The use of the wider strip seems to reduce the relative effectiveness of strip ribs in producing additional strength of

soil. Reinforcement layout plays a significant part in enhancing soil shear strength. Fabric reinforcement method is another way of improving soil shear strength which costs approximately 60% of the end dumping displacement method of dike construction (Haliburton et al., 1978).

A laboratory scale study was conducted by Shin et al. (1993) on geogrid, to improve the bearing capacity of weak soil. The study focused on determining the critical non-dimensional values for the geogrid reinforcement with depth. Additionally to obtain a maximum possible bearing ratio, the study also aimed at finding the location of first layer of geogrid with respect to the bottom of the foundation.

Geosynthetic can be used to design permanent as well as temporary earth structures which also ensures adequate factor of safety. It has been used increasingly in transport facilities like retaining walls, steep slopes, bridges pavements and foundation with weak/soft soil condition. In many cases, incorporating geosynthetics within the soil significantly reduces the cost of construction compared to unreinforced soil structures. A study conducted by Min et al. (1995) showed that the ultimate pullout load and interaction coefficient determined from repeated loading tests were found to be about 20% less compared to the results observed from sustained loading tests. Therefore, the use of a smaller Ci value compared to the one obtained in static test is recommended for the structures subjected to dynamic loading.

A reinforced earth slab may be used to transfer the load and to increase the load bearing capacity of the system. It is actually a thin layer of granular soil reinforced with horizontal layers of flat metal strips or ties having relatively high tensile strength, and ensures development of better frictional bond with the soil. The accuracy of the ultimate bearing

capacity design for the reinforced soil is similar to the regular footings. A study conducted by Verma and Char (1986) showed that sand subgrades reinforced with vertically placed galvanized rods significantly improves the bearing capacity of the soil.

Accoring to Fatani et al (1991), the reinforcement elements, consist of flexible, semi rigid or rigid metallic fibers, can be placed in the soil to increase the shear resistance. It is also reported that, with the use of reinforcement, peak and residual shear strength can be increased by up to 100% and 300% respectively. The study concluded that, the bearing capacity of a foundation depends on the following four factors; lateral spacing between strips, vertical spacing between layers, first layer depth below the footing, and number of reinforcement layers. Compared to the unreinforced soil, the bearing capacity can be improved by up to three times. However, bearing capacity improvement factor is limited to about two because of the practical considerations (Marto and Kasim, 2002).

Geogrid is a high modulus polymeric material with high tensile strength which is very useful to reinforce any construction material including the soil. Main feature of the geogrid is its opening between the longitudinal and transverse ribs which is called apertures. The opening should be sufficient to allow soil to pass through the geogrid. Giroud and Noiray (1981) suggested various pavement design methods for unpaved roads which are characterized by high allowable rut depths, low volume of traffic and no vehicle wander.

Geocell can be a potential element for the improvement of soil bearing capacity. Generally, it is a 1m deep open cellular structure constructed from a biaxial grid base layer with uniaxial grids forming vertical cells. The cells are usually filled with graded granular fill materials. The soil is contained and confined by a series of interlocking cells, constructed from

polymer geogrids (Figure 2.5). Potential failure plane is obstructed by the rigid geocell mattress and pushed down to a deeper stiff layer which is helpful to improve the load carrying capacity of the foundation soil. A case study presented by Robertson and Gilchrist (1987), described that the effectiveness of geocell mattress where a 14.76 ft. (4.5 m) high embankment was constructed on 13.12 ft. (4.0 m) thick compressible silty clay layer with an average undrained cohesion of 313 psf. (15 kpa) underlain by a stiffer material. It is also reported that, the use of this technique might result in a saving of about 31 % over the excavation, remove and replace method.

Figure 2. 5 Use of Geocells in pavement structures on weak foundation soil.

At present, several stablished ground improvement methods are being used widely as a relatively cheaper alternative to remove and replacement method. Some of the methods are briefly described in the following subsections.

2.2.7.1 Lime Stabilization

Admixtures are occasionally used for the purpose of stabilizing soil, especially for fine grained soil (Das, 2011). Lime is an example of such admixture. Properly proportioned

mixtures of lime can modify or stabilize and strengthen the soil. Purposes of using lime are; (a) to modify the soil, (b) expedite the process of construction, and (c) improving the strength and durability of soil layer. A study by Zhou et al. (2002) presented the suitability of lime for the improvement of weak fly ash ground. The major tests conducted to monitor the soil improvement included a series of unconfined and confined compression tests. Results obtained from the laboratory test results are shown in Figure 2.6. It is observed that, the lime addition resulted in an increased unconfined strength; the strength observed after 60 days is almost 7 times of the strength gained after 7 days. Based on the laboratory test results, 10% and 20% lime were mixed to construct lime and fly ash mixed columns in the field for testing (called Lime-FA columns or piles). Length of each columns was 9.6 m (31.5 ft.) and 0.5 m (1.64 ft.) in diameter. Results obtained from the load test conducted on this column group is shown in Figure 2.7. It is found that, when the axial load was below 100 KPa, addition of lime does not have any impact on bearing capacity. According to Das (2011), there are three ways for lime stabilization in the field:

i) Mixing proper amount of lime with the in situ material or the borrowed material at the site followed by addition of moisture and then compaction to desired level.
ii) Mixing lime and water with the soil collected from the site at designed proportion in a plant, which is then hauled back to the site for placement and compaction.
iii) High pressure injection of lime slurry into the soil up to a depth of 4 to 5 m (12 to 16 ft).

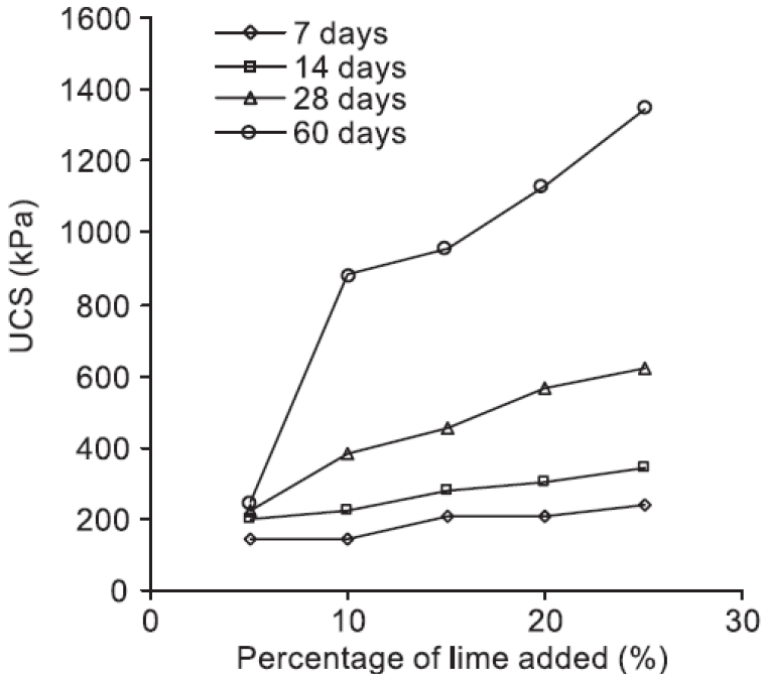

Figure 2. 6 Unconfined Compressive Strength (UCS) with added lime (Zhou et al., 2002).

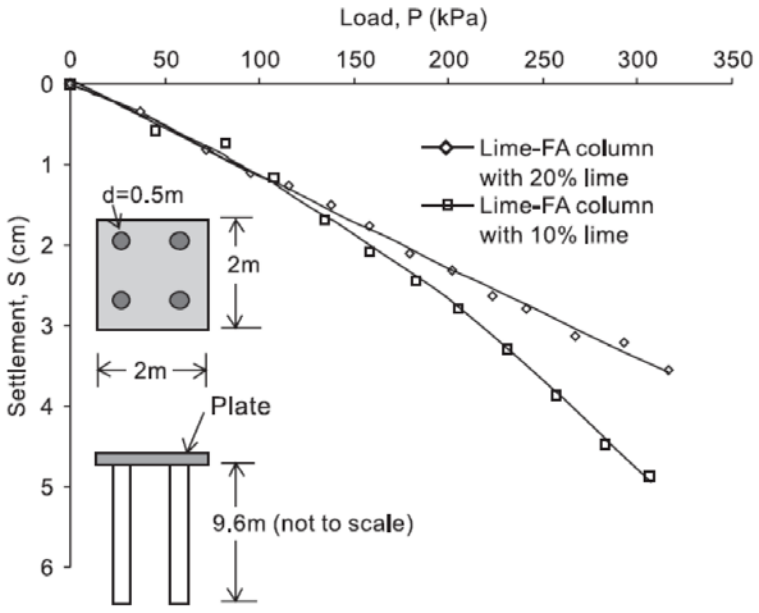

Figure 2. 7 Load vs settlement curves from field plate loading tests on a group of four Lime-FA columns (Zhou et al., 2002).

2.2.7.2 Cement Stabilization

Cement is another agent that can improve and stabilize soil. The use of cement has been increased for this purpose during the construction of highways and earth dams. Both sandy as well as clayey soil can be stabilized by cement. For clayey soil, mixing cement helps to decrease the liquid limit and increase the plasticity index and also workability of the soil. When the liquid limit of clayey soil is less than 45 to 50 and the plasticity index is less than about 25, this method is very effective (Das, 2011). Typical compressive strength of soils and soil-cement mixture is presented in Table 2.2. In case of untreated sandy clay compressive strength ranges from 70 – 280 kPa; whereas, when treated with cement, the soil may have a compressive strength as high as 1,730 to 3,460 kPa.

Tang et al. (2007) conducted an experimental program to investigate the effects of discrete short polypropylene fiber (PP-fiber) on the strength of cement treated and untreated clayey soil. The results obtained from the experiment showed that incorporating fiber reinforcement within the virgin soil and cemented soil increases the unconfined compressive strength (UCS). A significant improvement in the soil strength was observed due to the addition of cement from 0 to 5%; also the addition of increasing percentage of fiber caused an increase in compressive strength (Figure 2.8).

Table 2. 2 Typical Compressive Strength of Soils and Soil-Cement Mixtures (Das, 2011)

Material	Unconfined compressive strength range	
	kN/m²	lb/in²
Untreated soil:		
Clay, peat	Less than 350	Less than 50
Well-compacted sandy clay	70–280	10–40
Well-compacted gravel, sand, and clay mixtures	280–700	40–100
Soil–cement (10% cement by weight):		
Clay, organic soils	Less than 350	Less than 50
Silts, silty clays, very poorly graded sands, slightly organic soils	350–1050	50–150
Silty clays, sandy clays, very poorly graded sands, and gravels	700–1730	100–250
Silty sands, sandy clays, sands, and gravels	1730–3460	250–500
Well-graded sand–clay or gravel–sand–clay mixtures and sands and gravels	3460–10,350	500–1500

[a]Based on data from Mitchell, J. K. and Freitag, D. R. (1959). "A Review and Evaluation of Soil-Cement Pavements," *Journal of the Soil Mechanics and Foundations Division*, American Society of Civil Engineers, Vol. 85, No. SM6, pp. 49–73.

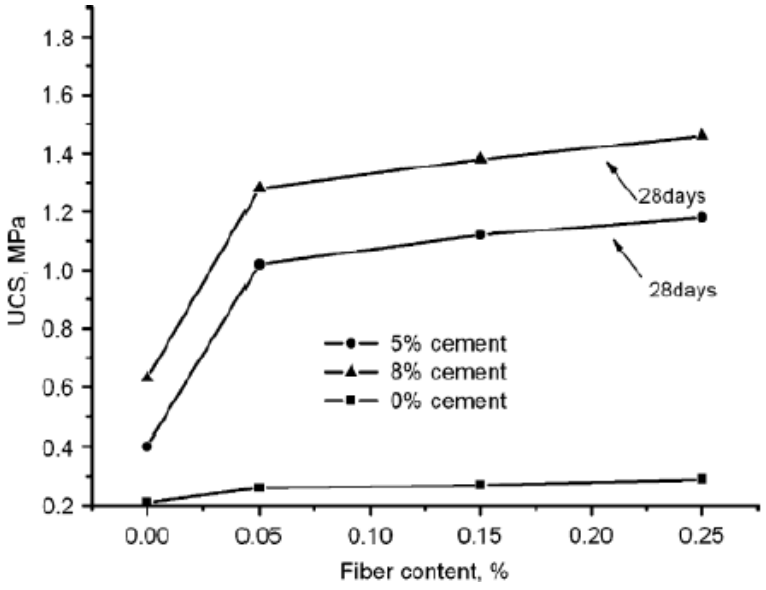

Figure 2. 8 The relationship between the UCS and fiber content (Tang et al., 2007).

2.2.7.3 Jet Grouting

Jet grouting is a soil stabilization technique where cement slurry is injected into the soil with very high nozzle pressure to form a soil concrete matrix. The injected cement grout

densifies the soil matrix by filling the voids without any essential change in the original soil volume or its structure. Soil stabilization by means of jet grouting occurs due to the hardening of grouted fluid within the soil body which forms like cemented columns and improve the bearing capacity of the ground. Some common application of this method are, underpinning of foundation, water control, support for excavation, and to seal the bottom of planned excavation. There are three basic systems of jet grouting that have been developed – single, double and triple rod systems where hydraulic rotary drilling is used to reach the design depth. This method is suitable for erodible soil like gravelly soil and clean sand but unsuitable for high plastic clay which is difficult to erode.

Case Study: Singapore Mass Transit System (Tornaghi, 1985)

Presence of several types of soils, such as beach, estuarine and fluvial deposits, marine clay and sedimentary soft rocks, makes the geology of the Singapore very complex. The study area of concern composed of a Beach sand and fill layer of 3 – 5 m (9.85 to 16.4 ft.) deep, overlie very soft peaty clay, marine clay and fluvial soils to a combined depth in excess of 15 m (49.2 ft.). In this tunnel project, the station area was excavated up to a depth of 15 m. To stabilize the soil, Jet grouting technique was utilized by means of vertical staggered holes along the two independent tunnel routes. To find out the density and unconfined compressive strength, soil samples were collected from different depth, before and after the jet grouting to conduct laboratory tests. The results obtained before and after the soil improvement is presented in Figure 2.9. It is observed that, for soft peat clay layer there is a little increase in unconfined strength with no significant change in bulk density, whereas for silty clay and medium stiff clay layer, a significance increase in both bulk density and strength was found.

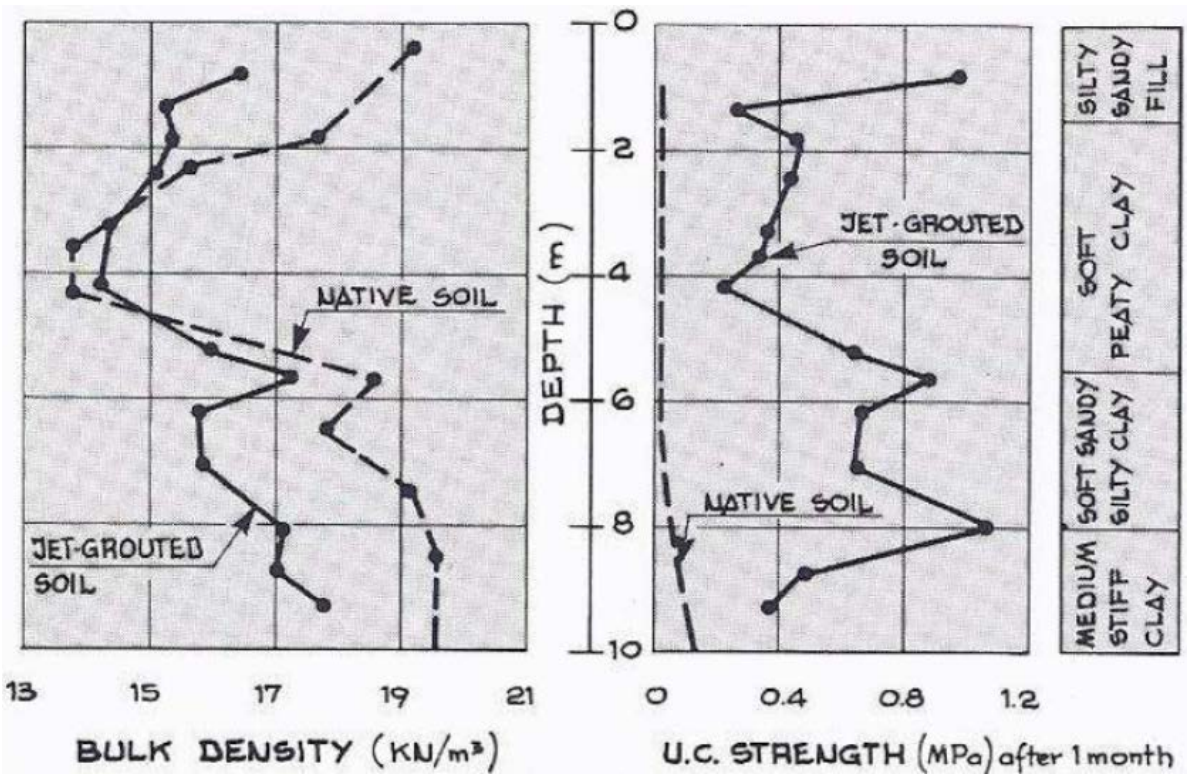

Figure 2. 9 Plots of bulk density and strength versus depth (mean values recorded in Singapore test area on samples of jet-grouted soil) (Tornaghi, 1985).

2.2.7.4 Dynamic Compaction

Dynamic compaction is a well stablished soil improvement technique to densify loose fill of cohesion less soil by dynamic loading of high impact energy. This compaction is done by dropping a heavy mass of 10 – 40 tons from a height generally varying between 10 – 25 m on to the predetermined grid points on the ground (Chow et al., 1992). According to Das (2011), degree of compaction achieved depends on:

- Weight of the hammer to be used,
- Drop height of the hammer,
- Spacing between hammer drop locations.

A case study was reported by Leonard et al. 1980, where the improvement of load bearing capacity was measured with cone penetration test. This site was located in Indianapolis where it was decided to construct a warehouse on an old spoil site. The spoil materials are loose, fine to medium sand with a thin gravelly seams of medium dense sand. Ground water was detected at a depth about 5 to 9 m (16.4 to 29.5 ft.) below the ground surface. Dynamic compaction method was used to improve the load bearing capacity of the soil with a 5.9 ton hammer, dropping from a height of 12 m (39.4 ft.) in a grid pattern. CPT tests were conducted in between the dropping points and it is observed that, tip resistance increased up to a depth of 5 m (16.4 ft.), and only within the sand layer (Figure 2.10).

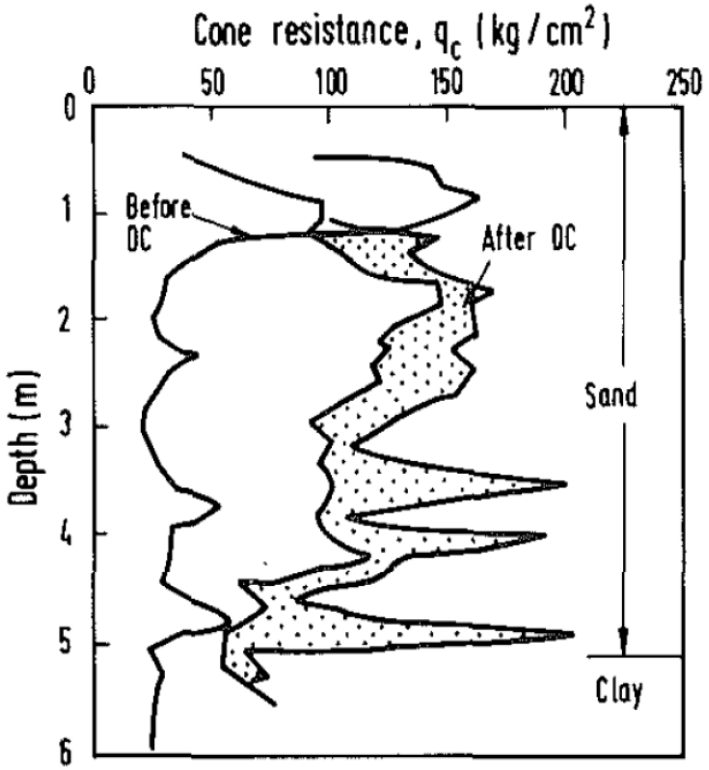

Figure 2. 10 Effect of dynamic loading on soil improvement with CPT (Chow et al., 1992).

2.2.7.5 Geopier

Rammed Aggregate Pier (RAP) systems proved to be efficient and cost effective as intermediate foundation solutions for supporting structures susceptible to settlement (Geopier, Tensar). Ground improvement technique introduced by Geopier are used to reinforce soils, including loose to dense sand, soft to stiff clay and silt, organic silt and peat, variable uncontrolled fill, and soils below the ground water. There are five different improvement methods which has been used for different projects.

The GP3 system (Figure 2.11a) utilizes replacement rammed aggregate pier elements as reinforcement for different soil types, which includes loose to dense sand, soft to stiff clay and/or silt, organic silt and peat, and variable uncontrolled fill materials. Achieving high density and high strength RAP elements of superior load support capacity is the goal for the vertical ramming. In this system, bearing capacity can be improved by up to about 10 ksf with superior settlement control.

Another improvement technique is the Geopier Impact system (Figure 2.11b) that uses a patented displacement mandrel. The main focus of this method is to improve poor soils, including soft clay and silt, loose sand, mixed layers of soil, uncontrolled fill, contaminated soils and soils underneath the groundwater table. Geopier Impact system is effective in treating different soil and groundwater conditions, and deep treatment for liquefaction. It increases the reach of RAP treatment depths beyond 40 feet.

The Geopier Rampact system (Figure 2.11c) is extremely cost effective method. In this method the displacement tapered mandrel is used to construct RAP elements by means of direct vertical ramming energy which densely compacts the successive lifts of high quality crushed

rock/aggregates to mold engineered elements of higher stiffness. Driving of the mandrel into the ground improves the soil matrix laterally and increases the corresponding stress. Another advantage of the Rampact elements is to provide adequate support in the relatively shallow deposits of man-made fill and other heterogeneous profiles as it does not require a casing.

Figure 2. 11 Rammed Aggregate Pier Systems. (a) GP3 system; (b) Impact system; (c) Rampact system; (d) Densipact system; (e) X1 system (www.Geopier.com).

The Densipact system (Figure 2.11d) is cost efficient in improving loose to medium dense granular soils (SP, SP-SM, SM) in places where it is required to increase the soil density. It can substitute dynamic compaction, massive remove and replacement, deep foundations, including driven piles, drilled shafts or augured cast-in-place piles and other forms of ground improvement. It has been found that the Densipact system can improve the bearing pressures up to about 14 ksf which ensures superior performance and reliability.

The Geopier X1 system (Figure 2.11e) forms replacement/displacement RAP elements as reinforcement for good to poor soils. It has the ability to build through zones that are susceptible to caving during drilling and facilitates construction flexibility. Visible inspection of the hole during drilling is possible to address change in ground conditions accordingly. It is recognized as an ideal solution for reinforcing a variety of soil types due to its cost effectiveness, performance, and flexibility.

2.2.7.6 Sand Compaction Pile

The sand compaction pile (SCP) is one of the effective and economic methods for ground improvement. It is widely used for ground stability improvement, prevention of liquefaction, reducing settlement etc. Installation of well-compacted sand piles in the ground with or without confinement is done to improve soft foundation soil. Nazir and Azzam (2010) conducted laboratory model tests to study the improvement of soft clay layer by using both partially replaced sand piles with or without confinement. Main purpose of their research was to evaluate the effectiveness of sand pile in increasing the bearing capacity and to control the settlement. Schematic view of the experimental model apparatus is shown in Figure 2.12 which consisted of cylinder shaped test box (diameter = 90 cm, height = 120 cm and thickness = 6

cm), having appropriate rigidity to maintain plain strain conditions by limiting all directional out of plain displacement. A model footing was made of steel circular plate with a diameter of 100 mm (3.94 inches), and thickness of 20 mm (0.8 inches). The normally consolidated soft clay bed was prepared by pouring the clay in layers, at a water content equal to its liquid limit (LL = 40). After the preparation of the clay bed, a steel pipe was pushed till the required depth followed by excavation of the soft layer inside the pipe. The pipe was then filled with sand and compacted in layers of 50 mm (1.97 inches) thick. Results obtained from this study showed that bearing capacity increases with increasing L/h ratio (L/h = 0, no replacement and L/h =1 = full replacement with sand) (Figure 2.13). It was observed that, with the full replacement of soft soil with sand layer, bearing capacity increased by almost 7 times.

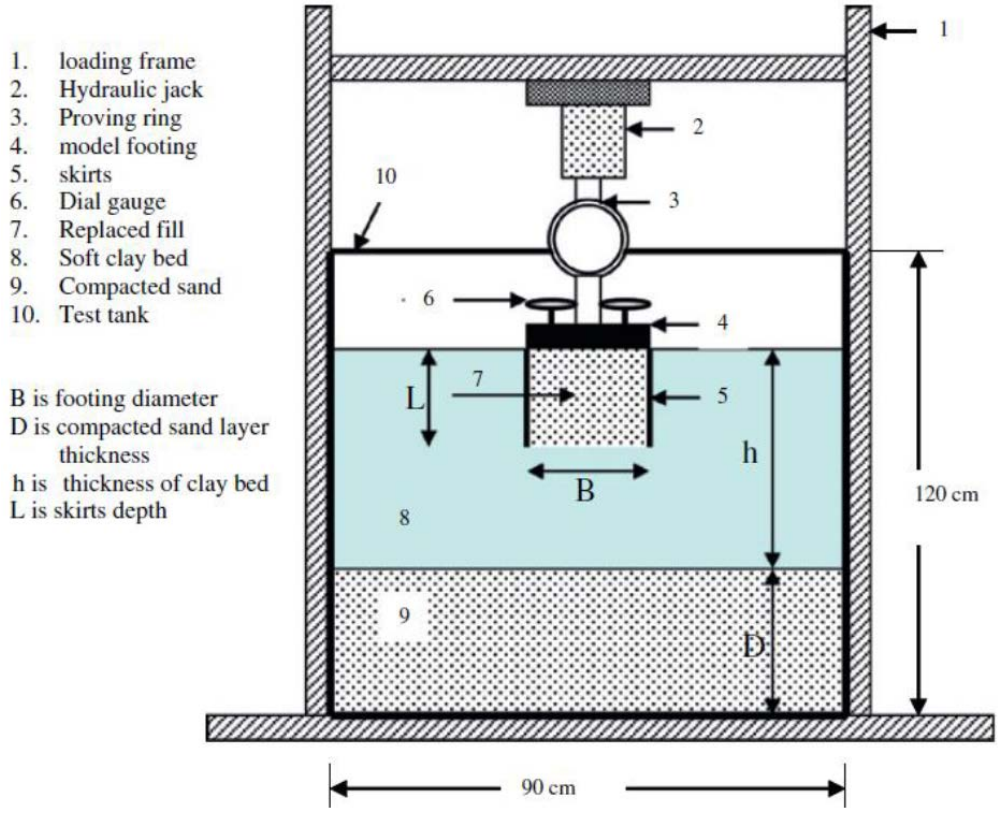

Figure 2. 12 Schematic diagram of the test set up (Nazir and Azzam, 2010).

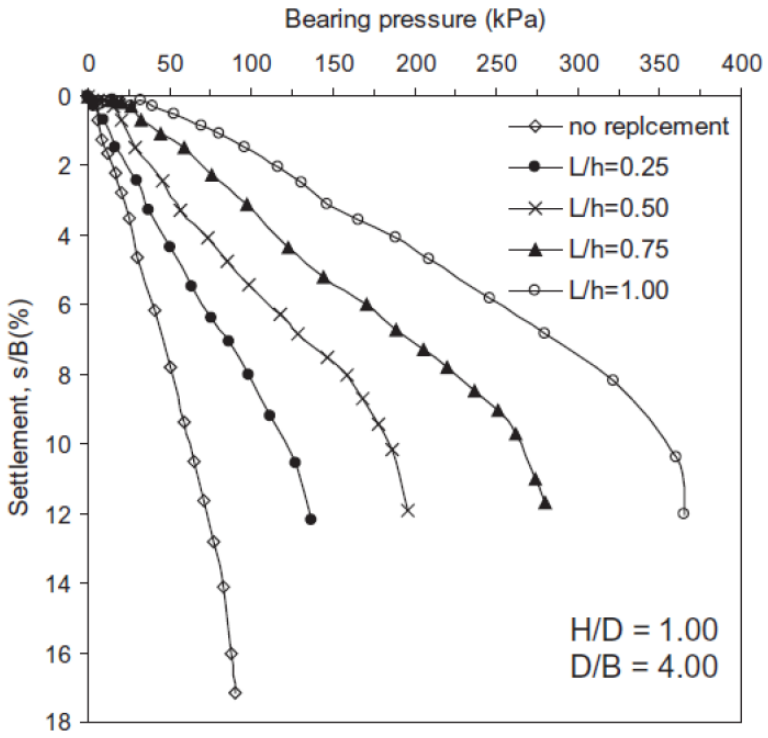

Figure 2. 13 Variation of bearing stress, q versus normalized settlement for different replaced depth for footing with skirts (Nazir and Azzam, 2010).

Sand compactions piles are constructed by driving a hollow mandrel. The bottom of the mandrel may be kept open or close depending upon the full or partial withdrawal. After the installation of mandrel, sand is poured from the top and is compacted by applying air pressure. Sand piles are usually 0.46 to 0.76 m (1.5 to 2.5 ft.) in diameter and are placed at about 1.5 to 3.0 m (5 to 10 ft.) center to center (Das, 2015). Basore and Boitano (1969) presented a case history on the densification of a granular subsoil having a thickness of about 9 m (30 ft) at San Francisco, California, using sand compaction piles which had diameters of 356 mm (14 in.). Figure 2.14a shows the layout of the sand piles. Improvement of the soil layers were identified by standard penetration resistance, N_{60}, before and after the construction of the sand piles, as shown in Figure 2.14b. These tests show that when the spacing vs pile diameter ratio exceeds about 4 to 5, the effect of densification is practically negligible.

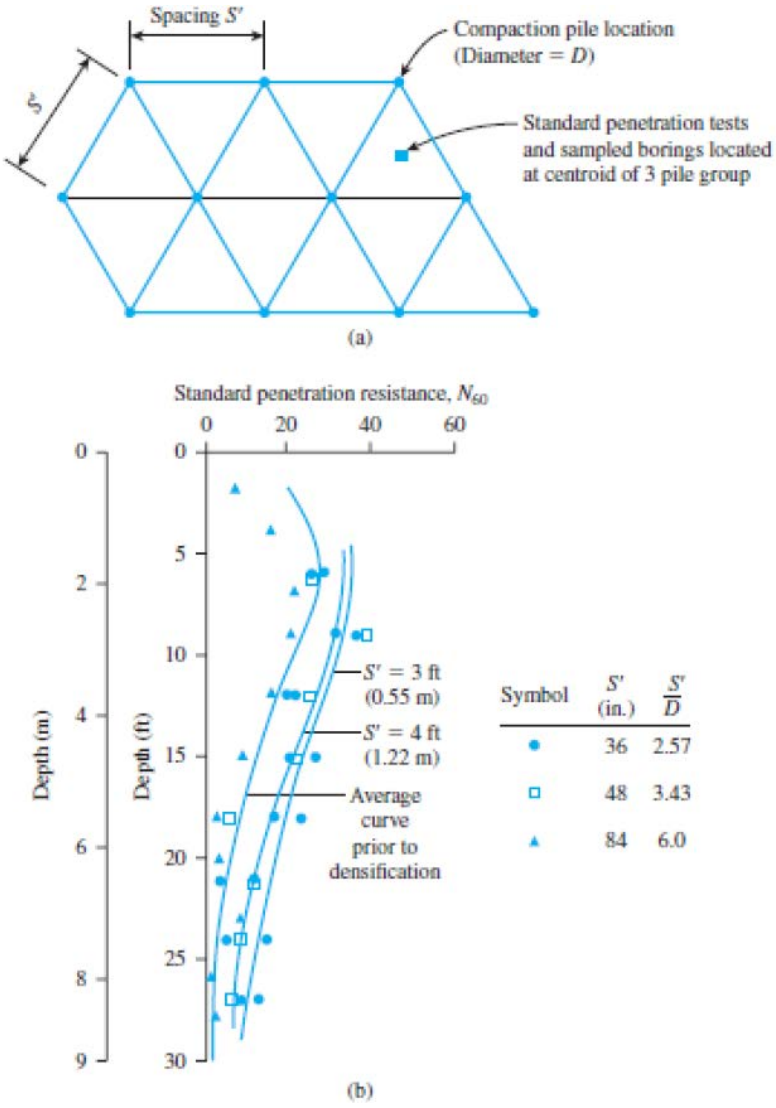

Figure 2. 14 Sand compaction pile test of Basore and Boitano (1969); (a) layout of the compaction pile; (b) standard penetration resistance variation with depth and S'.

2.2.7.7 Stone Column

As a ground improvement technique, the stone column method is economic compared to other expensive solutions. It is effectively used to increase the load bearing capacity of weak clay layers. The columns consists of crushed coarse aggregates of various sizes. The ratio at which stones of different sizes will be mixed depends on design criteria. Densification and/or reinforcement of the soil is accomplished with compacted granular columns or "stone

columns" by either top-feed or the bottom-feed method. Top feed method involves jetting of water to remove soft material, stabilize the probe hole, and ensure that the stone backfill reaches the tip of the vibrator. In Bottom Feed Vibro-Replacement method, the vibrator remains in the ground and no water is involved during the construction process.

Guetif et al. (2007), proposed a method for evaluating the improvement of the Young modulus of soft clay in which a vibro-compacted stone column was used. Based on the numerical study, a decrease in effective stress was found radially from the center of the stone column (Figure 2.15). Increase of vertical mean stress near the stone column indicates the increase of radial stress which will result in improvement of the Young modulus of soft clay, due to the consolidation.

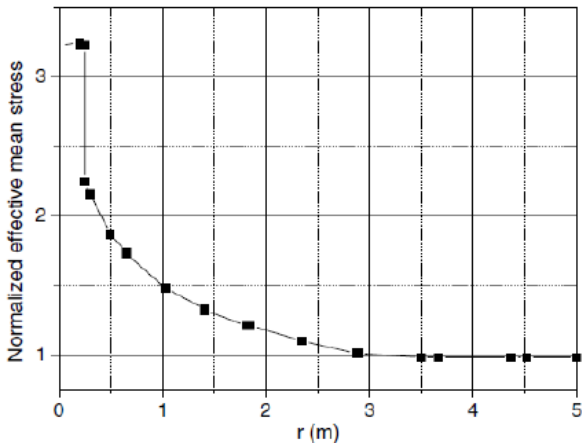

Figure 2. 15 Variation in normalized effective mean stress with distance from the column axis, in the reinforced soil after soft clay consolidation (Guetif et al., 2007).

The surrounding soil around the stone column provides confinement which ensures Load capacity of the columns. However, in case of very soft soils this lateral confinement might not be adequate and the formation of the stone column itself becomes doubtful (Murugesan and Rajagopal, 2009). Therefore, ideally wrapping individual stone columns with

suitable geosynthetic is recommended to improve the performance of stone columns. Load tests were conducted on the stone column installed at the center of the clay bed prepared in the large test tank (Figure 2.16a). The comparison of load bearing capacity of encased stone column (ESC) and ordinary stone column (OSC) is shown in Figure 2.16b. Ordinary stone column does not have much influence on bearing capacity; however, a significant improvement on load bearing capacity was observed for encased columns.

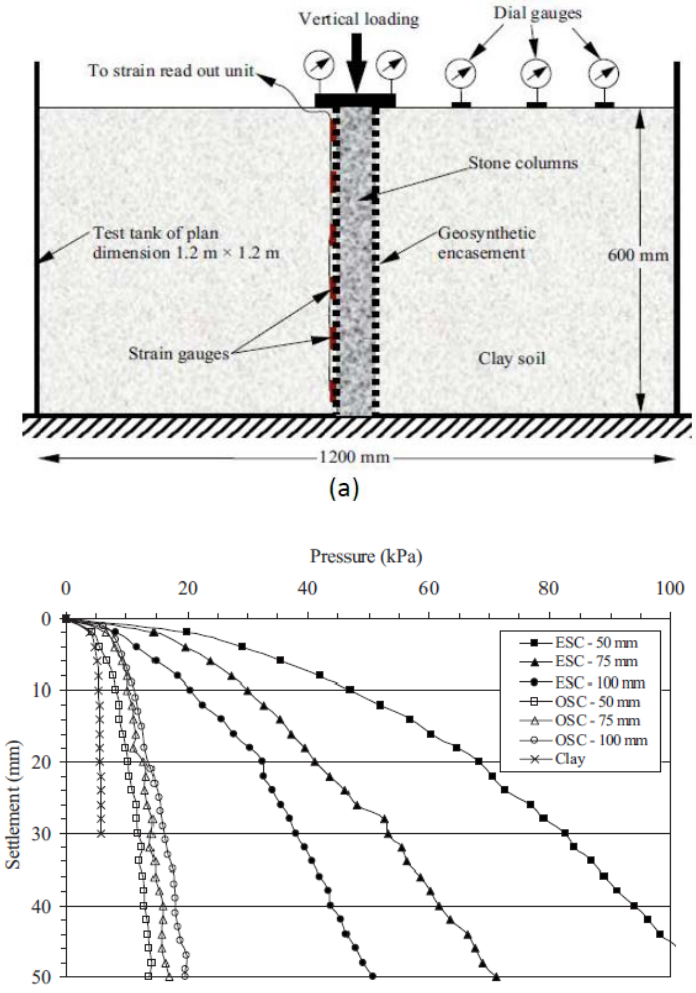

Figure 2. 16 (a) Test set up for single stone test column; (b) Comparison of load bearing capacity for Ordinary Stone Column (OSC) and Encase Stone Column (ESC) (Murugesan and Rajagopal, 2009).

2.2.7.8 Micropile

As a deep foundation element, micropiles are used to provide structural support, which require high-strength, small diameter steel casing and threaded bar to construct. They are also known as minipiles, needle piles, pin piles, and root piles. This technique has been used to support most types of structures. The advantage of micropiles are, they can be installed in a restricted access and low headroom interiors. These benefits allow them to be used for facility upgrades with limited disruption to normal operations.

Jenck et al. (2009) conducted a study to find out the settlement and arching effect in piled embankments using the three-dimensional (3D) finite difference model by FLAC 3D code. It was found that micropile treated soil can greatly reduce the settlement of the embankment and mitigate the seismic response of the embankment. Esmaeili (2012) conducted a study with micropile in lab scale to increase the bearing capacity of railway embankments and to avoid the deep sliding of loose subgrade. A typical cross-section of the test embankment with progressive failure surface is shown in Figure 2.17a & b.

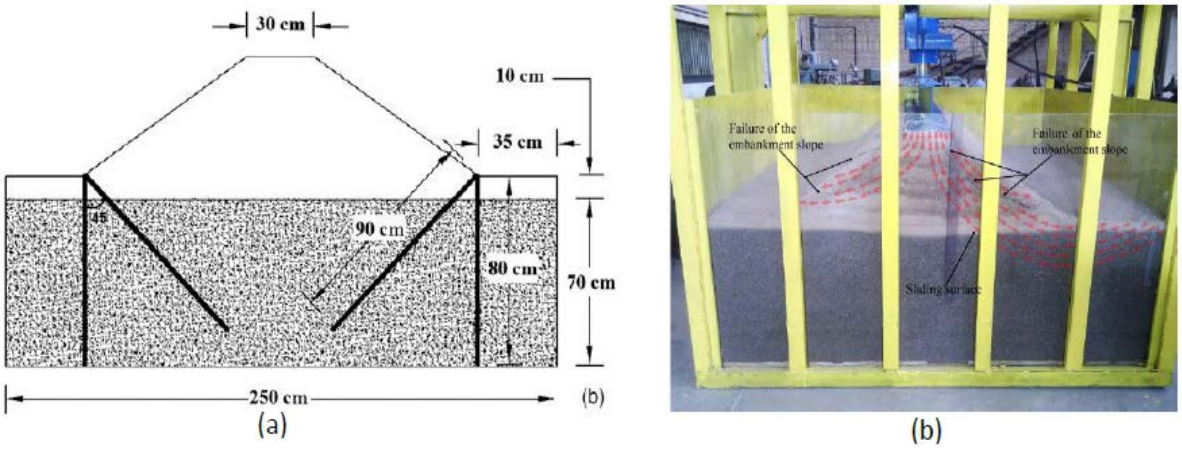

Figure 2. 17 (a) Arrangement of micropile for loading test. (b) Progressive sliding surface of the embankment (Esmaeili et al., 2012).

Three loading tests were performed, where the first test was conducted with no micropile, second and third loading tests were performed with 1 and 2 rows of micropile to observe the impact on bearing capacity (Figure 2.18). Test embankment was also modeled with Plaxis 3D code, to verify the results and it was found almost identical as shown in Table 2.3.

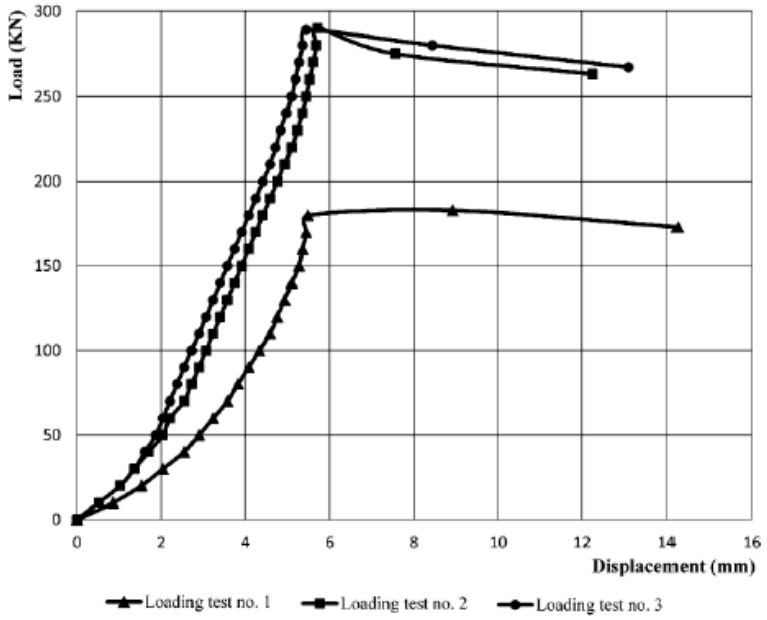

Figure 2. 18 Load displacement of embankment crest (Loading test no 1: no micropile; Loading test no.2: 1 row of micropile; Loading test no. 3: 2 rows of micropile) (Esmaeili et al., 2012).

Table 2. 3 Load bearing capacity of test embankment obtained from numerical and experimental results.

Test Number	**Numerical load-bearing capacity**	**Experimental load-bearing capacity**
1	258.30	254.16
2	404.17	402.78
3	404.17	401.39

2.2.7.9 Pile Supported Embankment

Pile supported embankment is a popular technique to improve the foundation to increase the structural stability and to reduce the structural deformations (Ariema and Butler, 1990). In recent years, geosynthetics have been used in combination with pile or column system to support embankment over soft clay foundations (Han and Collin, 2005).

Several researchers designed pile supported embankments without or with geosynthetic reinforcement. The former is considered as conventional pile-supported embankment while the latter is referred to as geosynthetic-reinforced pile supported embankment. Geosynthetic-reinforced embankment may be designed over piles with caps or on columnar systems. According to a study conducted by Hewlett and Randolph (1988), it is estimated that the pile covering as much as 10% of the area beneath the embankment may carry more than 60% of weight of the embankment due to arching action in the fill. A single geosynthetic reinforcement layer acts as a tensioned member while a multilayer system behaves similar to a stiffened platform (like a plate) which is due to the interlocking of geosynthetic reinforcement with the soil (Han and Gabr, 2002). These ground improvement engineering techniques have been practiced for more than two decades (Han and Collin, 2005).

Pile-supported embankments with geogrid reinforcement have been widely used in road engineering due to their economy and effectiveness (Lai et al., 2014). Load is transferred by arching action from geogrid to the piles. Nevertheless, many issues still remain in the application of such embankments; for example, excessive post-construction settlement and local instability (Zheng et al., 2009, Zhang et al., 2013) affect the service life and maintenance costs of roadways. For embankment constructed on highly compressible soils reinforced with

geosynthetics (GRPS – Geosynthetic Reinforced Pile Supported embankment), these issues are more severe, as most of the times load mobilization by soil arching effect remains unsuccessful, which has been proven to be a key factor for load transfer in embankments.

2.2.7.9.1 Load Transfer Mechanism

The interactions among pile or pile caps, foundation soil, fill material, and geosynthetic can be schematically described as shown in Figure 2.19. The embankment fill mass between pile-caps has a tendency to move downward under the influence of fill weight (W1), which occurs when the foundation is composed of soft soil. Part of this downward movement is restrained by shear resistance, τ, from the fill material above the pile caps. Pressure acting on the geosynthetic is somewhat reduced by the shear resistance; however, it increases the load applied on the pile caps. The load transfer mechanism from the fill mass on to the pile caps is known as “Soil Arching Effects” which was termed by Terzaghi (1943).

According to McNulty (1965), arching is the ability of the material to transfer load from one point to another in response to relative displacement between the locations. When reinforced with geosynthetics in combination to piles, the geosynthetic platform enhances the load transfer from the fill soil to the piles, which reduces the total and differential settlements. This reduction in differential settlement at the base of the structure is reflected at the surface. As observed by Russell and Pierpoint (1997), Han and Wayne (2000), Han and Gabr (2002), installation of geosynthetic reinforcement increases the load transfer efficiency and reduces the area replacement ratio of the columns (piles). Test conducted by Terzaghi (1936) and McNulty (1965) affirmed that the shear stress induced by soil arching increases with the displacement and fill thickness above the yielding soil portion (Han and Collin, 2005).

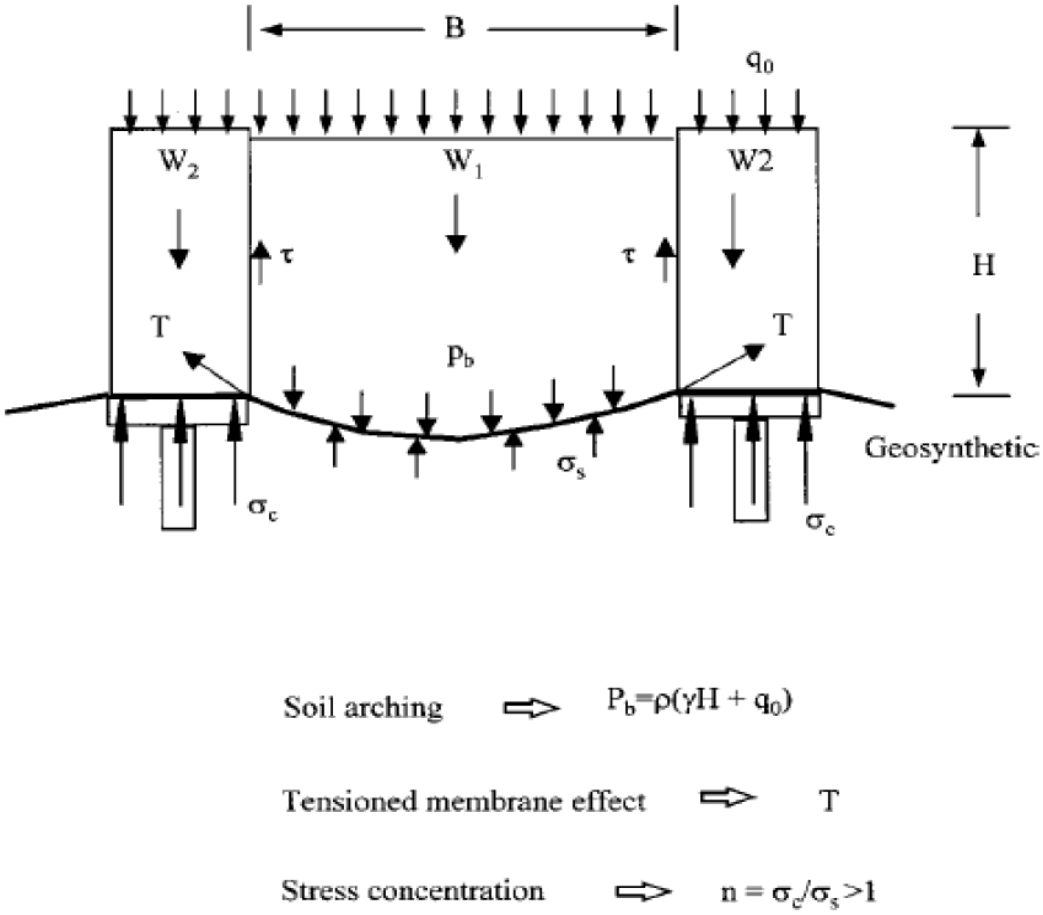

Figure 2. 19 Load transfer mechanism of geosynthetic reinforced pile-supported earth platforms (Reinaldo and Shao, 2003).

The degree of soil arching can be defined as follows:

$$\rho = \frac{p_b}{\gamma H + q_0} \tag{2.8}$$

where,

ρ = soil arching ratio (ρ = 0 represents the complete soil arching and ρ = 1 represents no arching)

p_b = applied pressure on top of the trap door (as shown in Figure 2.19)

γ = unit weight of embankment

H = height of the embankment

q_0 = uniform surcharge on the embankment

The pile caps are designed to cover an adequate plan area of the supported structure. Prime objective of the pile cap is to optimize the arching in the fill and thereby reducing the differential settlement. Circular pile caps are able to sustain more concentrated load than rectangular ones, which can be illustrated by the concept of distribution of earth pressure over the pile caps. Geosynthetic reinforcement further reduces the settlement and improves the load transfer efficiency of the whole system in addition to the ability to increase pile spacing.

In short, load transfer depends on the soil arching, tensioned member (or) stiffened platform effects and stress concentration (due to different stiffness between pile and soil). Effectiveness of each component depends on the type of fill materials, number of layers of reinforcement, modulus of pile and stiffness properties.

2.2.7.9.2 Numerical Study on Pile Supported Embankment

To understand the load transfer mechanism and settlement behavior of pile supported embankment, a number of numerical studies have been performed. A numerical study was conducted by Lai et al. (2014) to understand the difference between load transfer mechanisms of pile supported embankment with and without the geogrid reinforcement. Soil arching is the key mechanism which ensures the load transfer from the fill to the pile caps. Therefore, to understand the evolution of soil arching with increasing surcharge, a series of numerical simulations were conducted with the particle flow code PFC_2D. In the first stage, soil arching is developed and the effect is strengthened gradually. Soil arching is fully mobilized during the second stage and experiences a ‘‘forming-failure reforming’’ process with increasing

surcharge. So far, all these numerical models have been developed based on the laboratory model tests results.

Jenck et al. (2005) reported that, Ground improvement through vertical rigid piles is an interesting alternative method for foundations for roadways, railways, industrial pavements, waste water treatment plants and storage tanks constructed over soft soils. The aim of this technique is to ensure normal function of the structure and its durability by improving the soft soil layer that would reduce the probability of excess settlement. Load applied from the structure is transferred to a more rigid layer through a granular mat, built on the soft soil layer, reinforced by a vertical rigid pile grid. Loads from the structures transferring to the pile through the load transfer mat by arching action is shown in Figure 2.20. Main difference between the conventional techniques and this technique is that the piles are not directly connected with the structures. Lai et al. (2014) developed a DEM model based on the laboratory set up proposed by Jenck et al. (2009), as shown in Figure 2.21.

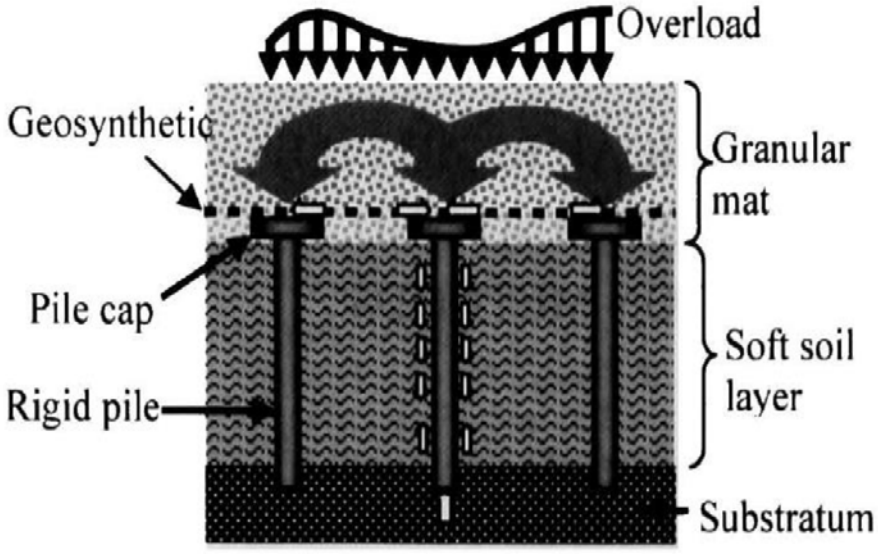

Figure 2. 20 Rigid pile improvement Principles (Jenck et al., 2005).

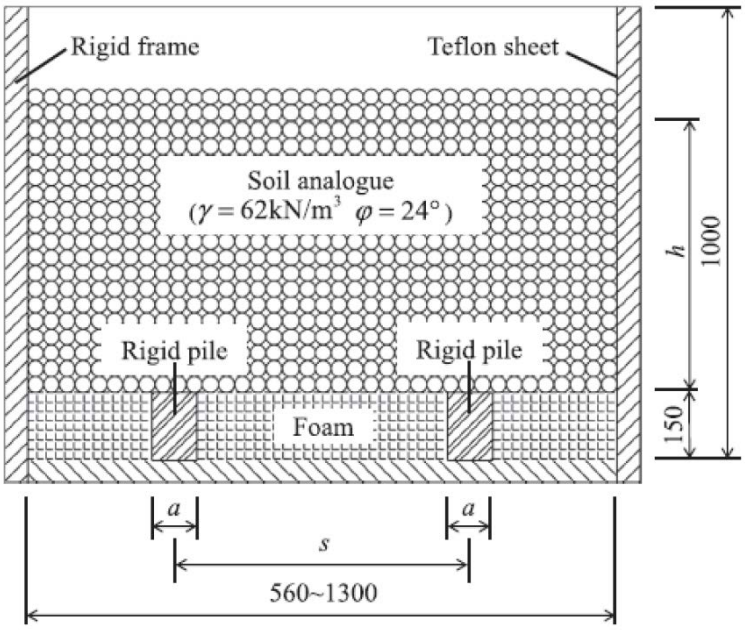

Figure 2. 21 Layout of the model test set up (Lai et al., 2014).

Based on the study conducted by Lai et al. (2014), the variation curves of efficacy versus surcharge for a particular case is shown in Figure 2.22. The variation of efficacy in this case can be divided into three stages:

a) Stage_1 (690 kPa): In this stage, the efficacy increases gradually. This indicates improved soil arching effect in the embankment and increase in the load sharing ratio of the piles.
b) Stage_2 (90 – 300 kPa): In this stage, the variation curve of efficacy shows a ‘‘step-shaped’’ decreasing trend with a few platforms. It is speculated that the stable soil arching in the embankment vanishes at the end of each platform. With further increase in surcharge, a new and stable soil arching is formed again. In other words, the soil arching in Stage_2 experiences a process of ‘‘forming failure–reforming’’ as the surcharge increases.

c) Stage_3 (≥ 300 kPa): In this stage, the efficacy decreases gradually. This indicates that once the surcharge exceeds a certain value, the embankment is unable to form a new stable soil arching.

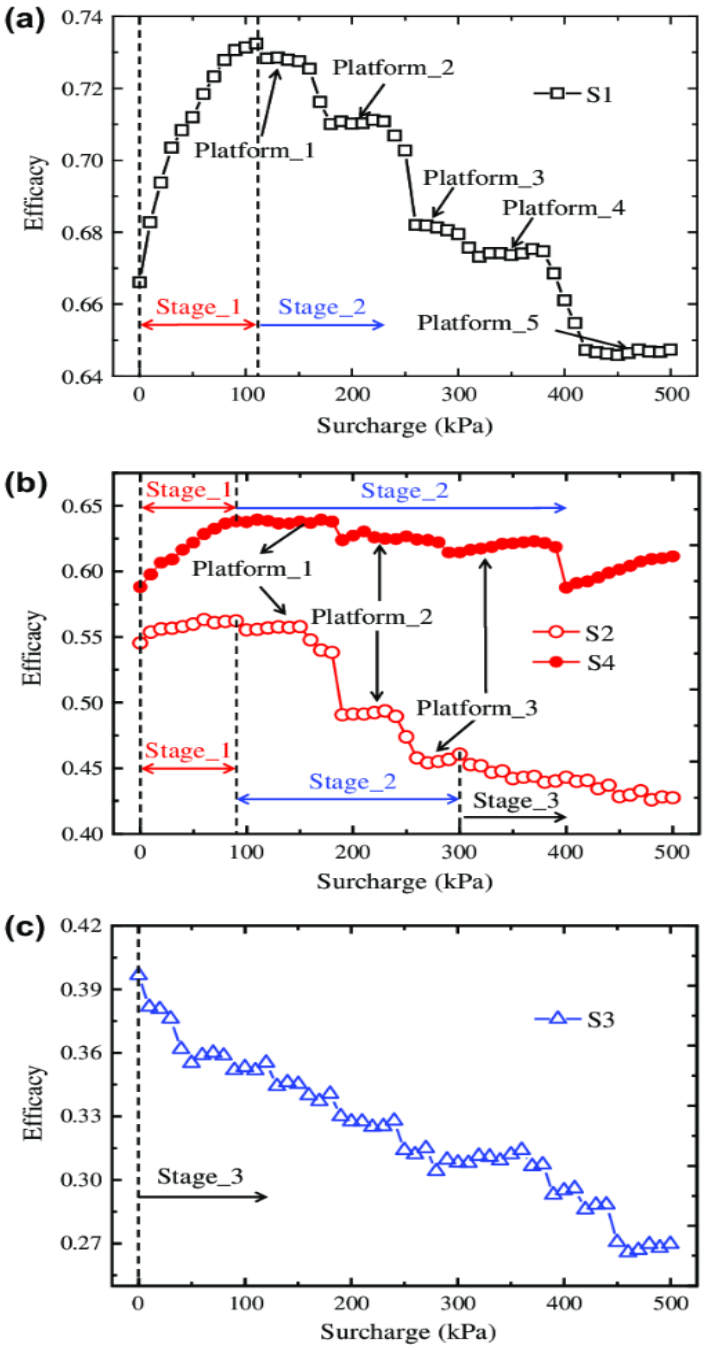

Figure 2. 22 Variation of efficacy vs surcharge (Lai et al., 2014).

To transfer surcharge loads through soil arching to the piles and to minimize deflection of the soil between pile, it is required to have a certain coverage area for the piles; i.e. piles need to be closely spaced and/or to have a larger pile caps. Based on the performance investigation of conventional pile-supported embankments, Rathmayer 1975 recommended the design criteria shown in Figure 2.23.

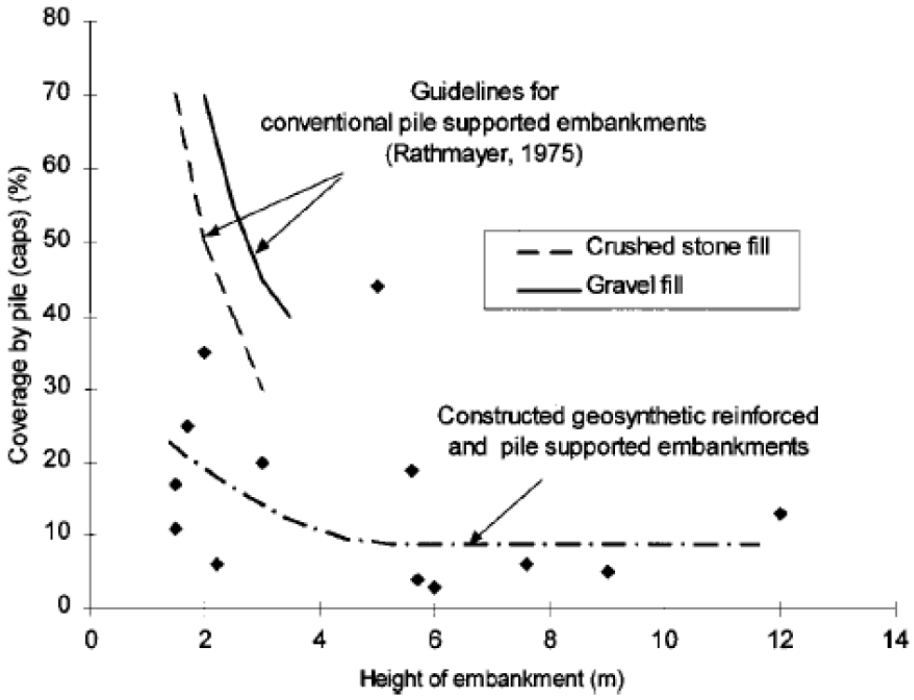

Figure 2. 23 Coverage by pile for constructed pile supported embankment (Han and Gabr, 2002).

Higher coverage area of the piles ensures higher load transfer through the piles. Use of geosynthetics can improve this scenario. According to Han and Gabr (2002), Geosynthetics are used to transfer the load from the structure to the vertical piles for (a) bridge approach slab (Reid et al., 1993), (b) subgrade improvement (Tsukada et al., 1993), (c) storage tank (ASCE Geo institute, 1997) (d) segmental retaining wall (Alzamora et al, 2000), (e) widening of existing road, as shown in Figure 2.24.

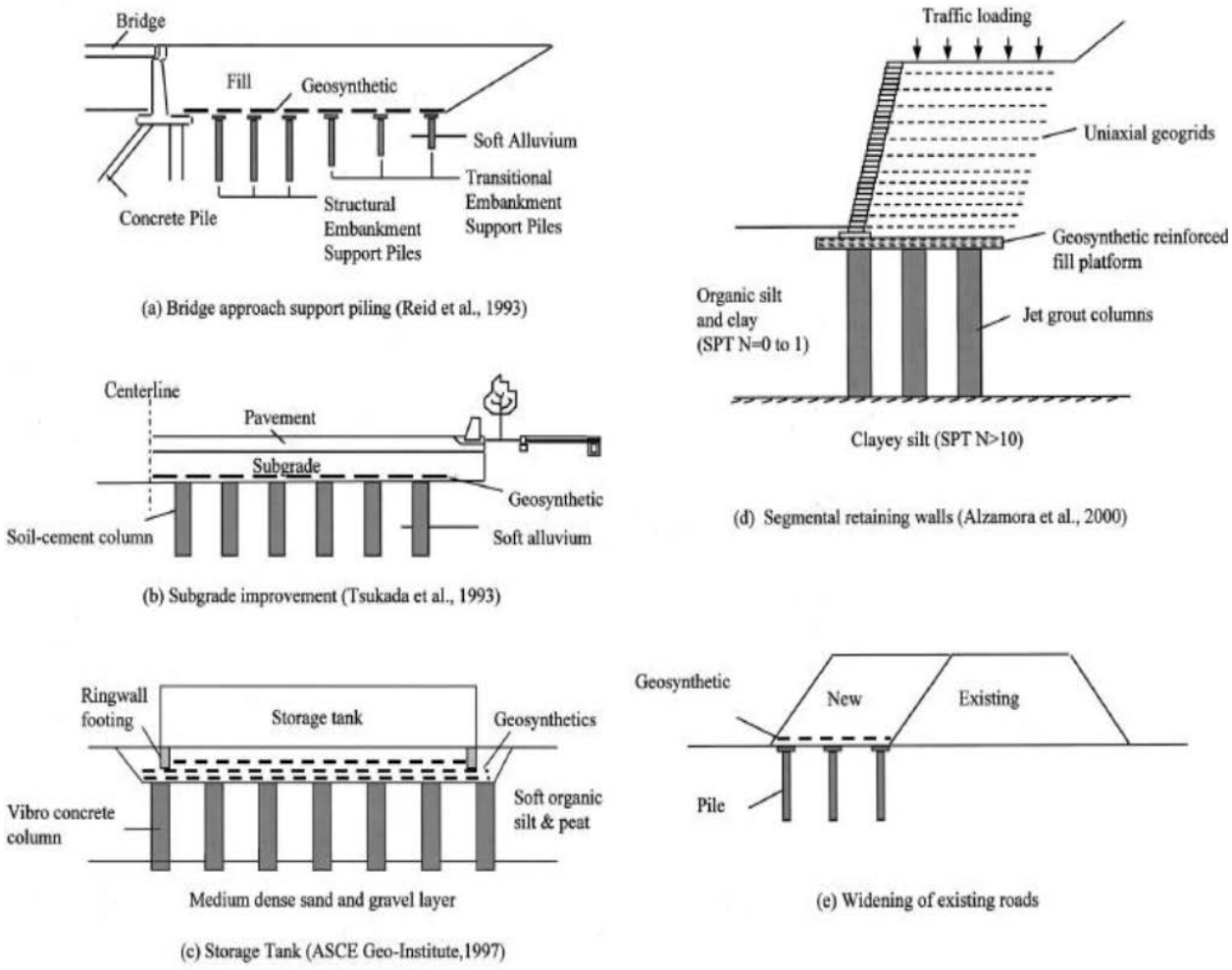

Figure 2. 24 Application of geosynthetic-reinforced and pile-supported platforms (Han and Gabr, 2002).

Han and Gabr (2002) performed a numerical modeling to evaluate the performance of fill height and pile modulus on maximum settlement. Based on the model, the impact of fill height and effect of pile modulus is presented in Figure 2.25a & 2.25b. For both cases, it was observed that, unreinforced embankment has larger settlement compared to the reinforced one.

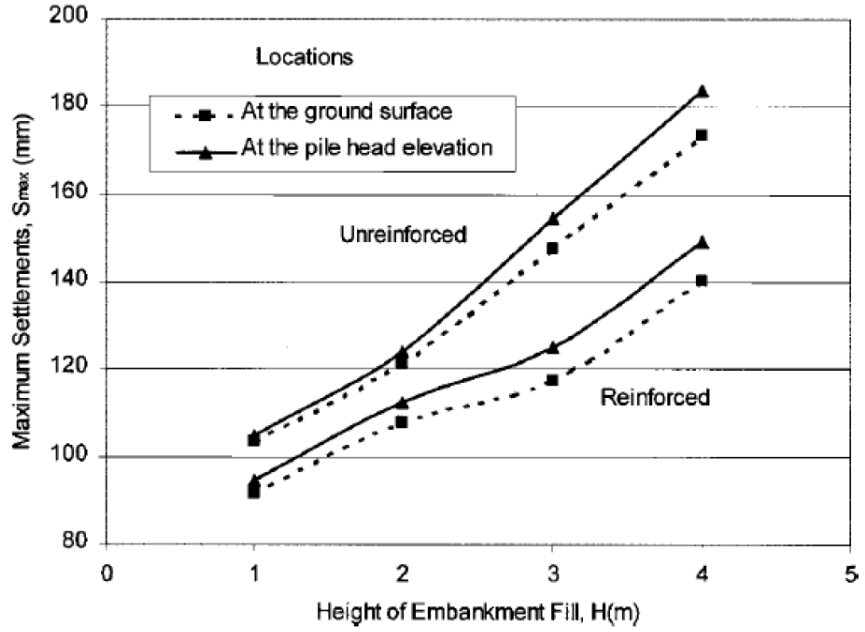

(a)

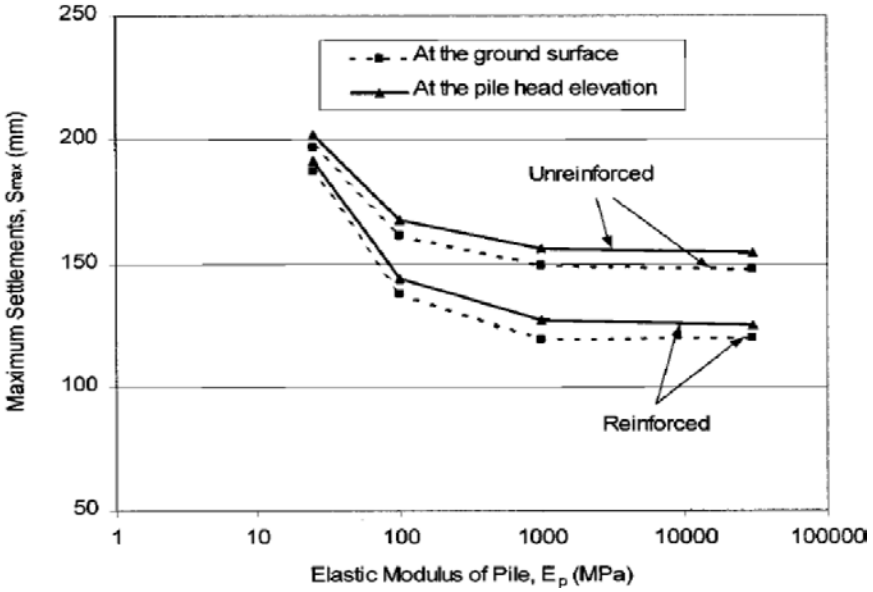

(b)

Figure 2. 25 Effect of embankment height (a) and pile elastic modulus (b) on maximum settlement of pile supported embankment on soft soil (Han and Gabr, 2002).

Most of the cases, geogrid is used as the load transferring element. Tension in the geogrid will decrease if the geogrid gains support from the compressible soil. On the other hand, if the geogrid does not gain any support from the compressible soil (similar to a geogrid

over a void), then the tension in the geogrid remains constant between the pile caps (Figure 2.26).

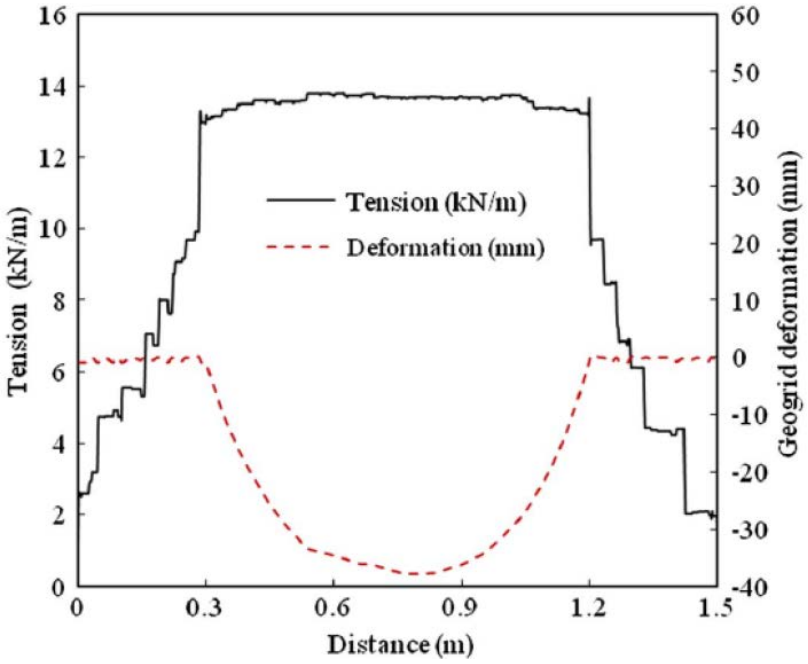

Figure 2. 26 Deformation and tension force on geogrid (Han et al., 2011).

2.2.7.9.3 Field Test on Pile Supported Embankment

Pile supported embankments provide an economic and effective solution for embankment constructed over soft ground; which also ensures rapid construction, small lateral deformation, and easily controlled settlements (Chen et al, 2009). A few case studies on pile supported embankment is discussed in this sub-section.

Field Test on Piled Embankment with Firm Substratum in TJ Highway

TJ highway is located in the southeast of Zhejiang province in China. The test location had a total length of the highway of 37.66 miles (60.6 km) and an embankment with a maximum height of 31.8 ft. (9.7 m) (Figure 2.27). The test site consists of soft soils (low plastic

clay, with high compressibility) with thickness varying from 16.40 to 65.62 ft. (5 to 20 m). Pre-stressed tube piles with square pile caps were used as the reinforcement for the soft ground. A test embankment of 413.40 ft. (126 m) long section was chosen in order to better understand the settlements and load share ratios of the pile-supported embankments on soft soils.

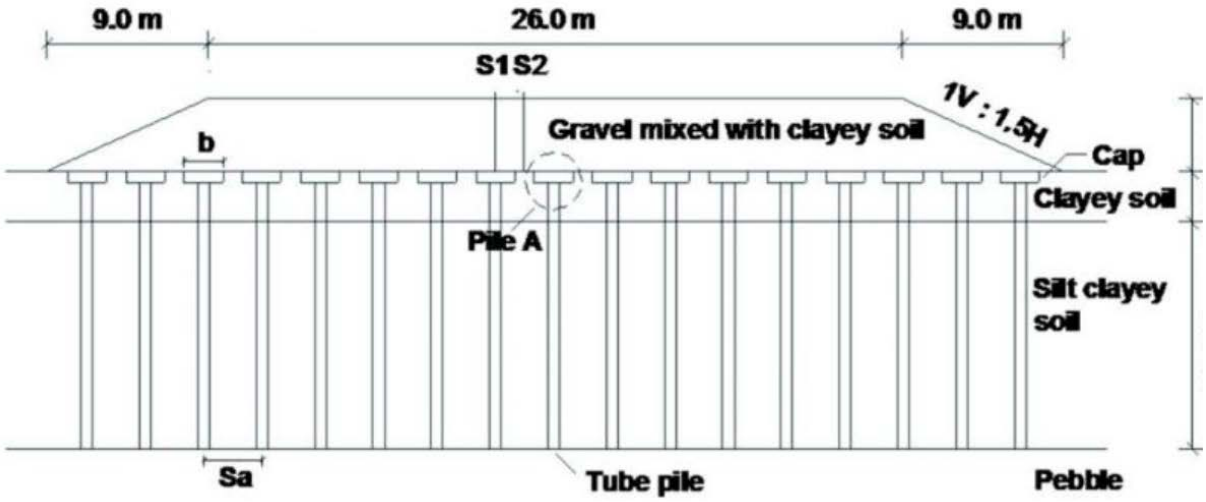

Figure 2. 27 Typical cross-section of the pile supported embankment (Chen et al., 2009).

Settlement data of the test section monitored up to 320 days is presented in Figure 2.28a. In this project earth pressure cells were used to measure the pressure acting on the soil and on the pile caps. From the results presented in Figure 2.28b, it is observed that, the earth pressures on the pile caps increased sharply with the embankment height. However, the earth pressures reached its peak within around 25–60 days, then decreased to relative steadily values in about 80 days. The decrease of the earth pressures on the soil is due to consolidation and the soil arching developed in the fill (Chen et al., 2009).

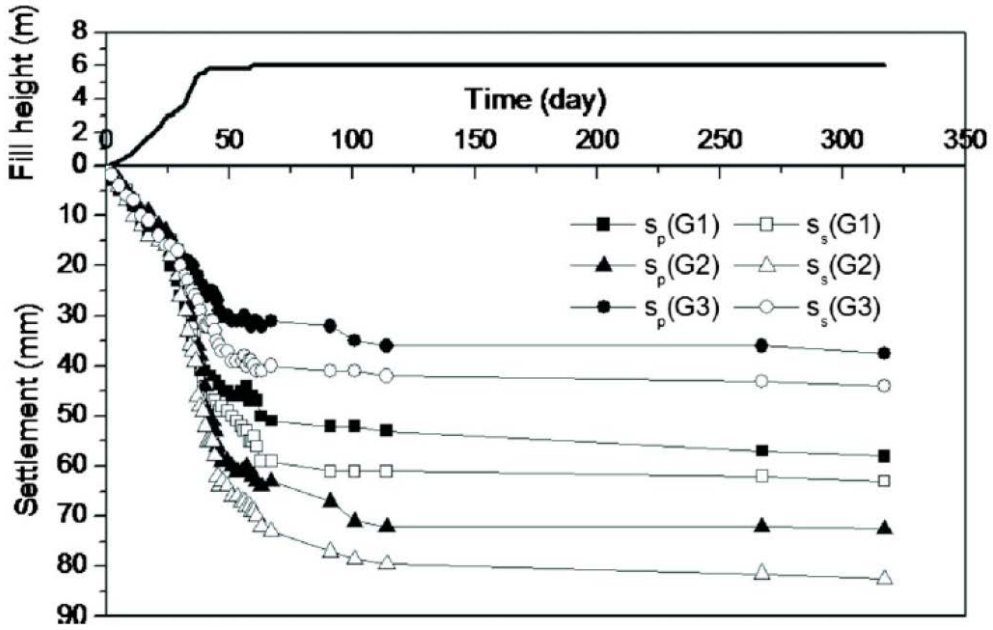

(a)

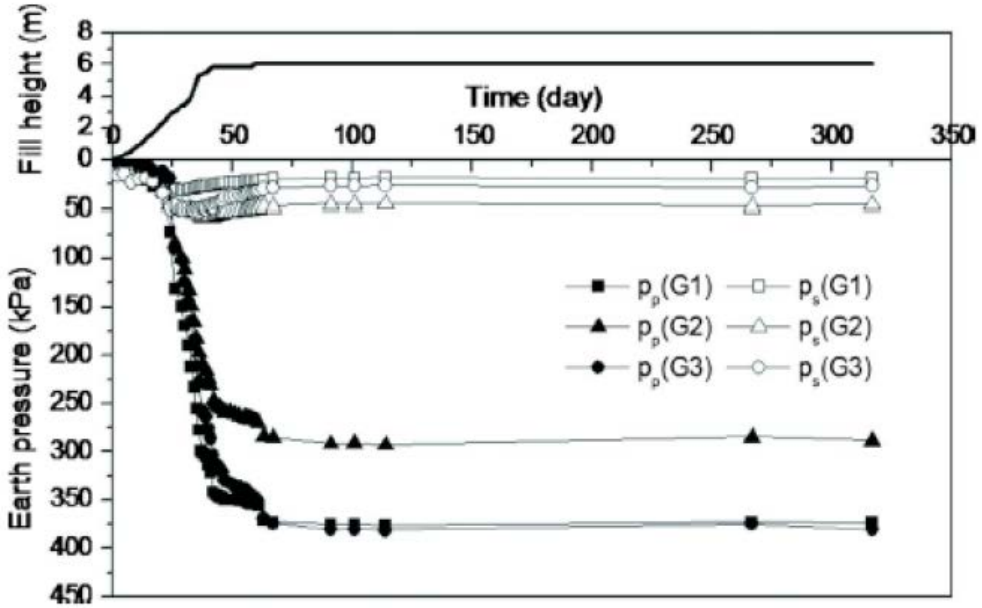

(b)

Figure 2. 28 Results for pile supported embankment test section in TJ highway; (a) settlement; (b) measured earth pressure (Chen et al., 2009).

Pile supported Embankment in Paris (Briancon and Simon, 2011)

The site discussed in this study is located 12.43 miles (20 km) northeast of Paris where the thickness of the soft soil layer was found to be between 26.25 and 34.45 ft. (8 and 10.5 m). The site soil was soft which consisted of clay and sandy clay of low plasticity and the depth of ground water was at 2 ft. Compressibility of the soil was reported to be between 1×10^{-6} m/s to 3×10^{-6} m/s. A preexisting clayey fill less than 6.56 ft. (2 m) thick, covered the soft soil. The selected test area of 170.6 ft. by 75.5 ft. (52 by 23 m) was divided into four instrumented sections (1R, 2R, 3R, and 4R), as shown in Figure 2.29a. Three sections were reinforced with rigid piles (2R, 3R, and 4R) and one unreinforced section (1R) was included for reference. Height of the embankment test sections was 16.40 ft. (5 m) with a length of 170.60 ft. (52 m) and a crown width of 26.25 ft. (8 m). The side slope was 2V to 1H (Figure 2.29b). More than 70 sensors were installed in the load-transfer platform, soft soil, and concrete piles. Pore-water pressure sensors (P) were used to measure the interstitial pressure in the soft soil, Earth pressure cells (E) to measure the load transfer under the embankment, Magnetic probe extensometer (M) was installed to measure the settlement of the soft soil, pressure transmitters (T) to measure the differential settlement between soil and pile at the pile head level. Earth pressure measured on pile tips as well as on the soil within the reinforced sections are shown in Figure 2.30. If the embankment is constructed without the piles, pressure on the soil would be 92.5 kPa in section 2R, 94.4 kPa in section 3R, and 94.8 kPa in section 4R. If the entire embankment were supported by just the piles, the pressure at the top of the piles would be 3,274 kPa in section 2R, 3,342 kPa in section 3R, and 3,354 kPa in section 4R. The comparison between the reinforced section (2R) and control section (1R) is presented in Figure 2.31. The results showed that the settlement was more than twice in control section as compared to the reinforced one.

Based on the results, the authors concluded that, pile supported embankment performs significantly better compared to the one without piles.

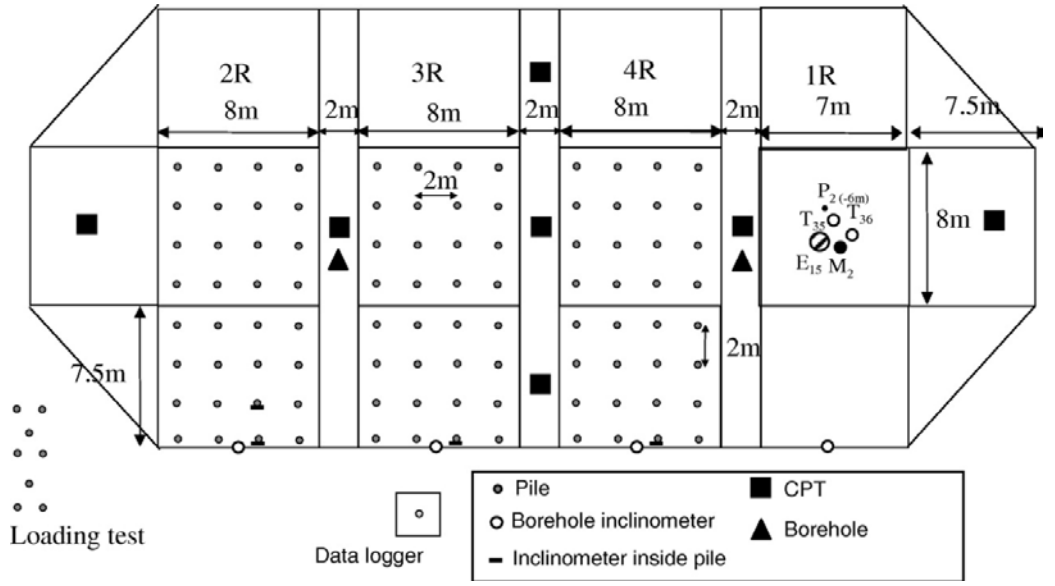

(a)

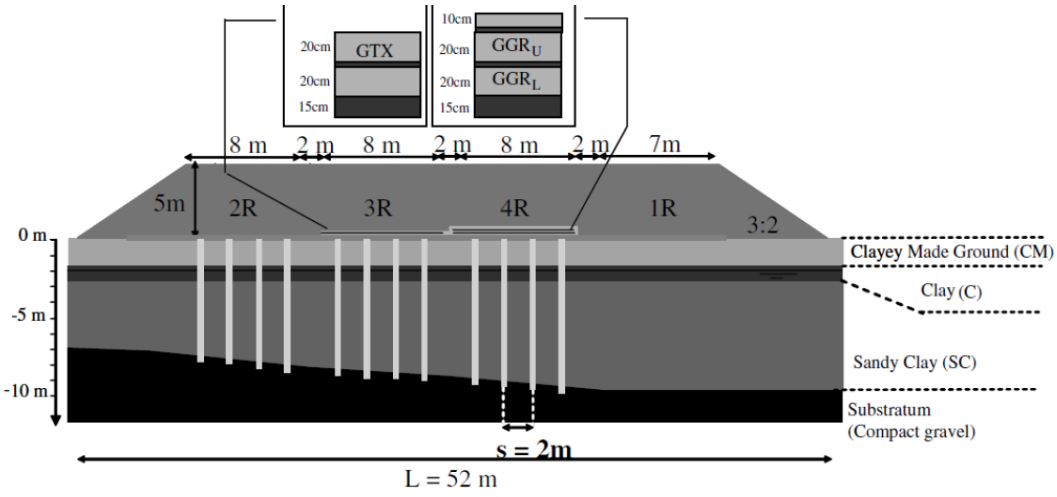

(b)

Figure 2. 29 (a) Top view of the embankment (instrumentation of four test sections); (b) Typical site cross-section and geometric characteristics (Briancon and Simon, 2011).

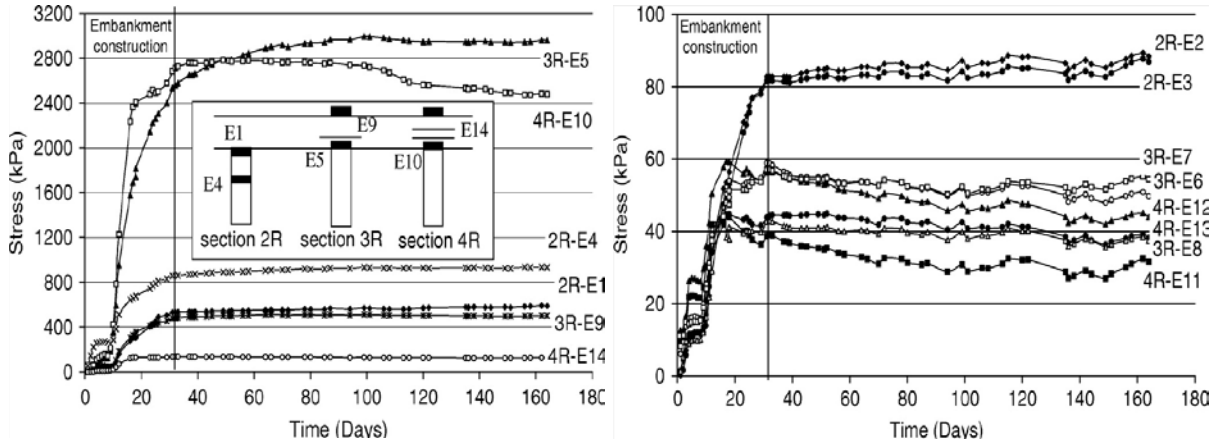

(a) (b)

Figure 2. 30 Pressure on concrete piles (a) and (b) soils within the reinforced section 2R, 3R and 4R (Briancon and Simon, 2011).

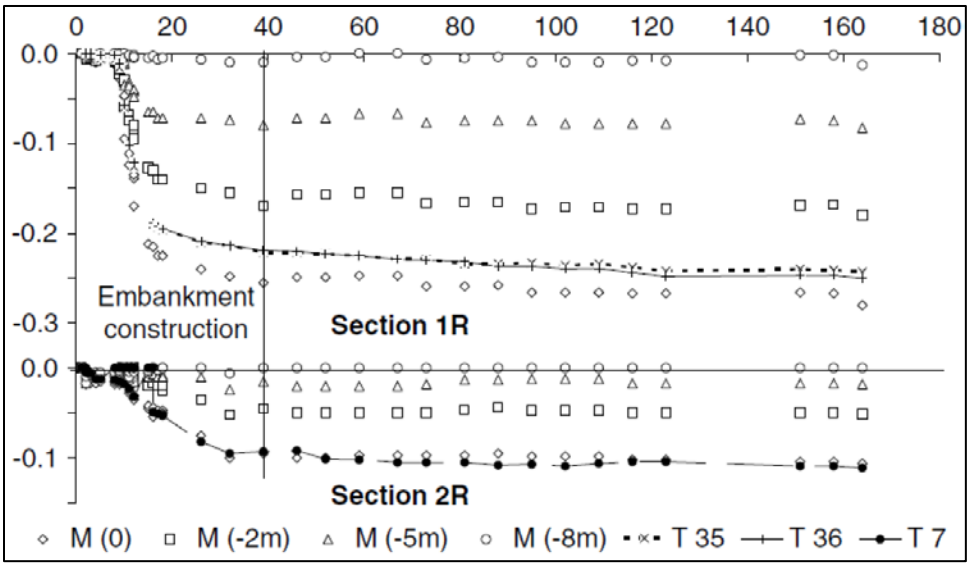

Figure 2. 31 Comparison of settlement between unreinforced (1R) and reinforced section (2R) (Briancon and Simon, 2011).

2.2.7.9.4 Beneficial Effect of Different Pile Supported Embankments

Numerous pile supported embankments have been reported over the time with or without geosynthetic reinforcement. According to Reid and Buchanan (1984), in past the use of piles in combination to geosynthetics helped to prevent differential settlement at the

approach embankment constructed over soft soil and a bridge abutment supported over a system of piles.

To support the embankment over a soft clay deposit for an airport project in Bangkok, Thailand, a chemico-lime pile instead of concrete pile was used which helped reducing the surficial settlement to about more than 50 percent (Hossain and Rao, 2006). Figure 2.32 illustrates the embankment supported by chemico-piles.

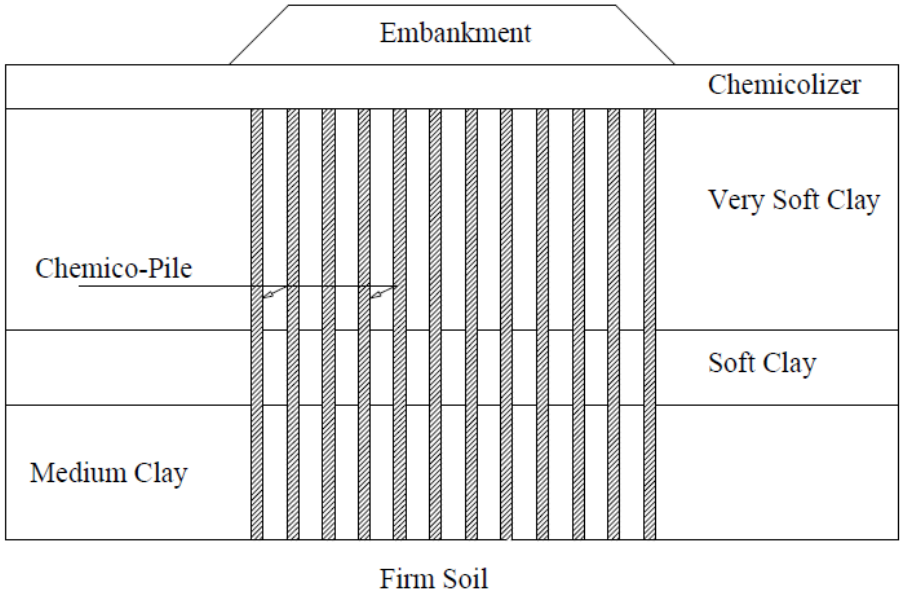

Figure 2. 32 Embankment with chemico-pile (Hossain and Rao, 2006).

Deep soil-cement lime mixed columns in place of conventional concrete piles are also used to support embankment constructed over soft soil. The use of soil-cement mixed columns in combination with a layer of geogrid under an embankment (pavement section) with a coverage ratio of 11% was found to be satisfactory in comparison to 50 – 70% coverage ratio of pile caps according to Han (1975).

Han and Gabr (2002) showed that the technique of using geosynthetic-reinforced earth platform in combination with vibro-concrete under a storage tank can minimize total as well as differential settlement in a soft soil terrain. Alzamora et al. (2000) reported that the technique of using geosynthetics is most effective in supporting segmental retaining wall. It is also commonly used to prevent the differential settlement case of widening the existing road embankment over soft soil where settlement has seized over a period of time.

However, all these techniques, described in subsection 2.2.7, for improving bearing capacity of weak foundation soil, can be expensive and sometimes really time consuming; therefore, development of a new, innovative, sustainable, and cost effective technique for bearing capacity improvement is necessary. One such method could be the use of recycled plastic pins (RPP).

2.3 Improvement of Sliding Resistance of MSE Wall Base

2.3.1 Background

Mechanically Stabilized Earth (MSE) walls are constructed by reinforcing the soil to support their own weight. There are widespread use of MSE wall; for example, to support bridges, sound walls, residential as well as commercial buildings, roadways, and railroads. Because of the rapid construction, cost-effectiveness, and better performance under seismic loading compared to other types of wall, mechanically stabilized earth (MSE) walls are one of the most preferred wall types (Christopher et al. 2005). In the United States highway system, more than 60,000 MSE walls over 35 ft. are in service (Alzamore and Barrows, 2007). First ever MSE wall in US was constructed in California (1972) and approximately 9,000,000 ft^2 (850,000 m^2) were added annually into the U.S. transportation system, which accounted for

more than fifty percent of all types of retaining wall usage (Berg et al. 2009). Because of their reliability, constructability and cost effectiveness, MSE retaining walls have been used in many federal, state and private projects over the last 30 years (Mahmood, 2009). The Texas Department of Transportation (TxDOT) is one of the leading transportation organizations in the application of MSE walls in United States. During August, 2010 to September 2011, 72% of the retaining walls were built as MSE wall (Table 2.4, Delphia, 2011).

Table 2. 4 Overall wall usage by TxDOT between August 2010 and September 2011.

Wall Type	**Area (ft^2)**	**(%)**
MSE	3,196,417	72
Concrete block (no r/f)	47,791	1
Cantilever drilled shaft	72,286	2
Soil Nailed	146,793	3
Rock Nailed	197,216	5
Tied-back	161,827	4
Spread footing	505,019	12
Other	22,389	1

Source: Delphia, 2011

The MSE walls constructed by TxDOT comprised of more than 20 percent of the MSE walls constructed annually in the U.S. transportation system (Aubeny et al., 2014). Apart from retaining soil or rock mass, MSE walls have been utilized to support heavily loaded structures, for example; bridges and towers (Adams et. al. 2011). However, in many cases lateral movement of MSE retaining structures have been observed and reported by different agencies

due to excessive lateral load and lack of lateral support or shear resistance at the base of the wall. Hence, remedial measure of this scenario is a must to avoid catastrophic failure of the structures supported by the wall.

2.3.2 Historical Development of MSE Wall

Space constraint leads to the use of retaining structures, which has become an essential element of every highway design projects. Retaining structures can be used for slope stabilization to minimize right-of-way for embankments. For many years, retaining structures were almost exclusively made of reinforced concrete and were designed as gravity or cantilever walls which are essentially rigid structures and cannot accommodate significant differential settlements unless founded on deep foundations (Berg et al., 2009). In addition, cost of reinforced concrete retaining wall increases rapidly with the type of retained soil and poor sub soil condition. According to Berg et al. 2009, Mechanically Stabilized Earth Walls (MSEWs) and Reinforced Soil Slopes (RSSs) are cost-effective soil-retaining structures that can tolerate much higher settlements compared to conventional reinforced concrete walls.

Since prehistoric times, inclusion of different reinforcing materials have been used to improve soil. In the earliest human history, people used straws, branches and sticks to reinforce mud dwellings and to improve the quality of adobe bricks. French settlers used sticks to reinforce mud dikes during the time of 17^{th} and 18^{th} centuries, along the Bay of Fundy in Canada. China have been using man-made soil reinforcement which include dikes of earth and tree branches for more than 1,000 years (e.g., western portion of the Great Wall). People along the Mississippi River also adopted the similar approach during 1880s. In England, wooden pegs were used for erosion and landslide control. Universally, bamboo or wire mesh was used

for the erosion control of the revetment. Live plant roots can also be used as reinforcing element for soil. In the early 1960s, the French architect and engineer Henri Vidal developed the modern methods of soil reinforcement for retaining wall construction. He termed the structure as Terre Armee (reinforced earth). His research led to the modern reinforced earth system that is known as MSE wall. In United States, the first wall to use this technology was built in 1972 on California State Highway 39, northeast of Los Angeles (Berg et. al., 2009). Since 1970's, due to economic and aesthetic benefits, use of MSE wall increased drastically all over the world. In 1970's, retaining structures using welded wire grids were introduced; while walls reinforced with geosynthetics were introduced in 1980's. According to Leshchinsky and Han (2004), use of geosynthetic reinforced wall increased dramatically in the 1990's. In current world, MSE wall is the first choice in most fill situations because of its reliability, cost-effectiveness and ease of construction.

2.3.3 Advantage of MSE Wall

Over the past 20 years, MSE walls have replaced the traditional concrete retaining wall, due to having numerous advantages compared to conventional reinforced concrete and concrete gravity retaining walls. The greatest advantage of MSE walls are their capability and flexibility to tolerate differential settlement due to poor subgrade condition. This eliminates the cost of foundation improvements, for example piles or pile caps to support conventional structures or remove and replace existing soil, which results in a cost savings of more than 50 percent (Berg et. al., 2009). In addition, due to its flexibility, observations in the seismically active zones showed that MSE walls have much higher resistance to seismic loading compared to concrete retaining structures. Other advantages of MSE walls are:

- Construction procedure is simple, rapid and do not require heavy or large equipment for construction.
- Experienced craftsmen with special skill for construction is not required.
- Requirement of site preparation is much lower compared to other alternatives.
- Construction operation requires less space in front of structure and can be constructed in areas where a concrete wall is almost impossible to construct.
- Can hold steep to vertical slopes which reduce the need for right-of way acquisition.
- Do not require rigid and unyielding foundation as the reinforced structures can tolerate deformation.
- MSE walls can be utilized as tall structures, which are technically feasible to heights more than 100 ft. (30 m).
- It can be used as a temporary structure in highway reconstruction projects as a cost effective solution for building temporary highway detours.
- This structure, when used with soil nailing method for excavation stabilization, offers a cost effective advantage; as the structural elements (nails and shotcrete facing) are comparatively inexpensive over conventional systems such as ground anchors and bracing systems (Christopher et. al., 1990).

For aesthetic considerations, various shapes and sizes of precast concrete facing elements can be made. Also to blend in to the environment, masonry units, timber and gabions can be used as facing of the wall.

2.3.4 Components of MSE Wall

MSE retaining (Figure 2.33) structures are cost-effective alternatives for most applications compared to reinforced concrete or gravity type walls that have traditionally been used to retain soil. The application include bridge abutments and wing walls, areas where the right-of way is restricted such that an embankment or excavation with stable side slopes cannot be constructed. They are especially suited for economical construction in steep-sided terrain, in ground subject to slope instability, or in areas with poor foundation soil. There are four major structural components while constructing MSE walls: i) Reinforcement, ii) wall facing, iii) reinforced backfill soil and iv) retained backfill. Reinforcements are used to strengthen soil at the back of the MSE wall. They are placed horizontally between layers of predetermined height as the backfill is placed in the reinforced zone of the wall. Wall facing is the component in the reinforced soil system, the purpose of which is to prevent soil from raveling out between the rows of reinforcements. Some of the common materials used for facing are precast concrete panels, dry cast modular blocks, gabions, shotcrete, welded wire mesh, metal sheets and plates, wood lagging and panels, wrapped sheets of geosynthetics etc. In the stability of the structure the facing plays a minor role and keep the wall straight. Reinforced backfill is the reinforced soil immediately at the back of the wall facing in which reinforcements are placed. With the placement of backfill soil, additional blocks/facing are laid. High quality backfill having good durability, drainage, and better soil–reinforcement interaction is required for MSE wall. This can be acquired from well graded granular material. In cases of MSE wall system that depends on friction between soil and reinforcing elements requirements are specified for backfill material of high frictional characteristics. Even in the systems of retaining wall with passive pressure on reinforcing elements, the quality of backfill is still critical (FHWA, 1995).

Retained backfill is the last component of MSE wall system. It is the fill material located between reinforced soil and native slope soil.

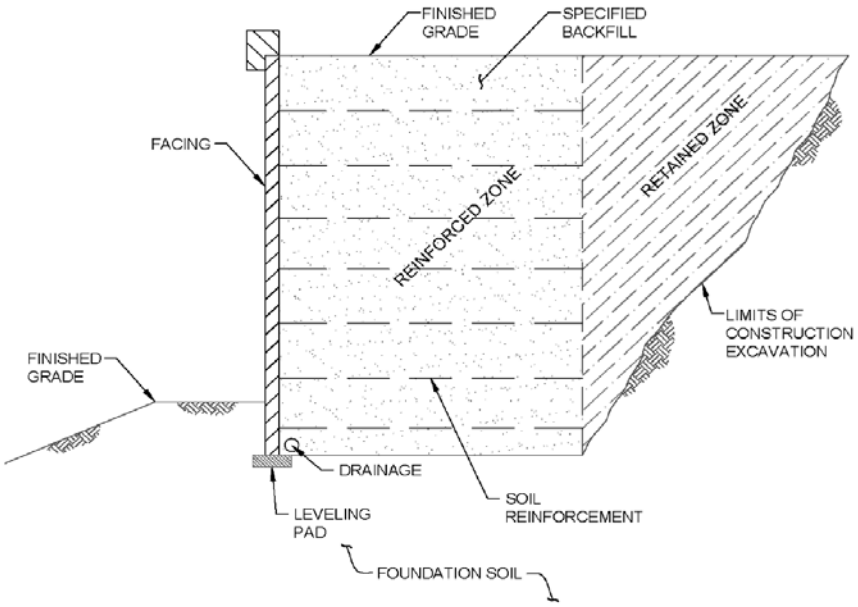

Figure 2. 33 Typical MSE Wall Section (FHWA, 1995).

2.3.5 Construction of MSE Wall System

MSE wall construction process can be divided into two sections based on the type of facing used; 1) MSE wall with precast panel facings and 2) MSE wall with flexible facings.

2.3.5.1 MSE Wall with Precast Panel Facing

MSE wall systems with precast panel facings are usually constructed following the sequence as follows: (A complete sequencing is presented in the Figure 2.34)

Preparation of subgrade:

Removal of all organic materials, vegetation, slide debris and other unstable materials from the area to be occupied by the retaining structure followed by compaction of subgrade soil to prepare a level ground. In unstable foundation areas, ground improvement is required.

Placement of a leveling pad for the construction of the facing elements:

The reason for the placement of a leveling pad is to provide a guide for facing panel construction; however, it does not have any structural foundation support. It is generally a concrete pad without reinforcement of only 1 ft. (300 mm) wide and 6 inches (150 mm) thick. A wider pad is required for the construction of Modular Block Wall (MBW).

Construction of first row of facing panels on the leveling pad:

Depending on the type of facing used, the first row of the panel might be of full or half-height. To maintain the stability and alignment, only the first tier of the panels need to be braced; while the subsequent rows are simply wedged and clamped to adjacent panels. However, full sized blocks are used throughout the height of wall without shoring for the construction with MBW units. Construction of facing panel and soil backfill should be done simultaneously.

Placement and compaction of reinforced fill on the subgrade to the level of the first layer of reinforcement:

It is important to ensure a consistent placement and compaction of fill material for good performance. Compaction should be maintained within the specific range of moisture content and at a specific density of 95 to 100 percent of AASHTO T-99 maximum density. It is recommended to perform the compaction in the dry side of optimum moisture content. Wall fill thickness must be controlled according to specification. Distribution of reinforcing elements and the height of individual lifts should not exceed 12 inches (300 mm). The reinforced fill should be dumped at the rear and the middle of the reinforcement and carefully

bladed towards the facing. Placement and compaction of the retained soil behind the reinforced volume should be done simultaneously.

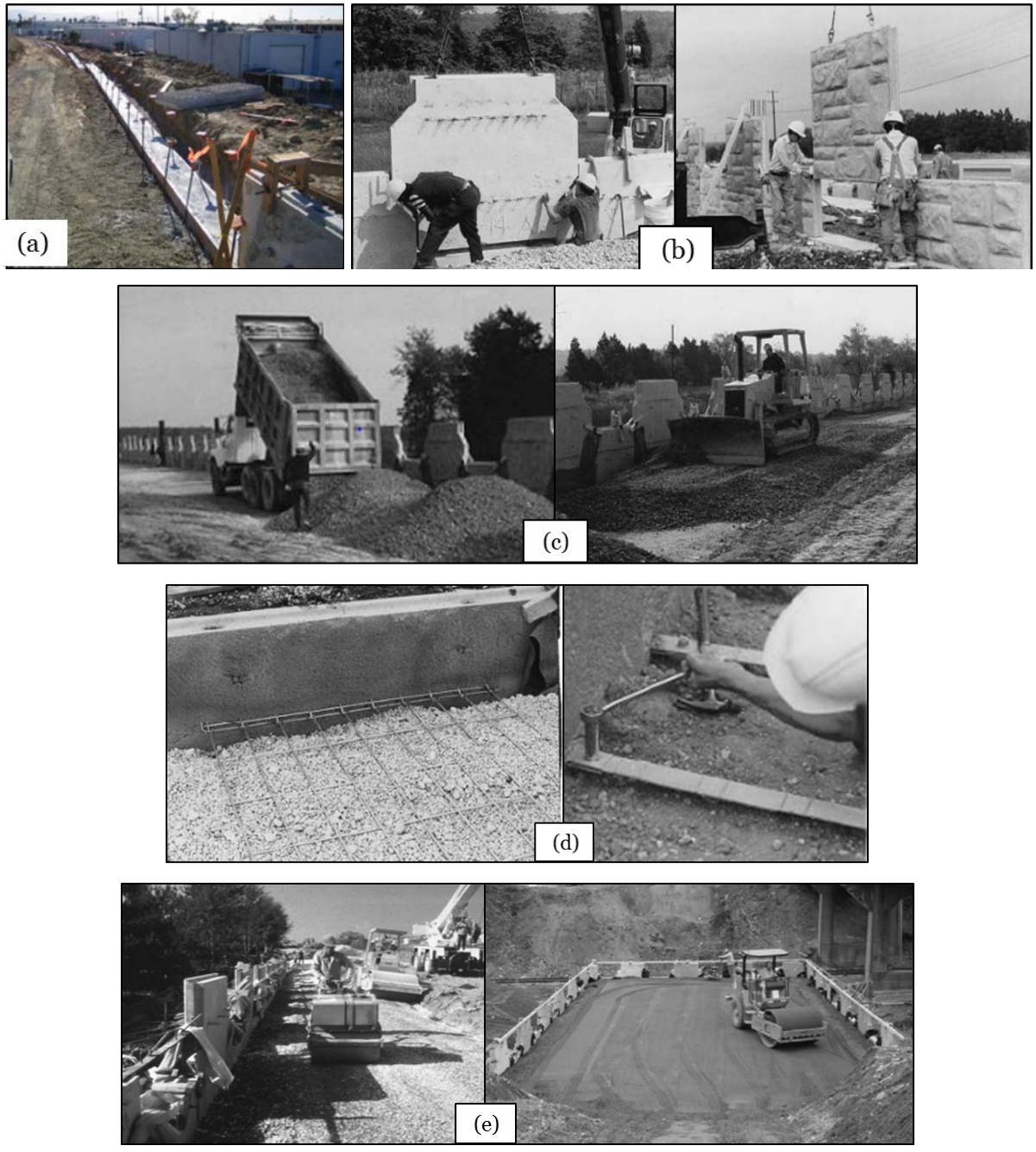

Figure 2. 34 Construction sequence of MSE wall with precast panel facing; (a) Leveling pad (Passe, 2000); (b) Precast panels erection; (c) Fill material spreading; (d) Placement and connection of reinforcement; (e) Compaction of reinforced fill material (Berg, 2009).

Placement of the first layer of reinforcements on the wall fill:

Once the compacted fill reaches the level of connection of the panel, the reinforcements are placed and connected to the facing panels. Generally, the reinforcements are placed perpendicular to the back of the wall panel.

The steps are repeated for each successive layers till the wall reaches its designed height.

Traffic barriers and copings Construction:

The final construction sequence is undertaken after the placement of final panel and the wall fill is completed to its final grade.

2.3.5.2 MSE Wall with Flexible Facing

Construction sequence of flexible-faced MSE walls are similar to that of walls with precast facing elements. In flexible faced MSE walls the reinforcing material also acts as facing material. Welded wire mesh, geotextiles, geogrids or gabions are some of the types of flexible facings used in the construction. The construction of the first level of facing element requires only a level grade. For MSE wall with flexible facing, a concrete footing or leveling pad required only if precast elements are to be attached to the system after construction.

Construction of the MSE wall with flexible facing follows the same sequence as outlined for segmental facings with the following exceptions:

Placement of first reinforcing layer:

The reinforcement should be placed on a level ground with the principal strength direction perpendicular to the face of the structure and should be secured with pins to restrict

their movement during placement of fill material. Reinforcement should have anisotropic strength properties (i.e., many geosynthetics). A minimum of 6 in. (150 mm) overlap should be ensured along the edges, perpendicular to the face while placing the adjacent reinforcing sheets. In case of using geogrid or wire mesh as reinforcement, the edges of two adjacent reinforcement sheet should be butted and clipped or tied together.

Face Construction:

Temporary face forms are used for placing the geosynthetic layers as shown in Figure 2.35. Form holders are required to ensure temporary support of forms at the face; the form holders should be placed at the base of each layer at horizontal intervals of approximately 4 ft. (1.20 m). For achieving and ensuring good compaction, these supports are essential. A geo textile or hardware cloth should be used when using geogrids or wire mesh, to ensure the retention of the wall fill material at the face. Precaution should be exercised when compacting the fill material within 3 ft. (~1 m) of the wall face; it is recommended to use a hand-operated vibratory compactor.

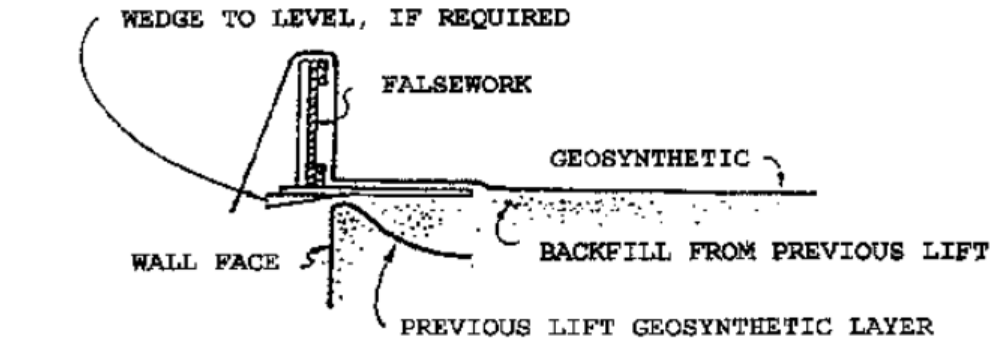

(1) PLACE FALSEWORK AND GEOSYNTHETIC ON PREVIOUS LIFT

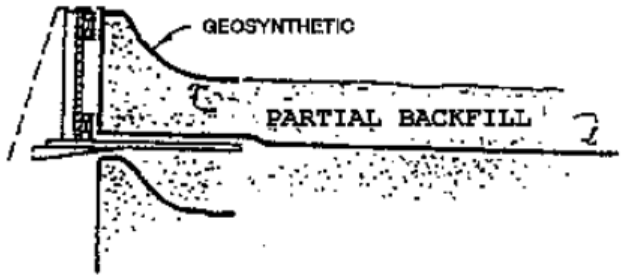

(2) PLACE/COMPACT PARTIAL BACKFILL AND OVERLAP GEOSYNTH

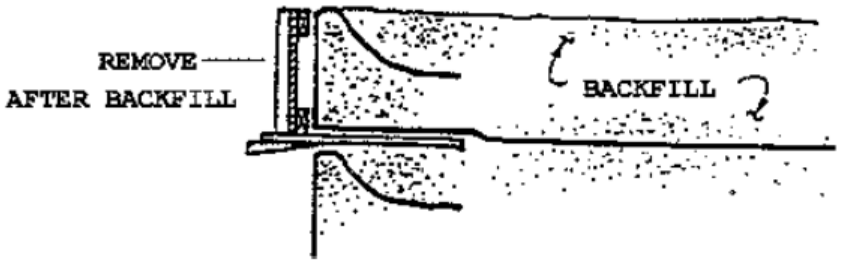

(3) PLACE/COMPACT REMAINDER OF BACKFILL LIFT

Figure 2. 35 Lift Construction sequence for flexible (geosynthetic) faced MSE wall.

2.3.6 Performance Criteria of MSE Wall

Performance criteria for MSE structures depends on the design requirements presented in Article 11.10 of 2007 AASHTO LRFD Specifications for Highway Bridges. Load and

resistance factors are considered in these requirements with respect to various failure modes and materials, and for various limit states. However, there is no specific method currently available to predict lateral displacement of the wall; major part of this displacement or lateral movement of the wall occurs during construction phase. The horizontal movement of the wall depend on the compaction effects, extensibility of reinforcement, length of reinforcement, reinforcement-to-panel connection details, and details of the facing system. Christopher et al. (1990) developed an empirical curve for the rough estimation of probable lateral displacement of simple structures that might occur during construction, based on the ratio of reinforcement length to wall-height and extensibility of reinforcement as shown in Figure 2.36.

Performance criterial of a MSE wall are both structure and site dependent. For a specific MSE structure system, safety factors or a consistent set of load and resistance factors including the tolerable movement of the structure, falls within the structure dependent performance criteria. During the design, few site-specific project criteria needed to be accounted for (Berg et. at., 2009):

Design limits and wall height:

To fulfill the geometric requirement of the project, required length and height must be established for the determination of the type of structure and external loading configurations.

Alignment limits:

It is required to establish horizontal (perpendicular to wall face) limits of bottom and top of wall alignment, as alignments vary with pounding of wall system. The alignment limit may restrict the type and maximum batter of the wall facing. This is more important for walls built particularly with Modular Block Wall (MBW) units.

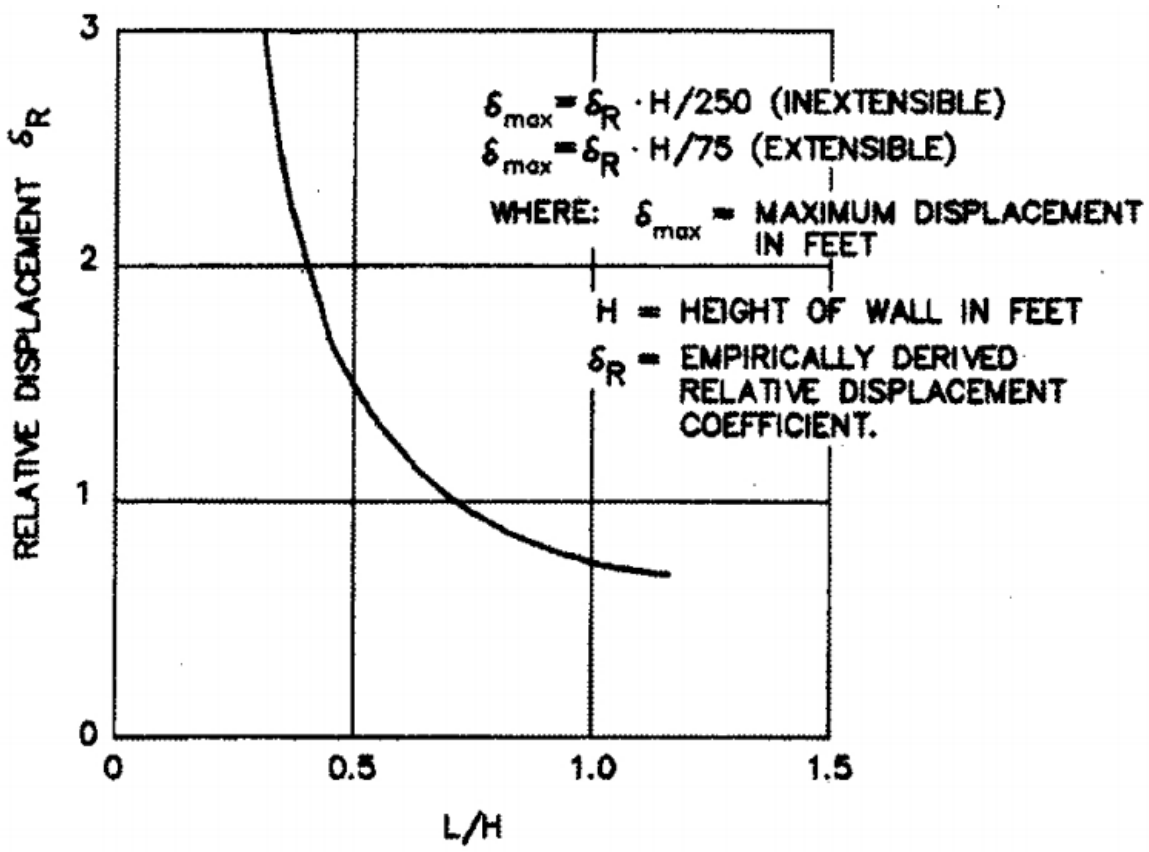

For L = 0.7 H
Metallic (inextensible) reinforcement ≈ ¾-in. per 10 ft of wall height
Geogrid (moderately extensible) reinforcement ≈1 in. per 10 ft of wall height
Geotextile (extensible) reinforcement ≈1.5 in. per 10 ft of wall height

Based on 20 ft high walls, relative displacement increases approximately 25% for every 400 psf surcharge. Experience indicates that for higher walls, the surcharge effect may be greater.

NOTE: This figure is only a guide. Actual displacement will depend, in addition to the parameters addressed in the figure, on soil characteristics, compaction effort, and contractor

Figure 2. 36 Empirical curve for the estimation of lateral displacement during construction for MSE walls (Christopher et. al., 1990).

Length of reinforcement:

For a MSE wall it is recommended that the minimum length of the reinforcement should be of 0.7H ("H" is the height of wall). However, if a surcharge load is present or where

foundation conditions affect lateral sliding and/or global/compound slope stability, longer lengths of the reinforcement are required. Typical required minimum length of reinforcement for different scenarios are listed in Table 2.5.

Table 2. 5 Typical values of minimum length of reinforcement.

Case	**Typical minimum L/H ratio**
Static loading with or without traffic surcharge	0.70
Slopping backfill surcharge	0.80
Seismic loading	0.80 to 1.11

External loads:

Loads from surcharge due to geometric requirement, adjoining footing loads, traffic loads, impact load from moving traffic are all considered within external loads. Magnitude of minimum traffic load is a uniform load equivalent to 2 ft. (0.6 m) of soil over the traffic lanes according to Article 3.11.6.4 (AASHTO, 2007).

Wall embedment:

For proper and stable construction, the wall needs to be embedded into the ground to a minimum depth from adjoining finished grade to the top of the leveling pad, which should be based on bearing, settlement, and slope stability considerations. Table 2.6 presents the recommended minimum embedment depth based on local bearing considerations which is currently in practice.

Table 2. 6 Minimum depth of embedment for MSEW (AASHTO, 2007).

Slope in front of the wall	**Minimum embedment depth to the top of leveling pad***
All geometries	2 ft. minimum
Horizontal (walls)	H/20
Horizontal abutments	H/10
3H : 1V	H/10
2H : 1V	H/7
1.5H : 1V	H/5

*Minimum depth is the greater of applicable values listed, frost depth, or scour depth.

A minimum horizontal bench of 4-ft (1.2 m) wide as measured from the face of the wall is necessary for the walls founded on slopes. The bench may be formed or the slope continued above that level (11.10.2.2, AASHTO, 2007), as illustrated in Figure 2.37. The purpose of this bench is to provide resistance against general bearing failure and to facilitate the access for maintenance inspections (C11.10.2.2, AASHTO, 2007).

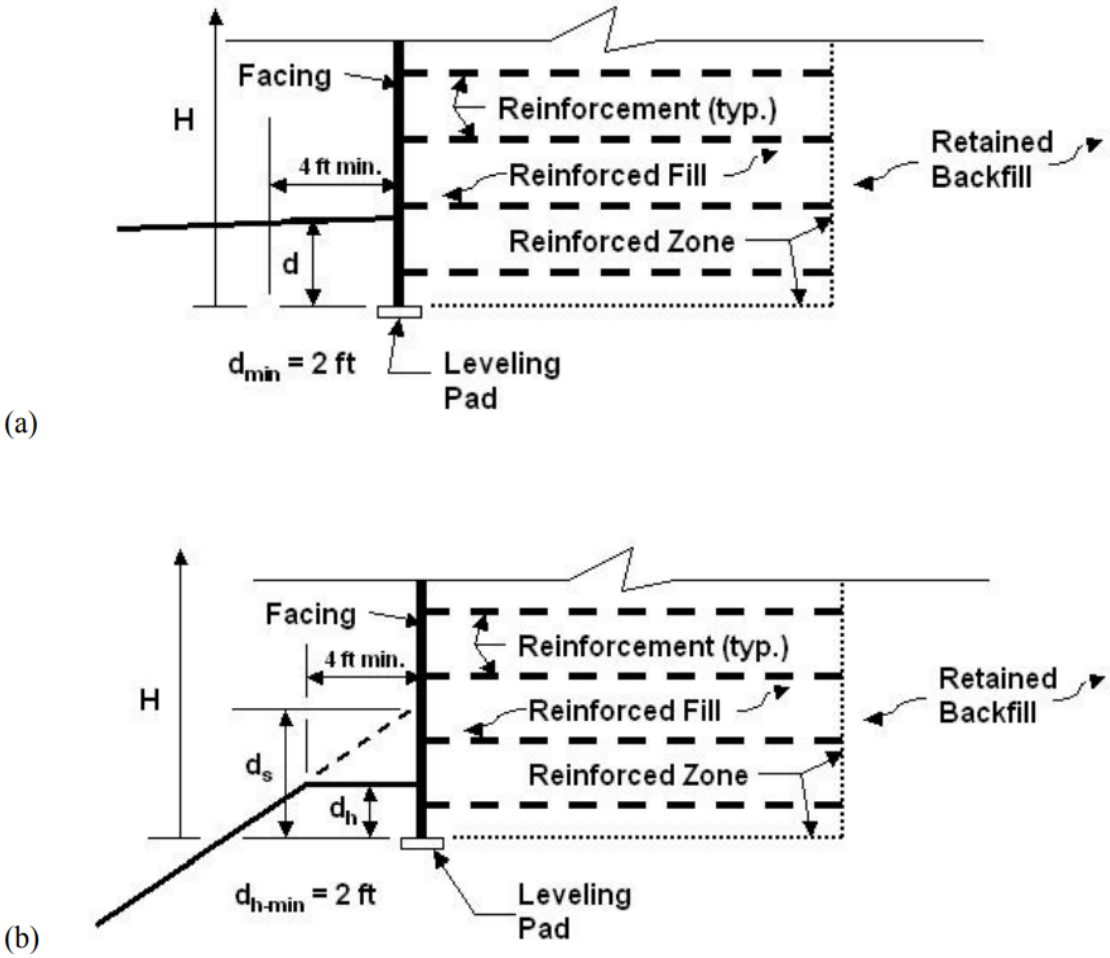

Figure 2. 37 Requirements of MSE wall embedment depth, (a) level toe condition and (b) benched slope toe condition (dh = minimum depth for horizontal slope and ds = minimum depth for sloping toe, from Table 2.6) (AASHTO, 2007).

2.3.7 External Stability of MSE Wall

Reinforced soil wall or MSE wall design includes determination of geometric requirements to prevent external failure. As with traditional gravity, semi gravity and cantilever retaining structures, four potential external failure mechanisms are usually taken into consideration while designing MSE walls, as shown in Figure 2.38. They include:

- Base sliding (or the lateral movement of the base)
- Overturning
- Bearing capacity failure
- Overall/global stability (Deep seated stability failure)

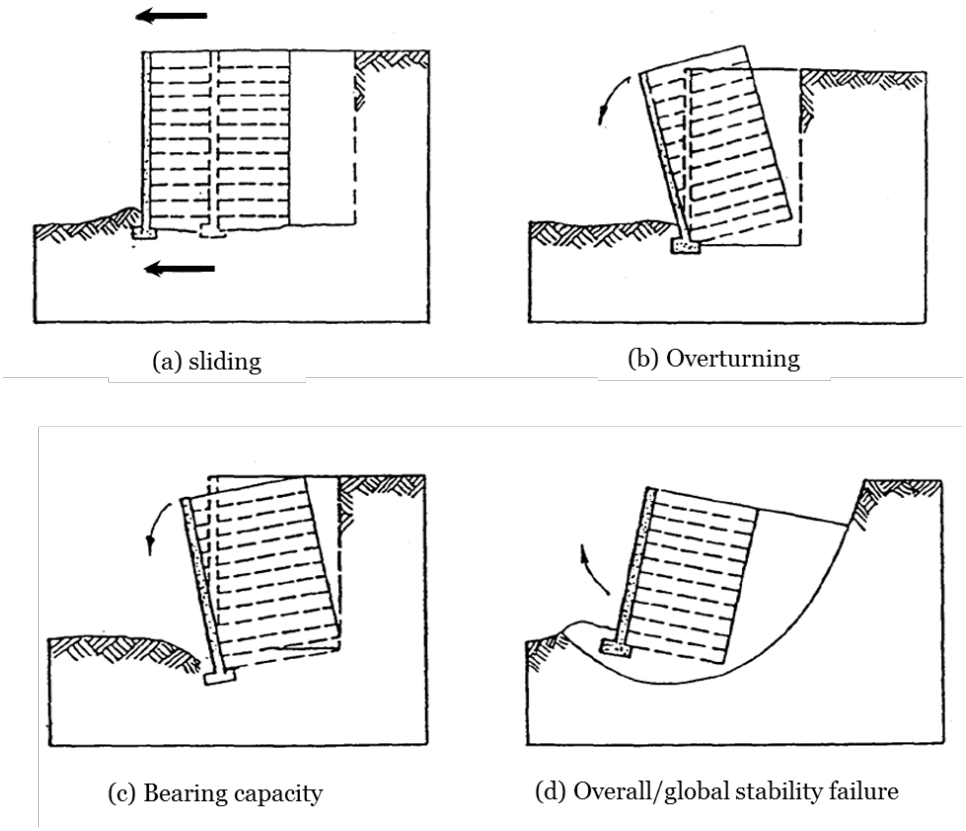

Figure 2. 38 Potential external stability failure mechanisms of a MSE wall.

Based on FHWA, external stability analysis for MSE wall are adopted from guidelines for conventional rigid retaining walls such as gravity walls and cantilever walls. The FHWA research project titled “Mechanically Stabilized Earth Walls and Reinforced Soil Slopes Design and Construction Guidelines” (Elias et. al., 2001) claimed that it is “justified” to adopt the external stability analysis. It has been reported that, between design and actual

performance, the sliding and overturning remains consistent. However, for the bearing capacity analysis, there are disagreement exists on the method used (Berg et al., 2009).

2.3.7.1 Bearing Capacity

Bearing capacity theory was derived by Terzaghi (1943). The ultimate bearing capacity can be calculated with the following equation. For a rigid footing, punching failure may occur when there is compression of the soil under the footing, accompanying by shear in the vertical direction at the edge of the footing as shown in Figure 2.39 (Berg et al., 2009). Heaving may not occur at the edge of the footing; however, heave may be seen at a certain distance from the edge of the footing. The main characteristic of the ultimate bearing capacity failure is relatively large settlement. Terzaghi proposed the equation below to calculate the ultimate bearing capacity:

$$q_u = cN_c + \gamma D_f N_q + \frac{1}{2}\gamma B N_\gamma \tag{2.9}$$

where,

q_u = Ultimate bearing capacity

c = Cohesion of foundation soil

N_c, N_q, N_γ = Bearing capacity factors

γ = Unit weight of foundation soil

D_f = Embedment factor for foundation

B = Width of footing

In case of MSE wall, Terzaghi's equation cannot predict the accurate bearing capacity, as it was derived based Prandtl's theory (1920) for plastic failure of metal under rigid punching;

however, the base of the MSE wall with reinforcement is relatively flexible. Therefore, the bearing capacity calculated based on this equation will yield a conservative result. Because of this limitation, many researchers have been trying to unify global stability and bearing capacity analysis; however, till now no breakthrough has been achieved (Aubeny et. al., 2014).

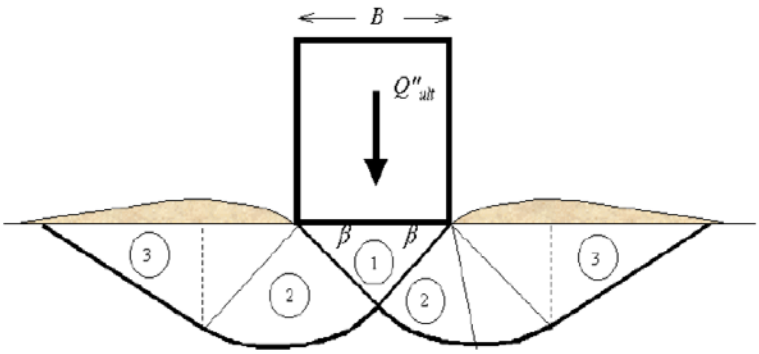

Figure 2. 39 Ultimate bearing capacity of rigid footing (Berg et al, 2009).

Leveling pad is used as the foundation for the facing wall; but surcharge is placed on the other side by backfill materials. The available bearing capacity equation ignores the effect of surcharge and probable failure pattern is shown in Figure 2.40.

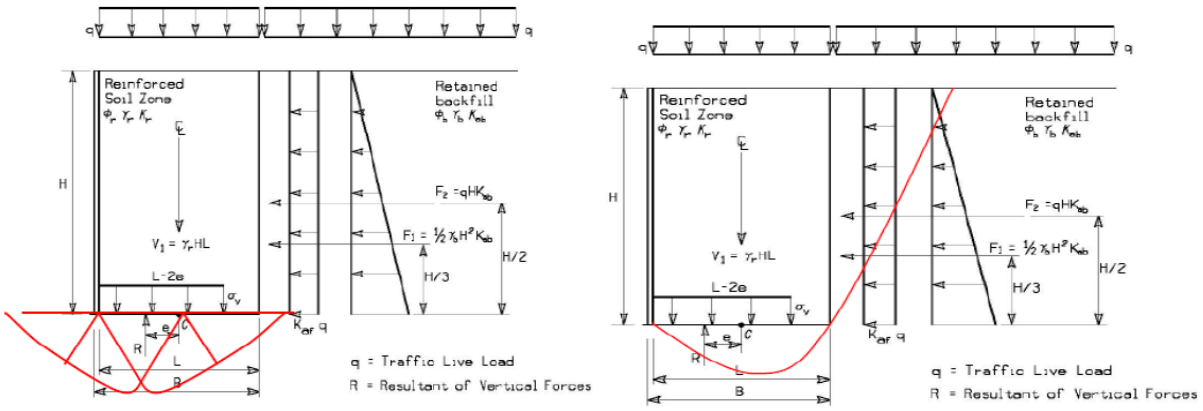

(a) Assumed Bearing Failure Zone of Current Practice

(b) Possible Failure Zone

Figure 2. 40 Bearing capacity of retaining walls (Berg et al., 2009).

One of the way to increase the bearing capacity of the foundation is, by increasing the width of the foundation, which can be done by increasing the length of the reinforcement at the base of the wall. According to the researchers, bearing capacity failure may lead to rotation about the toe of the MSE wall and increases the possibility of separation between reinforced zone and retained zone. Aubeny et at. (2014) reported that, the lack of bearing capacity for the MSE wall will not result in a punching failure because of the constant lateral force; and the wall movement will be dominated by rotation.

2.3.7.2 Sliding and Overturning

Unlike the bearing capacity analysis sliding and overturning of rigid wall has been well calibrated by practice. According to Leshchinsky and Han (2004), limit equilibrium method is suitable for the analysis of sliding which completely satisfy the equilibrium. There are almost no arguments present regarding checking of sliding and overturning. However, there are concerns among different researchers regarding the reliability of calculated FOS for MSE walls against sliding and overturning. A study done by Chalermyanont and Benson (2005) showed that, variability of the properties of the backfill materials can significantly influence the calculated FOS. In case of a retaining wall system (Figure 2.41), factor of safety against sliding can be calculated from the following equation:

$$F.S. = \frac{\gamma_r HL}{qHK_{0_f} + 0.5\,\gamma_f H^2 K_{0_f'}} \tag{2.10}$$

Here,

γ_r = unit weight of the reinforced soil

H = height of the wall

L = width of the foundation

q = surcharge

γ_f = unit weight of the fill soil

In Table 2.7, the FOSs of TxDOT and other agencies are listed for comparison. Spatial variation has been ignored, which results in higher probability of failure compared to rigid retaining wall designed with the same FOS.

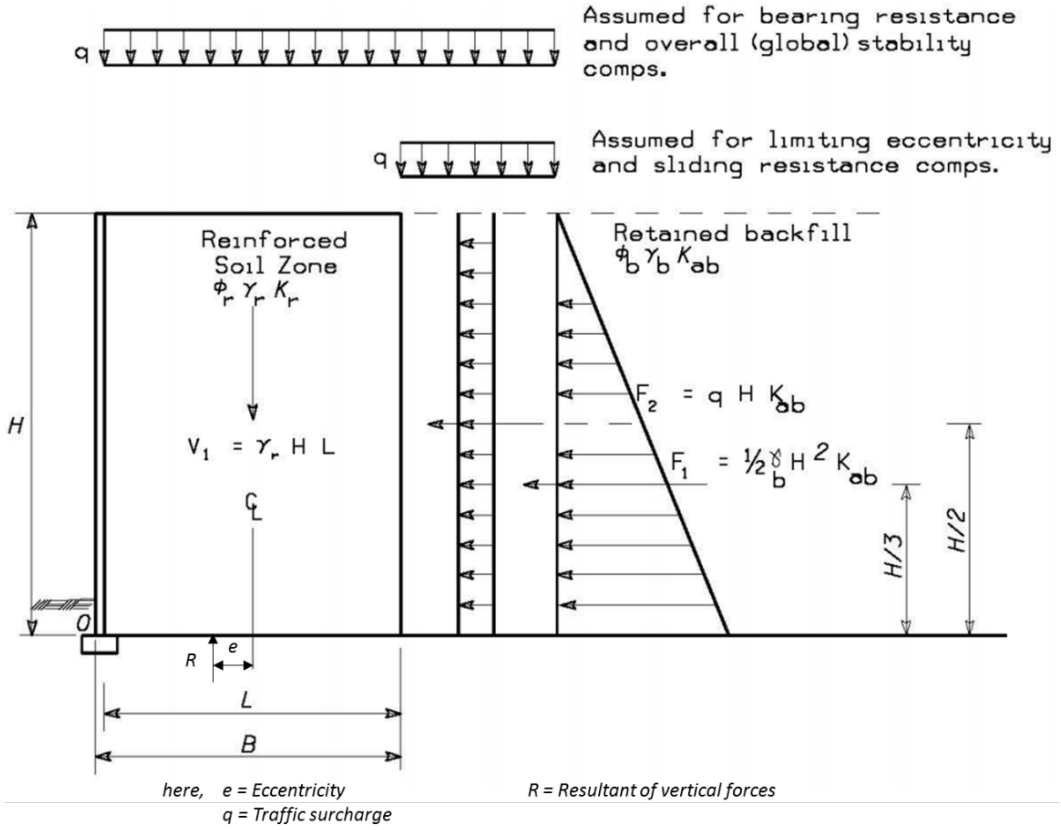

Figure 2. 41 Force diagram of retaining wall for sliding analysis; horizontal back slope with traffic surcharge (AASHTO, 2007).

Table 2. 7 Summary of Factor of Safety used on MSE Design Check (Aubeny, 2014).

Failure Mode	TxDOT	WisDOT (WisDOT 2006)	CalTrans (CalTrans 2004)
Sliding	FOS≥1.5	1.5 for spread footings on soil or rock and 1.0 for pile footings	1.5
Overturning	FOS≥2.0	1.3 (Global)	1.5
Bearing Capacity	FOS≥1.3 (global)	1.5 for footings on pile or rock 2.0 for footings on soil	3.0
Eccentricity, e	e<L/6 (middle third)	n/a	e<L/6, on soil e<L/4, on rock
Pullout	FOS≥1.5	1.5	1.5

2.3.8 Sliding Stability of MSE Wall System

The force responsible for initiation of sliding is the horizontal component of the thrust on the vertical plane at the back of the wall, generated due to loads from backfill soil, water, seismic load and surcharges. This is resisted by the shear force which is lesser of the shear resistance along the base of the wall and of a weak layer near the base of the MSE wall. Resistance to the lateral movement along the base is determined following the same process as spread footing on soil described in article 10.6.3.4 (AASHTO, 2007). Resistance against sliding failure (R_R) can be estimated by the following equation:

$$R_R = \varphi_\tau R_\tau \quad (2.11)$$

where,

φ_τ = resistance factor for shear resistance between soil and foundation (=1.0 for sliding: soil-on-soil)

R_τ = nominal sliding resistance between reinforced fill and foundation soil.

Passive resistance due to the embedment is ignored as there is a chance that soil might be removed through natural or manmade process (e.g. erosion, installation of utilities etc.) during the service life of the MSE wall. Also, the major part of the sliding occurs during the construction phase and during that time passive resistance is not present. In addition, shear strength from the facing system is also neglected as conservative approach.

Two specific cases, i) wall with horizontal backslope and ii) wall with sloping backfill, are considered for sliding. Calculation steps and equations to compute lateral movement/sliding for these two cases are described below (AASHTO, 2007; Berg et. at., 2009). Other loads or geometries, for different cases such as additional live load or dead load or surcharge loads, should be included in these equations.

1) Calculation of nominal thrust, per unit width, acting on the back of the reinforced zone:

Wall with horizontal backslope: (Figure 2.41)

Resultant force F_1, for the retained backfill is, $F_1 = \frac{1}{2} K_{ab} \gamma_b H^2$ (2.12)

Resultant force F_2, for a uniform surcharge is, $F_2 = K_{ab} q H$ (2.13)

where,

K_{ab} = active earth pressure coefficient for the retained backfill $= \tan^2 (45 - \frac{\emptyset'_b}{2})$; $\emptyset'_b$ is the friction angle of retained backfill.

γ_b = moist unit weight of the retained backfill soil

H = height of the retained wall

q = uniform live load surcharge = (γ_r) (h_{eq})

Wall with sloping backfill: (Figure 2.42)

Resultant nominal retained backfill force per unit width of wall, F_T is,

$$F_T = \frac{1}{2} K_{ab} \gamma_b h^2 \quad (2.14)$$

where,

K_{ab}= active earth pressure coefficient for sloping backfill = $\frac{sin^2(\theta+\emptyset'_b)}{\Gamma\, sin^2\theta \sin(\theta-\delta)}$; (here, $\Gamma = \left[1+\sqrt{\frac{\sin(\emptyset'_b+\delta)\sin(\emptyset'_b-\beta)}{\sin(\theta-\delta)\sin(\theta+\beta)}}\right]^2$; β is nominal slope of backfill behind wall in degrees; δ is the friction angle between retained backfill and reinforced soil which is set equal to β; θ is 90^0 for vertical or near vertical wall.)

h = summation of total height of wall, H, and slope at the back of the reinforced zone = H + L tan β

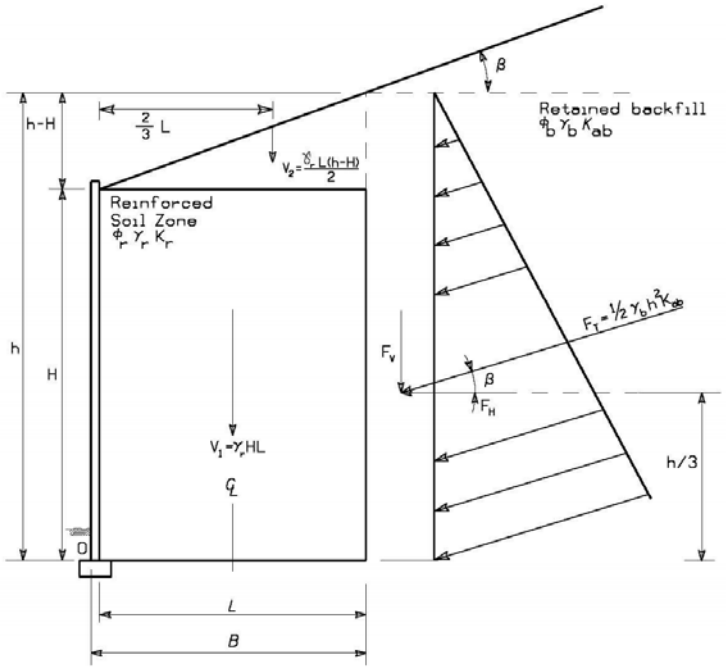

Figure 2. 42 Force diagram of retaining wall for sliding analysis: sloping backfill case (AASHTO, 2007).

It should be noted that, h - H for a broken backslope (Figure 2.43) should not exceed the upper crest height. If "S" is the height of broken backslope, then (H + L tanβ) ≤ (H + S); use (H + S) if (L tanβ) > S.

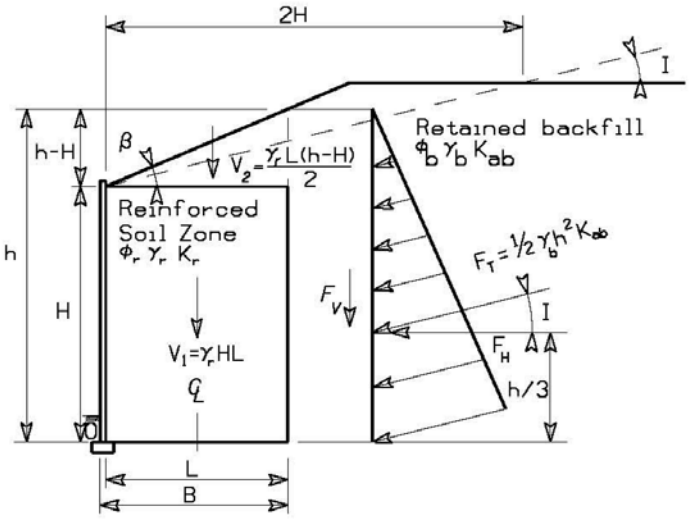

Figure 2. 43 Force diagram of retaining wall for sliding analysis: broken backslope case (AASHTO, 2007).

2) Calculation of nominal and factored horizontal driving forces

For horizontal backslope with a uniform live load surcharge:

$$\sum F = F_1 + F_2 \tag{2.15}$$

$$P_d = \gamma_{EH} F_1 + \gamma_{LS} F_2 \tag{2.16}$$

For sloping backfill condition:

$$F_H = F_T cos\beta \tag{2.17}$$

$$P_d = \gamma_{EH} F_H = \gamma_{EH} F_T cos\beta \tag{2.18}$$

For conservative design, the maximum EH load factor (=1.50) should be used in these equations as it will create the maximum driving force effect for the sliding limit state.

3) Determination of the most critical frictional properties at the base

Minimum friction angle, φ, should be chosen for three possibilities:

i) Sliding along the foundation soil, if its shear strength (based on $c'_f + \tan \varphi'_f$ and/or c_u for cohesive soils) is smaller than that of the reinforced fill material shear strength ($\tan \varphi'_r$).

ii) Sliding along the reinforced fill (φ'_r).

iii) Sliding along the weaker of the upper and lower soil-reinforcement interfaces, in case of sheet type reinforcement. Interface direct shear tests should be used for measuring the soil-reinforcement friction angle ρ. If testing is not possible, then it may be taken as $\frac{2}{3} \tan \varphi'_r$.

4) Calculation of the nominal components of resisting force and the factored resisting force per unit length of wall

For a horizontal backslope and uniform live load surcharge:

$$R_r = \gamma_{EV} V_1 x\, \mu \tag{2.19}$$

For sloping backfill condition:

$$R_r = [\gamma_{EV}(V_1 + V_2) + \gamma_{EV}\,(F_T \sin\beta)] x\, \mu \tag{2.20}$$

where,

μ = minimum soil friction angle φ [$\tan \varphi'_f$, $\tan \varphi'_r$, or (for continuous reinforcement) $\tan \rho$]

It should be noted that for conservative design the live load is excluded as it increases the sliding stability. Any external loads that tend to increase the sliding stability can only be

included when those loads are permanent. For considering minimum sliding resistance, the minimum EV load factor (= 1.00) should be used in the above equations.

5) Comparison between factored sliding resistance, R_f, and the factored driving force, P_d should be conducted to check if the resistance is greater.

6) The capacity demand ratio (CDR) for sliding should be checked, CDR = (R_f/P_d). The wall is safe against sliding if CDR > 1.0, if not, it is required to increase the length of the reinforcement, L, and repeat the process.

For the sliding stability, it is required to ensure that the shear resistance between the foundation soil and the backfill material at the base of the MSE wall is much higher compared to the driving forces responsible to initiate the lateral movement/sliding of the base of the wall.

2.3.9 Studies on Lateral Movement of MSE Wall

Stuedlein et al. (2007) presented a case study of a MSE wall for the third runway at Seattle-Tacoma international airport, located in Seattle, Washington. Approximately 1150 feet (350 m) long, two tier, 85 feet (26 m) tall MSE wall construction was required for the north side of third runway, with an exposed wall height of 77.5 feet (23.6 m). Subsurface condition reported for the area consists of 10 to 16.5 feet (3 to 5 m) of loose to medium dense slightly gravel, silty sand (including existing fill), 10 to 16.5 feet (3 to 5 m) of soft to medium stiff clayey silt and stiff to very stiff sandy silt over glacially overridden dense to very dense, slightly silty to silty, slightly gravelly to gravelly sand. It has also been reported that, there were deposits of very soft, silty, sandy peat of 10 feet (3m) deep beneath some portions of the wall footprint. All the materials and reinforcement selected and used for the construction of

the MSE wall met or exceed the minimum requirement set by AASHTO Standard Specifications for Highway Bridges. Construction of the MSE wall began on 18th February, 2005. It took about 88 days to complete the first tier of the wall. It took about 31 days to complete the construction of the second tier of the MSE which began on the 140th day from the beginning of construction. Performance of the wall was observed by monitoring displacements, tensile strains, and piezometric levels. A total of three inclinometers were installed to monitor the lateral movement of the wall. The results of inclinometer casing surveys are shown in Figure 2.44.

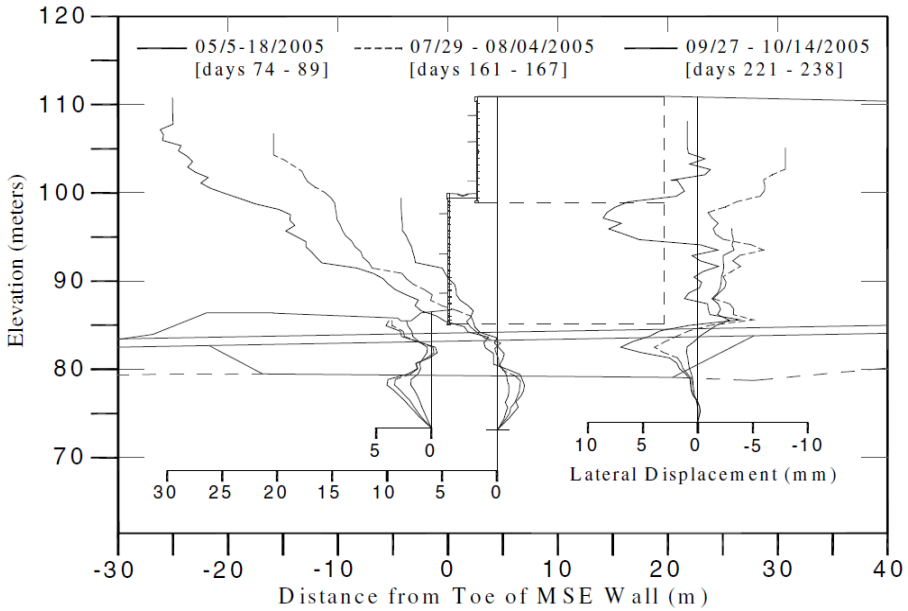

Figure 2. 44 Lateral Displacement in Front and within Retaining Soil Mass (Stuedlein et al., 2007).

From the monitoring data, it was noticed that within the glacially overridden and subgrade improved fill soils the lateral displacements are generally limited to less than 0.2 inches (5 mm), with a maximum of 0.28 inches (7 mm); and at the top of the wall the maximum movement was measured as 1.2 inches (30 mm). The authors pointed that, reason for this

movement might be due to the sharp geometrical change at the face of the wall and the shear stress concentration between the subgrade improved zone and native foundation soils. The profile of the lateral displacement of the inclinometer showed that with increasing height displacement increases. Maximum lateral displacement observed at the end of tier 1 construction, near the end of tier 2 construction and the final inclinometer observation was found to be 0.35, 0.79 and 1.22 inches (9, 20 and 31 mm) respectively. Lateral movement results from the displacement monitoring points (DMP) at the tallest portion of the wall face are shown in Figure 2.45 for three displacement profiles corresponding to the end of tier 1 construction, end of tier 2 construction and the final survey. It was found that the maximum movement of the wall face was about 0.4 inches (10 mm). This small amount might be due to the delay in face panel construction and baseline survey.

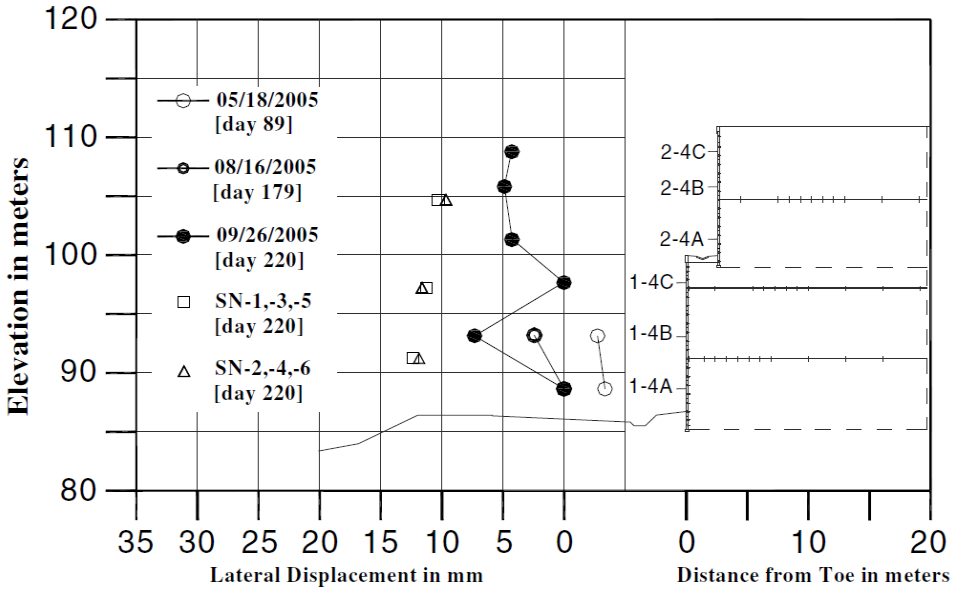

Figure 2. 45 Lateral Displacement of the face of MSE wall (Stuedlein et al., 2007).

Stuedlein et al. (2010) conducted another study on a four-tier, 1,430 ft. (436 m) long, 150 ft. (~46 m) tall MSE wall, constructed for the expansion of the Seattle-Tacoma

International Airport by introducing a third runway west of two existing runways. It was reported that, fill slopes of 2H: 1V were used wherever possible; however, due to the possibility of the fill slopes intruding the wetlands in some areas, MSE wall construction became necessary. The wall has a face area of approximately 130,200 ft^2 (12,100 m^2) and an exposed height of 137.5 ft. (41.9 m). The authors believed that based of the literature it was the tallest MSE wall in the western hemisphere. The subsurface investigation reported that before construction, below the wall footprint, there were 10 – 12 ft. of soft peat, interlayered with loose to medium dense silty sand and sandy peat, over glacially overridden dense to very dense, slightly gravelly, silty to very silty sand. Due to the poor soil condition at the shallow depth and inconclusive ground improvement test results, the soil was excavated up to 12 ft. (4 m) to the top of the dense to very dense glacially overridden soils and replaced with densely compacted granular backfill to provide a high strength foundation for the MSE wall. According to the authors, the wall was designed and the materials were chosen based on AASHTO Standard Specifications for Highway Bridges (AASHTO 1996 and Interim Updates). The authors reported that the Construction of the MSE wall began on 5th January, 2005. It took about 58 days to complete the first tier, 48 ft. (14.6 m) tall section. On day 72, 38.4 ft. (11.7 m) tall second tier construction started which took 41 days to complete; for the 3rd and 4th tier construction, it took 44 and 42 days to complete to heights of 37.7 and 26 ft. (11.5 and 7.9 m) that began on days 131st and 205th respectively. Between days 406 and 420 the final grading operation was conducted to bring the MSE wall to design elevation. Vertical inclinometer was used to monitor lateral movement of the MSE wall during the performance monitoring period. The results from the inclinometer data are shown in Figure 2.46. From the monitoring data it was reported that the maximum lateral displacement within the reinforced soil mass was

observed just above the toe of the wall. At the end of second tier construction the maximum lateral movement was found to be 0.3 inches (8 mm) which increased with increasing wall height and found to be a value of 1.8 inches (45 mm) at the end of tier 4 construction. Figure 2.46 also shows the lateral movement of the wall facing. It was noted that the lateral movement of the wall facing follows an irregular pattern. The maximum movement was found to be near the base of the wall. The authors reported that, based on the survey results showed prior to tier 3 construction, the lateral displacement was insignificant. However, the displacement kept rising with the increasing wall height. At the end of tier 3 construction, the lateral displacement was found to be approximately 1.2 inches (30 mm) near the wall base which increased to about 3.5 inches (90 mm) at the end of tier 4 construction.

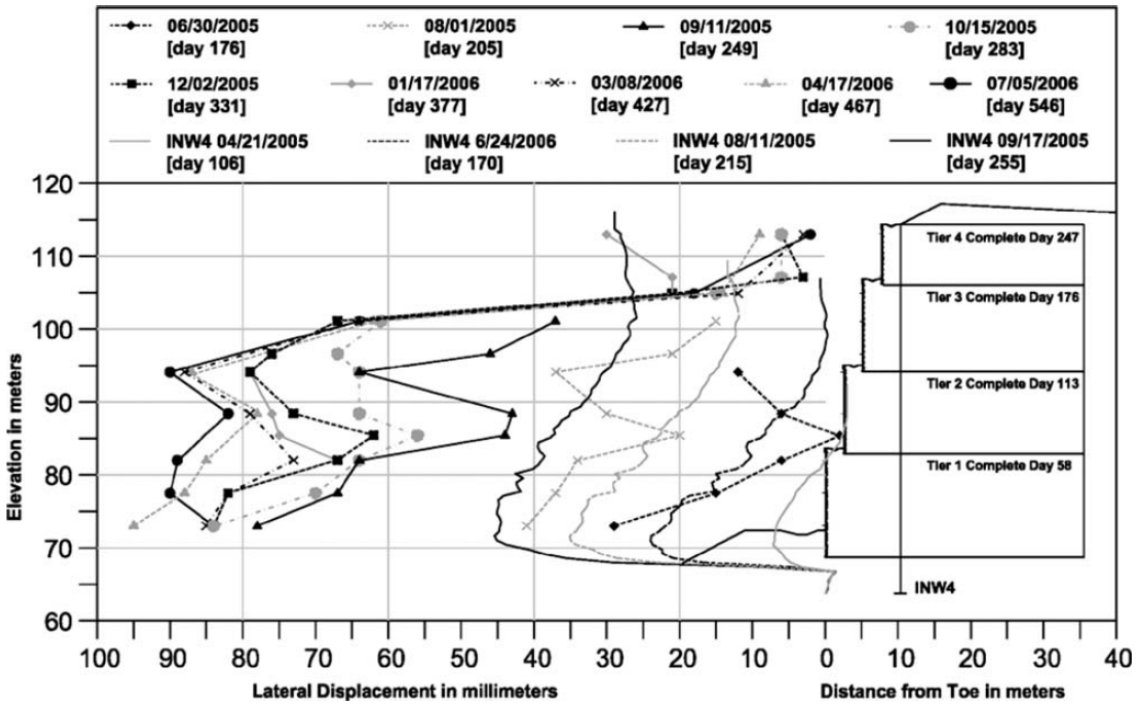

Figure 2. 46 Lateral displacement of wall facing within the reinforced soil mass and subgrade soil (Stuedlein et al., 2010).

Chalermyanont & Benson (2005) conducted a parametric study based on Monte Carlo simulation to identify the parameters responsible for the external stability of the MSE wall and developed a reality based design method. For external stability analysis, the researchers considered three modes of failure: sliding, overturning, and bearing capacity. For the external stability assessment, the reinforced soil was treated as a rigid mass using the similar procedures used for conventional gravity-type wall systems. A schematic showing how MSE walls were modeled is shown in Figure 2.47a. Parameters used in calculating external stability of a MSE wall are the wall height, length of reinforced soil mass, backfill friction angle, backfill unit weight, friction angle of the foundation soil and unit weight of the foundation soil. Force acting on the retaining system is also shown in Figure 2.47b. Probability of failure for each cases are shown in Figure 2.48. From the parametric study it has been reported that, the mean and coefficient of variation of the backfill friction angle are significant for sliding. It is also observed that, unit weight of the fill has insignificant impact on sliding failure.

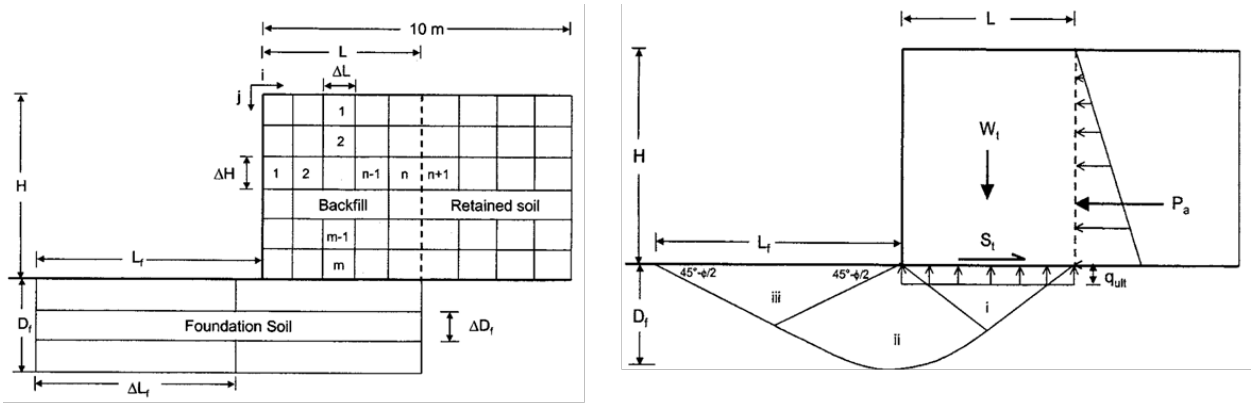

(a) (b)

Figure 2. 47 (a) Mechanically stabilized earth wall model showing cells and effective foundation area; (b) Schematic of forces and stresses acting on a mechanically stabilized earth wall (Chalermyanont & Benson, 2005).

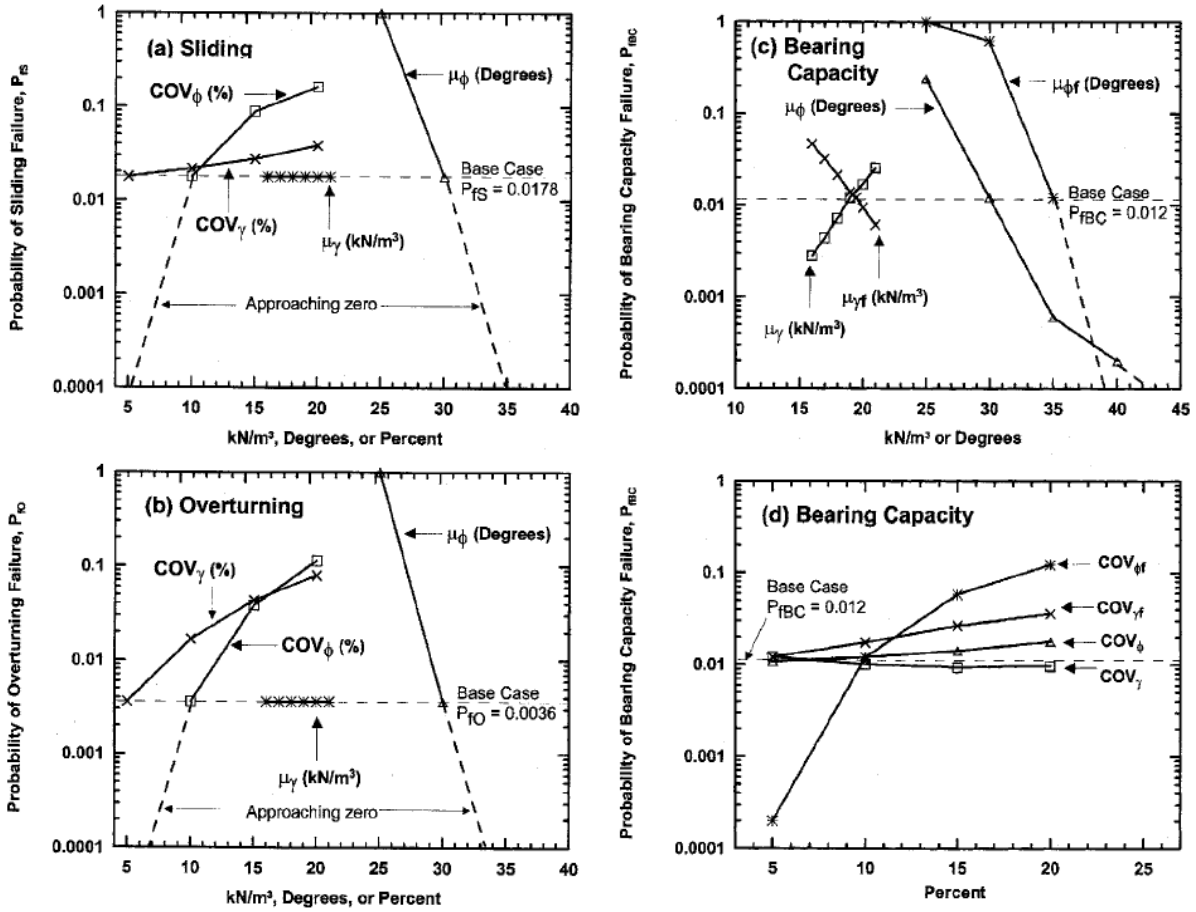

Figure 2. 48 Probabilities of failure based on parametric analysis: (a) sliding, (b) overturning, (c) bearing capacity (μ_φ, μ_γ,$\mu_{\varphi f}$ and $\mu_{\gamma f}$), (d) bearing capacity (COV_φ, COV_γ,$COV_{\varphi f}$ and $COV_{\gamma f}$) (Chalermyanont & Benson, 2005).

Horpibulsuk et al. (2011) presented a study of the performance of a fully instrumented test wall that is reinforced with an inextensible earth reinforcement composed of longitudinal and traverse members. The test section was built on a hard stratum and the MSE wall of the section was 19.69 ft. (6 m) high. The top the wall was 29.53 ft. (9 m) long and 19.69 ft. (6 m) wide and at the base it was 39.37 ft. (12 m) long and 68.9 ft. (21 m) wide. Schematic diagram of the test wall is shown in Figure 2.49a. Segmental concrete block of 4.92 x 4.92 x 0.46 ft. (1.5 x 1.5 x 0.14 m) in dimension was used as the facing panels for the wall. It took about 20 days for the construction to be completed (the sequence is shown in Figure 2.49b).

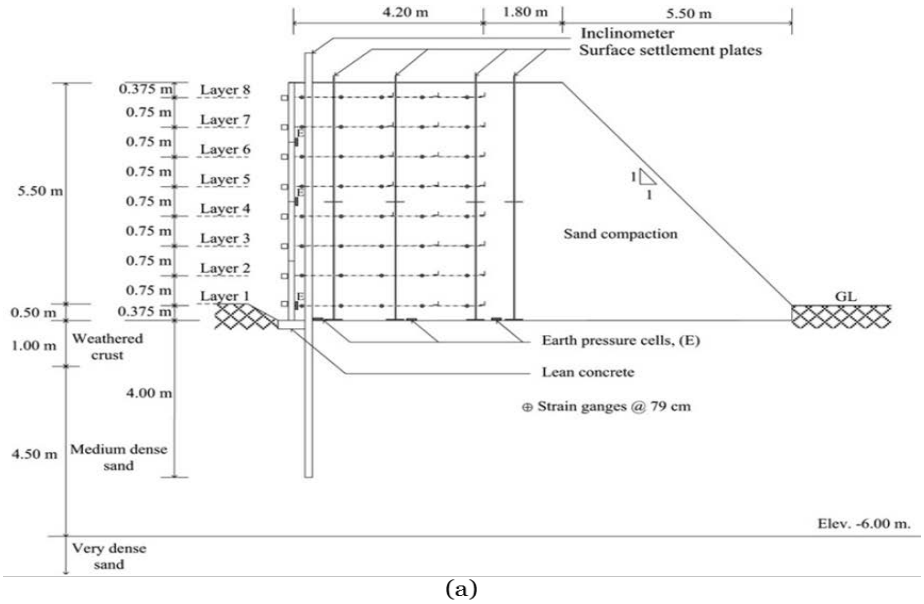

(a)

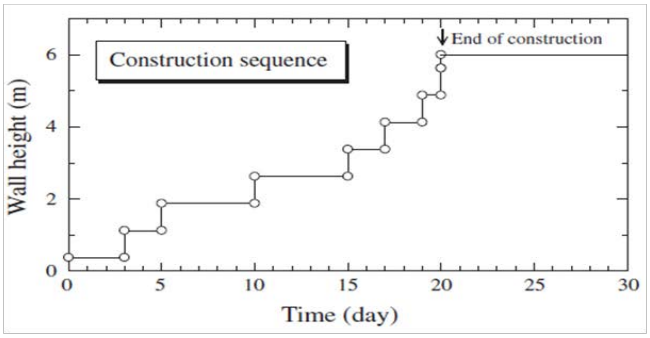

(b)

Figure 2. 49 (a) Schematic diagram of test wall with instrumentation; (b) construction sequence of test wall (Horpibulsuk et al., 2011).

The authors measured the lateral movement of the segmental panel at the end of construction by a theodolite at the center of each panel. The results are shown in Figure 2.50a. It was found that the maximum lateral movement occurs at the top of the wall as show in the Figure 2.50a. However, according to the authors this plot is misleading. Since all the panels are connected, the value found and showed in the graph is cumulative value. Therefore, the maximum lateral movement cannot be at the top. To justify the claim, the authors plotted a relative lateral movement of the panels as shown in Figure 2.50b. Difference between lateral movements of two continuous facing panel is the relative movement. It is noticed from the plot

that the lateral movement of the top by itself is the lowest while the base movement is the highest; which indicates that with depth the lateral movement increases due to the increasing lateral earth pressure of the backfill during construction. A vertical inclinometer was installed near the face of the wall to monitor the lateral movement of the wall facing. Lateral movement of the wall based on the inclinometer reading is shown in Figure 2.50c. Maximum deformation of 9 mm was reported after 47 days of construction. Based on the results, the authors reported that due to the stiff foundation soil, settlement induced lateral movement is almost negligible.

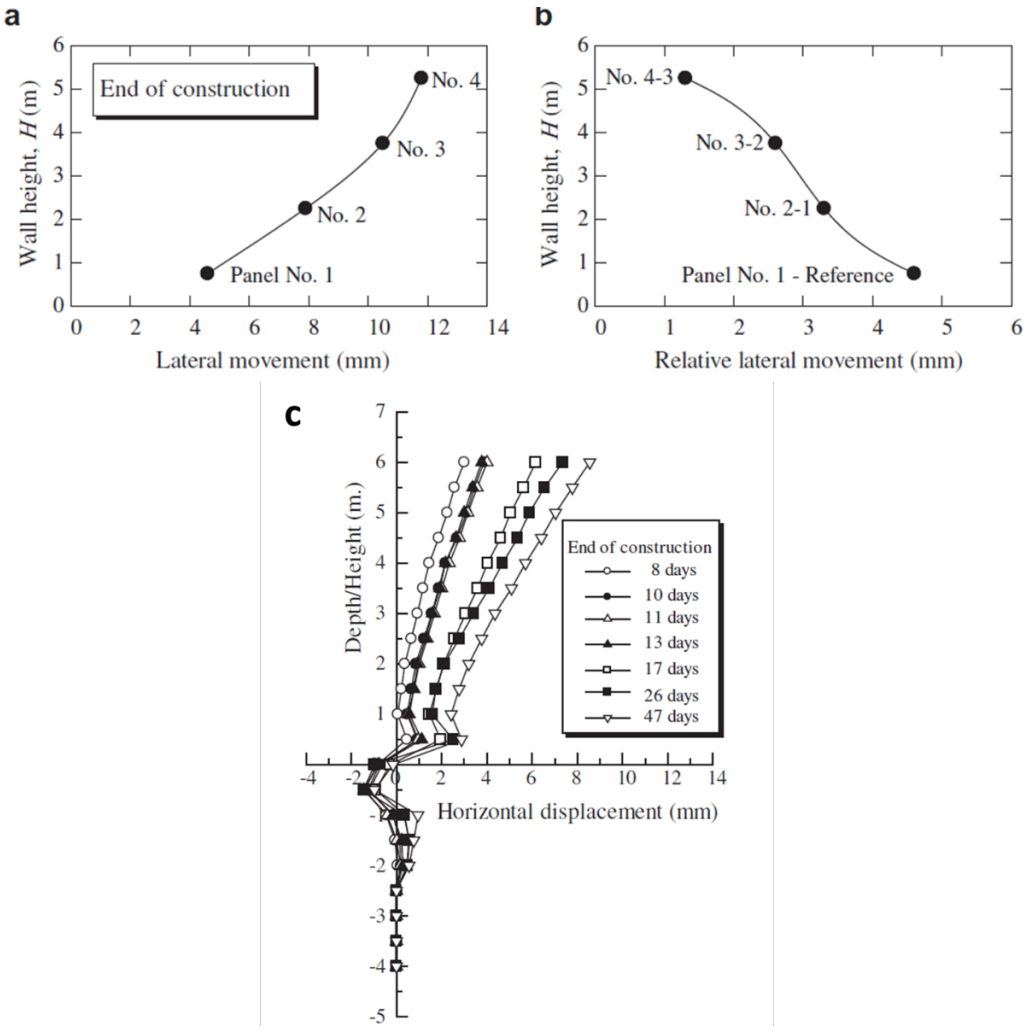

Figure 2. 50 Lateral movement of wall; (a,b) at the end of construction for each segmental panel; (c) after the completion of construction (Horpibulsuk et al., 2011).

Suksiripattanapong et al. (2012) conducted a numerical analysis of the same above discussed bearing reinforcement earth (BRE) wall using PLAXIS 2D. The authors obtained the parameters for the model developed from the conventional laboratory test and back analysis from the laboratory rotary pullout test. They modeled the reinforcement as geotextile; and used the soil/reinforcement interface parameter, R (0.65 and 0.75 for bearing reinforcement of 2 and 3 transverse members respectively), as equivalent frictional resistance. Plane strain problem was used for modelling the BRE wall and for the backfill and foundation soil, the finite element mesh involved 15-node triangular element. According to the authors, due to absence of ground water table the simulation was performed in drained condition. The finite element mesh and boundary conditions used by the authors are shown in Figure 2.51.

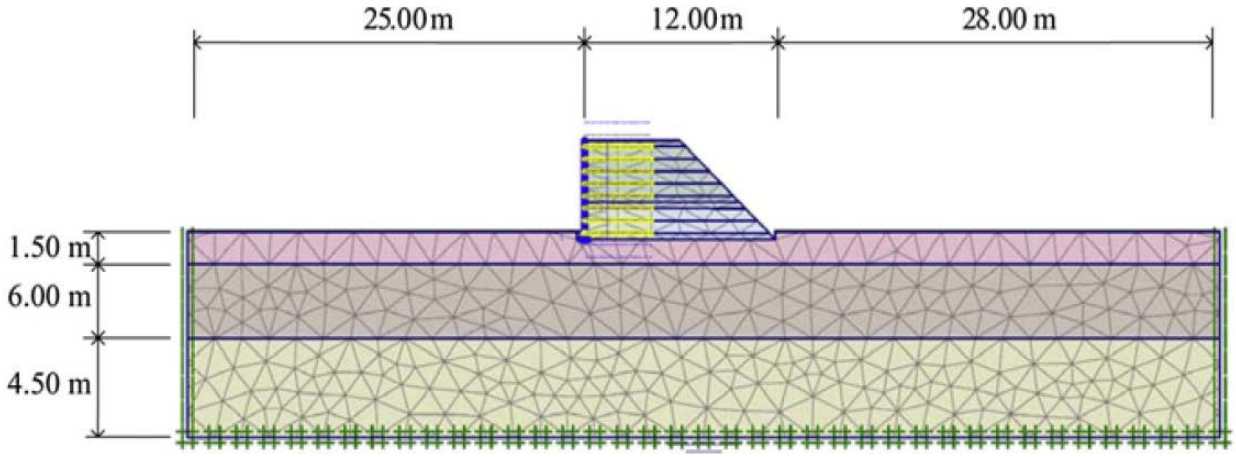

Figure 2. 51 Finite element model of BRE wall (Suksiripattanapong et al., 2012).

The behavior of the soil layers were simulated using Mohr-Coulomb model. The authors compared the measured lateral movement with the simulated data from the calibrated model; the result is shown in Figure 2.52. The lateral movement measured is the cumulative movement during construction (measured by theodolite) and after construction (measured by inclinometer). From the plot it can be noticed that model predicted lateral movement is

relatively higher compared to the measured data. According to the authors, this might be due to the stiffness of the inclinometer pipe that might be preventing the lateral movement of the soil and also the inclinometer casing was installed near the leveling pad, which might also be obstructing the inclinometer movement. The authors also reported that the lateral movement is dependent on the soil/reinforcement interface parameter, R and found that lower the R value, higher the lateral movement is. The reinforcement is providing additional resistance against sliding/lateral movement, which is higher with higher R value.

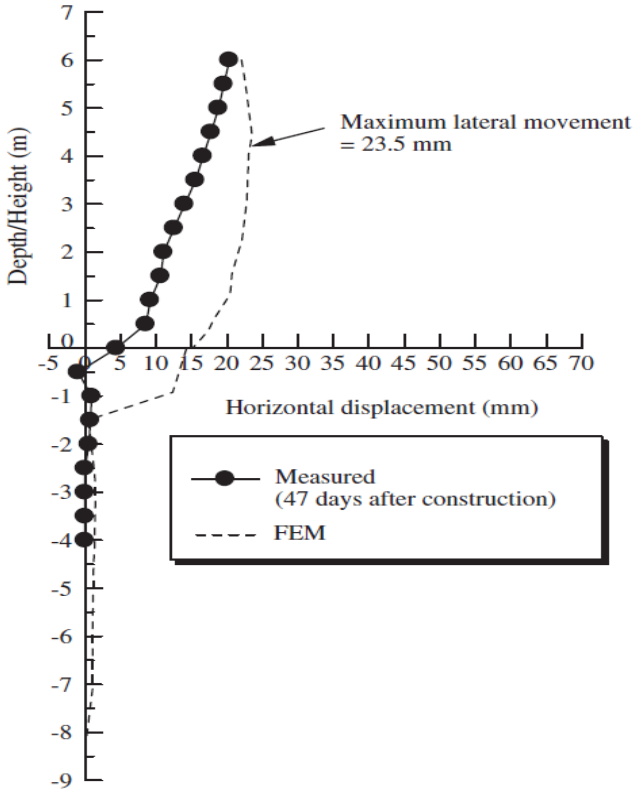

Figure 2. 52 Comparison between the simulated and measured lateral movements (Suksiripattanapong et al., 2012).

2.3.10 Problems Associated with Lateral Movement of Retaining Structures

Retaining structures are used generally to support steep to vertical slopes, highway structures like roads and bridges to minimize need for right–of–way acquisition, to stabilize

the slope of embankment etc. Deformation of the retaining wall might result in minor to catastrophic failure of these structures, e.g. embankment slope failure, deformation of highway roads and bridges etc. Lateral movement of the MSE retaining structure might result in panel opening and washout/loss of drainage materials resulting in failure of retaining wall.

Babu et al. (2016) presented a forensic analysis of a cantilever retaining structure for road approach embankment and reported that lateral displacement is one of the form of distresses present among other distresses like vertical and rotational displacement. The authors conducted a back analysis of failure and reported that the mechanism of failure is a combination of sliding and overturning. Lateral movement observed in the field are presented in the Figure 2.53. A maximum lateral displacement of 24.8 inches (630 mm) was observed at the right of the east side at 1+208.7 chainage as shown in the figure.

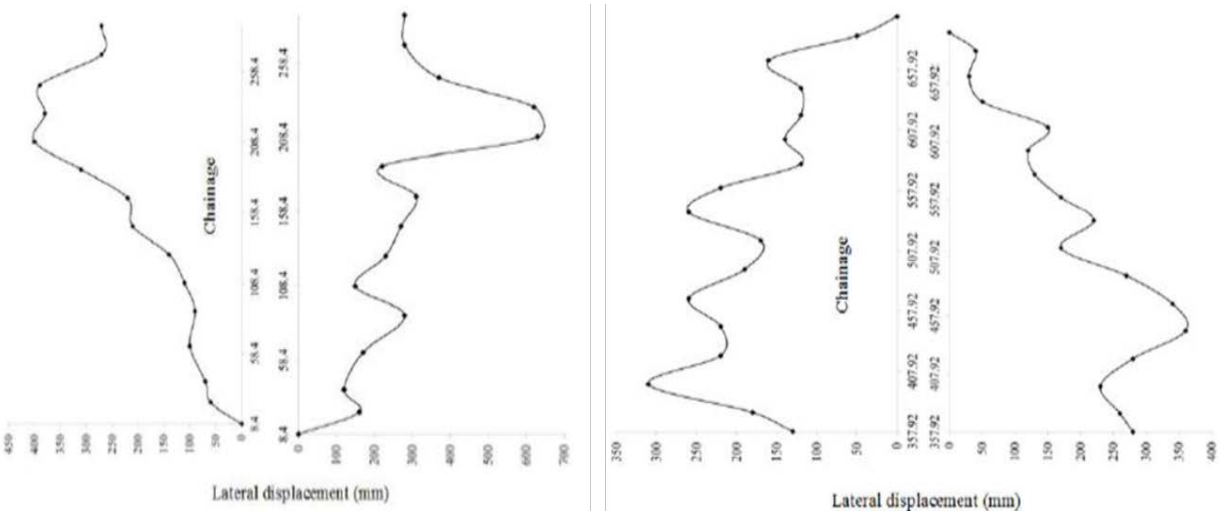

Figure 2. 53 Lateral Displacement patterns of retaining wall on the left and right side of the east end (Babu et al., 2016).

Actual field scenario of the laterally displaced wall is shown in Figure 2.54a. Due to the excessive lateral movement, separation between wall and road approach embankment was

observed; which resulted in distress on flexible pavement constructed on the embankment as shown in Figure 2.54b.

(a) (b)

Figure 2. 54 (a) Laterally displace wall in the field; (b) Distress on the flexible pavement as a result of lateral movement (Babu et al., 2016).

Sliding or lateral movement of MSE wall occurs when there is insufficient shear resistance against sliding force. The shear resistance generates from the shear force between foundation soil and the backfill material at the base of the MSE wall. Also the length of reinforcement introduces a considerable portion of resistance against sliding force. A low cost MSE wall without proper consideration for sufficient base shear resistance is bound to slide outward due to lateral earth pressure. As a result it might affect the structure near the base of the wall. Figure 2.55 shows distress in pavement resulting from lateral movement of a MSE wall adjacent to the base of the wall.

Figure 2. 55 Distress in pavement structure resulting from the lateral movement of MSE wall base (Schmidt and Harpstead, 2011).

2.3.11 Importance of Shear Key to Restrict Lateral Movement of MSE Wall

For a conventional retaining structure, the resistance against sliding is primarily due to friction between the foundation soil and the bottom of the base slab. This friction highly depends on the normal force from the weight of the wall and the weight of the backfill soil on the heel of the base slab. Higher the normal force greater is the frictional resistance. However, due to higher lateral pressure this resistance is not always sufficient to restrict the sliding of the wall. Therefore, two approach can be taken into consideration; one is to increase the weight of the wall or to increase the length of heel slab which is effective but expensive solution; the second approach is introduction of a shear key at the base slab of the wall. Figure 2.56 shows schematic of a conventional wall with shear key at the base slab. Use of shear key introduces

additional resistance against sliding through the generation of passive pressure from the soil in front of the shear key. Passive earth resistance increases with the increasing height of the shear key. Introducing a shear key is much more cost effective compared to the former approach. Even a small depth of shear key can generate considerable resistance against sliding. A study done by Sarath et al. (2011) showed that, use of shear key can almost completely resist the sliding tendency of the wall and increases the factor of safety against sliding significantly.

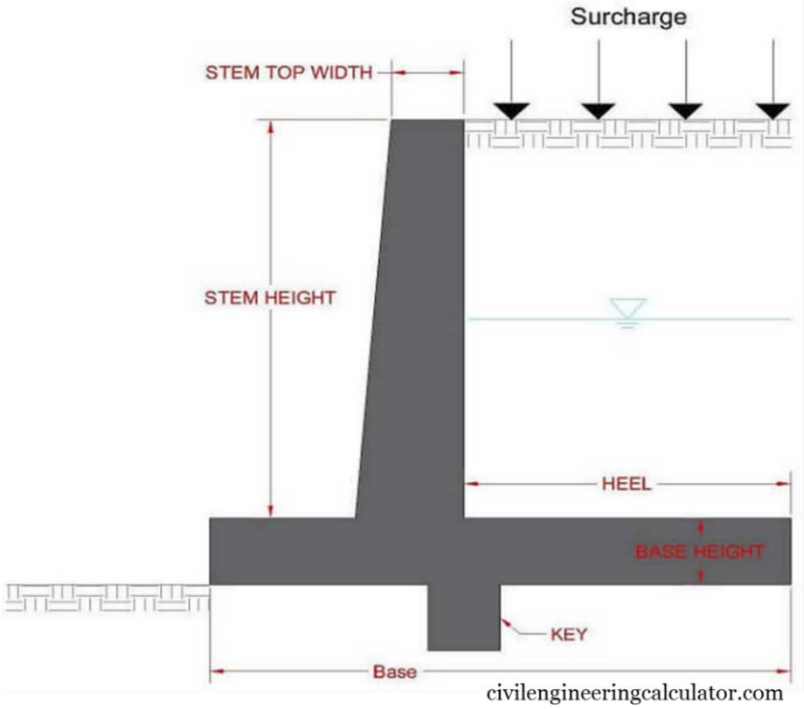

Figure 2. 56 Schematic of a conventional retaining wall with shear key to resist lateral movement.

The authors reported that the best location for shear key is under the heel which resulted in greater factor of safety. Also, by increasing the depth of the key sliding resistance can be significantly improved. The authors performed a numerical study using Plaxis 2D to show the effect of depth (0.5 m to 2 m) of shear key for varying φ values to increase the factor of safety against sliding. The results are shown in Figure 2.57.

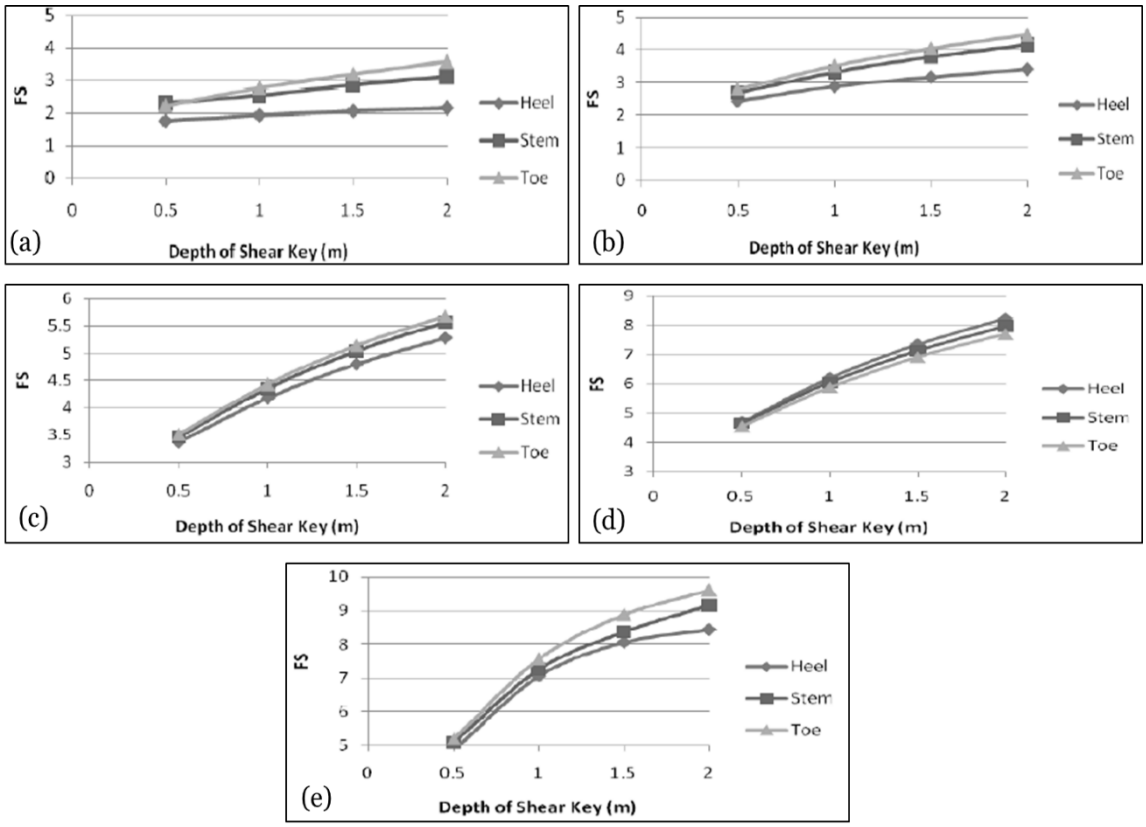

Figure 2. 57 Change in factor of safety with depth of shear key for (a) φ = 25°; (b) φ = 30°; (c) φ = 35°; (d) φ = 40°; (e) φ = 45° (Sarath et al., 2011).

Similarly, in case of MSE wall, if a sort of shear key can be introduced within base the structure, it can limit the lateral movement of the wall significantly by incorporating additional resistance due to passive earth resistance.

A study conducted by Kim and Bilgin (2007) showed that, concrete key size under the MSE retaining wall significantly reduces the lateral displacement of the wall. The authors studied the effect of concrete key size for varying lengths of reinforcement and friction angles of foundation soil. Commercially available finite element software, PLAXIS was used for performing numerical analysis. The model was developed by studying a 10 m-high MSE wall. It was reported that the longer key length is more effective in reducing deformation compared

to shorter reinforcement length. Figure 2.58 shows the detail geometry of MSE wall used for analyzed model.

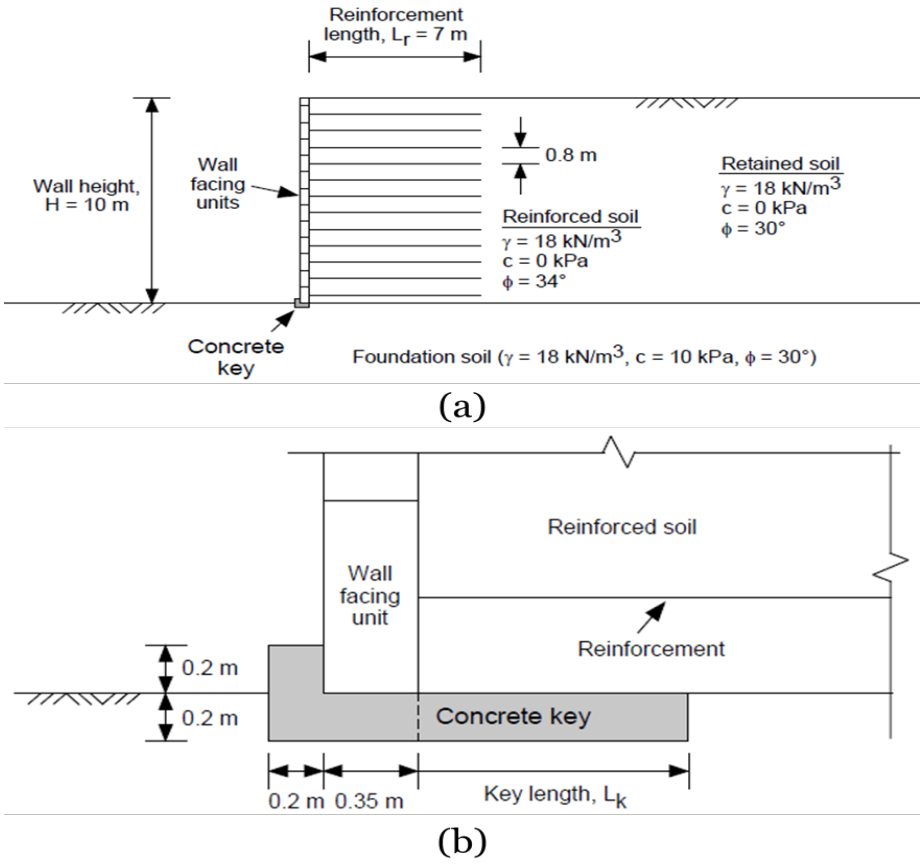

Figure 2. 58 Schematic and baseline model of MSE wall for numerical analysis; (a) Detail of MSE wall; (b) Detail of concrete key (Kim and Bilgin, 2007).

Kim and Bilgin (2007) used two-dimensional plane strain analysis for finite element modeling with triangular elements of 15-nodes. Soil layers were used to simulate loading, each lifts were of 2.62 ft. (0.8 m). The authors assumed one uniform soil layer as subsurface soil. Results from the parametric study showed that with the increasing size (length) of concrete key lateral deformation decreases regardless of the reinforcement length and foundation soil strength. Figure 2.59 shows the results generated in the study, where each curve is the representation of the final deformed shape of the wall face for varying key length (L_k), length

of reinforcement (L_r) and friction angle of foundation soil (φ_{sub}) values. The additional shear resistance generated due to the concrete key reduces the lateral movement of the wall facing significantly.

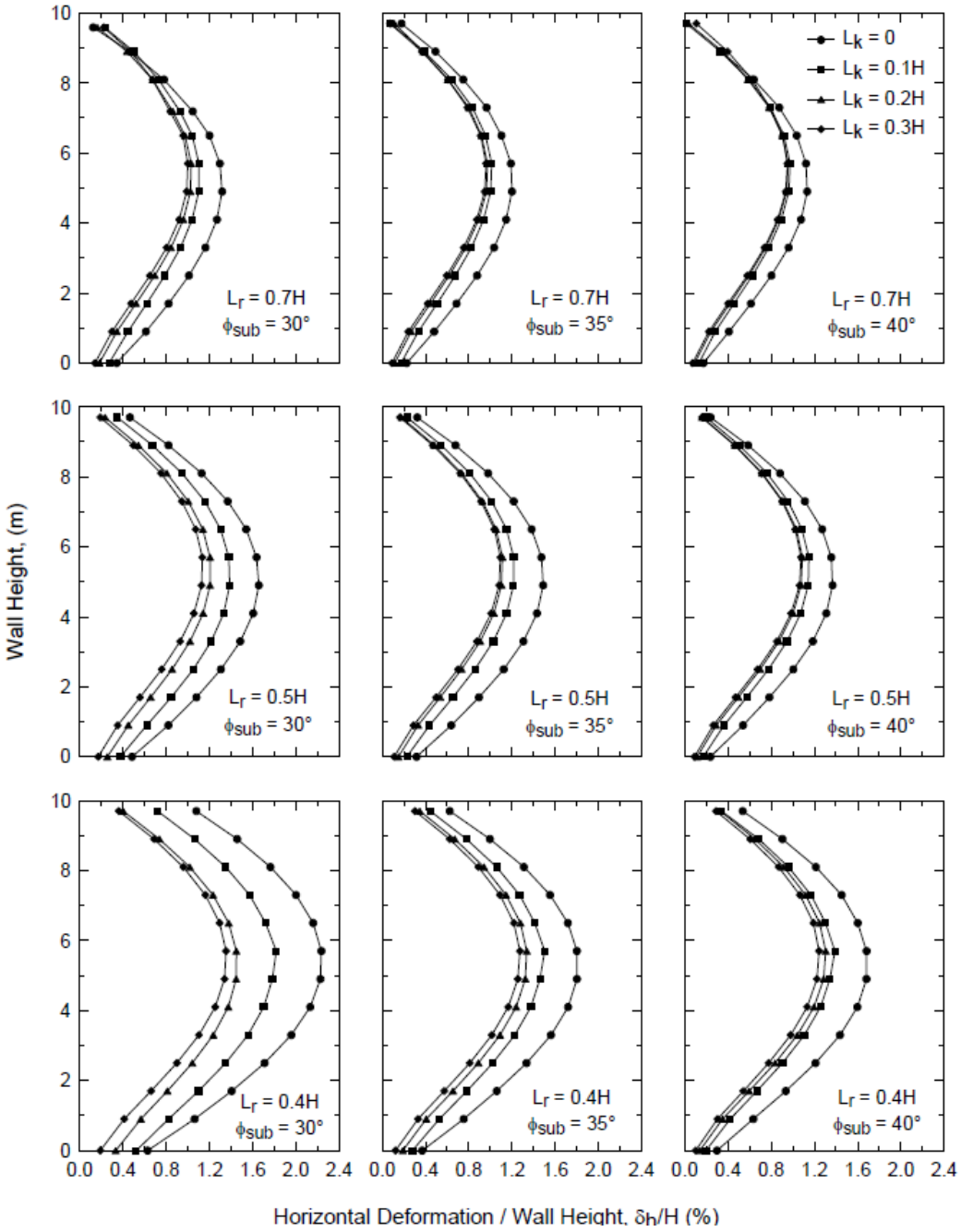

Figure 2. 59 Effect of concrete key on the lateral deformation of MSE wall (Kim and Bilgin, 2007).

However, concrete acts as a structural element which is rigid in nature and might limit the benefit of MSE wall to perform well under differential movement. Also, it is relatively expensive to construct a continuous concrete key. Therefore, a suitable and cost effective solution is necessary. Introducing piles at the base of the reinforced soil of retaining wall can be effective as they might act as composite structure to resist sliding and also improve factor of safety against global failure. However, concrete piles are expensive and timber piles are subject to degradation thus have much lower design life. Therefore, Recycled plastic pins can be such an alternative, which is a cost effective solution and also resistant to chemical and biological degradation.

2.4 Recycled Plastic Pins (RPP)

Recycled plastic pin is also commercially known as plastic lumber which is fabricated using recycled plastic and other waste materials like polymers, fly ash and saw dust (Chen et al., 2007). From the standpoint of environmental and life cycle cost analysis (LCCA), the recycled plastic pin (RPP) is under serious consideration as structural materials for marine and waterfront application (Khan, 2014). RPP is a sustainable material which require almost no maintenance and resistant to moisture, corrosion, rotting and insects. Typically, more than 50% of the feedstock used for plastic lumber composed of polyolefin in terms of high density polyethylene (HDPE), low density polyethylene (LDPE) and polypropylene (PP) (Khan, 2014). The polyolefin used in the combination acts as adhesive that helps combining high melt plastics and additives such as fiberglass, wood fibers within a rigid structure.

2.4.1 Green Engineering

According to EPA (United States Environmental Protection Agency), the design, commercialization, and use of products in a way that reduces pollution and waste, promotes sustainability, and minimizes risk to the environment without sacrificing viability and efficiency is termed as green engineering. An excellent example of green engineering can be Recycled Plastic Pins (RPP), which reduces the waste volume entering into the landfill, provides additional market for RPPs and can be an economical solution to numerous geotechnical projects.

The rapid growth of population resulted in an increased volume of waste generation. Annually, a total of 1.3 billion tons of municipal solid waste (MSW) is generated, which is expected to increase by almost double by the year 2025. 10 % of this waste is composed of plastic waste, which amounts to approximately 130 million tons. In USA, the amount of generated plastic waste is approximately 32.5 million tons, which is 13 % of the total waste volume. However, plastic waste occupies a large volume of landfill space, even though they are lightweight material. In addition, plastic waste, being a non-degradable part of the MSW stream, once buried in the landfill stays and occupies the space forever. Therefore, a huge landfill space can be saved if diversion and reuse of this non-degradable waste is ensured. At the same time, it ensures additional space availability for new waste and increases the operational life of a landfill.

The plastic and plastic products, being non-degradable, poses problem for landfill. However, this non-degradable nature becomes advantageous, when they are used in projects related to civil engineering infrastructure. RPP made out of recycled plastic bottles, when used

in slope stabilization, ground improvement or other purpose, they can perform well for a long time by preserving their engineering characteristics. This minimizes the overall repair and maintenance cost of the project. Hence, the use of RPP demonstrates the perfect example of sustainable engineering solution (Hossain et al., 2017).

2.4.2 Manufacturing Process of RPP

The production process of plastic lumber begins with collection of raw materials followed by cleaning and pulverizing the raw materials. Approximately 600 mineral water/soda bottles are used for one 4 in. x 4 in. RPP (Figure 2.60). The resulting product is melted in an extrusion machine at a production site. Two methods of manufacturing process for recycled plastic lumber are presented by Malcolm (1995) such as the Injection molding process and the continuous extrusion process.

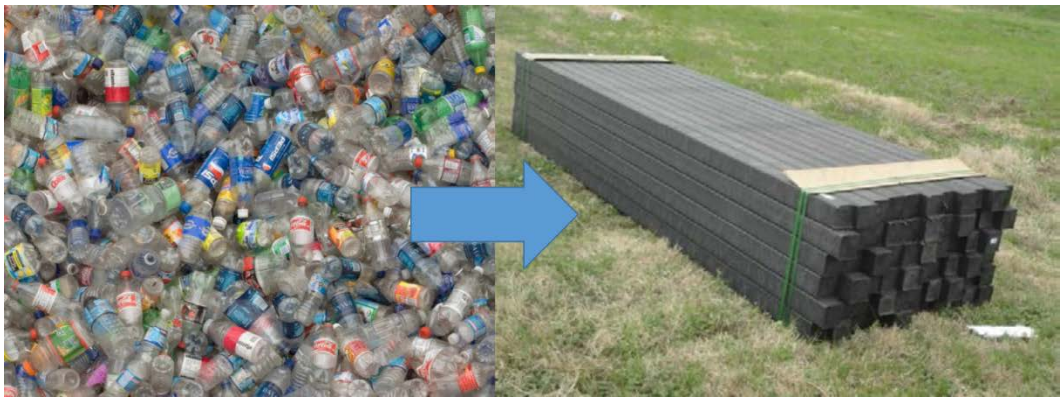

Figure 2. 60 Recycled Plastic Pins (Hossain et al., 2017).

The injection process involves injection of molten plastic into a mold that defines the shape and length of the product followed by uniform cooling and then removal of the finished product. This process is relatively simple and inexpensive; however, the volume produced is limited (Malcolm, 1995). On the other hand, the continuous extrusion process allows

production of varying length of the RPP. During this process, the molten plastic is continuously extruded through series of dies which shape the materials during its cooling. However, it becomes challenging to ensure uniform controlled cooling of the sample to prevent warpage and caving of the lumber. Also, a considerable investment is required in comparison to the injection molding process. However, the continuous extrusion process requires less labor and suitable for mass production.

Another widely used manufacturing process of the recycled plastic pin is the compression molding process (Lampo and Nosker, 1997) where other materials are mixed with batches consisting of 50-70% of thermoplastics by melting. An automatically adjusted scraper is used to remove the melted material from the plasticator followed by pressing it through a heated extruder die into premeasured, roll-shaped loaves. The loaves are then processed through a press-charging device that fills a sequence of compression molds alternately. The finished products are cooled to a temperature of 40 °C within the mold and ejected into a conveyor to be carried to a storage area.

2.4.3 Engineering Properties of RPP

Bowders et al. (2003) conducted a study on the different engineering properties of RPP to evaluate a wide varieties of production standard. As a part of the study uniaxial compression test and four point flexure test were performed; the results are presented in Table 2.8 and Table 2.9 respectively.

Table 2. 8 Uniaxial compression test results of different RPP samples (Bowders et al., 2003).

Specimen Batch	No. of Specimen tested	Nom. Strain Rate (%/min)	Uniaxial Compressive Strength (MPa)		Young's Modulus, $E_{1\%}$ (MPa)		Young's Modulus, $E_{5\%}$ (MPa)	
			Avg.	Std. Dev.	Avg.	Std. Dev.	Avg.	Std. Dev.
A1	10	-	19	0.9	922	53	390	27
A2	7	0.005	20	0.8	1285	69	378	15
A3	6	0.006	20	0.9	1220	108	363	27
A4	3	0.004	20	0.9	1377	165	363	25
A5	4	0.006	12	1	645	159	225	17
A6	4	0.006	13	0.9	786	106	238	34
B7	2	0.007	14	0.5	541	36	268	3
B8	2	0.006	16	0.4	643	1	308	0.5
C9	3	0.0085	17	1.1	533	84	387	40

Table 2. 9 Four point bending test results of various RPP samples (Bowders et al., 2003).

Specimen Batch	No of Specimens Tested	Nom. Def. Rate (mm/min)	Flexural Strength (MPa)	Secant Flexural Modulus $E_{1\%}$ (MPa)	Secant Flexural Modulus $E_{5\%}$ (MPa)
A1	13	-	11	779	662
A4	3	4.27	18	1388	-
A5	3	5.74	11	711	504
A6	4	3.62	10	634	443
B7	1	4.05	9	544	425
B8	1	5.67	-	816	-
C9	2	3.21	12	691	553

A comparative experimental study, following ASTM 695-85, on the compressive strength of Recycled Plastic Lumber on a total of 10 plastic samples, obtained from eight manufacturers having great variation in composition, was conducted by Lampo and Nosker (1997). The study included an effective cross sectional area which was calculated based on a specific gravity measurement to calculate the mechanical properties of the material. The authors reported that the compressive strength test was performed at 0.1 in/min rate. Based on the experimental results, the modulus, ultimate strength at 10% strain and yield strength at 2% offset were calculated from the load-displacement data.

To minimize effect of voids when comparing the material properties and effect from different extrusion method, the modulus and ultimate strength are normalized by dividing with specific gravity to determine specific modulus and specific strength. Based on the study, the compressive strength results are presented in Table 2.10. In addition, the comparisons of compressive strength between different samples are presented in Figure 2.61 and Figure 2.62.

According to the experimental study conducted by Lampo and Nosker (1997), the compressive strength for RPP lumber ranged between 1.74 to 3.5 ksi and the tensile strength varies between 1.25 to 3.5 ksi. However, it was also concluded that the RPP reaches its ultimate strength at different strain level compared to softwood.

Table 2. 10 Average values of specific gravity, modulus, specific modulus, yield stress, ultimate stress, ultimate strength and specific strength for each sample type of RPP (Lampo and Nosker, 1997).

Sample	Specific Gravity	Modulus (ksi)	Specific Modulus (ksi)	Yield Stress (ksi)	Ultimate Strength (ksi)	Specific Strength (ksi)
51A	0.2789	38.00	121.83	0.71	0.78	2.80
1B	0.7012	61.93	88.33	1.38	1.89	2.70
2D (BR)	0.8630	85.28	98.92	1.67	2.32	2.69
2D (G)	0.8098	116.03	143.30	2.10	2.86	3.53
1E	0.862	80.79	93.84	1.77	2.42	2.81
1F	0.7888	108.20	137.06	2.19	2.81	3.56
1J(B)	0.7534	93.26	123.86	1.90	2.36	3.13
1J(W)	0.9087	110.08	121.25	2.16	2.83	3.11
23L	0.7856	191.45	243.66	1.71	1.93	2.46
1M	0.5652	57.87	102.25	0.96	1.23	2.18
1S	0.9090	80.50	88.47	1.67	2.05	2.26
1T	0.8804	117.92	133.58	2.25	3.12	3.54
9U	0.774	86.73	111.53	1.83	2.41	3.11

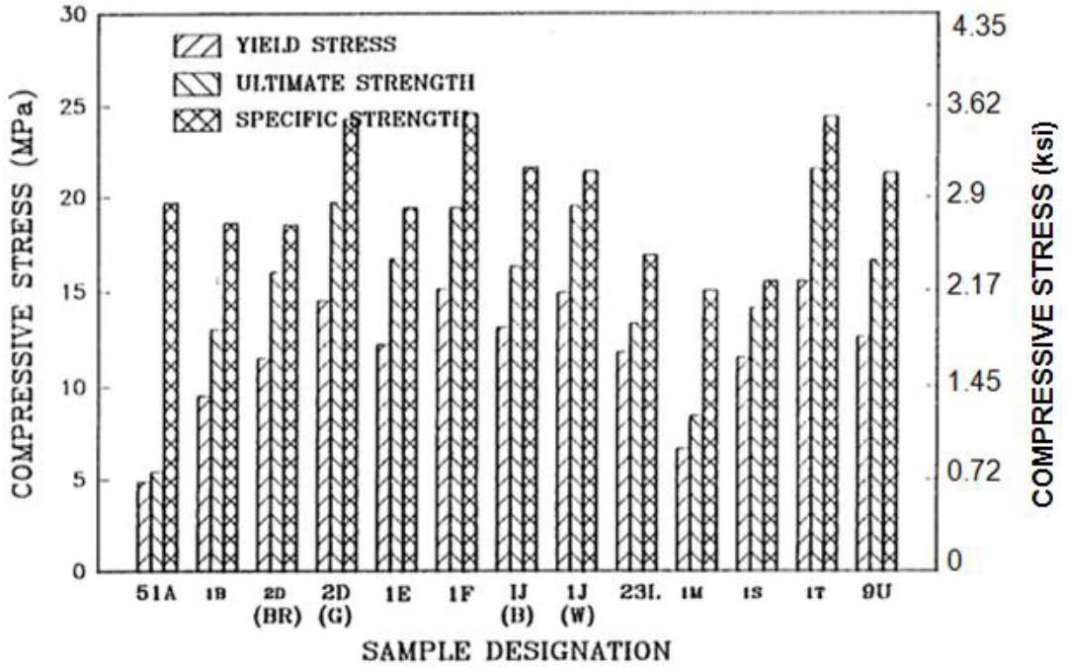

Figure 2. 61 Comparison between compressive strength of RPP (Lampo and Nosker, 1997).

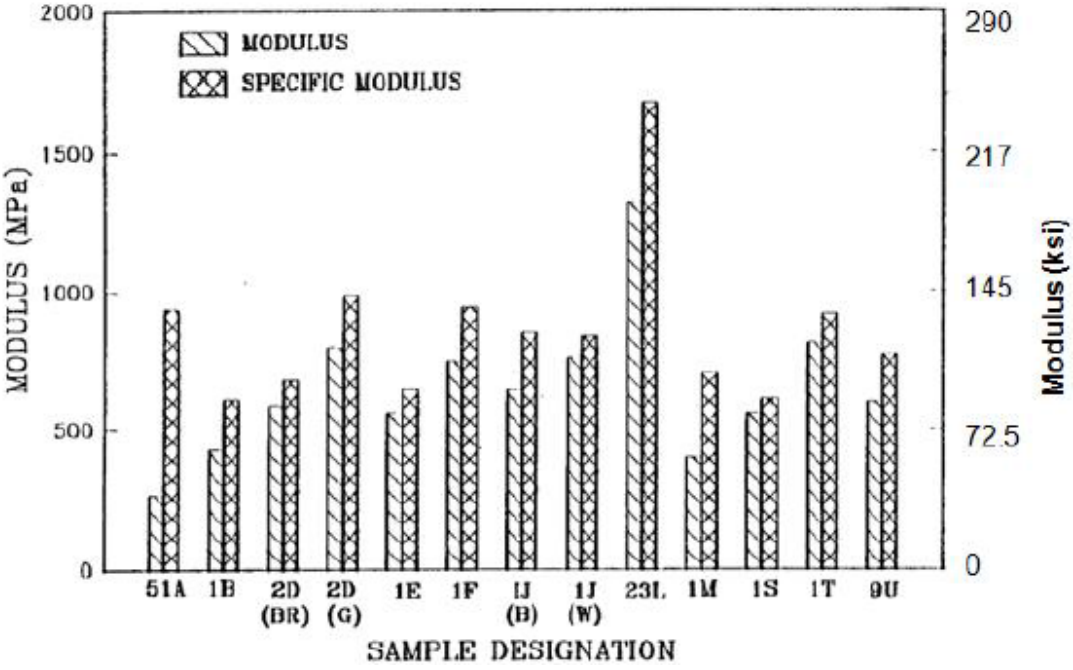

Figure 2. 62 Comparison between Compressive modulus of RPP (Lampo and Nosker, 1997).

A study conducted by Breslin et al. (1998) showed the comparison between different test results from literature as presented in table 2.11. The authors reported that adding different

additives like fibers, glass, polystyrene etc. into plastic lumber increases the stiffness of the final product.

Table 2. 11 Engineering properties of recycled plastic pins (Breslin et. al, 1998).

Product	**Composition**	**Compressive Strength (psi)**	**Modulus of Elasticity (psi)**	**Tensile Strength (psi)**	**Source**
TRIMAX	HDPE / Glass Fiber	1740	450 000	1250	TRIMAX literature SUNY at Stony Brook
TRIMAX	HDPE / Glass Fiber			1189	www.lumberlast.com
Lumber Last	Commingled recycled plastic	3755 (ultimate) (D198)	140 000 (D790)	1453 (ultimate) (D198)	www.ecpl.com
Earthcare recycled maid	Post-consumer milk jugs	0.79 (Density)	3205 (D695)	93 000–102 500 (D790)	Zarillo and Lockert (1993)
Hammer's plastic	80%HDPE/20%LDPE	2708	89 814		Zarillo and Lockert (1993)
	HDPE/LDPE (20PSGF)	4247	527 000		
	HDPE/LDPE (40PS20GF)	3514 (D695)	653 000 (D790)	1793 (D638)	
Superwood Selma, Alabama	33%HDPE/33%LDPE/33%PP	3468 (D695)	146 171 (D790)	1793 (D638)	Beck, R. (1993)

Table 2. 11 Engineering properties of recycled plastic pins (Breslin et. al, 1998). (contd.)

Product	Composition	Compressive Strength (psi)	Modulus of Elasticity (psi)	Tensile Strength (psi)	Source
California recycling company	100% Commingled	81 717			Beck, R. (1993)
	10% Polypropylene	79 319			
	50% HDPE	92 636 (D790)			
RPL-A	HDPE/Glass fibers	2000			Smith and Kyanka (1994)
RPL-B	49% HDPE/51% wood fiber				Smith and Kyanka (1994)
Rutgers University	100% Curb tailings	3049	89 500		Renfee et al. (1989)
	60% Milk bottles, 15% Detergent bottles, 15% Curb tailings, 10% LDPE	3921	114 800		Renfee et al. (1989)
	50% Milk bottles, 50% Densified PS	4120 (D695)	164 000 (D790)		
Earth care products	HDPE		173 439 (D790)		www.ecpl.com
BTW recycled plastic lumber	Post-consumer	1840–2801	162 000		BTW/Hammers Brochure

Plastic is susceptible to temperature. At higher temperature it is weak and shows ductile behavior; however, at lower temperature plastic is much stronger and brittle in nature. Figure 2.63 presents the effect of temperature change on tensile strength of HDPE (Malcolm 1995).

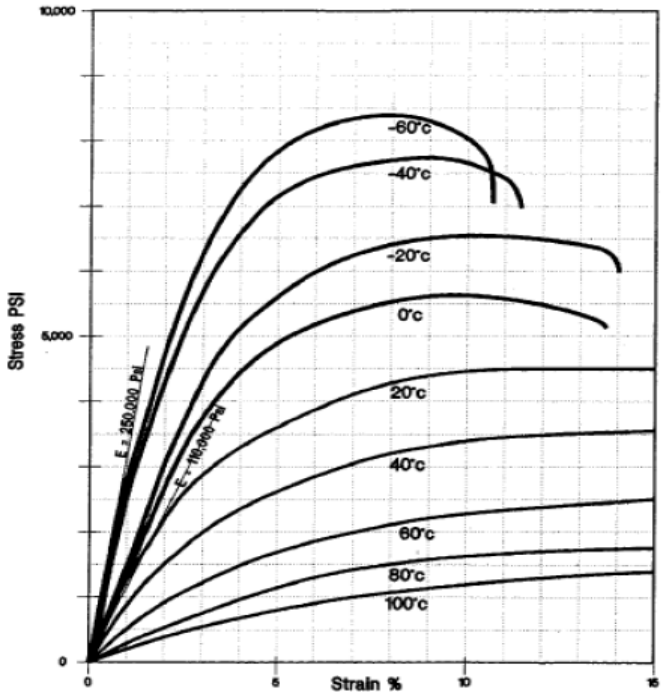

Figure 2. 63 Tensile strength of HDPE for different temperature (Malcolm, 1995).

Ahmed (2012) conducted a comparative study between RPP, wood and bamboo piles. Based on the study, wood showed to have highest compressive and flexural strength among these three alternatives; however, RPP has the advantage of facilitating greater soil movement which was found to be upto 19%. The most attractive part that led to the consideration of using RPP in place of other alternatives is its ability to perform well under different environmental and chemical conditions. The author reported that, for different environmental conditions the maximum decrease in RPP strength was only 8%, whereas for wood and bamboo the value was found to be about 50% and 65% respectively. The durability and strength properties of RPP presents it to be a potential economic alternative over other materials.

2.4.4 Long Term Engineering Properties of RPP

Breslin et al. (1998) conducted a study on the long term engineering properties of RPP. During the study, the plastic lumber samples were removed from the deck and taken to the laboratory for testing. At the beginning the authors investigated the initial engineering properties of recycled plastic pins that was manufactured by continuous extrusion process. For the long term properties test, the plastic lumbers were collected at 2 year intervals during monitoring periods. The authors reported that there was not any noticeable change such as warping, cracking and discoloration in the RPPs.

The effect of outdoor weathering and environmental effects including the degradation due to UV radiation, thermal expansion and combined effects of moisture and temperature on the mechanical behavior of RPP were determined by Krishnaswamy and Francini (2000). No significant variation of the flexural modulus and strength of RPP according to ASTM D6109 before and after the hygrothermal cycling, as presented in Table 2.12.

Table 2. 12 Comparison of flexural properties of RPP before and after hygrothermal cycling (Krishnaswamy and Francini, 2000).

	Secant Modulus (psi)	**Stress at 3% strain (psi)**
Before cycling	97,800 ± 6,400	1,900 ± 120
After cycling	113,600 ± 14,400	2,400 ± 400

Lynch et al. (2001) conducted a study to investigate the effect of weathering on the mechanical behavior of recycled HDPE based plastic pins. A three point bending test was performed to obtain the flexural properties of weathered deck boards to compare against

original flexural properties as per ASTM D796. Before the weathering action, the original flexural properties was determined to be 171 ksi for flexural modulus and 2.5 ksi for flexural strength. The three-point bending test results of the weathered samples obtained from the study are presented in table 2.13 and table 2.14.

Flexural properties of RPP when the exposed and unexposed side was tested in tension, are presented in table 2.13 and table 2.14 respectively. Comparison between the two results suggests that both modulus and strength increased after the outdoor exposure. Based on the results, it was found that the modulus increased by 28% and 25% when the exposed and unexposed sides are tested in tension respectively. In addition, for both cases, the strength at three percent strain increased by 4% from the original value.

Table 2. 13 Results of three-point bending test of different RPP samples after weathering (exposed surface was subjected to tension) (Lynch et al., 2001).

Sample	**Modulus (ksi)**	**Strength at 3% strain (ksi)**	**Ultimate strength (ksi)**
1A	240.47	2.77	3.43
2A	213.79	2.48	3.12
3A	200.88	2.44	2.86
4A	214.22	2.55	3.32
5A	227.42	2.73	3.31
AVERAGE	219.30	2.59	3.21

Table 2. 14 Results of three-point bending test of different RPP samples after weathering (unexposed surface was subjected to tension) (Lynch et al., 2001).

Sample	Modulus (ksi)	Strength at 3% strain (ksi)	Ultimate strength (ksi)
1B	217.56	2.77	3.49
2B	204.50	2.47	3.05
3B	190.29	2.45	3.05
4B	219.30	2.43	3.11
5B	234.67	2.76	3.25
AVERAGE	213.26	2.58	3.19

2.4.5 Creep of RPP

The recycled plastic pin is a nearly isotropic material having considerable strength, durability and workability which can be reinforced to increase the strength by forming a composite material. It is strong as wood; however, being visco-elastic material, it is susceptible to creep and deflection under sustained load. A study conducted by Malcolm (1995) showed the creep behavior of a 3.5 in. x 3.5 in. RPP under sustained mid span bending stress of 516.70 psi. Figure 2.64 presents the generated creep curve in this study.

According to Chen et al. (2007), variety in manufacturing process is responsible for variation in engineering properties of commercially available materials. The polymeric materials show higher creep compared to timber, concrete or steel, while they are more resilient against environmental degradation. Van Ness et al. (1998) tested on RPPs collected from various commercial sources and concluded that, RPP containing oriented glass fiber is more resistant against creep.

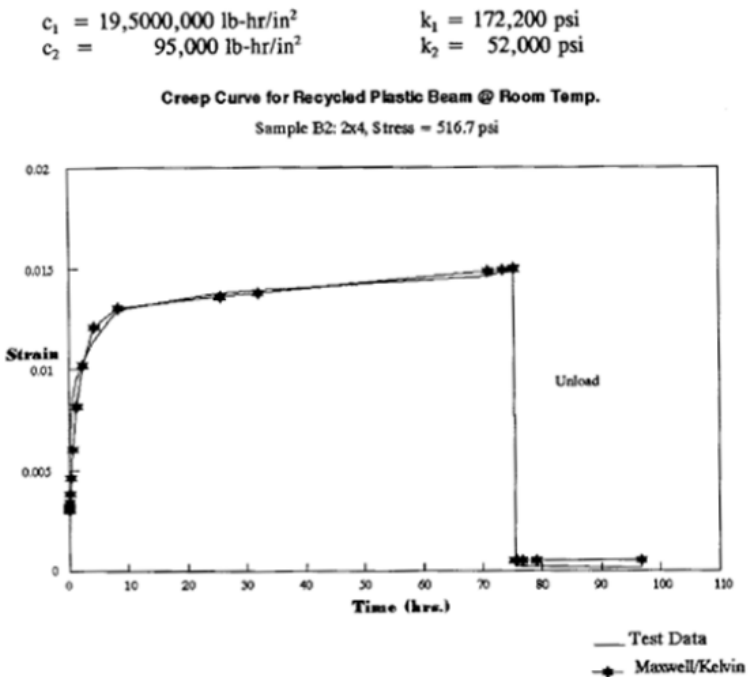

Figure 2. 64 Creep behavior of RPP beam at room temperature (Malcolm, 1995).

Lampo and Nosker (1997) reported that, for any load bearing application, creep is a serious concern while using RPP. Inheriting the viscoelastic properties of plastic, a plastic lumber will sag under static sustained loading which increases with increasing temperature. Civil engineers generally study this time dependent variable to develop load-duration factors for design purpose. To develop the design guideline for plastic lumber, this effect is extremely crucial which should be taken into account.

2.5 Utilization of Recycled Plastic Pin for Geotechnical Projects

Recycled Plastic Pins (RPP) are becoming more and more popular as a cost effective and sustainable solution for slope stabilization compared to conventional techniques (Loehr and Bowders, 2007, Khan, 2014). Compared to other piles, e.g. concrete or steel piles or other structural materials, RPP weighs much less and is more resistant to chemical and biological degradation. The compressive strength of each RPP is sufficient enough to carry vertical load

from the structure above. In addition, previous studies showed the use of RPPs in the failed area of the slope to provide additional resistance along the sliding plane to increase factor of safety. The theoretical calculation as well as practical application proved that RPP is suitable to resist lateral load and increase the factor of safety of highway slopes. Therefore, it might also be used effectively as reinforcement to act as a shear key and provide additional resistance against sliding or lateral loading for any retaining type structure for example MSE retaining structures.

2.5.1 Field Performance of RPP

Parra et al. (2003) conducted a field performance study on slope sites that had been stabilized with RPP. The authors reported that the sites experienced recurring surficial sliding, ranging from depth of 3 ft. (0.9 m) to 5 ft. (1.5 m). It has to be noted that the soil in the sites were composed of mainly clayey soil. Khan (2014), had presented field performance and numerical modeling of RPP for shallow slope stabilization. Field performance of RPP based on their analysis are discussed in the following sub-sections.

2.5.1.1 Interstate-70 (I-70) Emma Field Test Site

The test site is located on I-70, about 65 mi (105 km) west of Columbia, Missouri, having a slope height of 22 ft. (6.7 m) with 2.5H: 1V side slope that forms eastbound entrance ramp to I-70 in Saline County. The slope soil is composed of mixed lean clays with scattered cobbles and construction rubble (concrete & asphalt). The slope experienced recurring slides over the past few decades in four areas of the embankment, denoted as S1, S2, S3 and S4 as shown in the Figure 2.65a. Slide areas of S1 and S2 were considered and stabilized with RPP while area S3 and S4 served as control section. A 3 ft. (0.9m) staggered grid covered the failed

area for stabilization based on the laboratory test results on soil samples and back analyzed failure condition. The installation of the RPP took place during November and December of 1999 and the installation was done approximately perpendicular to the slope. For the S1 area a total of 199 pins were installed and for S2 area total installed pins were 163; the layout is shown in Figure 2.65b.

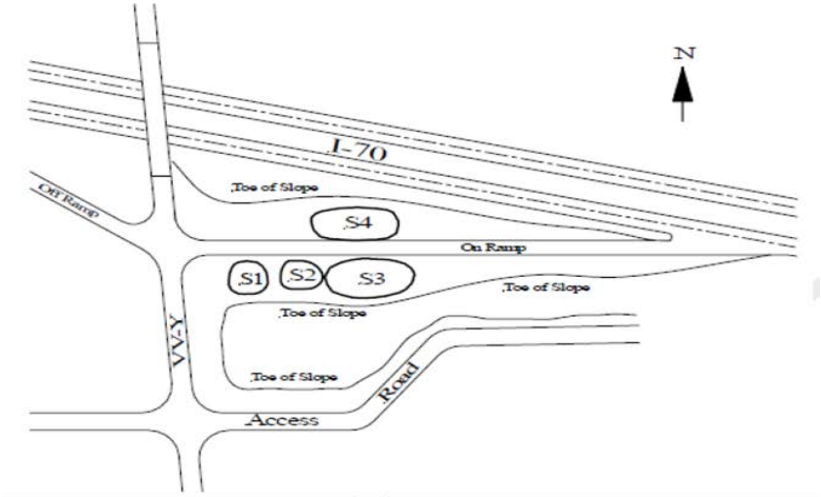

(a)

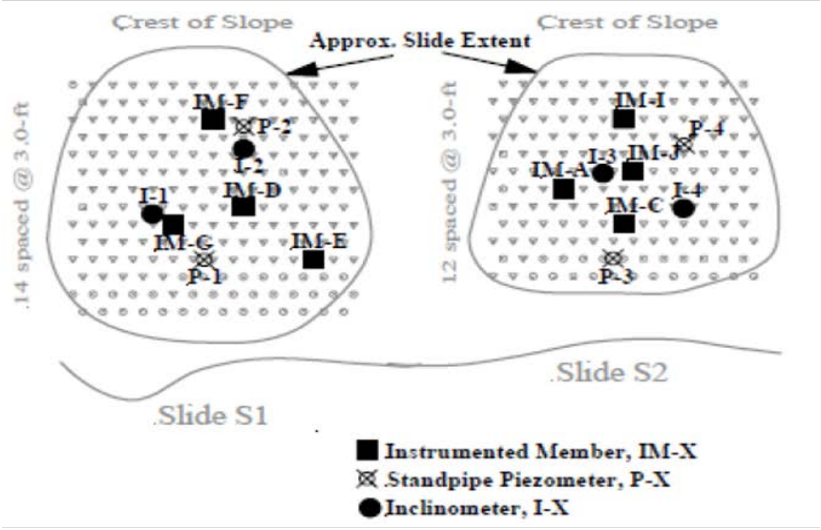

(b)

Figure 2. 65 (a) I-70 site slide areas Location; (b) RPP layout plan for the slide area S1 & S2 (Parra et al., 2003).

Inclinometers were installed to monitor lateral displacement of the sections. Figure 2.66 presents the depth vs. cumulative lateral displacement and cumulative lateral displacement vs. time plot developed from field monitoring data. Based on the data, it was reported that, for the first year the movement was minimum followed by an increased maximum movement of about 0.8 inches (20 mm) during next 6 months. After that, the lateral movement became minimum. According to Parra et al. (2003), the control sections (S3 and S4) failed during late spring while in the reinforced sections, very small movement was observed.

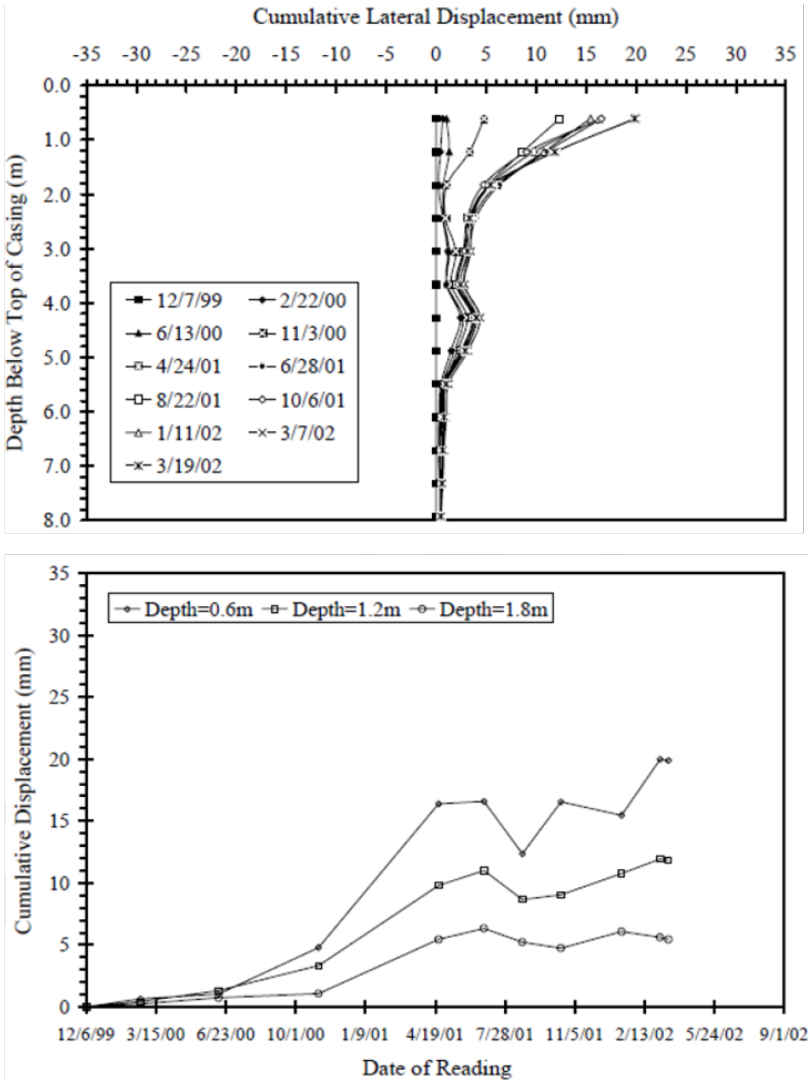

Figure 2. 66 Performance monitoring from Inclinometer I-2 at I-70 Site (Parra et al., 2003).

2.5.1.2 US 287 Slope Site

The slope site is located over Highway US 287, near the St. Paul overpass in Midlothian, Texas. The location is presented in Figure 2.67. The slope was constructed during 2003 – 2004 with a maximum slope height of about 30 to 35 ft. and a side slope of 3H: 1V. Cracks were observed near the shoulder during September 2010, which eventually resulted in the need for the slope to be stabilized to restrict further movement.

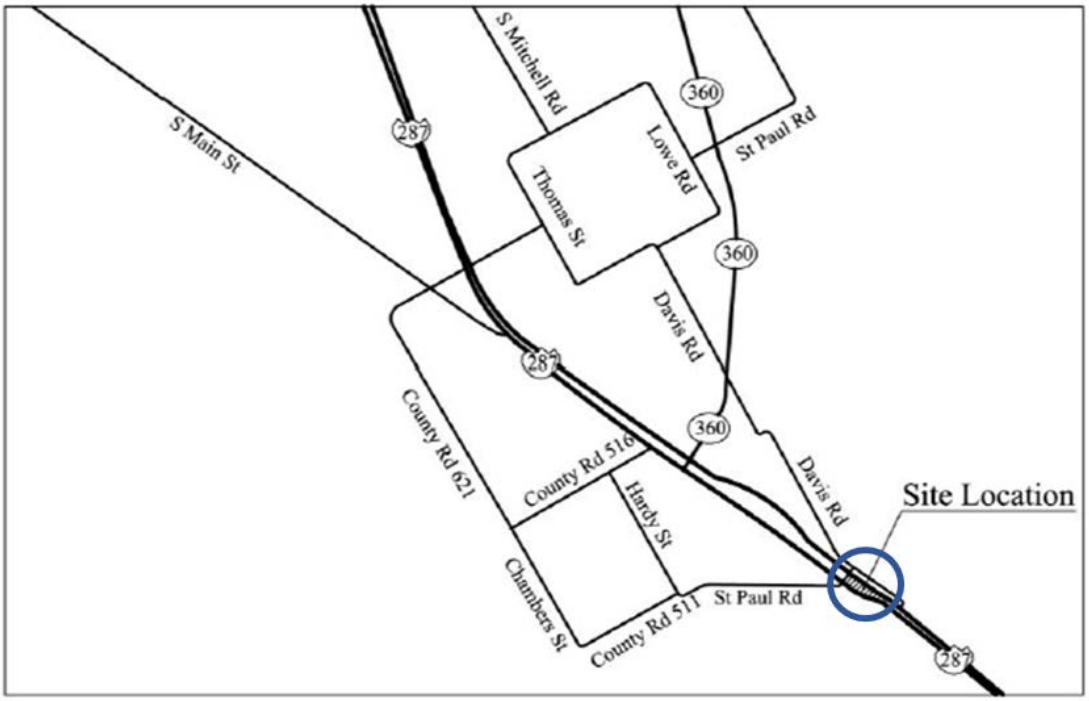

Figure 2. 67 Site location map for the slope at US 287 (Khan, 2014).

Three 50 ft. sections were selected and two of them were reinforced with RPP while the third one served as a control section. The layout of RPP installed in site US 287 is presented in Figure 2.68. Slope movement was monitored using three inclinometers for three sections.

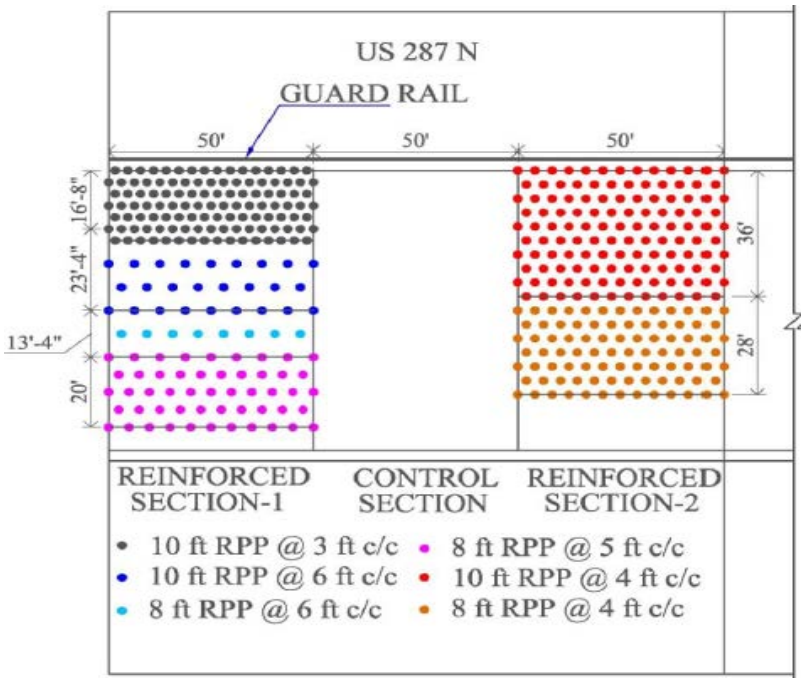

Figure 2. 68 Proposed layout of RPP for the slope at US 287 (Khan, 2014).

The performance monitoring results of the US 287 slope indicated that the unreinforced control sections had significant settlement (as much as 15 inches) at the crest of the slope. In addition, a total of 3 inch increments in settlement had taken place during the year. However, almost no increment in settlement was observed at the reinforced section. A total settlement of the reinforced section was found to be 2 to 4 inch, which was significantly less compared to the unreinforced section. Figure 2.69 and Figure 2.70 presents the total and incremental settlement for control and RPP reinforced test sections respectively. The lateral displacement of the test section had taken place after 1 year of construction which was about 1.5 inch. After 1 year the horizontal displacement became less than 0.1 inches in the reinforced section. A total of three inclinometers were installed to monitor the horizontal displacement; inclinometer 1 and 3 was installed in the reinforced section 1 and 2, while inclinometer 2 was installed in control section. Figure 2.71 presents the results of inclinometer 1 and 3. From the results, it

can be noticed that after the initial movement during the load mobilization period (little more than a year) the movement became almost constant. For the inclinometer 1, maximum horizontal movement was observed to be 1.3 inches while for inclinometer 3, it was found to be 1.8 inches.

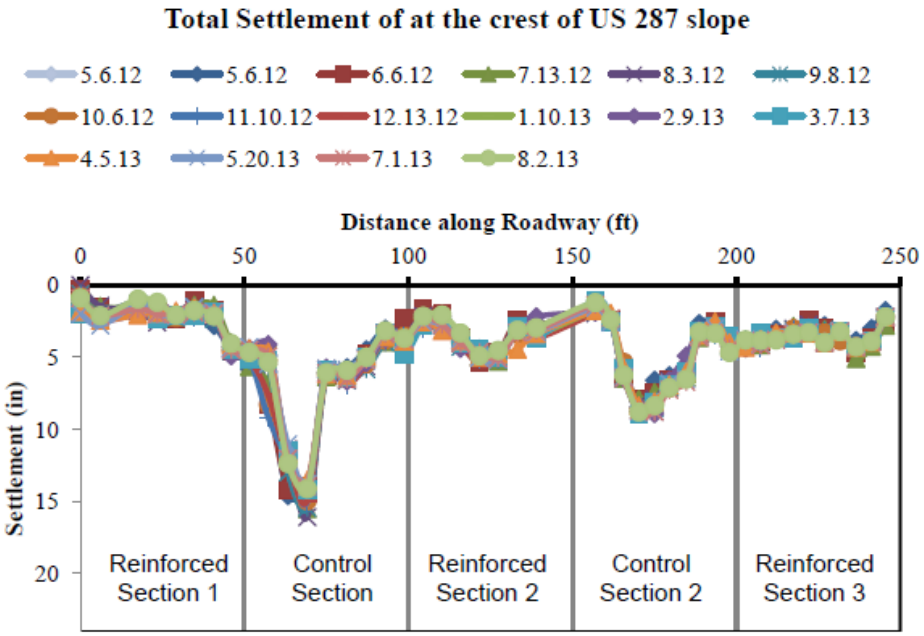

Figure 2. 69 Total Settlements with time along the Crest of US 287 Slope (Khan, 2014).

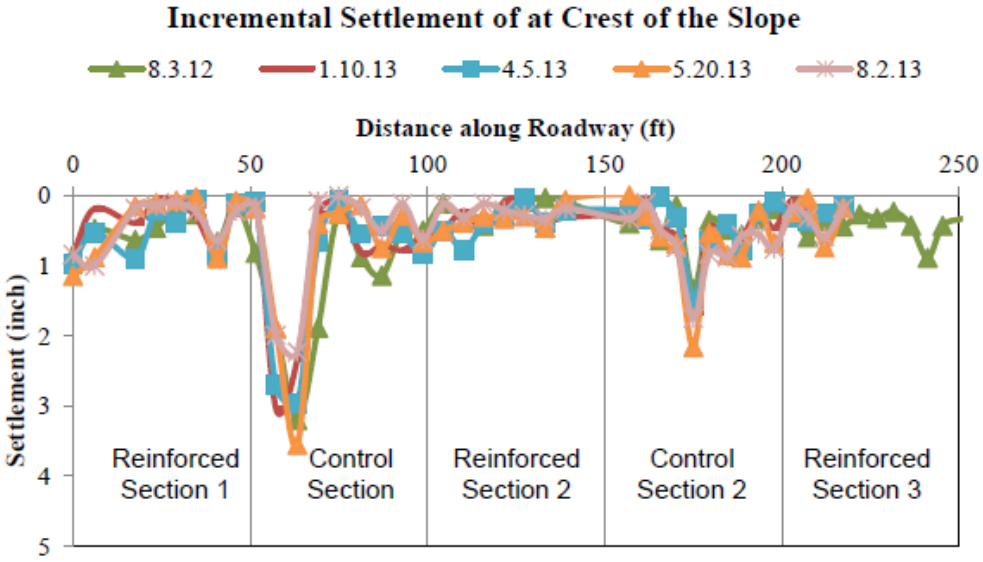

Figure 2. 70 Incremental Settlements in US 287 Slope (Khan, 2014).

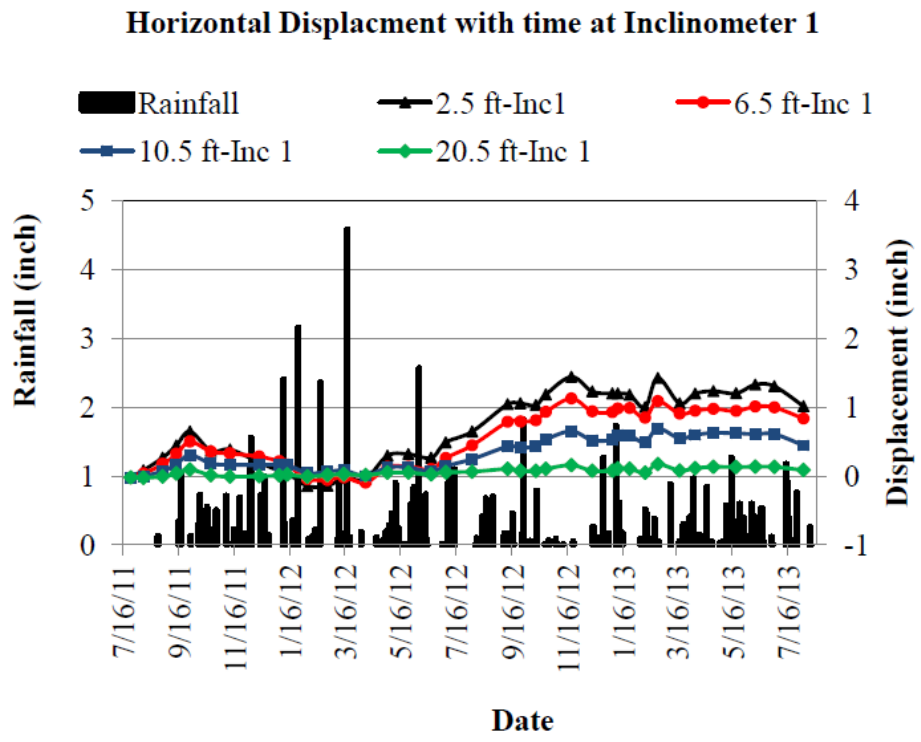

(a)

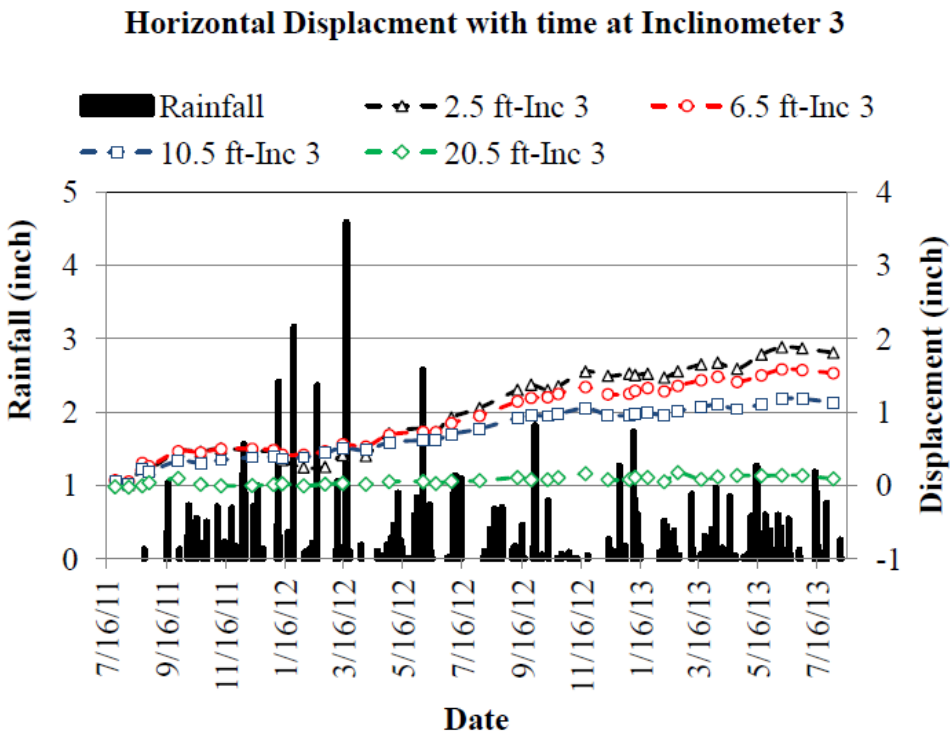

Figure 2. 71 Variation in Horizontal Displacement for the (a) Reinforced Section 1, and (b) Reinforced Section 2 (Khan, 2014).

CHAPTER 3

METHODOLOGY

This chapter presents the adopted methodology for the current study. Site selection, site investigation, sample collection and testing, field installation and instrumentation are discussed in this chapter.

3.1 Project Background

The objectives of the current study was to establish a new, efficient, cost effective and sustainable method for improving unsuitable foundation soil, i.e. to improve the bearing capacity of weak soil and to increase the sliding resistance or shear resistance of the MSE wall base, using Recycled Plastic Pins. Most of the cases, in north Texas region, top layer (2 – 5 ft.) of soil is not suitable as foundation for road embankment. For sites with weak foundation soil, it is sometimes more economical to provide a ground (foundation) improvement plan to allow the safe use of the superstructures rather than changing the type of structures. However, if the foundation soil is very stiff, and MSE retaining structures are constructed over it, chances of base sliding becomes much higher compared to the bearing capacity failure. Therefore, use of RPP might become a potential solution to improve the bearing and shearing capacity of such soil types. If used appropriately in the weak foundation soil, RPP might increase the load bearing capacity of the soil by transferring a significant portion of the load from the structure to a deeper stiff layer as well as densifying the soft soil layer. In addition, RPP might act as shear key at the base of the MSE wall if utilized in a proper designed manner and increase the sliding resistance of the MSE wall base.

To successfully evaluate the effectiveness of RPPs, a field scale study needed to be conducted. Therefore, a number of test sections were constructed with and without the reinforcement (RPP). The appropriate site location for the construction of the test sections were identified based on the site investigation. Site selection was followed by the field installation and instrumentation of the test sections. The field investigation and study on the test sections were conducted in two phases; phase I included construction of the vertical and lateral loaded test sections in the selected site location. In phase – II, loading height at the back of the wall in the lateral loaded test sections was increased for further testing; while for the bearing capacity analysis, new site location was selected and new vertical test sections were constructed for verifying the results obtained from phase – I.

3.2 Site Investigation

Site investigation is very important to determine the suitability of any location that will serve the purpose of research. The site investigation work was carried out according to the recommendation of TxDOT Geotechnical Manual, Section 1- “Soil Survey”. Prior to the commencement of site investigation, site boundary was set up and appropriate number of boring locations were marked at a distance of about 100 ft. for soil drilling.

3.2.1 Drilling

Continuous-flight augers were used for drilling and required power was delivered from the truck mounted drilling rigs. Continuous-flight auger used was 5 ft. long with an inside diameter of 2.75 inches. Tip of the auger was attached to a cutter head and each of the subsequent sections are added to increase the reach of the drilling rig to go deeper. During drilling, the pilot assembly and center rods were removed after certain depth for the collection

of soil sample and conducting Standard Penetration Test (SPT). A total of eleven drillings were conducted for several site investigation with a total drilling depth of about 20 ft. Disturbed/remolded soil samples were collected and stored in airtight containers/zip lock bags to preserve the field moisture content. Figure 3.1 shows the setup of drilling rig and collection of remolded samples.

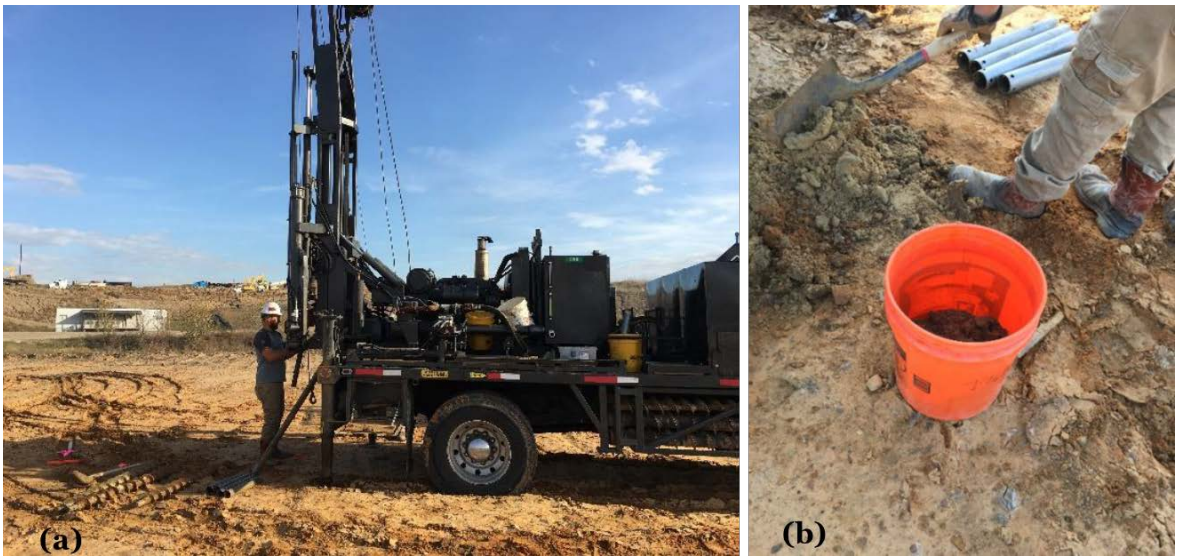

Figure 3. 1 (a) Drilling Rig set up; (b) Collection of remolded sample.

3.2.2 Undisturbed Soil Sample Collection

Undisturbed soil sampling was carried out by using a thin-walled Shelby tube sampler with outer diameter of 3 inch. Prior to soil sampling, bottom of the hole was measured to confirm the depth at which the soil sample was taken. The sample tube was lowered down to the bottom of the hole and pushed into the soil. When the sample tube reaches the required depth, the tube was then carefully taken out to the surface. An extruder was used to extrude the undisturbed soil sample from the Shelby tube sampler as shown in Figure 3.2a. To retain the field moisture, extruded samples were covered with a moisture bag and carefully stored in

a storage box (Figure 3.2b) before transporting to the laboratory for testing. In this project, 3 undisturbed soil samples were collected for each bore holes.

(a) **(b)**

Figure 3. 2 (a) Extruding undisturbed sample; (b) Undisturbed soil samples in a storage box.

3.2.3 Standard Penetration Test

The standard penetration test was carried out in accordance with ASTM D 1586, which is also recommended by the TxDOT Geotechnical manual. This method covers the determination of resistance of penetration of a split barrel sampler and obtaining disturbed soil for identification purpose. The split barrel sampler was driven into the soil by means of a 63.5 kg hammer, falling freely from a height of 30 inch onto an anvil which is attached to the top of the rod. A trip release mechanism and guiding assembly was used to control the falling hammer and the driving energy was thus transmitted through the rods to the SPT sampler. The sampler was driven 18 inch into the soil and the number of blows required for each 6 inch of penetration was recorded. The blow count for the last 12 inch of penetration was considered as the SPT N-value.

For safety reasons, it is recommended that boreholes should be plugged after the drilling has been completed with backfill materials, cement grouting or preferably bentonite. Hence, Bentonite slurry was used to plug the boreholes as shown in the Figure 3.3.

Figure 3. 3 Preparation of Bentonite Slurry. (b) Filling drilling holes with Bentonite slurry.

3.3 Laboratory Testing

Laboratory tests were performed on both undisturbed and disturbed/remolded samples. Strength test was performed on undisturbed samples and physical and mechanical properties were determined with the remolded samples taken from the field. The laboratory tests included moisture content test, Atterberg limit test and unconfined compression tests.

Moisture content of the soil samples collected from different depths, were determined according to the standard test method ASTM D4643 – 08.

Atterberg limit test, i.e., the liquid limit and plastic limit test, as described in ASTM standard D4318 were performed for samples collected from different depths.

The purpose of UCS test is to determine the unconfined compressive strength of cohesive soil sample. Soil strength was measured with the universal master loader capable of performing unconfined compression test, which is an unconsolidated undrained (UU or Q-type) test where the lateral confining pressure is equal to zero (atmospheric pressure).

3.4 Site Selection

For the current study, a suitable study location was required for the construction of the test sections to assess the effectiveness of RPP in improving the bearing capacity of weak foundation soil and increasing the sliding resistance of the MSE wall base. A total of four location was selected for soil investigation, which was carried out in two phases. Each phase included investigation of two locations for identifying appropriate soil condition, for the purpose of constructing the test sections. For field scale investigation, considerably soft foundation soil was required for the sections to be tested for bearing capacity improvement; while for test sections to assess increase in lateral resistance for MSE wall base, stiff foundation with a slope at the back was required. The following sub-sections includes the investigation reports and selection of the appropriate location.

3.4.1 Site Investigation for Location 1

The first site was located near the active zone of the City of Denton Landfill, Denton, Texas as shown in Figure 3.4a. This area of the site location was about 22,000 sq. ft. and easily accessible through the hauling routes. Figure 3.4b shows the condition of the site of location 1. This section represents the soil investigation results based on three borings conducted on the Location 1 during 2nd December, 2016.

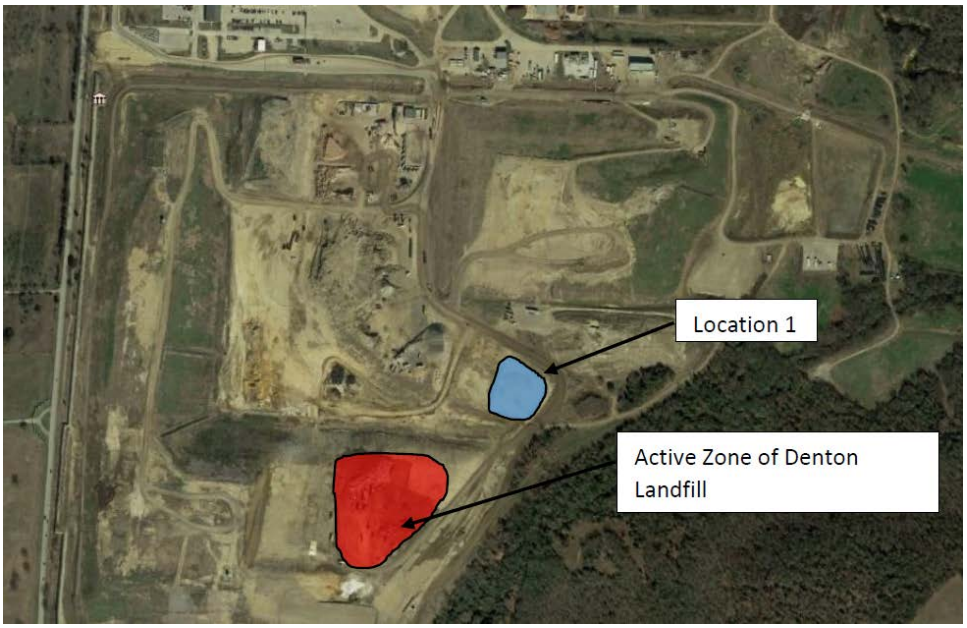

(a)

(b)

Figure 3. 4 (a) Site location 1, located near to the active zone of the City of Denton Landfill, Denton, Texas; (b) site condition of location 1.

The main purpose of this soil investigation was to obtain and understand the sub soil condition to determine the suitability of this area for the construction of the test sections. Some specific information is given below:

a) Name of the project: Soil Investigation at Location 1 (S1)

b) Location: The City of Denton Landfill, Denton, Texas

c) Client: Texas Department of Transportation

d) Field Work: 2nd December, 2016

e) Scope of Work: Number of bore holes – 03

Drilling depth – 20 ft.

Standard Penetration Test (SPT) – 12 nos.

Undisturbed sample – 09 nos.

Bulk/Remolded sample – 12 nos.

3.4.1.1 Soil Boring Results

The subsurface conditions, as interpreted from the field investigation program, indicate a subsurface profile consisting of low to medium plasticity clay and silt. Water table was not detected during the field investigation and range of moisture content was found to be between 12 and 18%. The boring log for BH1_S1, BH2_S1 and BH3_S1 are provided in Appendix A.

Summary of quantity of field work is shown in the following Table 3.1.

Table 3. 1 Summary of field tests.

No.	Bore Hole ID	Date of Boring	Drilling Depth (ft.)	No. of Undisturbed Samples	No. of SPT tests
1	BH1_S1	12-02-16	20	03	04
2	BH2_S1	12-02-16	20	03	04
3	BH3_S1	12-02-16	20	03	04

3.4.1.2 Moisture Content Test Results

Moisture contents were determined from the bulk sample collected during drilling. Moisture content results indicates that, soil is in dry side of the optimum moisture content with very low permeability. Depth wise moisture variation is shown in Figure 3.5. It is observed that, this area is very dry and range of moisture varied from 10 to 15%.

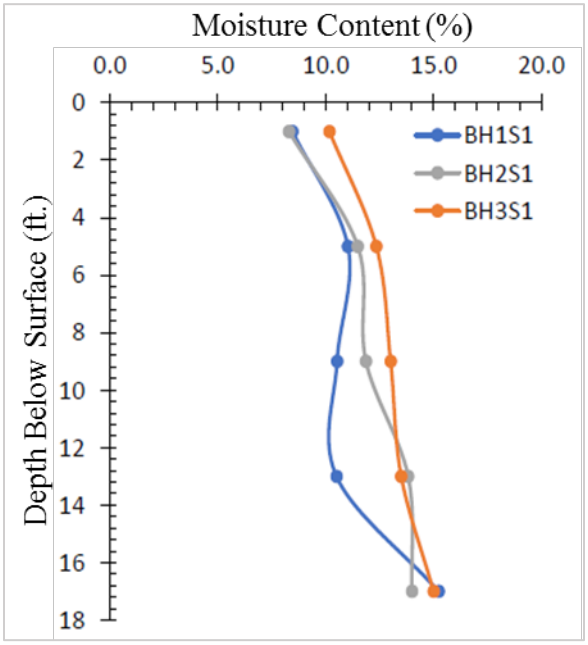

Figure 3. 5 Depth wise moisture variation for the boreholes in Location 01.

3.4.1.3 Atterberg Limit Test Results

Liquid limit and plastic limit tests were performed on samples collected at different depth from the three borings. From the test results it was found that plasticity index varies from 5 to 12 and range of liquid limit was between 20 and 30. Based on the plasticity chart this soil may be classified as low plastic clay (CL). The Atterberg limit test results are presented in Figure 3.6.

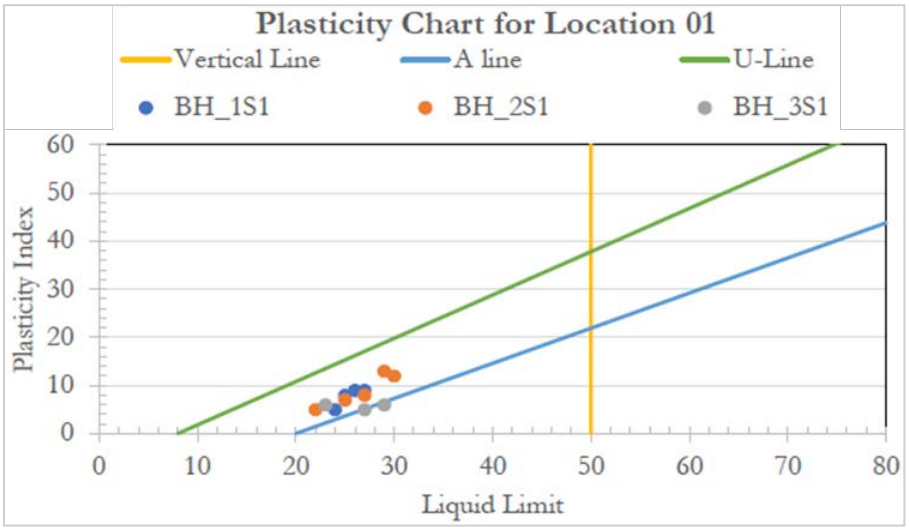

Figure 3. 6 Plasticity chart for the soil samples collected from location 1.

3.4.1.4 UCS Test Results

The unconfined compressive strength (q_u) is the maximum value σ_1, which may or may not coincide with the maximum force measurement (depending on the area correction). It is also equal to the diameter of Mohr's circle as indicated in Figure 3.7. The undrained shear strength (S_u) is typically taken as the maximum shear stress, or

$$S_u = \frac{1}{2} q_u \tag{3.1}$$

In this study UCS test has been conducted on undisturbed sample collected in thin walled Shelby tubes at two different depths of 4 ft. and 10 ft. respectively. Axial stress vs strain curve obtained from 4 ft. depth is shown in Figure 3.7 and corresponding Mohr circle diagram is shown in Figure 3.8, which indicates the undrained shear strength of 550 psf. For the sample collected from 10 ft. depth, axial stress vs strain curve and corresponding Mohr circle diagram is shown in Figure 3.9 and Figure 3.10 respectively. Undrained shear strength at 10 ft. depth was found as high as 5400 psf, indicating very stiff soil layer.

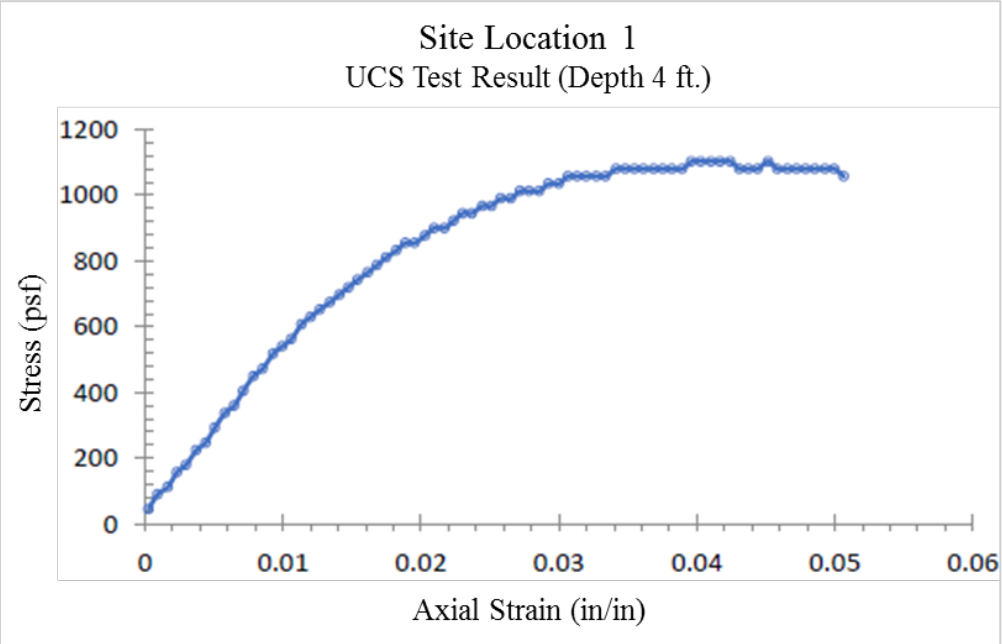

Figure 3. 7 Stress vs Strain Curve obtained from UCS test conducted on sample collected from 4 ft. depth at location 1.

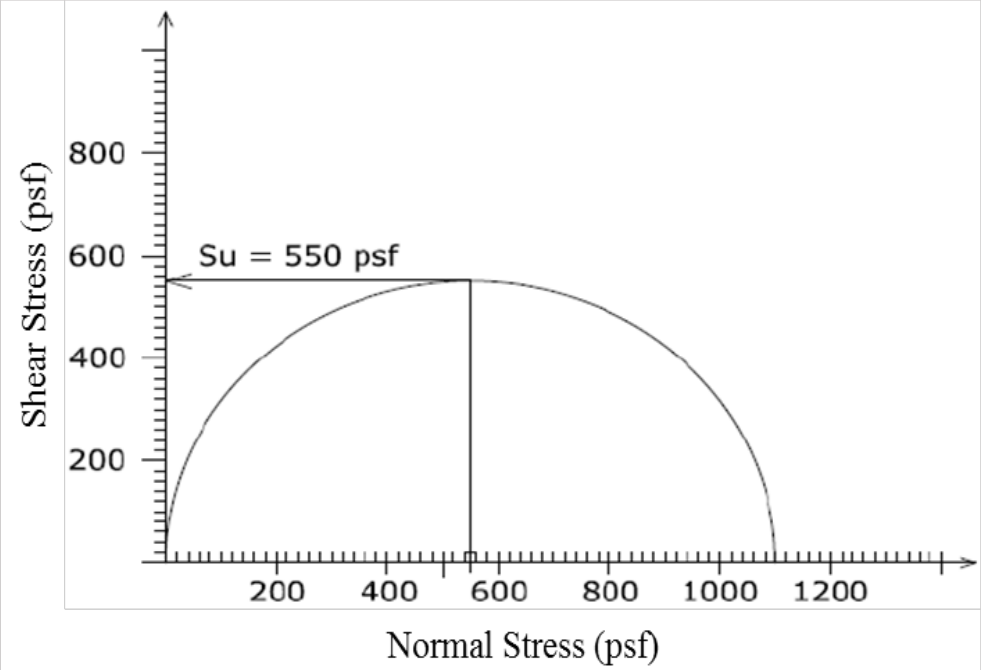

Figure 3. 8 Mohr circle diagram showing undrained shear strength at a depth of 4 ft. from Location 1.

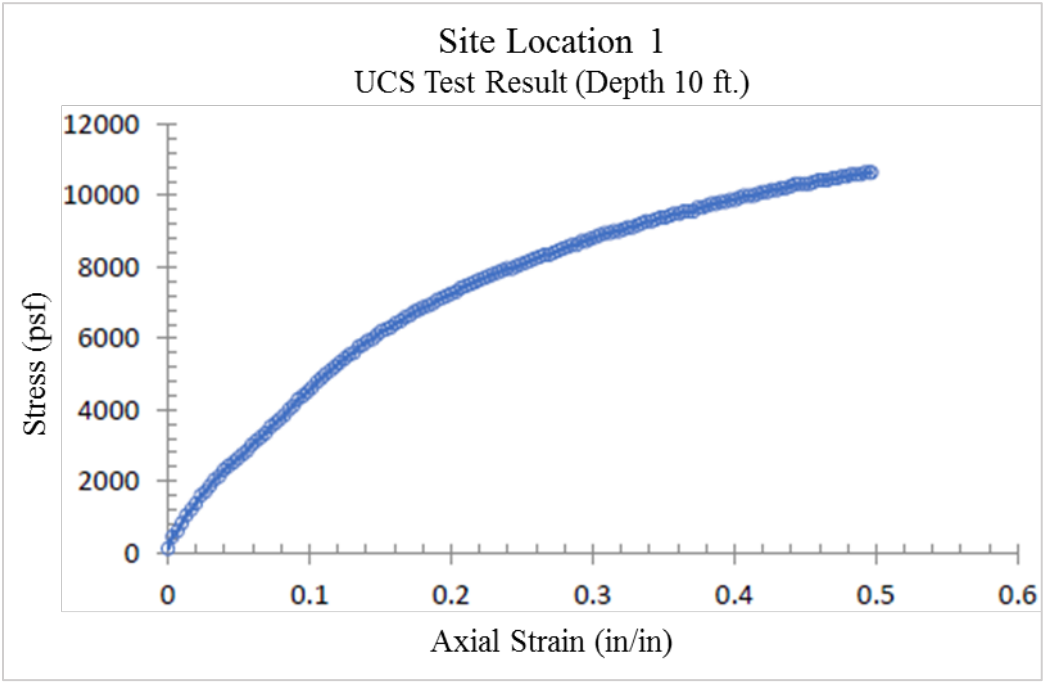

Figure 3. 9 Stress vs Strain Curve obtained from UCS test conducted on sample collected from 10 ft. depth at location 1.

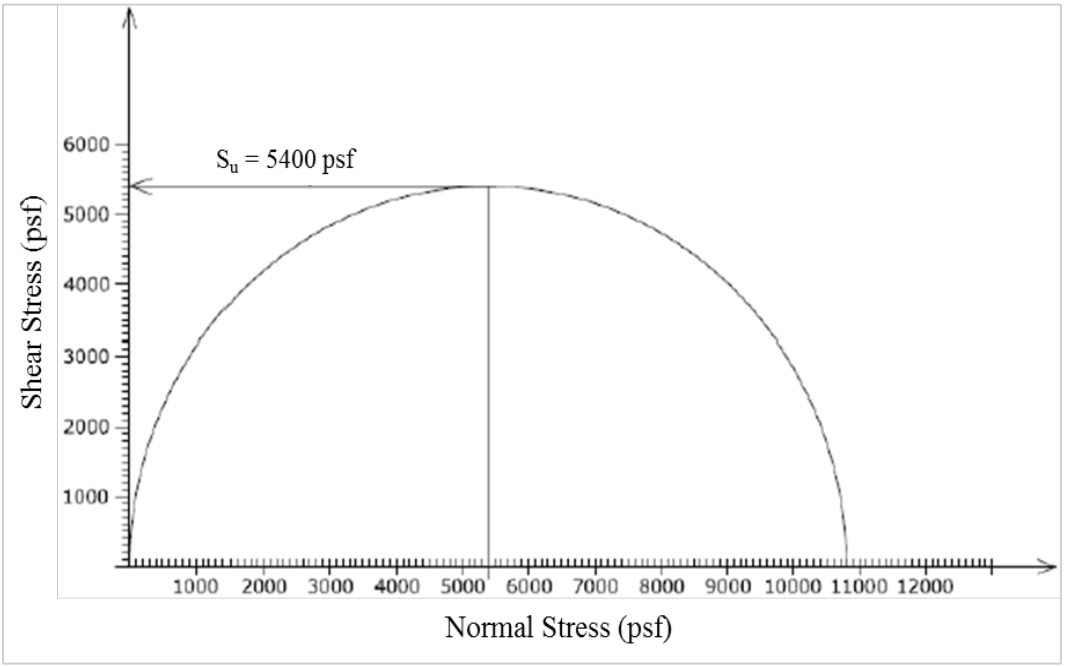

Figure 3. 10 Mohr circle diagram showing undrained shear strength at a depth of 10 ft.

3.4.1.5 Bearing Capacity Analysis

Typically, the minimum factors of safety for embankment structures are from 1.3 to 1.5. Figure 3.11 illustrates the resisting and driving forces related to embankment failure. The weight of the fill tries to move the soft foundation soil and the embankment moves counter clockwise to the right. Pavement at the top is supported by the internal strength of the embankment layers and strength of the foundation soil. Failure may occur in a circular fashion as shown in Figure 3.11 or it may be a semi-circle, in a block mode, or wedge. The basic principles are the same in all three modes of failure.

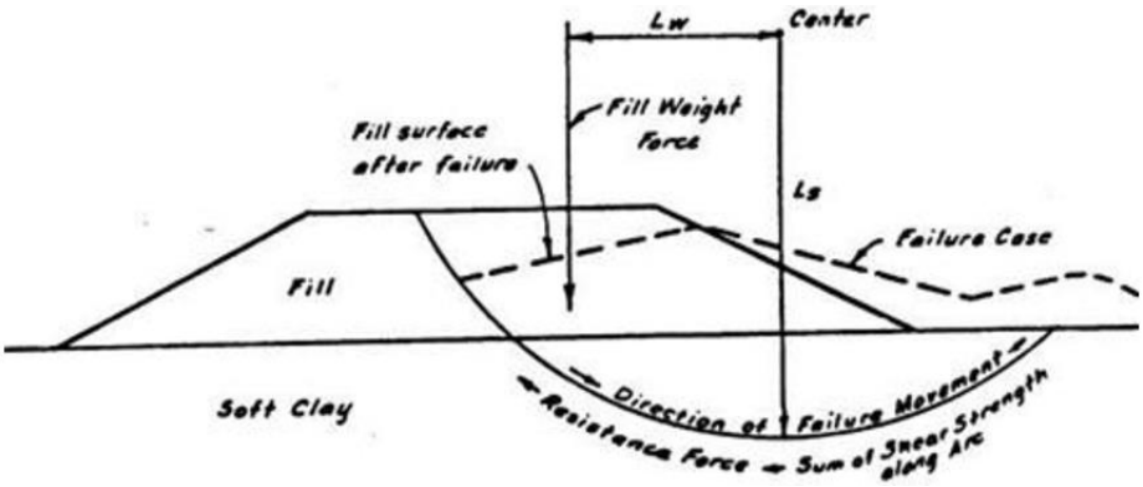

Figure 3. 11 Resisting and Driving Forces for Embankment Failure.

In this study, the focus is to increase the resisting force of the weak foundation soil by incorporating Recycled Plastic Pin as reinforcement. A number of test sections are to be constructed within a short time; therefore, undrained shear strength parameters are used to determine the bearing capacity of foundation soil using Skempton's equation (Eqn.3.1) for undrained bearing capacity. Skempton's undrained bearing capacity factor (N_{cu}) has been used which depends on size and depth of the foundation. As the test sections are square in shape and foundation will be set up on ground level, the value of N_{cu} will be equal to N_c. When the

friction angle is zero for the cohesive soil, undrained bearing capacity will be the multiplication of undrained shear strength and N_c and the simplified equation will be Eqn. 3.3.

Skempton's equation is widely used for undrained clay soils:

$$q_u = s_u .N_{cu} + q_o \quad (3.2)$$

where, N_{cu} = Skempton's bearing capacity factor, $N_{cu} = N_c.s_c.d_c$

here, s_c is a shape factor and d_c is a depth factor.

$N_q = 1$, $N_\gamma = 0$, $N_c = 5.14$

$s_c = 1 + 0.2$ (B/L) for $B \leq L$

$d_c = 1+$ Ö (0.053 D/B) for $D/B < 4$

When the foundation is on the ground surface, $q_o = 0$; Shape factor, $s_c = 1$; and Depth factor, dc = 1

$$q_u = 5.14\ s_u \text{ or } (2+\pi)\ s_u \quad (3.3)$$

Based on Eqn. 3.3 and undrained shear strength at location 1, the ultimate bearing capacity at 4 ft. depth was calculated to be 2827 psf. or 1.285 tsf. Based on the field SPT data, N value for the top layer of soil was 11, which indicates the soil is stiff and compressive strength is in between 1 to 2 tsf. Based on undrained shear strength parameter as well as field SPT value, it is confirmed that, top soil within location 1 was not sufficiently weak rather the ultimate bearing capacity is too high which can carry a load of 24 ft. embankment before obtaining a factor of safety below 1. As the soil of this location was not categorized as weak soil, further soil investigation was required to find a suitable location to construct the test sections for phase – I investigation.

3.4.2 Site Investigation for Location 2

The second location was also in the City of Denton Landfill, which was located just beside the treatment plant road (Figure 3.12) and considerably far from the active zone of the landfill.

Main advantage of this location was its topography as it had sufficient area to construct the vertical loaded test sections as well as sloping ground suitable for the construction of the lateral loaded test sections. This zone was readily accessible through the treatment plant road which is connected with South Mayhill road, Denton, Texas. Total available area in this zone was about 40,000 sq. ft. which is almost twice in size from Location 1. A total of three drilling location was selected, where two of them were located at the top (BH1_S2 & BH2_S2) and third one (BH3_S2) was located near the toe of the slope on the western side as shown in Figure 3.12. This section represents the soil investigation results based on three borings conducted on the Location 2 during 10th March, 2017. The main purpose of this soil investigation was to obtain and understand the sub soil condition to determine the suitability of this area for the construction of the test sections. Some specific information is given below:

a) Name of the project: Soil Investigation at Location 2 (S2)

b) Location: The City of Denton Landfill, Denton, Texas

c) Client: Texas Department of Transportation

d) Field Work: 10th March, 2017

e) Scope of Work: Number of bore holes – 03

Drilling depth – 20 ft.

Standard Penetration Test (SPT) – 12 nos.

Undisturbed sample – 09 nos.

Bulk/Remolded sample – 12 nos.

(a)

(b) (c)

Figure 3. 12 (a) Location of the soil borings; (b) flat surface; (c) sloping ground.

3.4.2.1 Soil Boring Results

The subsurface conditions as interpreted from the field investigation program, indicate a subsurface profile consisting two distinguished soil layers (Figure 3.13). Top few feet was expected to be weak soil lied over very stiff soil.

Water table was not detected during the field investigation, however, from initial investigation it was noticed that the soil had varying moisture content with depth. The boring log for BH1_S2, BH2_S2 and BH3_S2 are provided in Appendix B.

Summary of quantity of field work is shown in the following Table 3.2.

Table 3. 2 Summary of field tests.

No.	Bore Hole ID	Date of Boring	Drilling Depth (ft.)	No. of Undisturbed Samples	No. of SPT tests
1	BH1_S2	03-10-17	20	03	04
2	BH2_S2	03-10-17	20	03	04
3	BH3_S2	03-10-17	20	03	04

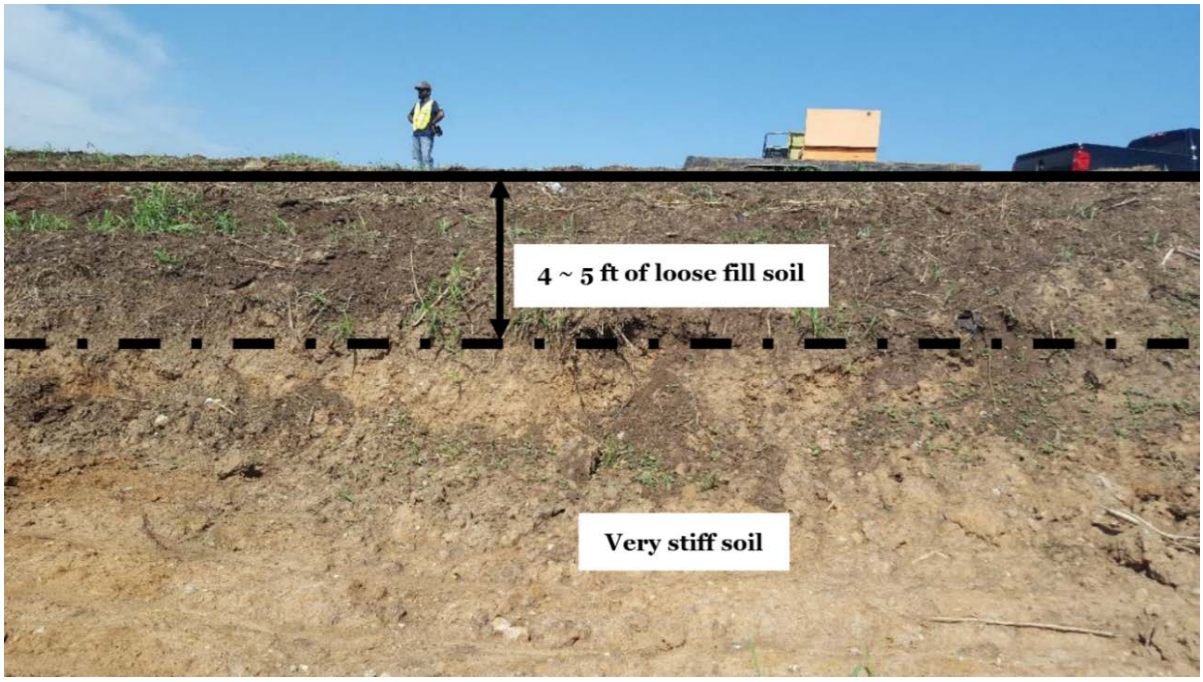

Figure 3. 13 Two distinguish soil layers in site location 2.

3.4.2.2 Geophysical Testing: Resistivity Imaging

The use of geophysical methods is becoming popular all over the world for evaluating subsurface conditions of soil at shallow depth and for geo-hazard studies (Hossain et al. 2010; Hossain et al. 2011). Geophysical methods have the ability to generate an "image" of the subsurface which will provide a qualitative information of moisture contents, presence of larger voids etc. Examples of applications include: study of lithology, evaluation of faulting and karst conditions, mapping of bedrock, determination of groundwater elevations, determination of material layer thickness and monitoring of dam and levee seepage. For the purpose of the current project, Resistivity Imaging (RI) has been used to investigating the project site.

For this location in concern, Resistivity Imaging (RI) was used for enhanced mapping of lateral and vertical variations in subsurface moisture content. A total of five test sections were proposed to be constructed where, three of them will be used for vertical loading (Zone 1, 2 and 3) and the remaining two will serve as lateral loading test section (Zone 4 and 5), as shown in Figure 3.14. Resistivity Imaging was performed along a line, which is also shown in Figure 3.14. The RI investigations were conducted using 8-channel unit. The system consists of 56 electrodes and these electrodes were placed at 4 ft. spacing. The RI results obtained from the test is shown in Figure 3.15. Higher resistivity indicates relatively dry soil and lower resistivity indicates higher moister content.

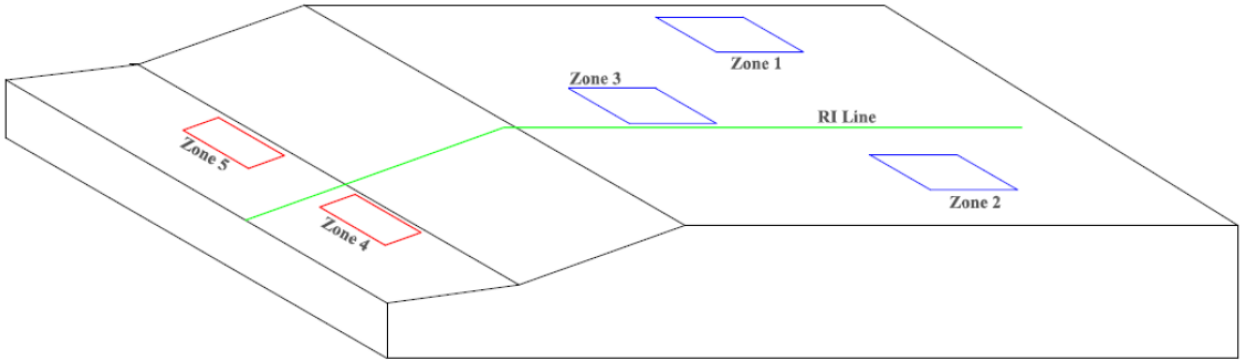

Figure 3. 14 Resistivity Imaging through the possible locations of the test section.

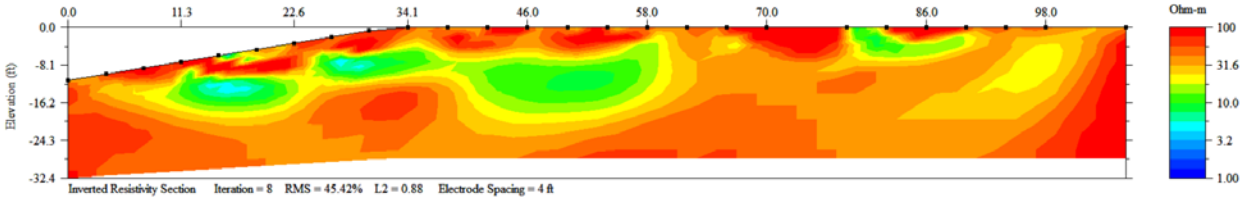

Figure 3. 15 Resistivity Imaging Results showing seepage along the slope.

3.4.2.3 Moisture Content Test Results

Moisture content of the bulk soil samples collected from different depth during drilling, were determined according to the standard test method ASTM D4643 – 08. Moisture content results indicate that, there was some accumulation of water in top few feet, indicating a perched water table, which was in good agreement with the resistivity imaging result. Maximum moisture content of about 20% was observed at a depth of about 4 ft. for borehole BH1_S2. No ground water table was detected during the site investigation. Depth wise moisture variation profile is shown in Figure 3.16.

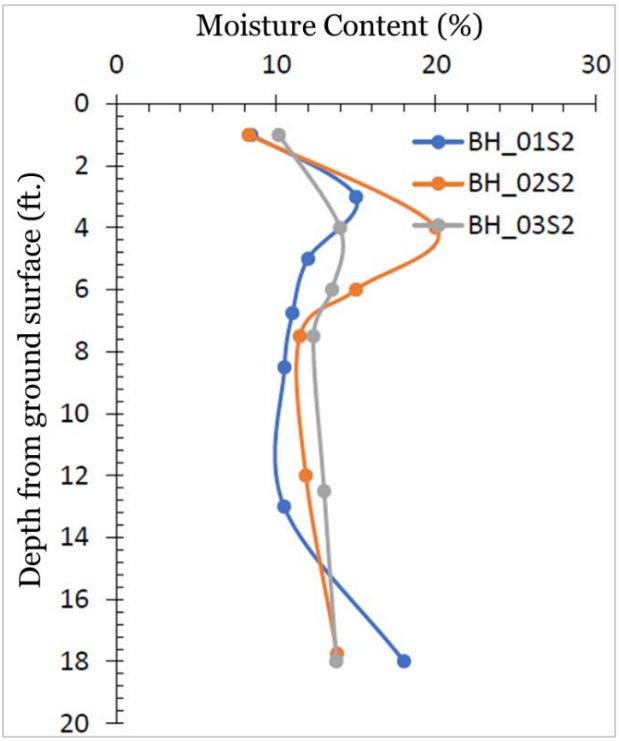

Figure 3. 16 Depth wise moisture variation for the boreholes in Location 02.

3.4.2.4 Atterberg Limit Test Results

The liquid limit and plastic limit test as described in ASTM standard D4318 were performed for the samples collected from different depths of the three borings. Plasticity index varies from 18 to 20 and range of liquid limit was between 25 and 48. Based on the plasticity chart this soil may be classified as low plastic clay (CL). The Atterberg limit test results are presented in Figure 3.17.

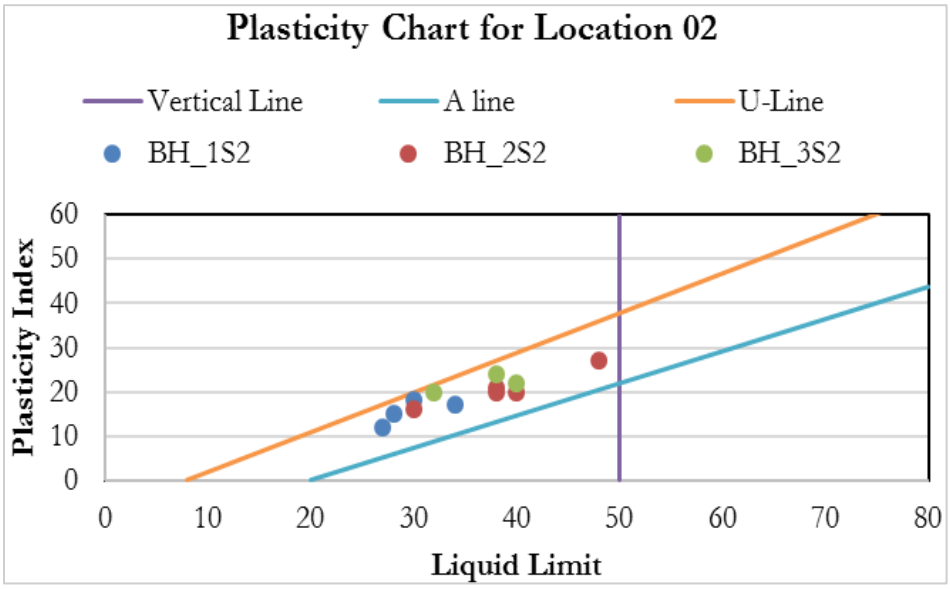

Figure 3. 17 Plasticity chart for the soil samples collected from location 2.

3.4.2.5 Unconfined Compressive Test Results

UCS tests were conducted on undisturbed sample collected in thin walled Shelby tubes at two different depths of 4 ft. and 10 ft. respectively. Axial stress vs strain curve obtained from 4 ft. depth is shown in Figure 3.18 and corresponding Mohr circle diagram is shown in Figure 3.19. Based on the plot it was found that the undrained shear strength of the soil layer was 120 psf. For the sample collected from 10 ft. depth, axial stress vs strain curve and corresponding Mohr circle diagram is shown in Figure 3.20 and Figure 3.21 respectively. Undrained shear strength at 10 ft. depth was found to be as high as 5000 psf, indicating very stiff soil layer; which is almost same for the foundation soil at the toe of the slope.

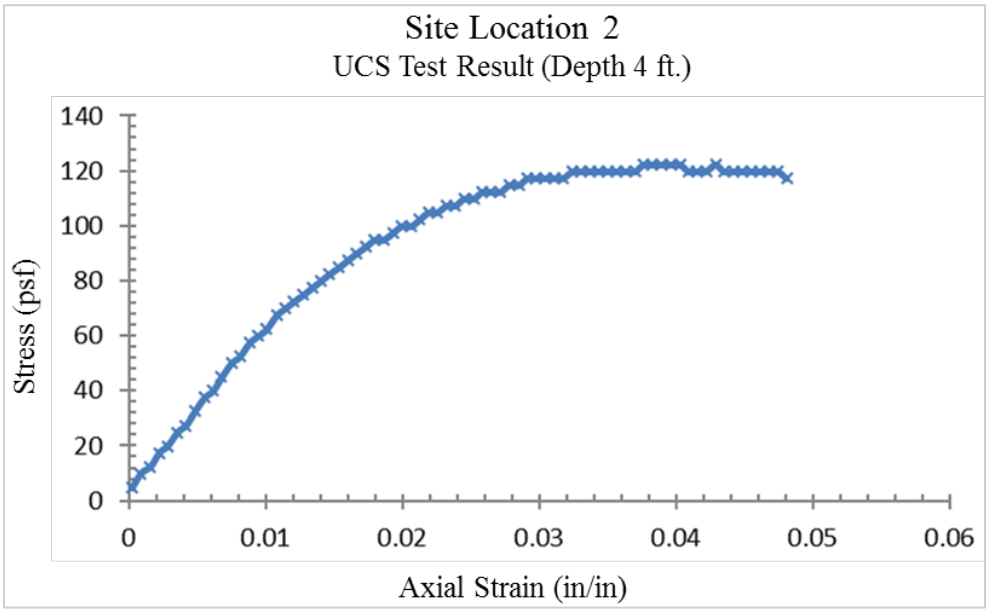

Figure 3. 18 Stress vs Strain Curve obtained from UCS test conducted on sample collected from 4 ft. depth at location 2.

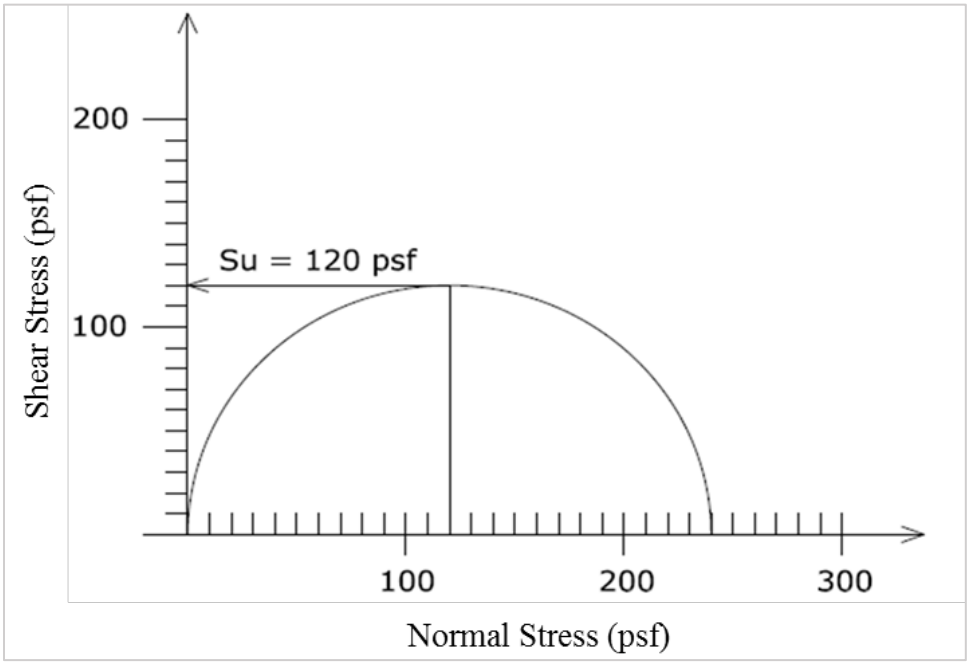

Figure 3. 19 Mohr circle diagram showing undrained shear strength at a depth of 4 ft. from Location 2.

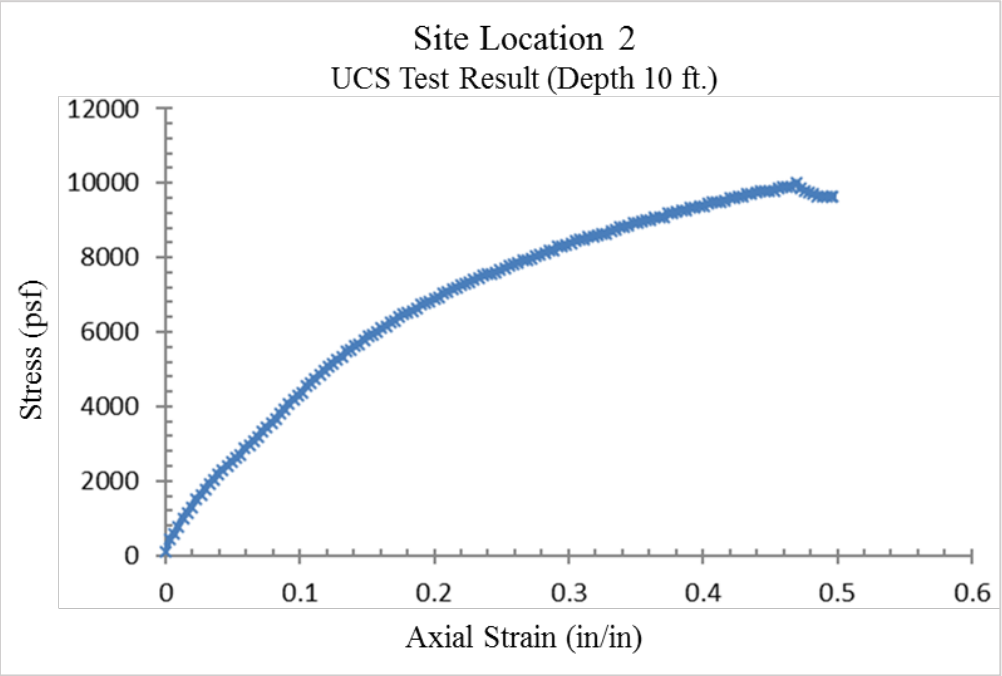

Figure 3. 20 Stress vs Strain Curve obtained from UCS test conducted on sample collected from 10 ft. depth at location 2.

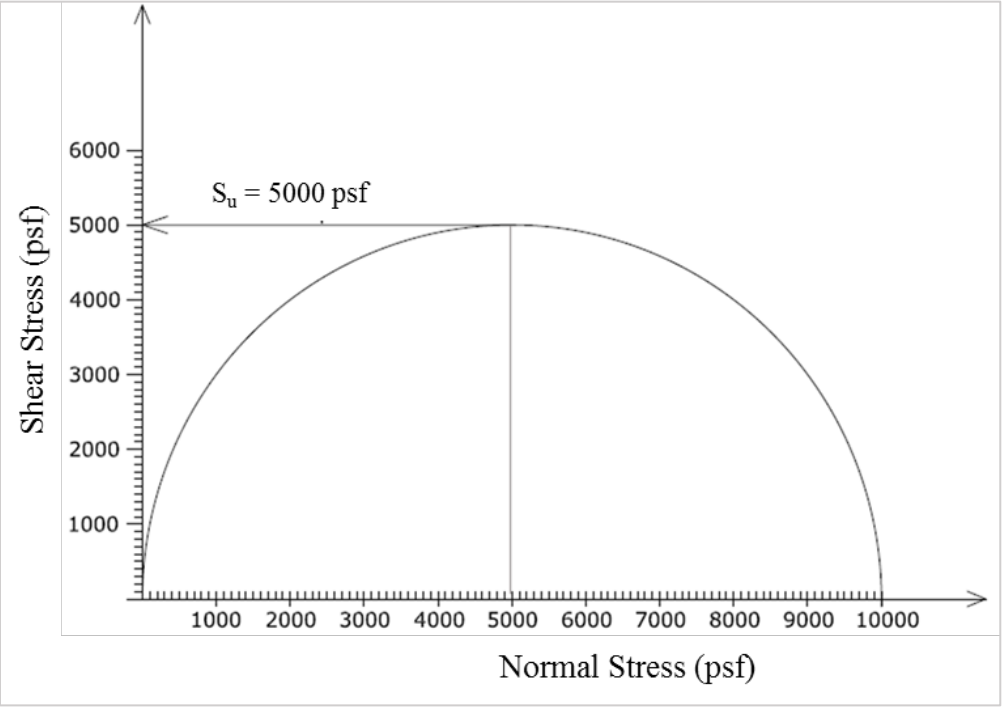

Figure 3. 21 Mohr circle diagram showing undrained shear strength at a depth of 10 ft. from Location 2.

3.4.2.6 Bearing Capacity Analysis

Based on Eqn. 3.3 and undrained shear strength at location 2, ultimate bearing capacity for 4 ft. depth is 616.8 psf or 0.28 tsf. Based on the field SPT data, N value for the top layer (from BH2_S2) of soil was 4, which indicates the soil is stiff and compressive strength will be in between 0.25 to 0.50 tsf. Based on undrained shear strength parameter as well as field SPT value, it was confirmed that, top soil within this zone was weak. To maintain a factor of safety of 1.5, maximum allowable loading is 411.2 psf which is equivalent to an embankment height of 3.43 ft. (considering the unit weight of fill material as 120 pcf). In addition, the soil layer near the toe of the slope was found to be composed of really stiff soil.

3.4.3 Recommendation for the Test Sections for Phase – I Construction

The purpose of the site investigation was to determine a suitable location to construct the vertical and lateral loaded test sections. Based on the site investigation and laboratory testing report it was concluded that the site location 2 was suitable for the construction of both vertical and lateral loaded test sections. A suitable sub soil profile was developed for the site location as shown in Figure 3.22.

Three vertically loaded test sections needed to be constructed, where for two of them the foundation soil was reinforced with Recycled plastic pin (different sizes) and the remaining one served as control section. Determination of loading size for the test section was one of the critical issue, as it should represent the embankment loading. Typically embankment foundation is considered as strip footing where depth of foundation is zero and breadth to length ratio is taken as infinity. For the construction of embankment test section, depth of

foundation was recommended to be zero but breadth to length ratio was taken as 1, which means a square type footing and failure can be occurred at any plane.

In addition, two laterally loaded sections needed to be built for the study; one RPP reinforced section and the other as control section. The foundation on which the retaining structure was constructed, needed to be cleaned and levelled before construction of the test sections. For the construction of the test sections it was critical that the test sections should be constructed in such a way that it represent the MSE retaining structures.

Five specific zones have been defined to set up the test sections; three for vertical loaded test sections on the flat soft soil surface, while the other two for lateral loaded test sections, as part of Phase – I construction and monitoring. The suggested location of the test sections are shown in Figure 3.23.

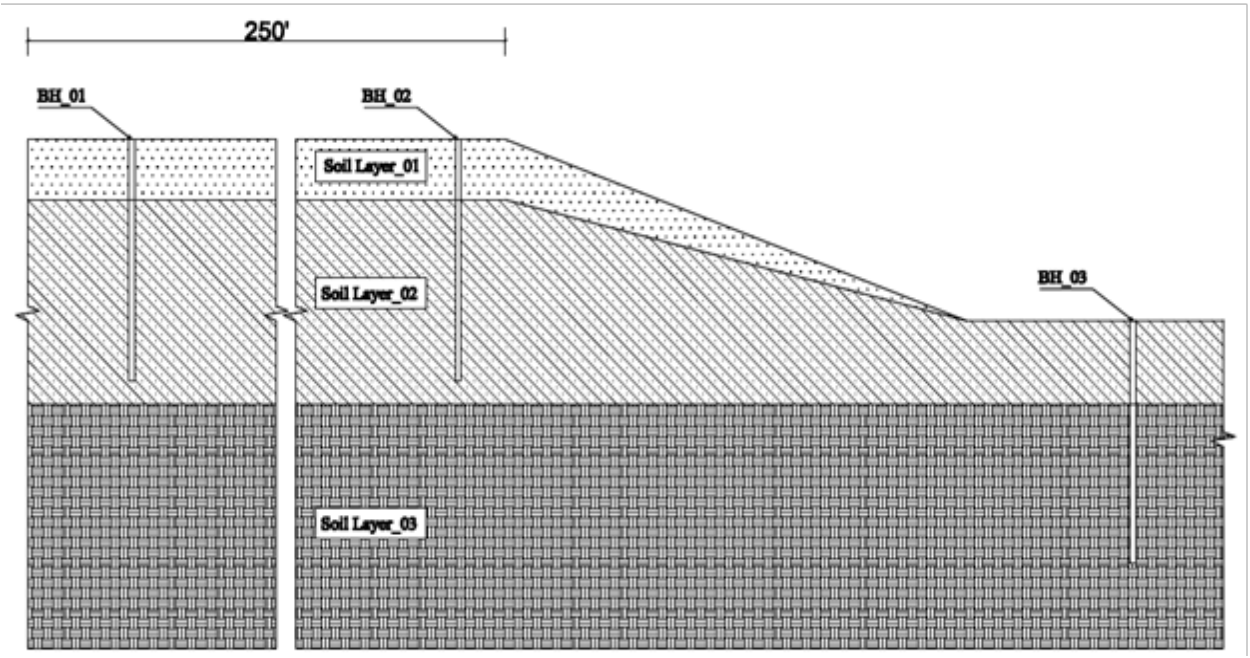

Figure 3. 22 Developed soil profile of the site location 2.

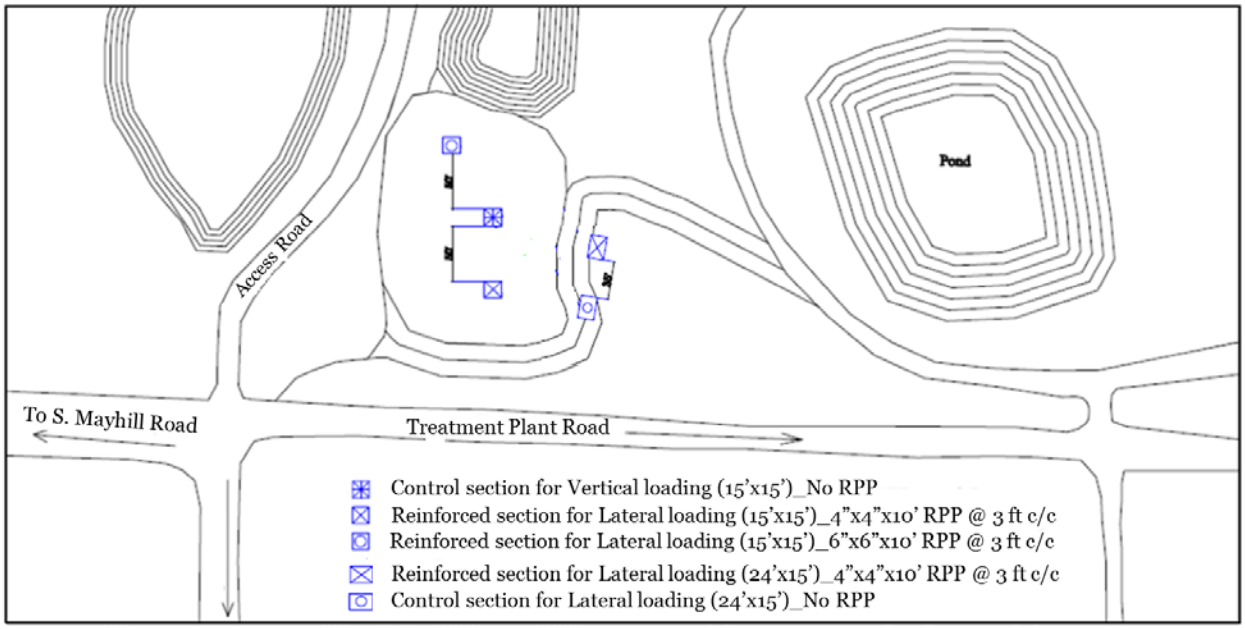

Figure 3. 23 Locations for different test sections in site location 2.

3.4.4 Site Investigation for Location 3

The third location was provided by the Hunter Ferrell Landfill, Irving, Texas which is located just beside the nursery & close to the Lonestar cricket ground (Figure 3.24) and considerably far from the active zone of the landfill. Total available area in this zone was about 28,000 sq. ft. of relatively flat surface (Figure 3.25). The location is easily accessible through the access road. This section represents the soil investigation results based on three borings conducted on location 3 during 9th February, 2018. The main purpose of this soil investigation was to obtain and understand the sub-soil condition to determine the suitability of this area for the construction of the test sections. Some specific information is given below:

a) Name of the project: Soil Investigation at Location 3 (S3)

b) Location: Hunter Ferrell Landfill, Irving, Texas

c) Client: Texas Department of Transportation

d) Field Work: 9th February, 2018

e) Scope of Work: Number of bore holes – 03

Drilling depth – 20 ft.

Standard Penetration Test (SPT) – 12 nos.

Undisturbed sample – 09 nos.

Bulk/Remolded sample – 12 nos.

Figure 3. 24 Site location 3, located far from active zone of landfill.

Figure 3. 25 Site condition of location 3.

3.4.4.1 Soil Boring Results

The subsurface conditions, based on the field investigation program, indicate a subsurface profile consisting of mostly high plasticity clay and silt. Water table was not detected during the field investigation and range of moisture content was between 19 to 28%. The boring log for BH1_S3, BH2_S3 and BH3_S3 are provided in Appendix C. The laboratory test results are presented here. Summary of quantity of field work is shown in the following Table 3.3.

Table 3. 3 Summary of the field tests.

No.	Bore Hole ID	Date of Boring	Drilling Depth (ft.)	No. of Undisturbed Samples	No. of SPT tests
1	BH1_S3	02-09-18	20	02	04
2	BH2_S3	02-09-18	20	02	04
3	BH3_S3	02-09-18	20	02	04

3.4.4.2 Moisture Content Test Results

Moisture content of the bulk soil samples collected from varying depth during drilling, were determined according to the standard test method ASTM D4643 – 08. Maximum moisture content of about 28% was found at a depth of about 19 ft. for BH1_S3. No ground water table was detected during the site investigation. Depth wise moisture variation profile is shown in Figure 3.26.

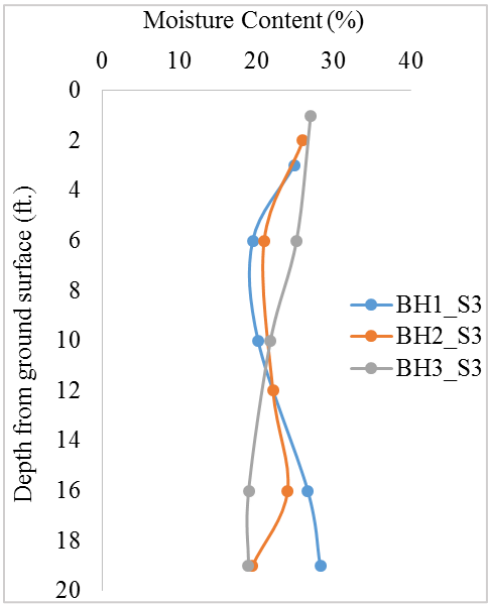

Figure 3. 26 Depth wise moisture variation for the boreholes in Location 03.

3.4.4.3 Atterberg Limit Test Results

Liquid limit and plastic limit test were performed for the samples collected from different depths of the three borings. Plasticity index varied from 33 to 49 and range of liquid limit was between 47 and 65. Based on the plasticity chart this soil may be classified as high plastic clay (CL). The Atterberg limit test results are presented in Figure 3.27.

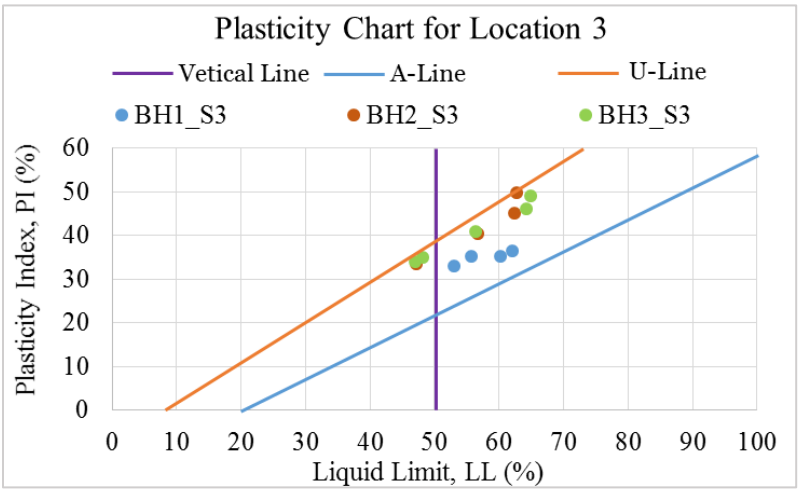

Figure 3. 27 Plasticity chart for the soil samples collected from location 3

3.4.4.4 Unconfined Compressive Test Results

UCS tests were conducted on undisturbed sample collected in thin walled Shelby tubes at two different depths of 5 ft. and 15 ft. respectively. Mohr circle diagram for 5 ft. depth is shown in Figure 3.28. From the plot it was found that the undrained shear strength at 5 ft. depth was 705 psf. For the sample collected from 15 ft. depth, Mohr circle diagram is shown in Figure 3.29. Undrained shear strength at 15 ft. depth was found to be as high as 6,500 psf, indicating very stiff soil layer.

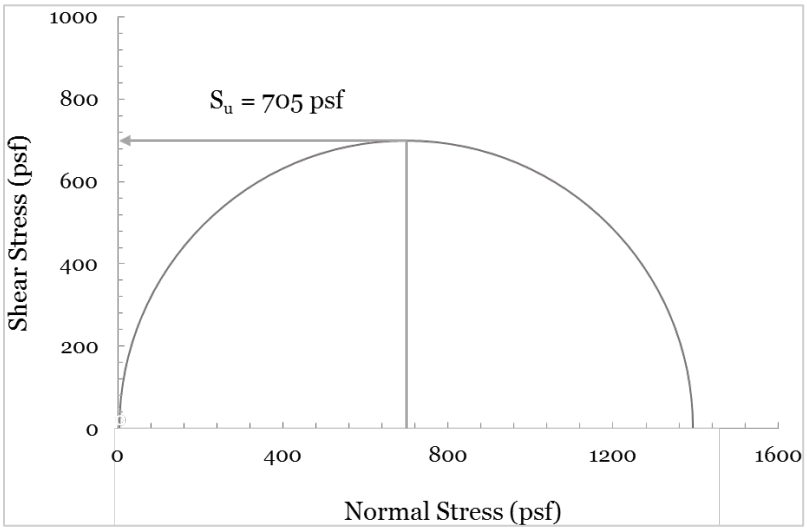

Figure 3. 28 Mohr circle diagram for undrained shear strength at 5 ft. depth for location 3.

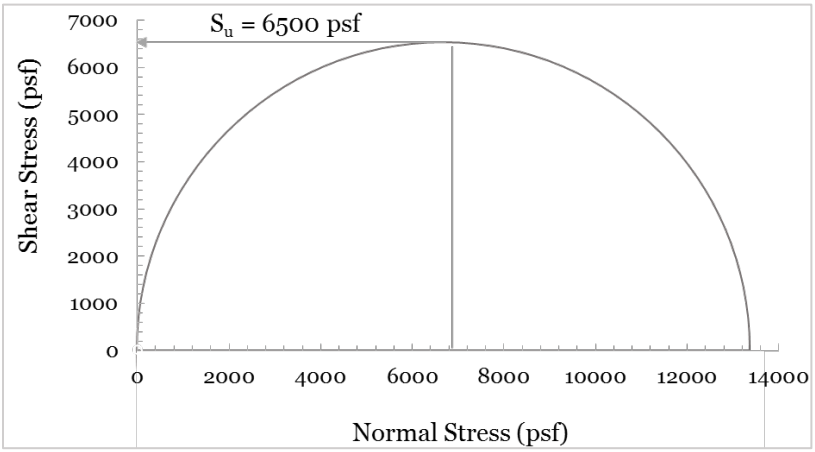

Figure 3. 29 Mohr circle diagram for undrained shear strength at 15 ft. depth for location 3.

3.4.4.5 Bearing Capacity Analysis

Based on Eqn. 3.3 and undrained shear strength at location 3, ultimate bearing capacity at 5 ft. depth is 3,600 psf or 1.64 tsf. Based on the field SPT data, N value for the top layer of soil was 11, which indicates the soil is stiff and compressive strength will be in between 1 to 2 tsf. Based on undrained shear strength parameter as well as field SPT value, it is confirmed that, top soil within this zone is not weak rather the ultimate bearing capacity is too high to support the load of 30 ft. embankment before obtaining a factor of safety below 1. As the soil at this location was not categorized as weak soil, further soil investigation was required to find a suitable location to construct the test sections.

3.4.5 Site Investigation for Location 4

The fourth location was also provided by the Hunter Ferrell Landfill, Irving Texas which is located near the active phase of landfill as shown in the Figure 3.30. Total available area in this zone was about 80,000 sq. ft. and easily accessible through the hauling roads inside the landfill. This section represents the soil investigation results based on two borings conducted on location 4 during 8th March, 2018. The main purpose of this soil investigation was to obtain and understand the sub-soil condition to determine the suitability of this area for the construction of the test sections. Some specific information is given below:

a) Name of the project: Soil Investigation at Location 4 (S4)

b) Location: Hunter Ferrell Landfill, Irving, Texas

c) Client: Texas Department of Transportation

d) Field Work: 8th March, 2018

e) Scope of Work: Number of bore holes – 02

Drilling depth – 20 ft.

Standard Penetration Test (SPT) – 8 nos.

Undisturbed sample – 04 nos.

Bulk/Remolded sample – 8 nos.

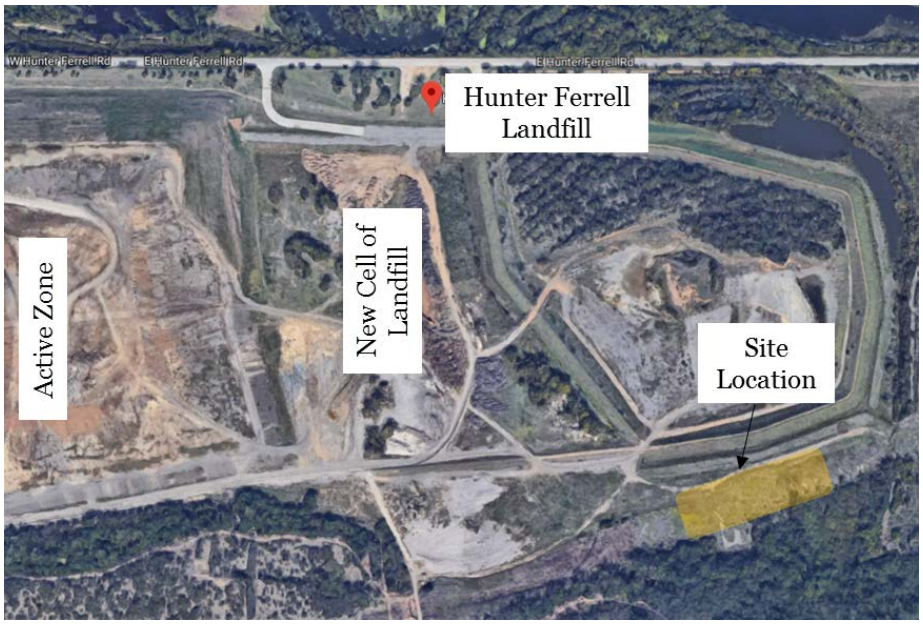

Figure 3. 30 Location 4, close to the new cell of landfill.

3.4.5.1 Soil Boring Results

The subsurface conditions, as interpreted from the field investigation program, indicate a subsurface profile consisting of mostly high plasticity clay. Like other site locations, water table was not detected during the field investigation and range of moisture content was between 20 to 28%. The boring log for BH1_S4 and BH2_S4 are provided in Appendix D.

Summary of quantity of field work is shown in the following Table 3.4.

Table 3. 4 Summary of the field tests.

No.	Bore Hole ID	Date of Boring	Drilling Depth (ft.)	No. of Undisturbed Samples	No. of SPT tests
1	BH1_S4	03-8-18	20	02	04
2	BH2_S4	03-8-18	20	02	04

3.4.5.2 Moisture Content Test Results

Moisture content test results of the bulk soil samples collected from different depth during drilling indicated that, the top soil had more moisture compared to soil layers underneath. This might be due to the extremely low permeability of clay present in the project site. Maximum moisture content of about 28% was observed at a depth of about 2 ft. for BH1_S4. No ground water table was detected during the site investigation. Depth wise moisture variation profile is shown in Figure 3.31.

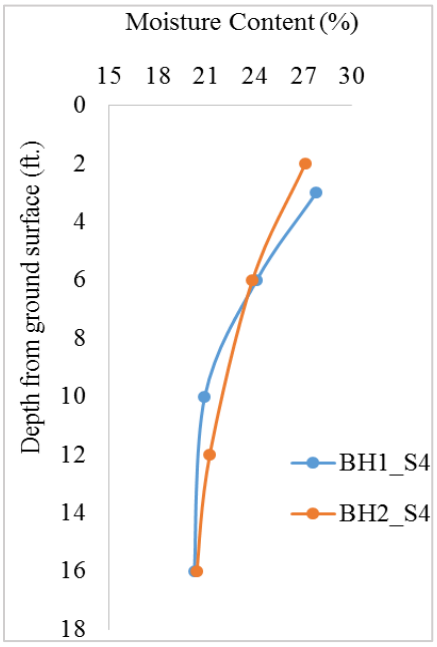

Figure 3. 31 Depth wise moisture variation for the boreholes in Location 04.

3.4.5.3 Atterberg Limit Test Results

Liquid limit and plastic limit test were performed for the samples collected from different depths of the two borings. Plasticity index varies from 36 to 48 and range of liquid limit was between 51 and 66. Based on the plasticity chart this soil may be classified as high plastic clay (CL). The Atterberg limit test results are presented in Figure 3.32.

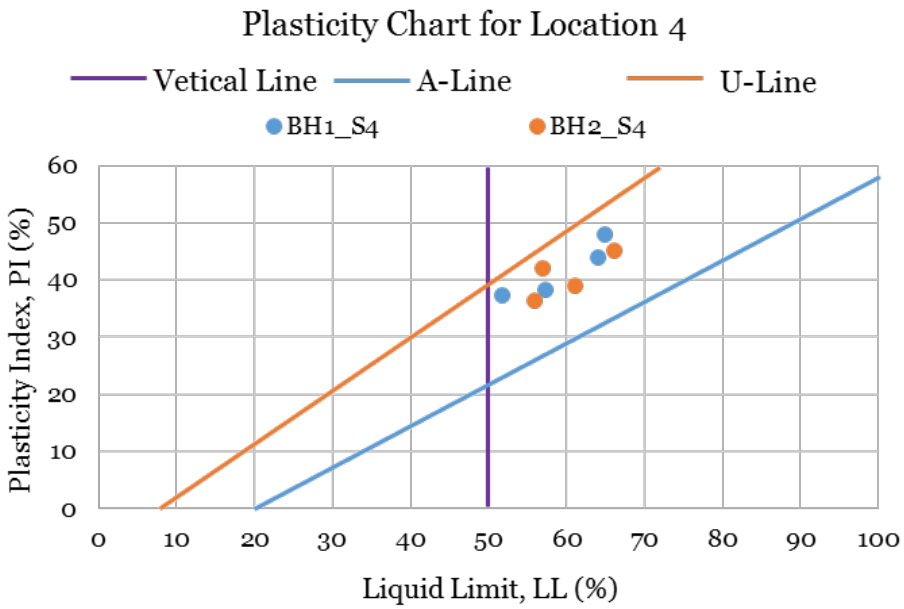

Figure 3. 32 Plasticity chart for the soil samples collected from location 4.

3.4.5.4 Unconfined Compressive Test Results

UCS tests were conducted on undisturbed soil samples collected in thin walled Shelby tubes at two different depths of 5 ft. and 15 ft. respectively. Mohr circle diagram for 5 ft. depth is shown in Figure 3.33, which indicates the undrained shear strength at 5 ft. was found to be 140 psf. For the sample collected from 15 ft. depth, Mohr circle diagram is shown in Figure 3.34. Undrained shear strength at 15 ft. depth was found as high as 6,400 psf, indicating extremely stiff soil layer.

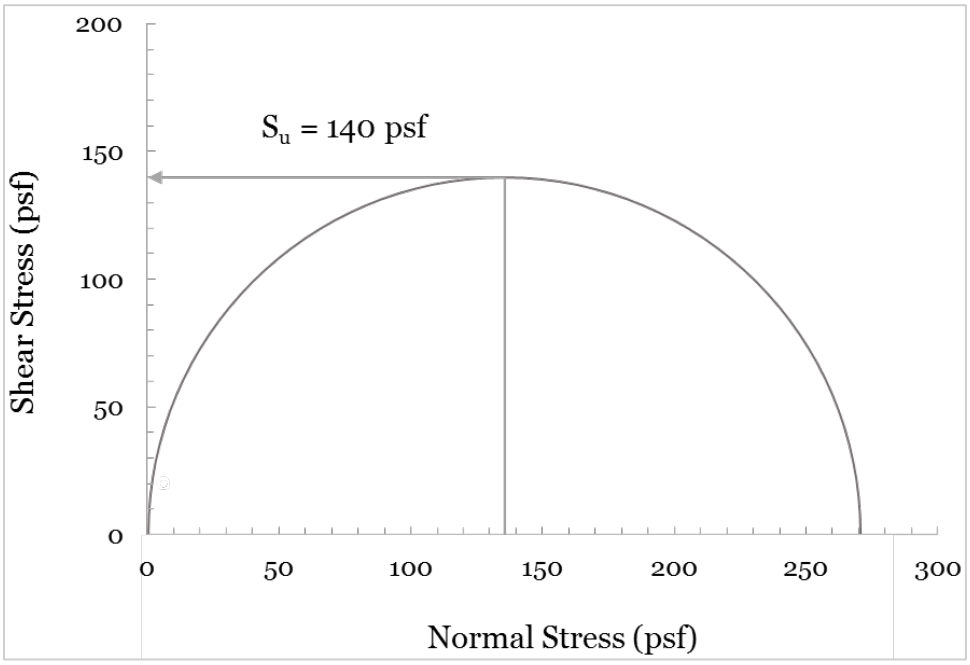

Figure 3. 33 Mohr circle diagram showing undrained shear strength at a depth of 5 ft. for location 4.

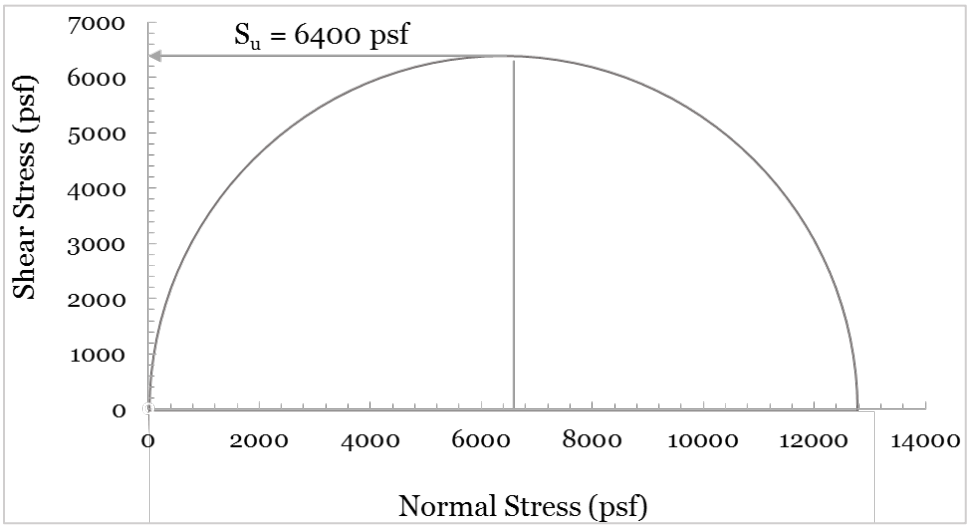

Figure 3. 34 Mohr circle diagram showing undrained shear strength at a depth of 15 ft. for location 4.

3.4.5.5 Bearing Capacity Analysis

Based on Eqn. 3.3 and undrained shear strength at location 4, the ultimate bearing capacity at 5 ft. depth was calculated to be 719.6 psf or 0.33 tsf. Based on the field SPT data,

N value for the top layer (From BH1_S4) of soil was 5, which indicates that the compressive strength will be in between 0.25 to 0.50 tsf. Based on undrained shear strength parameter as well as field SPT value, it was confirmed that, top soil within this zone was weak. To maintain a factor of safety of 1.5, maximum allowable loading is 479.73 psf which is equivalent to an embankment height of about 4 ft. (considering the unit weight of fill material as 120 pcf).

3.4.6 Recommendation for the Test Sections for Phase – II Construction

The purpose of the site investigation was to determine a suitable location to construct the vertical loaded test sections for phase II construction and monitoring for settlement. Based on the site investigation and laboratory testing report, it was concluded that the site soil condition of the site location 4 is suitable for the phase – II construction of the vertical loaded test sections.

Two test sections were required to be constructed where foundation soil of one of them needed to be reinforced with 4 in. x 4 in. RPPs at 3 ft. c/c and the other as control section (without any RPP reinforcement). Determination of loading size for the test section was one of the critical issue; for this phase of construction, boxed soil load were to be applied on top of the foundation to ensure uniform loading.

Two specific zones have been defined to set up the test sections for Phase – II construction and monitoring.

3.5 Reinforcing Mechanism Using RPP

3.5.1 Improvement of Soil Bearing Capacity

Recycled Plastic Pins in combination to the geosynthetic can significantly improve the bearing capacity and thus can take care of a considerable portion of settlement for weak foundation soil. The interactions between piles, foundation soil and geosynthetic are schematically presented in Figure 3.35. Embankment constructed on a soft foundation has a tendency to move downward under the influence of the embankment fill mass "W". For a reinforced section, RPP restricts the vertical movement of soil mass directly above it. This soil mass above the RPP/pile provides additional shear resistance, τ, which partially restrains the downward movement of the embankment fill mass above the gate. The shear resistance reduces pressure acting on the geosynthetic; however, load applied on the piles increases. This mechanism of load transfer is termed as "soil arching" effect by Terzaghi (1943). In addition, driving RPP in weak foundation soil helps densifying the soil matrix and improves the stiffness of the foundation.

The geosynthetic, when used in combination to the piles, it enhances the load transfer from fill soil to the piles which reduces both total and differential settlements between the piles. According to Terzaghi (1936) and McNulty (1965), shear stress induced by soil arching increases with increasing displacement and height above the yielding portion. Therefore, reduction in settlement due to the use of geosynthetic reduces the shear stresses, τ, which results in minimization of the effect of soil arching to the RPPs. This results in reduced load transfer to the piles; however, load on the piles may be increased by the vertical component of the tensioned member (geosynthetic). Also, the load transfer to the pins/piles largely depends

on the strength of geosynthetic. In short, load transfer mechanism is the combination of soil arching of the embankment, tensioned membrane effect of geosynthetic, and stress concentration due to the difference in stiffness between RPP and soil.

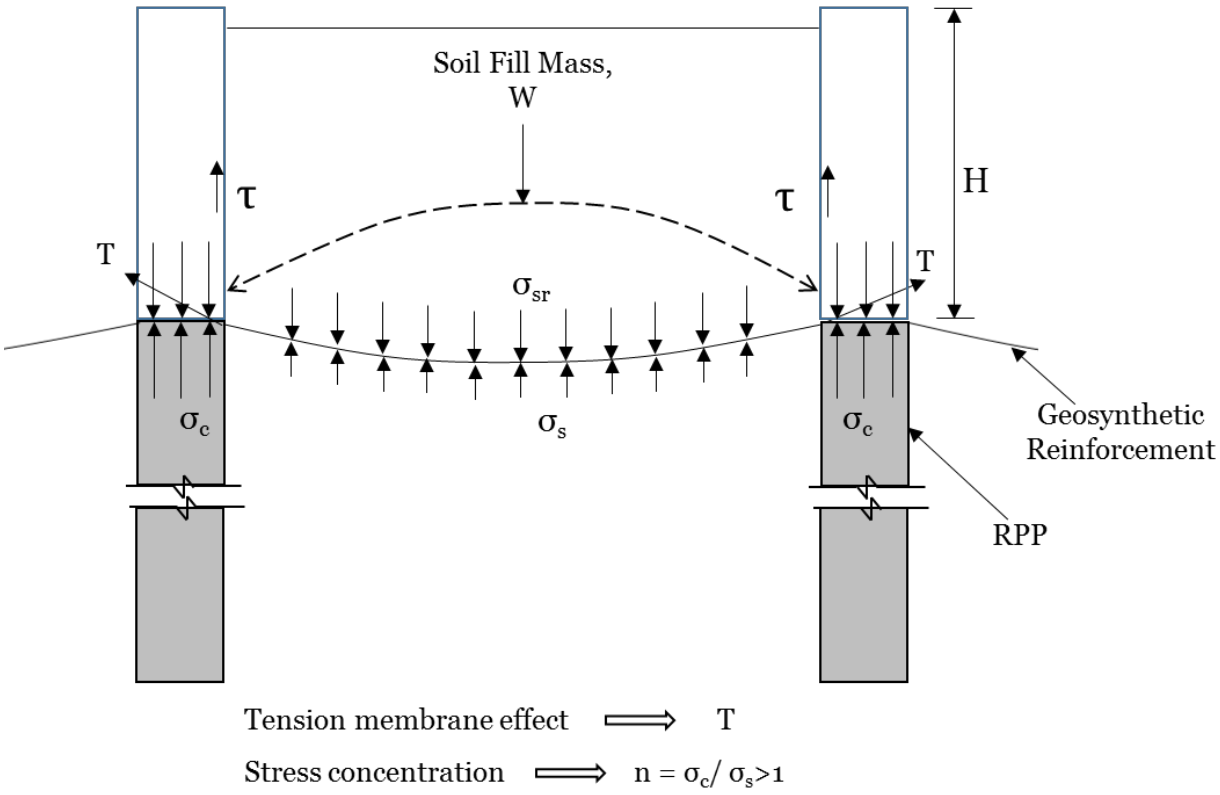

Figure 3. 35 Mechanism of load transfer for geosynthetic reinforced RPP-supported earth embankment (modified from Han, 1999; and, Han and Gabr, 2002).

The improved bearing capacity of the reinforced section can be back calculated from the field results using the following equation:

$$q = \frac{p}{s\prime} \cdot s \tag{3.4}$$

where,

q = Improved bearing capacity of the reinforced section

p = Load applied to the test sections (same for both reinforced and control section)

s = Settlement of the control section due to load p

s’ = Settlement of the reinforced section due to load p

3.5.2 Increasing Resistance against Sliding of the MSE Wall Base

For slope stabilization, plastic pin is used to provide additional resisting force along the slip surface and restrict the sliding of the soil mass and increases the factor of safety (Khan, 2014). The general definition of factor of safety is the ratio of resisting force (FR or moment MR) to the driving force (FD or moment MD). Figure 3.36 represents a schematic diagram of slope reinforcement using RPP.

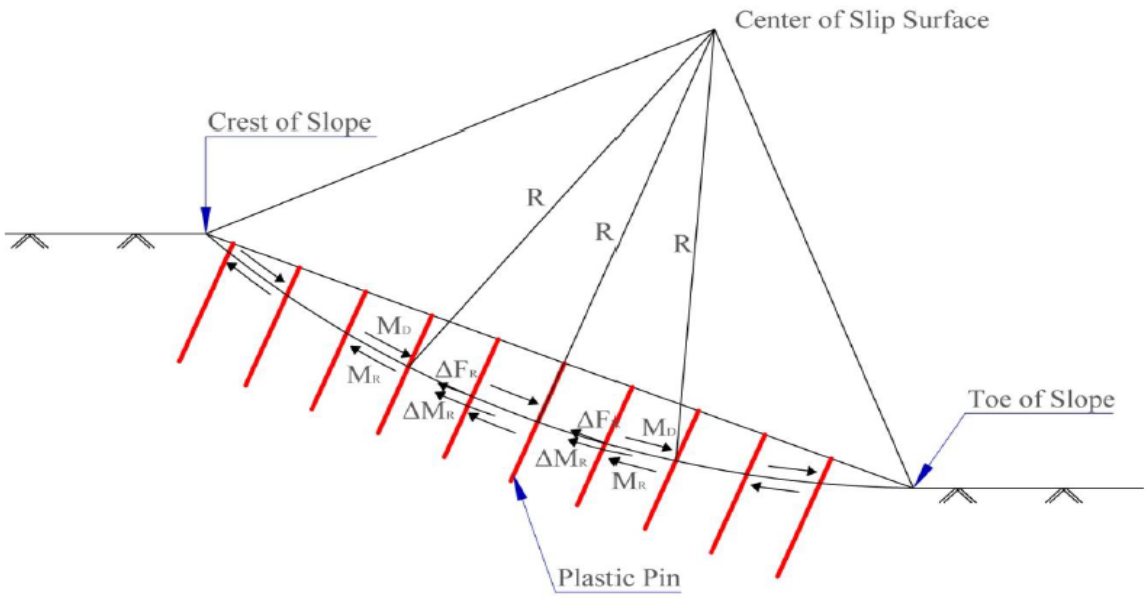

Figure 3. 36 Schematic of Resistances for RPP reinforced slope (Khan, 2014).

RPP provides significant lateral support or resistance against the slip surface of the slope and thus stabilize the slope. Which also proves, RPP has significant lateral load resisting capacity. Therefore, when RPPs are driven into the foundation soil at the base of the retaining wall keeping a certain portion above ground followed by the construction of the retaining

structures, they might perform as part of the structural element of the wall, which will provide additional resistance against lateral movement of the wall against the foundation soil. A typical diagram of the structure reinforced with RPP is shown in Figure 3.37. Factor of safety against sliding may be defined as:

$$FS_{sliding} = \frac{\sum F_R}{\sum F_D}; \quad (3.5)$$

Here, $\sum F_R$ = sum of all horizontal resisting force

$\sum F_D$ = sum of all driving force

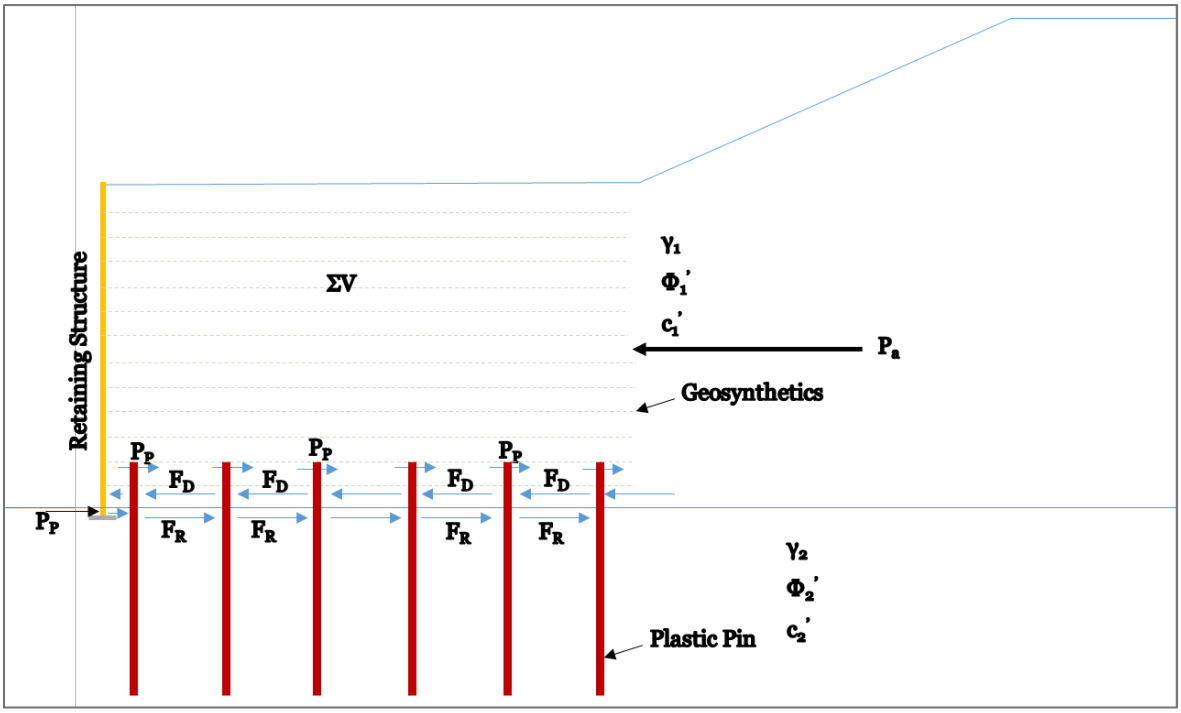

Figure 3. 37 Schematic of RPP reinforced retaining structure.

Shear strength of the soil below the base may be represented as:

$$\tau = c'_a + \sigma' \tan\delta' \quad (3.6)$$

where

δ' = angle of friction between the foundation soil and reinforced soil

c'_a = adhesion between the foundation soil and reinforced soil

The maximum resisting force generated from the soil per unit length of the wall along the bottom of the reinforced base is,

$$R' = \tau \text{ (area of the cross section)}$$

$$= \tau \text{ (B x 1)}$$

$$= B\sigma'\tan\delta' + Bc'_a$$

$$R' = (\Sigma V) \tan\delta' + Bc'_a \quad (3.7)$$

In addition, passive resisting force, Pp is also a part of the horizontal resisting force. Hence,

$$\Sigma F_R' = (\Sigma V) \tan\delta' + Bc'_a + P_p \quad (3.8)$$

On the other hand, the only horizontal force responsible for the sliding of the wall facing is due to the active pressure from the backfill material, which can be expressed as,

$$\Sigma F_D = P_a \cos\alpha \quad (3.9)$$

The factor of safety against sliding,

$$\text{FS (sliding)} = \frac{(\Sigma V)\tan\delta' + Bc'_a + P_p}{P_a \cos\alpha} \quad (3.10)$$

For MSE retaining structure passive force generated at the face of wall is ignored in calculation, and $\alpha = 0^o$; hence, the factor of safety equation becomes,

$$\text{FS (sliding)} = \frac{(\sum V)tan\delta' + Bc'_a}{P_a} \quad (3.11)$$

Here, $P_a = \frac{1}{2}\gamma_1 K_a H'^2$ (3.12)

Typically, the factor of safety against the base sliding of a retaining wall system is recommended as 3.0. If the desired factor of safety is not obtained several alternatives may be investigated according to Das, B.M. (2011).

a) Increase the width of the base slab
b) Using a deadman anchor
c) Reducing the value of Pa, by Elman and Terry (1988) method
d) Use a key to the base slab.

The usual and effective approach is to use a concrete shear key, which improves the sliding resistance considerably. However, a continuous concrete shear key at the base of MSE retaining wall increases the cost of construction and it is labor intensive. Therefore, instead of continuous shear key, RPP may be introduced to increase the base sliding resistance of the MSE retaining wall. The RPP when used in the composite system, might work similar to a shear key for the structure. If a key is included, it should provide additional passive force, P_P.

If RPP is installed at the base of the retaining wall system, base resistance is expected to increase as the pressure from lateral load acting on the wall will be transferred to the RPP thus reducing the effective pressure at the back of the wall. For the lateral loaded test sections, RPP was proposed to be installed in such a way that 8 ft. will be driven into the ground and 2 ft. will be kept extended above the ground to act as a cantilever beam which will carry the

lateral loads generated from the backfill soil. Total tip deflection of RPP acting as a cantilever beam with uniformly distributed load and rectangular cross section can be expressed as:

$$\Delta = \frac{pL^4}{8EI}\left[1 + \frac{E}{2G}\left(\frac{D}{L}\right)^2\right] \quad (3.13)$$

Here,

Δ = deflection of pin head

L = length of the extended portion of the pin

E = modulus of elasticity of RPP

I =moment of inertia

D = equivalent diameter

The additional deflection due to shear deformations is given by the second term in the brackets. The effect of shear deformations increases with increasing E/G ratios and decreasing slenderness ratios (L/D).

RPP incorporates additional passive resistance force, P_{RPP}. With the addition of RPP, Equation for the factor of safety against sliding becomes,

$$\text{FS (sliding)} = \frac{(\sum V)tan\delta' + Bc'_a + P_{RPP}}{P_a} \quad (3.14)$$

This additional passive force should increase the factor safety against sliding significantly, which need to be evaluated from field performance analysis.

3.6 Material Selection

The composition of a typical RPP includes, High Density Polyethylene, HDPE (55% – 70%), Low Density Polyethylene, LDPE (5% -10%), Polystyrene, PS (2% – 10%), Polypropylene, PP (2% -7%), Polyethylene- terephthalate, PET (1%-5%). In addition, varying amounts of additives e.g. sawdust, fly ash, fiberglass, wood fiber (0%-5%) is also present (Malcolm, 1995). A study conducted by Nosker and Renfree (2000) presented the evaluation of the recycled plastic lumber and its applications on different civil engineering applications. The successful utilization of the recycled plastic lumber for the structural application depends largely on the elastic modulus and the time-dependent mechanical behavior (creep). During the production process, glass and wood fibers are added to the recycled plastic composites to improve the mechanical properties and stiffness of the recycled plastic pin. It has been reported in previous studies that the use of glass and wood fiber additives improve the modulus of elasticity for plastic lumber significantly (Breslin et al. 1998; Lampo and Nosker, 1997, Nosker and Renfree, 2000). Specially, recycled plastic lumber that contains oriented glass fiber was found to be most creep resistant over time (Van Ness et al., 1998).

RPP is commercially available in different lengths, sizes and shapes (i.e. rectangular, circular, square). Moreover, the composition of RPP also varies, as it is manufactured from the recycled plastics from different sources. Based on available options, 4 in. x 4 in. and 6 in. x 6 in. fiber-reinforced RPP was selected due to its improved elastic modulus and creep resistant behavior for the construction of the test sections. For the vertical loaded test sections, both 4 in. x 4 in. and 6 in. x 6 in. RPP were used; while for the lateral loaded test sections only 4 in. x 4 in. RPP was utilized.

3.7 Design of the Test Section

Main purposes of this study was to assess the effect of RPP in improving bearing capacity of the foundation soil and increasing resistance against base sliding of the face of a MSE retaining structure. For field scale evaluation of the effect of RPP both vertical and lateral loaded test section were needed to be constructed; the design details of the test sections is presented in the following sub-sections.

3.7.1 Vertical Loaded Test Sections

RPP might become a potential remedy for improving bearing capacity of the weak foundation soil. When applied in combination to the geosynthetic, the geosynthetic reinforced RPP can provide additional support to the structure to restrict both total and differential settlement. To evaluate the effectiveness of RPP in improving bearing capacity of weak foundation soil, three test sections were proposed to be constructed at the designated site location at the City of Denton Landfill, Denton, Texas for the phase – I construction and monitoring. In phase – II construction and monitoring, two sections were proposed to be constructed at the Hunter Ferrell landfill, Irving, Texas to verify the conclusion found from phase – I. For the phase – I, one section was constructed as a control section having no plastic pin reinforcement; foundation soil for the other two test sections were reinforced with 4 in. x 4 in. and 6 in. x 6 in. RPPs respectively and designated as reinforced test sections. For phase – II, one control section and one 4 in. x 4 in. RPP reinforced section were constructed. All of the sections were identical having an effective dimension of 15 ft. x 15 ft.

As part of the phase – I construction, Two reinforced sections were proposed for the vertical loading test sections. One of the sections (BR_01) was reinforced with 4 in. x 4 in.

RPP and another section (BR_02) was reinforced with 6 in. x 6 in. RPP. To understand the effect of RPP size on improvement of bearing capacity, 3 ft. c/c spacing was used for both RPP reinforced test sections. The third section (BC_01) was loaded without any RPP reinforcement, to have a control section, for the purpose of comparing the deformation with the reinforced sections. A thin layer of geogrid was to be placed on top to facilitate the soil arching that will ensure mobilization of load from the fill material. All the test sections were loaded with native soil, mostly medium to high plastic clay for the construction of 6 ft. height embankment sectio. Proposed layout and cross sections of the test sections are presented in Figure 3.38, Figure 3.39 and Figure 3.40.

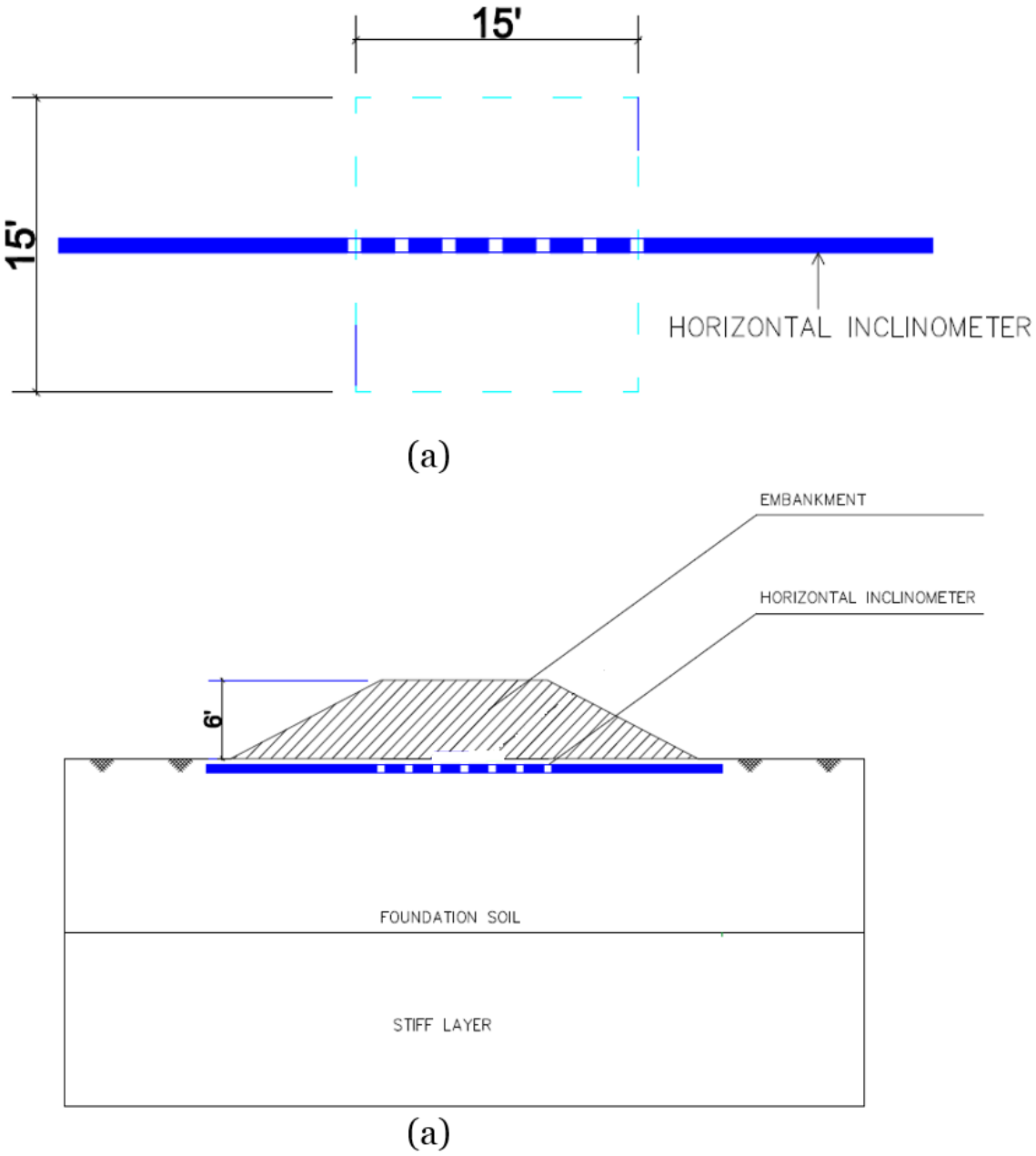

Figure 3. 38 (a) Proposed layout of control section; (b) section details of the control section.

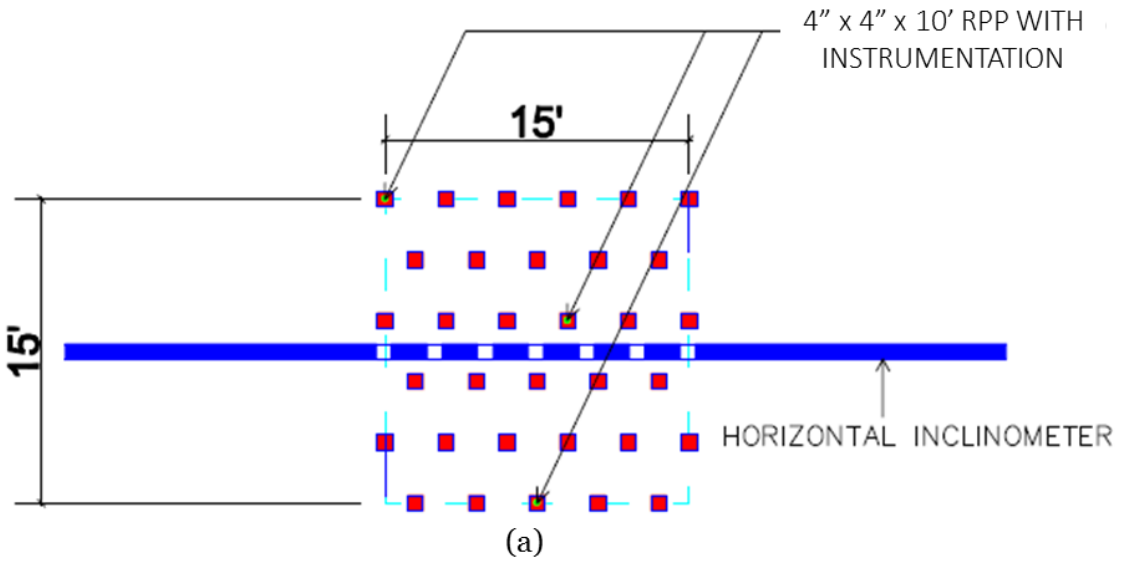

(a)

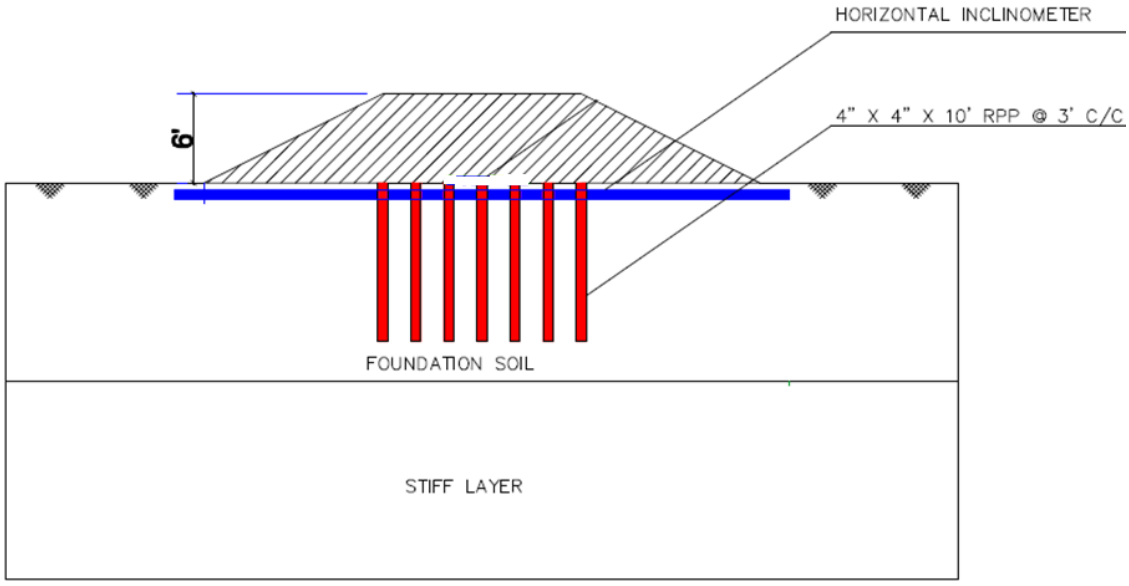

(b)

Figure 3. 39 (a) Proposed layout of 4" x 4" RPP reinforced section; (b) section details of the 4" x 4" RPP reinforced section.

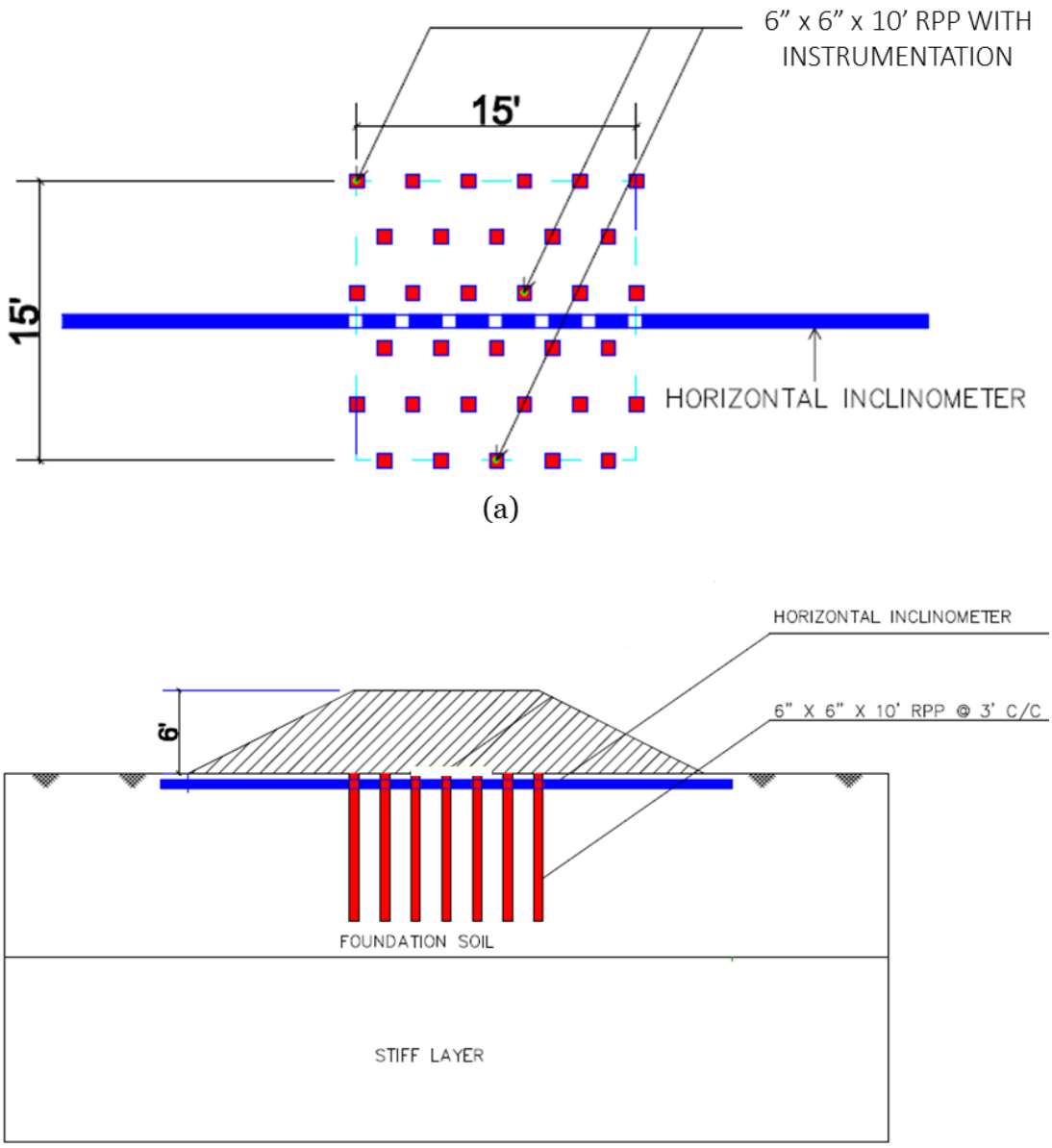

Figure 3. 40 (a) Proposed layout of 6" x 6" RPP reinforced section; (b) section details of the 6" x 6" RPP reinforced section.

For the phase – II construction, a total of two test sections were constructed. One of the sections (BR) was reinforced with 4 in x 4 in RPP and another as control section (BC) without any reinforcement. Identical to phase – I, a thin layer of geosynthetic was placed on top of the foundation. Both the test sections needed to be loaded with a soil height of 5 ft. The native soil

was found to be sandy silt. The boundary of the sections was constructed with galvanized steel pipe and pressure treated wooden plank to create a boxed loading to ensure uniform loading on the foundation. Proposed layout is presented in Figure 3.41 and Figure 3.42.

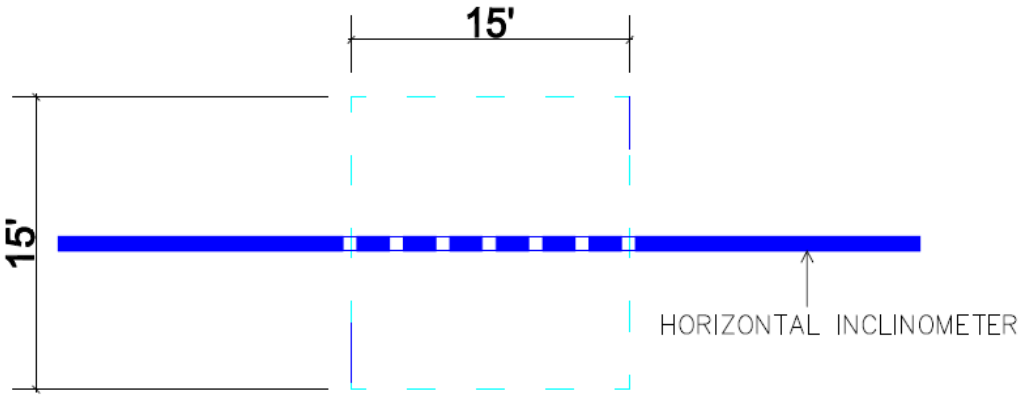

(a)

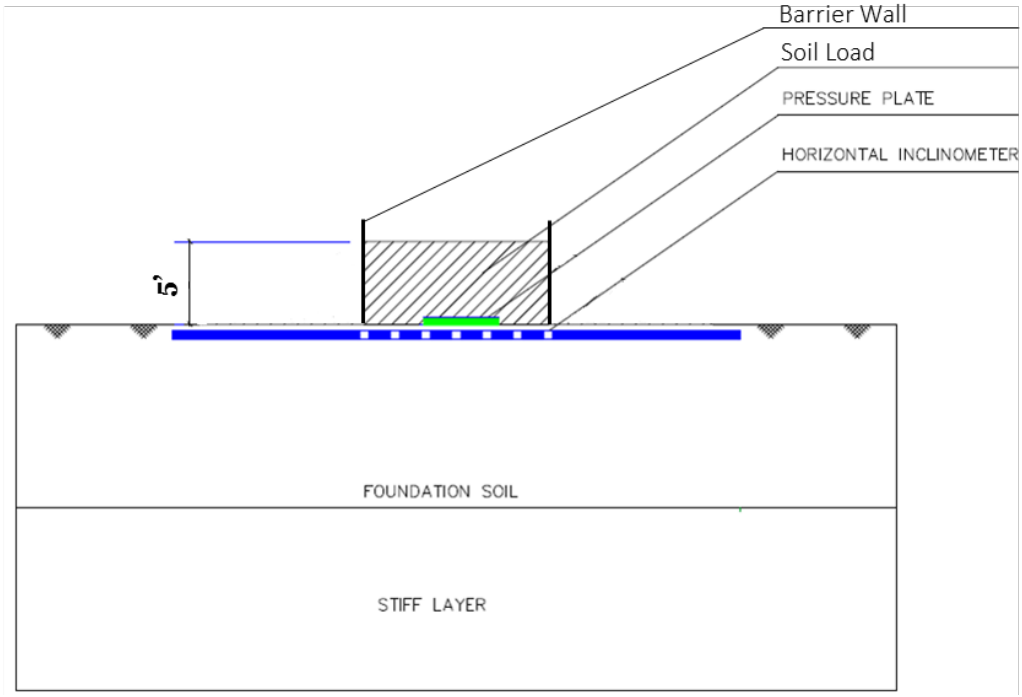

(b)

Figure 3. 41 Phase – II construction; (a) proposed layout of control section; (b) section details of the control section.

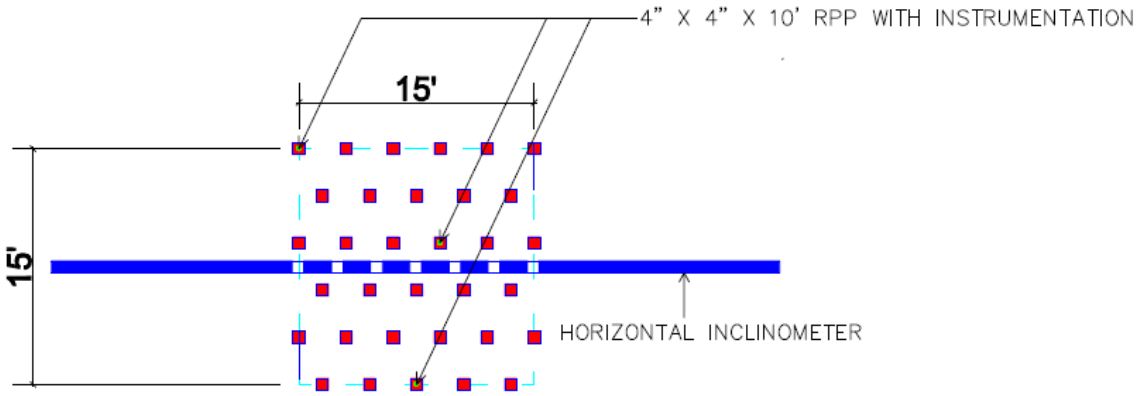

(a)

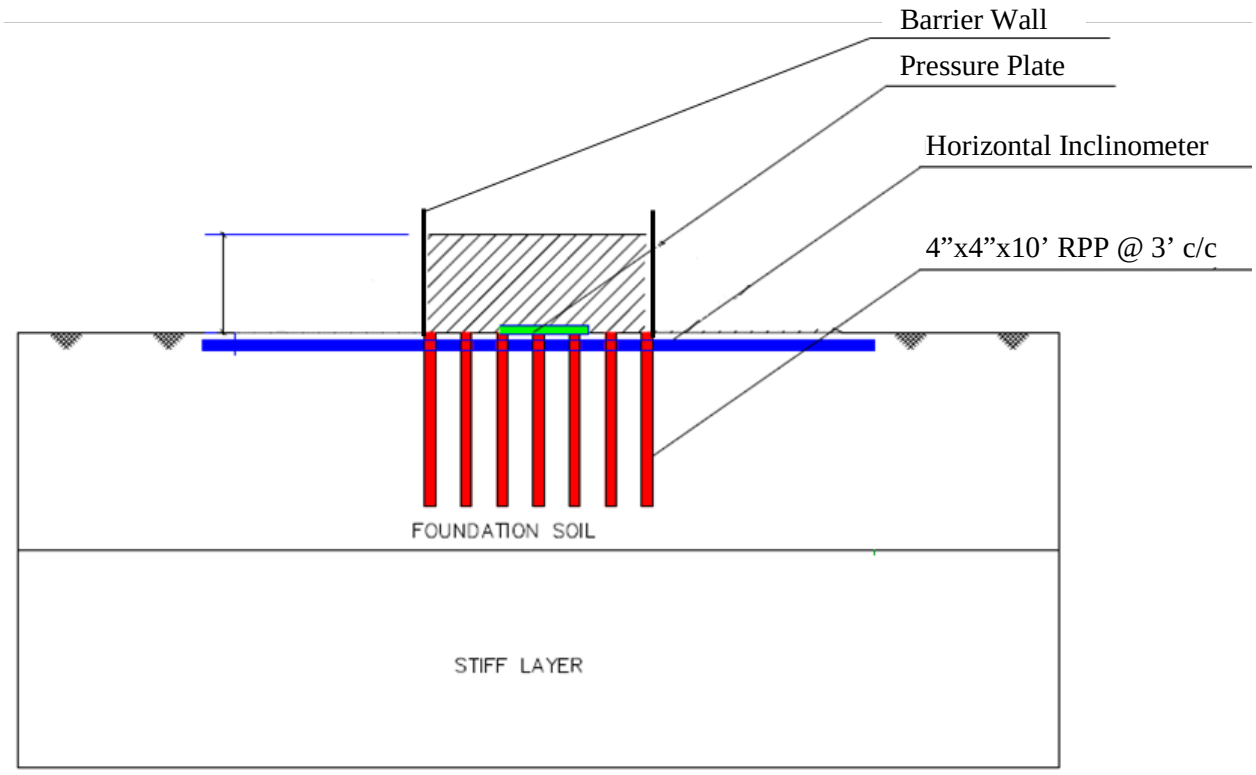

(b)

Figure 3. 42 Phase – II construction; (a) proposed layout of 4" x 4" RPP reinforced section; (b) section details of the reinforced section.

3.7.2 Lateral Loaded Test Sections

RPP has the potential and proved to be capable of resisting lateral force from sliding soil mass in slope. Therefore, they might become potential solution to the sliding of MSE wall base. To evaluate the effectiveness of RPP in providing additional resistance against sliding of the MSW wall base, field test was required. Hence, two test sections were proposed to be constructed at the designated site location at the City of Denton Landfill, Denton, Texas. One as a control section having no plastic pin reinforcement; the other section was reinforced with RPP and designated as reinforced test section. Both of the sections were identical having a dimension of 24 ft. (front) x 15 ft. (sides)

RPPs were proposed to be installed near the toe of an existing slope, where the retaining wall section (SR_01) were to be built. Due to the possibility of base sliding, RPPs of 4 in. x 4 in. were installed with 3 ft. spacing, which eventually expected to act as shear key to restraint the base sliding of the wall. All the RPP in this zone were to be driven 8 ft. into the ground, keeping 2 ft. above ground. The extended part was attached with the base of the wall section to resist the possible sliding due to the lateral load as well as load from the surcharge that will be placed on top of the wall section or slope. Another retaining wall test section (SC_01) with the same geometry and loading condition was constructed adjacent to the reinforced section. This retaining wall served as control section (SC_01), to be compared with the performance of the reinforced section (SR_01). Proposed layout and cross sections of the test sections are presented in Figure 3.43 and Figure 3.44.

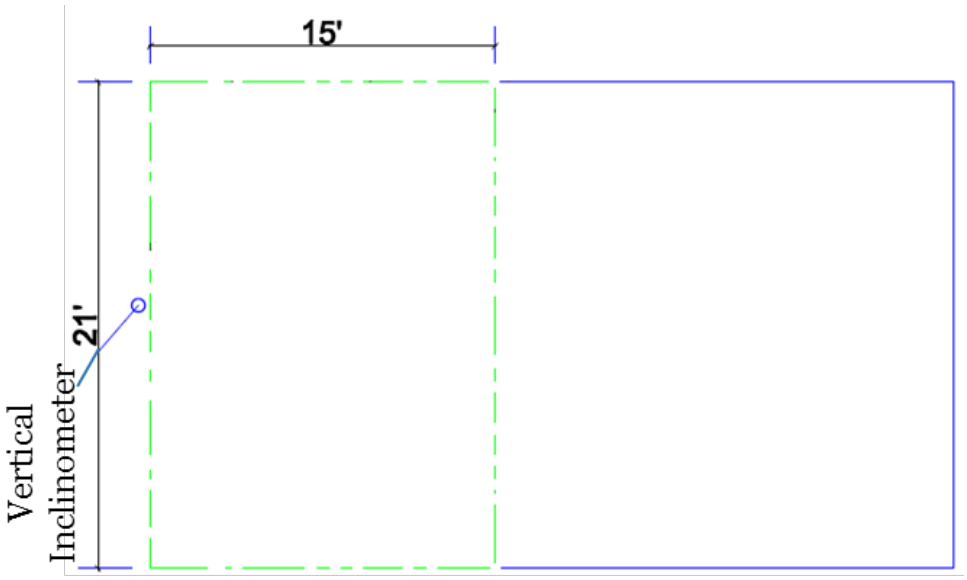

(a)

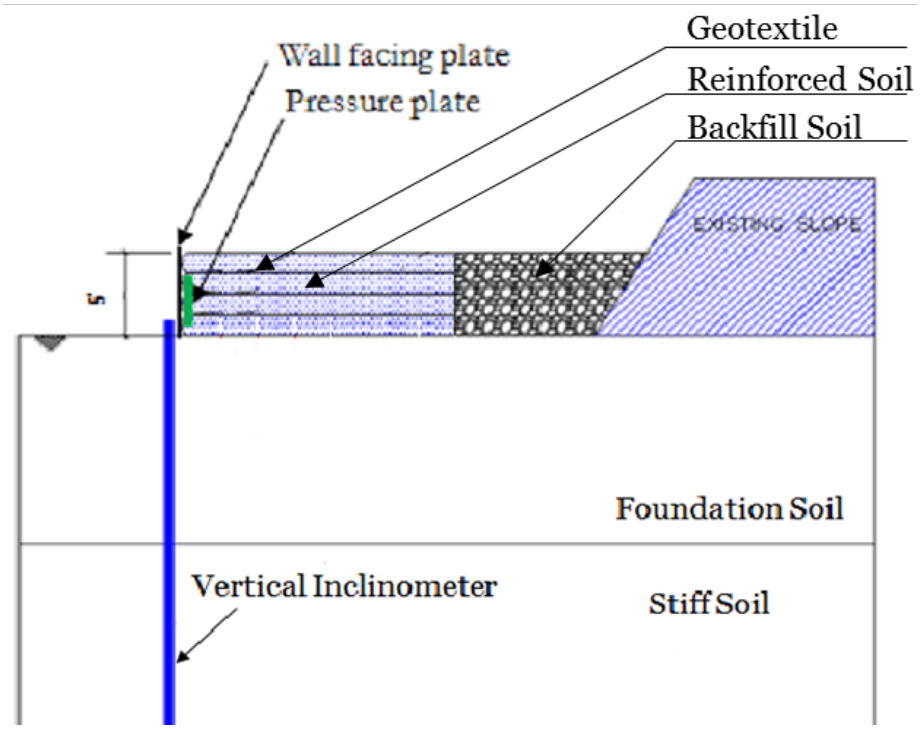

(b)

Figure 3. 43 (a) Proposed layout of control section; (b) Section details of the control section.

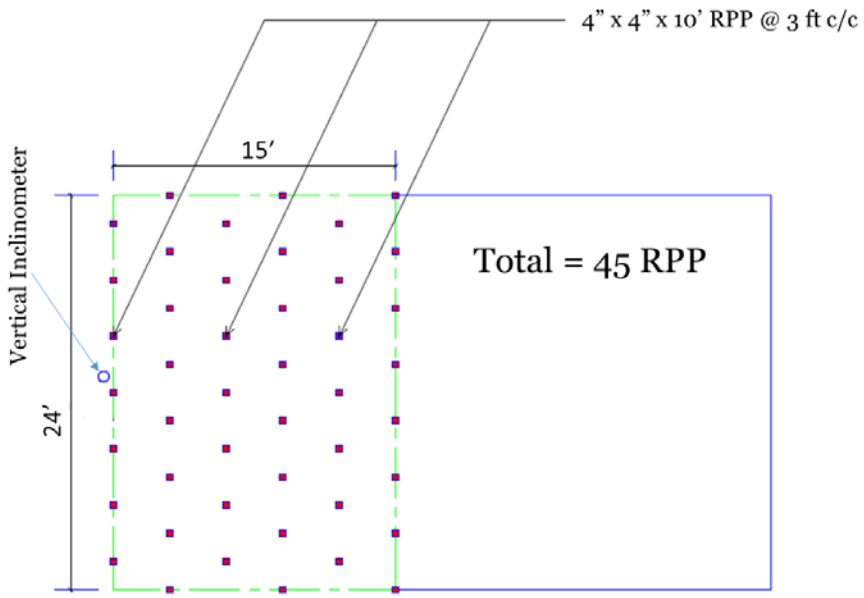

(a)

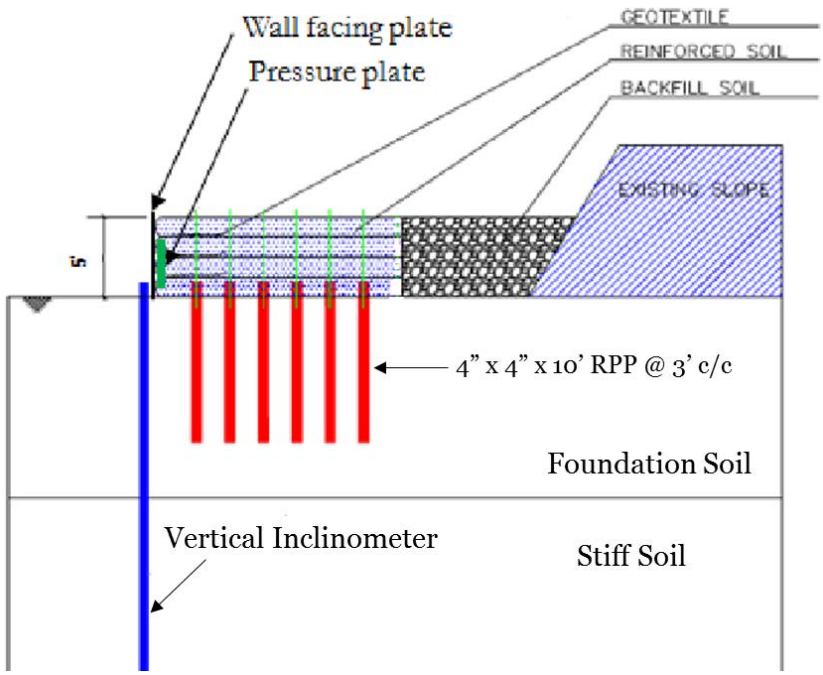

(b)

Figure 3. 44 (a) Proposed RPP layout of reinforced section; (b) Section details of the reinforced test section.

For the phase – II construction, load at the back of the existing lateral sections were increased for further evaluation of the effectiveness of RPP.

3.8 Field Installation of RPP

The field installation of RPP for both vertical and lateral loaded test sections for phase – I were carried out during July, 2017. The size of RPP installed included 4 in. x 4 in. and 6 in. x 6 in. The pin installation process for phase – II construction was similar to phase – I. The detail installation program is presented in this section.

According to a study done by Sommers et al. (2000) on different construction techniques for field installation of RPP, the mast-mounted pseudo vibratory hammer system performed well for RPP installation. The mast-mounted hammer system maintains the alignment of the hammer and restricts imposing additional lateral loads during the RPP driving process (Bowders et al., 2003). A similar crawler-type drilling rig that had a mast-mounted vibrator hammer (model: Klemm 802 drill rig along with KD 1011 percussion head drifter) was utilized by Khan (2014), during the highway slope stabilization on US 287. According to Khan (2014), the crawler-type rig was suitable for the installation process over the slopes, as no additional anchorage is required to maintain the stability of the equipment, which reduces labor, cost and time of the installation process. However, Tamrakar (2015) reported that, a crawler mounted rig with pseudo vibratory hammer (model: Casagrande M9-1) was not suitable due to the steepness of the slope at the crest. Further installation work was carried out with an excavator equipped with Hydraulic breaker (model: deer 200D with FRD, F22 hydraulic hammer). In this study, RPP installation was carried out with an excavator equipped with hydraulic breaker (model: Volvo EC 130).

The site investigation program indicated that soil near the toe of the slope was medium stiff to stiff clay layer, while on top flat portion the soil was found to be relatively soft. Before

installation of RPP, site preparation was necessary as the location was densely covered with vegetation. The site location was cleaned and levelled using a Caterpillar track loader 973D and a Caterpillar 160H motor grader as shown in the Figure 3.45.

(a)

(b)

Figure 3. 45 Site preparation for (a) Vertical loaded test sections; (b) Lateral loaded test sections.

3.8.1 Installation of RPP for Vertical Loaded Test Section

For the vertical loaded test sections, RPP of 4 in. x 4 in. and 6 in. x 6 in. sizes were used as reinforcement for foundation soil. The RPPs installed for these test sections were driven into the ground in a way that the top of each RPP is flashed to the ground surface. RPP installation photographs at vertical loaded test sections are presented in Figure 3.46. RPP driving time was measured during the installation process. Based on the measured driving time, the average installation time, as well as the driving rate, is summarized in Table 3.5. According to Khan (2014), Installation time per RPP is the summation of the time required to install and to maneuver the drilling equipment to the next location. Average RPP driving time at vertical section is shown in Table 3.5.

It was observed that, average driving time for 4 in. x 4 in. section varied from 3.2 to 4.3 minutes whereas for 6 in. x 6 in. section it varied from 5.25 to 10.76 minutes. Larger size of RPP showed higher resistance as well as more energy and time required to install.

Figure 3. 46 Installation of RPP for the vertical loaded test section.

Table 3. 5 Average RPP Driving Time at the vertical loading test sections.

Location of RPP	Row Number	RPP Spacing (ft.)	Average RPP Driving Time (min)	Average RPP Driving Rate (ft./min)
BR_01 (4” x 4”)	1	3	3.45	2.9
	2	3	4.30	2.3
	3	3	3.50	2.9
	4	3	3.25	3.1
	5	3	3.50	2.9
	6	3	3.20	3.1
BR_02 (6” x 6”)	1	3	10.76	0.9
	2	3	8.08	1.2
	3	3	7.50	1.3
	4	3	5.50	1.8
	5	3	5.25	1.9
	6	3	5.25	1.9

Based on the study, the average driving rate for the whole test section with 4 in. x 4 in. was 2.87 ft. /min, which signifies that for vertical loaded sections a 10 ft. long 4 in. x 4 in. RPP could be installed within approximately 3.5 minutes. For locations like such, a total of approximately 115 to 135 RPPs of 4 in. x 4 in. can be installed each day.

For the 6 in. x 6 in. RPP section, the average driving rate was 1.5 ft. /min, which signifies that for the test sections a 10 ft. long 6 in. x 6 in. RPP could be installed within

approximately 6.7 minutes. For locations like such, a total of approximately 50 to 70 RPPs of 6 in. x 6 in. can be installed each day.

3.8.2 Installation of RPP for Lateral Loaded Test Section

For lateral loaded test section, 4 in. x 4 in. 10 ft. long RPP was used, which played the role of shear key to reinforce and increase the sliding resistance of MSE wall base. RPPs in this test section were driven up to 8 ft., keeping 2 ft. above ground surface to form a composite structure with the reinforced soil body of the retaining structure. As the soil was very stiff at the site location, steel pin of 3.95 in. x 3.95 in. cross-section and 8 ft. long was used to make a hole up to the desired depth. RPPs were later installed in to those holes by hammering with hydraulic breaker. A total of 45 RPPS were installed in 6 rows which followed a staggered pattern. The RPP installation photographs are presented in Figure 3.47.

Figure 3. 47 Installation of RPP for the Lateral loaded test section.

The RPP driving time was measured during the installation process. Based on the measured driving time, the average installation time, as well as the driving rate, is summarized in Table 3.6. It was observed that, average driving time for 4 in. x 4 in. section up to a depth of 8 ft. varied from 4.55 to 5.65 minutes.

Table 3. 6 Average RPP driving time for the lateral loading test section.

Test Section	Row Number	RPP Spacing (ft.)	Driving Depth of RPP (ft.)	Average RPP Driving Time (min)	Average RPP Driving Rate (ft./min)
	1	3	8	4.55	1.8
	2	3	8	4.76	1.7
SR_01	3	3	8	5.65	1.4
(4” x 4”)	4	3	8	5.34	1.5
	5	3	8	5.50	1.5
	6	3	8	4.80	1.6

Based on the study, the average driving rate for the whole test section was 1.58 ft. /min, which signifies that for lateral loaded test sections a 10 ft. long, 4 in. x 4 in RPP could be installed (up to a depth of 8 ft. keeping 2 ft. above ground) within approximately 5 minutes. This indicates that a total of 75 to 95 RPPs can be installed per day if the site condition is somewhat close to that observed in the current study.

3.9 Instrumentation

Instrumentation refers to tools used by researches to measure variables of concern during data-collection process. Proper selection of instrumentation is a must for efficient collection of data. It has been cited in many studies as the pacing factor of research (National Academy of Sciences, National Academy of Engineering, and Institute of Medicine, 2006). Therefore, instrumentation for this research has been done according to the need of the research. Instrumentation for the vertical and lateral loaded test sections are presented in the following sub-sections.

3.9.1 Instrumentation for Vertical Loaded Test Section

To evaluate the performance of the reinforced sections, horizontal inclinometers and pressure plates were installed. Summary of the instrumentation for the test sections are listed in Table 3.7.

Table 3. 7 Instrumentation for the test sections.

No.	Section ID	Type	List of Items
01	BR_01	Reinforced section for bearing capacity	• 33 RPP (4” x 4” x 10’) • Horizontal inclinometer
02	BR_02	Reinforced section for bearing capacity	• 33 RPP (6” x 6” x 10’) • Horizontal inclinometer
03	BC_01	Control section for bearing capacity	• Horizontal inclinometer

For the phase – II construction, in addition to the above instrumentation, pressure plates were also installed in both of the test sections to monitor pressure transfer to the ground surface.

3.9.1.1 Installation of Horizontal Inclinometer

Purpose of the horizontal inclinometer is to monitor the vertical deformation of the foundation soil under structural loading. For each test sections, one horizontal inclinometer casing was installed. As the foundation is on the ground surface, approximately 6 inches deep trench was created to install the inclinometers for each sections. Play sand was utilized to create a level bed inside the trench to set the inclinometer casing on a level surface. After placing the inclinometer on the sand bed, it was covered with adjacent soil up to the existing ground level. Figure 3.48 presents the installation steps of horizontal inclinometer for the vertical loaded test sections.

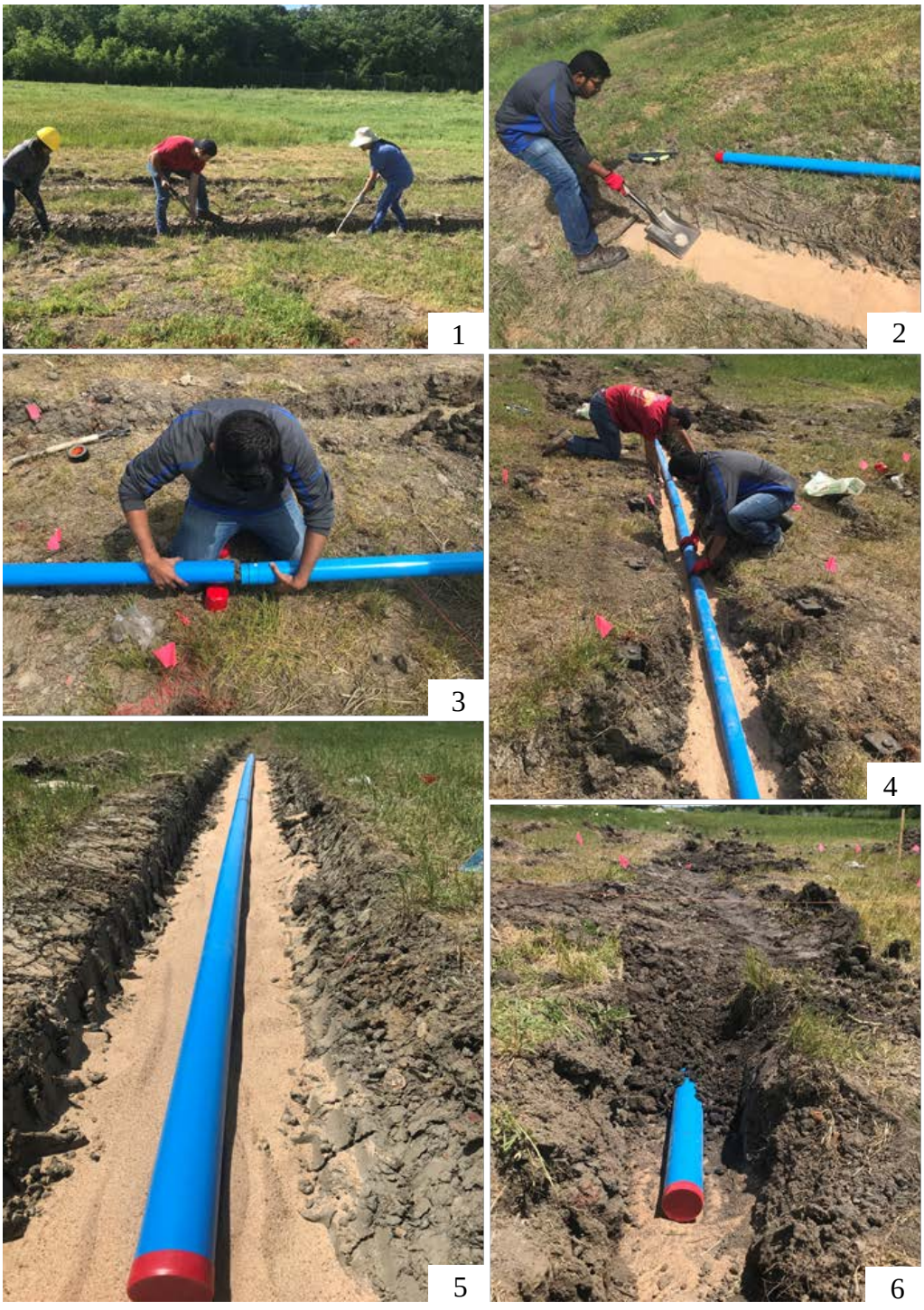

Figure 3. 48 Installation of horizontal inclinometer for the vertical loaded test section.

3.9.1.2 Installation of Pressure Plate

Earth pressure cells also called total pressure cells, are designed to measure the stresses of embankment fill on the soil. In the current study, Model 4800 Earth Pressure Cell was used to measure vertical earth pressure acting on the ground or on the RPP. To connect the pressure plate to the top of the RPP, a steel pile cap of 10 inches diameter was constructed and connected to the RPP before placing the pressure plate. Schematic Diagram of the Earth Pressure Cell and field placement is shown in Figure 3.49.

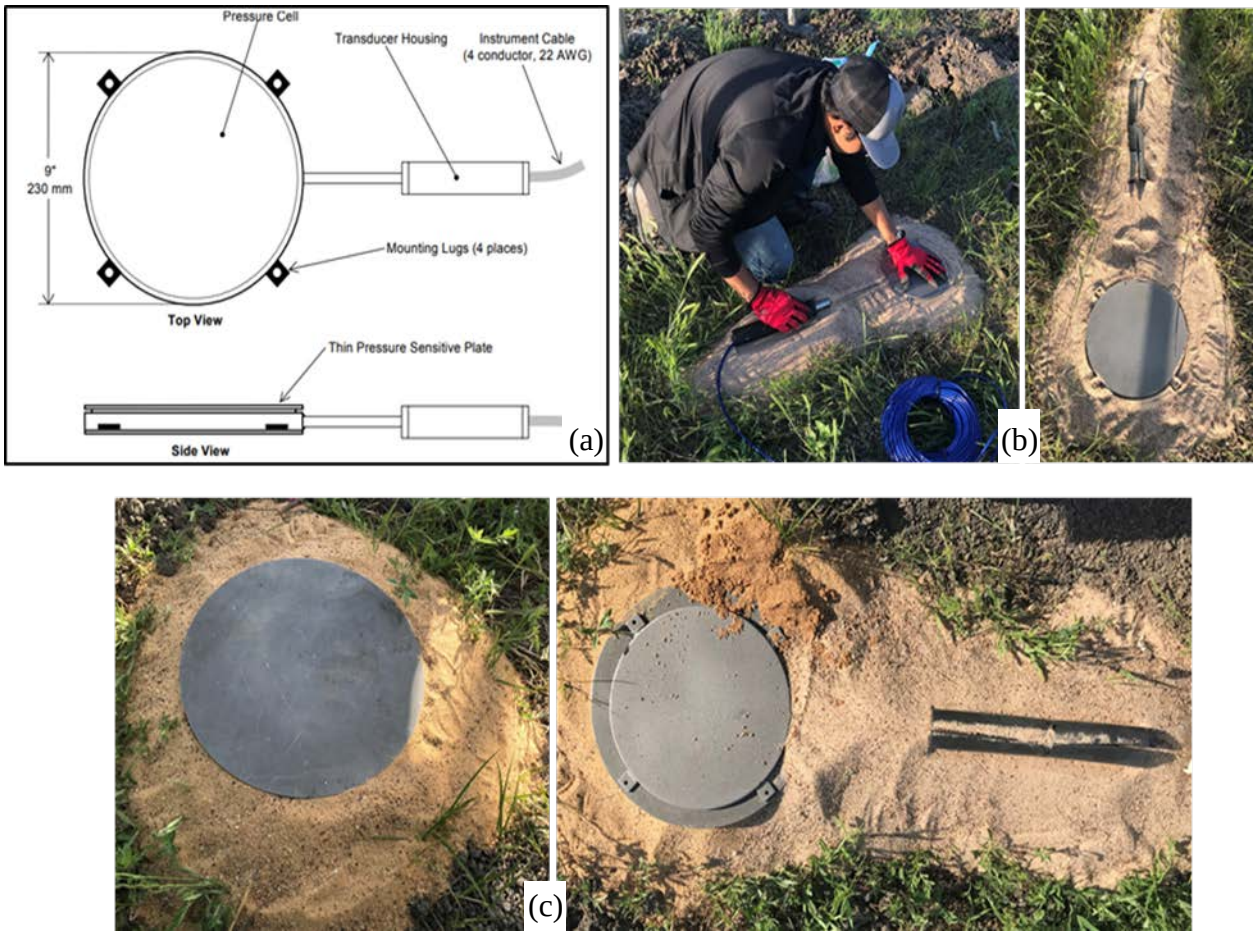

Figure 3. 49 (a) Model 4800 circular earth pressure cell; (b) placement of pressure cell on the ground; (c) installation of pressure plate on RPP.

3.9.2 Instrumentation of Lateral Loaded Test Sections

To evaluate the performance of the RPP as shear key for the retaining wall section, vertical inclinometers and pressure plates were installed. Summary of the instrumentation for lateral loaded test sections are listed in Table 3.8. The table lists the complete instrumentation for the test sections. Difference between phase – I and phase – II is the addition of pressure plates in later phase.

Table 3. 8 Instrumentation for the lateral loaded test sections.

No.	Section ID	Type	List of Items
01	SR_01	Reinforced section for shear resistance	• 45 RPP (4”x4”x10’) • Earth pressure plate • Vertical inclinometer
02	SC_01	Control section for shear resistance	• Earth pressure plate • Vertical inclinometer

3.9.2.1 Installation of Vertical Inclinometer

Purpose of the vertical inclinometer is to monitor the lateral movement of the base of the retaining structure. Two vertical inclinometer casings were installed close to the outside face of the retaining wall of Control Section (SC_01) and Reinforced Section (SR_01) respectively. Depth of the inclinometer casings were 20 ft. from the ground surface and major part of the deformation were expected near the ground surface. Photograph of vertical inclinometer casing placement is shown in Figure 3.50.

Figure 3. 50 Placement of vertical inclinometer for the lateral loaded test sections.

3.9.2.2 Installation of Pressure Plate

Earth pressure cells are designed to measure the stresses or the pressure of soil on the structure. In the current study, Model 4810 Earth Pressure Cell was used to measure lateral earth pressure acting on the face of the wall. Schematic Diagram of the Earth Pressure Cell and field placement is shown in Figure 3.51.

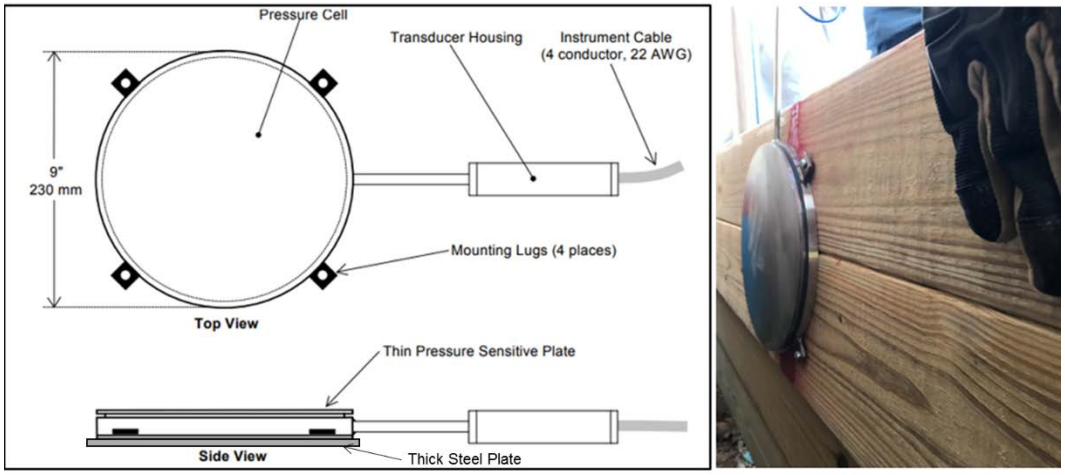

Figure 3. 51 (a) Model 4810 circular earth pressure cell; (b) placement of pressure cell at the inside face of the wall.

3.9.3 Data Acquisition System

After the installation of the pressure sensors, the cables from the sensors were connected to an automatic data acquisition system (data logger) to monitor the pressure applied on the foundation (for vertical section) or on the back of the wall. Two four channel data logger (LC – 2 x 4), one for vertical loaded test sections and one for lateral loaded test sections, were set up in the field to accommodate all the pressure sensors. The LC – 2 x 4 is a self-contained data logger that can measure the data at a continuous interval. For the current study, the interval was set to 60 minutes which permitted storing of 24 data per day. The setup for the logger for both type of test sections are presented in Figure 3.52.

The inclinometers installed in the test sections were monitored on a weekly basis for the first few months; after that it was decided to monitor on monthly basis when the variation was found to be really low. The performance monitoring results and analysis is presented in chapter four.

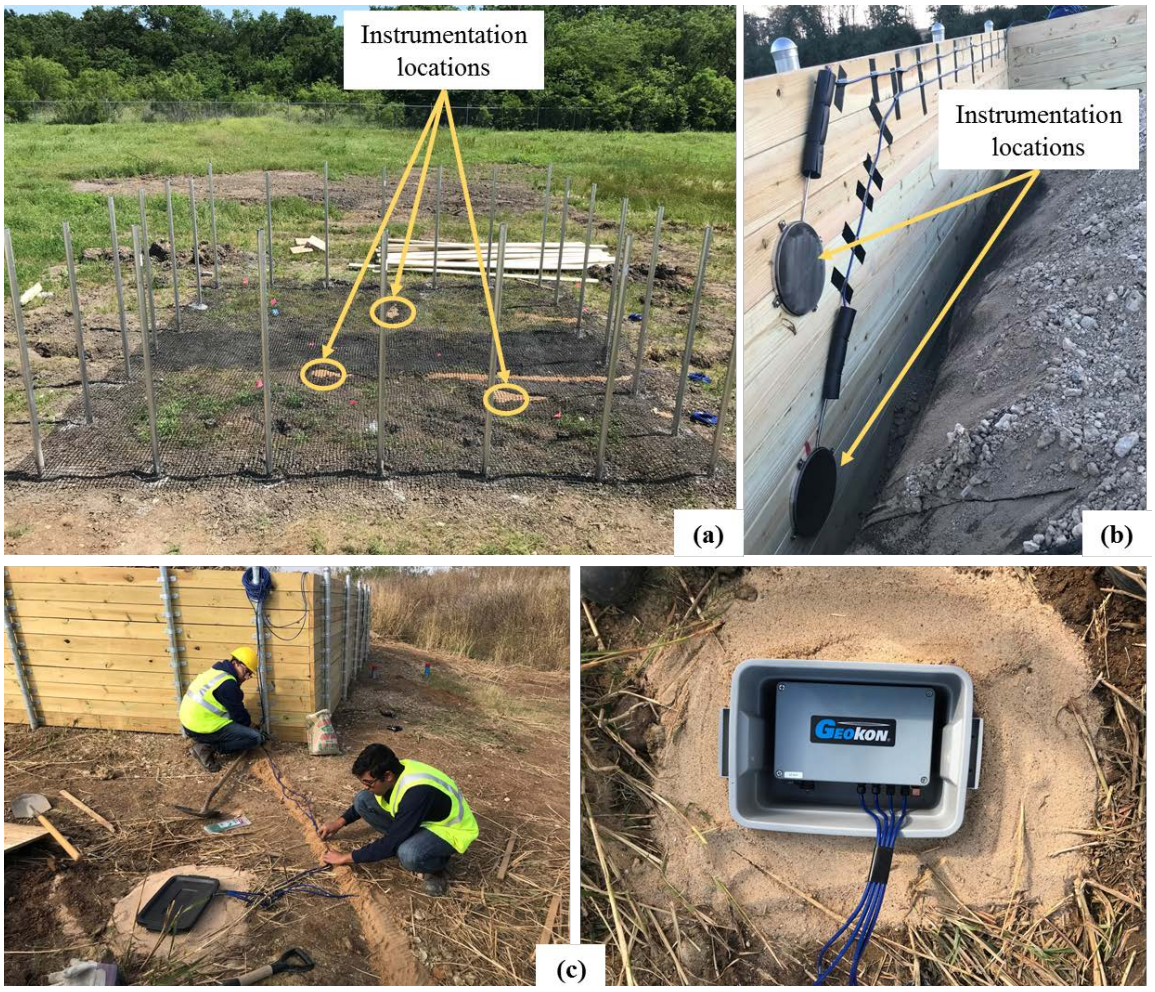

Figure 3. 52 Data collection: Instrumentation locations for (a) vertical loaded test section, (b) lateral loaded test section; (c) data logger setup.

3.10 Construction of the Test Sections

Followed by the installation of RPP and other instrumentations, construction of the test sections took place. The details of the construction of the test sections is presented in the following sub-sections.

3.10.1 Construction of Vertical Loaded Test Sections

Construction of the vertical loaded test sections, as described before, was divided into two phases. Construction of the test sections for phase – I began on 12th July, 2017 and ended

on 14th July, 2017. Phase – II construction began on May 8th, 2018 and completed on May 31st, 2018.

3.10.1.1 Phase – I Construction

For the phase – I construction, a total of three vertical loaded test sections were constructed on July 12, 2017. One of the test sections were constructed as control section without any RPP and the other two as reinforced section with 4 in. x 4 in. and 6 in. x 6 in. RPP as reinforcement for foundation respectively. Once the instrumentation was completed, a thin layer of high strength bi-axial geogrid was placed on the base to mobilize the load from the soil to the RPP by arching action. Medium to high plastic clay, which was readily available native soil, was used fill material. Approximately 100 cubic yards of soil was used to load each section up to a height of 6 ft. Construction sequence of vertical loading section is shown in Appendix E.

3.10.1.2 Phase – II Construction

The objective of phase – II construction was to validate the claim in phase – I of foundation soil improvement due to RPP reinforcement. The sections were constructed using a barrier wall instead of embankment loading for the new construction to ensure uniform load over the foundation soil. The wall was constructed using raw pressure treated 2 in. x 6 in. wooden planks which were supported by 3/8" galvanized schedule 40 steel posts. The steel posts were embedded 3 ft. into the ground by drilling into the ground and grouted with concrete and was spaced at 3 ft. Once the concrete was set in place and the posts were stiff enough, the wooden planks were connected to the posts using brackets and screws. Once the barrier wall construction was completed, silty sand of 5 ft. height was used as fill material to apply load on

the test sections. A layer of geogrid was placed to improve the load transfer efficiency before load application. Figure 3.53 presents the construction steps of the test sections for phase – II.

Figure 3. 53 Phase – II construction: (a) Installation of steel post and geogrid placement; (b) Connecting wooden planks with the post and wall construction; (c) Loading the test sections and completed test section.

3.10.2 Construction of Lateral Loaded Test Sections

Construction of the lateral loaded test sections was also done in two phases. Construction of test section for phase – I began on 12th July, 2017 and ended on 14th July, 2017. Phase – II construction began on November 6th, 2017 and completed on November 10th, 2017.

3.10.2.1 Phase – I Construction

Two retaining walls were constructed for lateral loaded test sections. One of the retaining walls (SR_01) contains RPP as reinforcement for the wall base, where 2 ft. of the RPP was kept extended above the ground surface with 8 ft. anchorage in the ground; the other retaining wall (SC_01) had no RPP reinforcement and thus designated as control section. Geosynthetic was used to reinforce the backfill soil in several layers. The retaining walls were constructed to a height of 4 ft. for each section. Both of the sections were constructed identically to compare the test results. Compaction of soil was conducted for each layer and caution was exercised while compacting soil close to the face of the wall. Construction of the retaining walls began on 13th July, 2017 and completed on 14th July, 2017. Construction sequence of lateral loading section is shown in Appendix F. Figure 3.54 presents some of the photographs of phase-I construction.

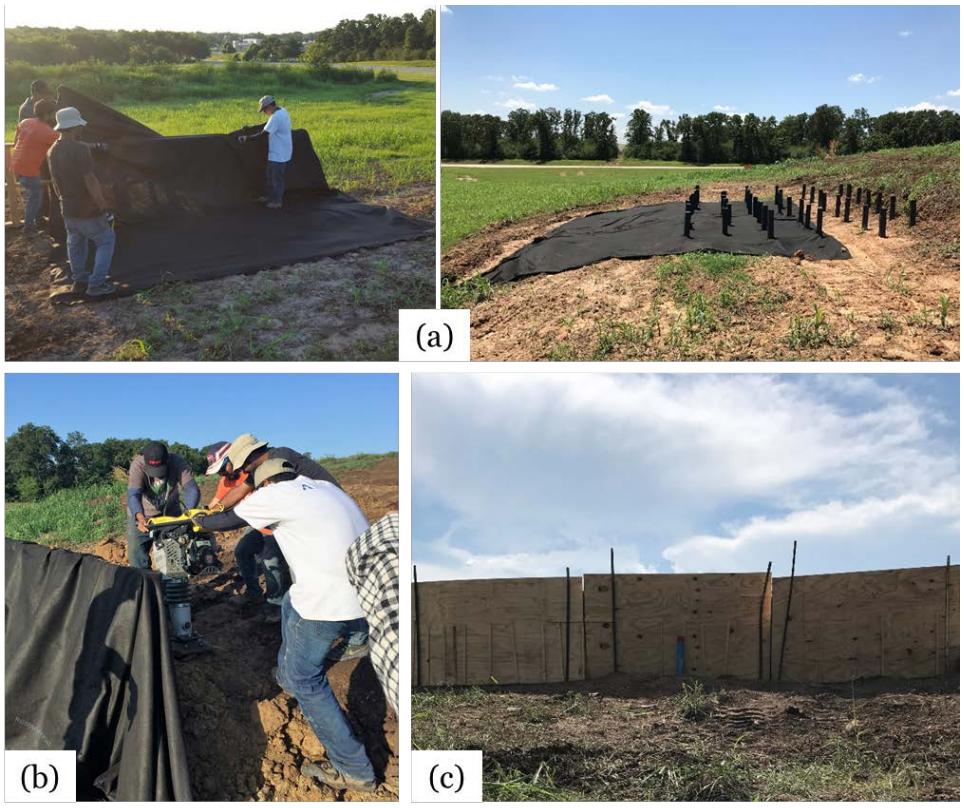

Figure 3. 54 Construction of the test sections: (a) Placement of geosynthetic layer; (b) Compaction of soil layer; (c) Completed wall.

3.10.2.2 Phase – II Construction

The objective of phase – II construction was to provide a relatively better facing system suitable and capable to sustain higher loading height. For the new wall, raw pressure treated 2 in. x 6 in. wooden planks were used and 3/8 in. galvanized schedule 40 steel post was installed at 5 ft. spacing as support to the wooden planks. Posts were installed by drilling 2 ft. into ground and grouted with concrete as shown in Figure 3.55a. Once the concrete was set in place and the posts were stiff enough, the wooden planks were connected to the posts using brackets and screws as shown in Figure 3.55b. During installation of the new wall facing, pressure sensors were attached to the inside face of the wall (Figure 3.55c).

Figure 3. 55 (a) Installation of steel post; (b) Connecting wooden planks with the post; (c) Installing pressure sensor at the inside face of the wall facing.

The old facing was carefully removed once the new facing were up to a certain height. The extended portion of the wooden planks for the new facing were sawed and screwed with side facing of the wall as presented in Figure 3.56a. The complete wall is shown in Figure 3.56b.

Figure 3. 56 (a) Sawing to shape and connecting corners using screws; (b) Complete wall facing of the test section.

Once the new facing construction was completed, the test sections were loaded with backfill soil up to a height of 5 ft. using a front end loader as shown in Figure 3.57a. However, due to the equipment being too heavy and possibility of excess lateral pressure generation during backfilling, it was decided to manually fill the immediate back of the wall facing (Figure 3.57b).

Figure 3. 57 (a) Backfilling test section; (b) Manually spreading soil near the facing; (c) Complete wall after backfilling.

CHAPTER 4

RESULTS AND DISCUSSION

The results obtained from the field scale study to evaluate the effectiveness of Recycled Plastic Pins (RPP) in improving the performance of unsuitable ground, to carry load with reduced settlement or to increase the shear resistance against the sliding of the MSE wall base, are presented in this chapter. Major problems with weak foundation soil includes bearing failure of structures in the form of excessive differential and total settlement, lateral pressure and global or local instability (Han and Gabr, 2002). On the other hand, for MSE retaining structure constructed on stiff foundation soil, a major concern is the failure of the structure by excessive lateral movement of base of the wall facing due to lack of sufficient shear resistance against sliding. In the current study, RPP has been utilized as reinforcement for unsuitable soil in both scenarios; however, the application concept is slightly different. For the former case, RPP was used for foundation reinforcement (similar to pile supported structures) which might help with soil densification and improving the load supporting capacity of the soil. When applied in combination to geosynthetics it ensures the load mobilization of the fill material to the RPPs. For the latter case, RPP, when incorporated in design and construction at the base of MSE retaining structure, might perform as shear key for the MSE wall base to provide additional shear resistance against base sliding of the wall. Numerous test sections have been constructed in the field as part of the study to assess the performance of RPP for both cases. Construction of the test sections were carried out in two phases as described in the previous chapter.

This chapter includes the performance monitoring results obtained from field monitoring data for the test sections for both phase – I and phase– II. Comparison between the results for the related test sections are also presented and discussed.

4.1 Performance of Vertical Loaded Test Sections

The purpose of the vertical loading test section was to determine the effectiveness of RPP to improve the excessive settlement scenario of structures (e.g. embankment) constructed on weak foundation soils. The following sub-sections present the analytical study for the RPP reinforced foundation and the performance monitoring of the test sections for both phase – I and phase – II.

4.1.1 Analytic Study on Vertical Loaded Test Sections

Recycled plastic pins help densifying the foundation soil when driven into the foundation. In addition, it creates a RPP – soil composite; the stiffness of which improves considerably depending on the size and spacing of RPPs. Due to the RPP reinforcement, the new composite foundation becomes capable of supporting the load from the structure with reduced settlement. The potential of RPP in improving the weak foundation soil can be evaluated using analytical method.

Settlement of the foundation soil can be divided into two parts; elastic settlement which depends on load, and consolidation settlement or time dependent settlement. However, in absence of water table, no consolidation settlement takes place. In the current study, from the field investigation of the site location no water table was found. Therefore, the predominant type of settlement for the foundation soil at the study location under load should only be elastic

settlement (Se). The theory of elasticity may be used to determine the elastic settlement of a foundation soil. According to Das (2011), if the foundation is perfectly flexible, the theoretical expression of elastic settlement is,

$$S_e = q_0(\alpha B')\frac{1-\mu_s{}^2}{E_s} I_s I_f \quad (4.1)$$

where,

q_0 = net pressure applied on the foundation

μ_s = Poisson's ratio of the soil

E_s = average modulus of elasticity of the soil under the foundation

B' = B/2 for center of the foundation; or B for the corner of the foundation

I_s = Shape factor

I_f = depth factor

α = a factor that depends on the location on the foundation where settlement is to be calculated

= 4 (for center of the foundation); 1 (for corner of the foundation)

For the current study, a section was considered having a square foundation of width, B = 15 ft. and applied load was due to the soil fill material of 6 ft. height with a unit weight, γ = 115 pcf. Therefore, the net pressure applied on the foundation was, q_0 = 115 x 6 = 690 psf. The average modulus of elasticity of the soil under the foundation was calculated to be, E_s = 124762 psf. and poisons ratio, μ_s = 0.25. For a square foundation on the ground surface, shape factor (I_s) and depth factor (I_f) is considered to be 1.0. For a foundation under uniform load, the maximum stress is usually experienced at the center of the foundation, therefore, maximum

settlement will take place at the center of the foundation. Hence, the maximum settlement of the foundation can be calculated using equation 4.1.

S_e = 690 x 4 x (15/2) x $\frac{1-0.25^2}{124762}$

= 0.156 ft.

= 1.87 inches.

Which is excessive considering the allowable settlement to be 1 inch. The bearing capacity of the foundation for 1 inch settlement can be back calculated using equation 4.1.

$$q_u = \frac{S_e}{(\alpha B')\frac{1-\mu_s{}^2}{E_s}} \tag{4.2}$$

$$= \frac{(1/12)}{\left(4\,x\frac{15}{2}\right)\frac{(1-0.25^2)}{124762}} = 369.67 \cong 370 \text{ psf.}$$

If RPPs are driven into the foundation soil, it is expected to improve the support capacity of the existing foundation soil. Driving RPP into the soft foundation soil without replacement of soil ensures densification of the soil matrix, creating a composite foundation of improved stiffness. Modulus of elasticity of the RPP is E_{RPP} = 28.8 x 10^6 psf. If 4 in. x 4 in. RPPs are driven into the foundation soil at 3 ft. c/c spacing in a staggered pattern, the equivalent average modulus of elasticity of the RPP – soil composite becomes, E_{eq_s} = 279501 psf. Settlement for the new reinforced foundation can be calculated using equation 4.1.

S_e = 690 x 4 x (15/2) x $\frac{1-0.25^2}{279501}$

= 0.0694 ft.

= 0.83 inches.

A reduction in settlement of about 56% may be obtained through the use of 4 in. x 4 in. RPP at 3 ft. c/c spacing. The bearing capacity for the improved foundation for 1 inch settlement can be calculated using equation 4.2.

$$q_u = \frac{S_e}{(\alpha B')\frac{1-\mu_s{}^2}{E_{eq_s}}}$$

$$= \frac{(1/12)}{\left(4\, x\frac{15}{2}\right)\frac{\left(1-0.25^2\right)}{279501}} = 828.15 \cong 828 \text{ psf.}$$

Which shows, compared to the unreinforced section, a bearing capacity improvement of about 2.24 times may be obtained due to the use of 4 in. x 4 in. RPP at 3 ft. c/c.

Using the same analytical process, settlement and bearing capacity for foundation reinforced with different size and spacing of RPP can be determined. Table 4.1 shows calculated predicted settlement for the foundation soil reinforced with 4 in. x 4 in., 6 in. x 6 in. and 10 in. x 10 in. RPP at 2 ft., 3 ft. and 4 ft. spacing. Table 4.2 presents bearing capacity of different RPP reinforced section for 1 inch settlement.

Table 4. 1 Settlement calculated for RPP reinforced foundation soil due to 6 ft. soil load.

Settlement (inches)			
RPP size / **Spacing (ft.)**	**4 in. x 4 in. RPP**	**6 in. x 6 in. RPP**	**10 in. x 10 in. RPP**
2	0.55	0.32	0.12
3	0.83	0.49	0.21
4	1.11	0.74	0.36

Table 4. 2 Bearing capacity of the reinforced foundation (for 1 inch settlement).

Bearing Capacity (psf.)			
RPP size / Spacing (ft.)	**4 in. x 4 in. RPP**	**6 in. x 6 in. RPP**	**10 in. x 10 in. RPP**
2	1260	2174	5942
3	828	1403	3242
4	619	933	1936

Based on the calculation it was noticed that bearing capacity can be improved by as much as 16 times compared to the unreinforced section by the use of RPP. A significant reduction in settlement was found for each of the reinforced sections based on the analytical solution. Figure 4.1 shows a comparative bar chart of foundation settlement between different RPP reinforced sections and control section (without RPP reinforcement).

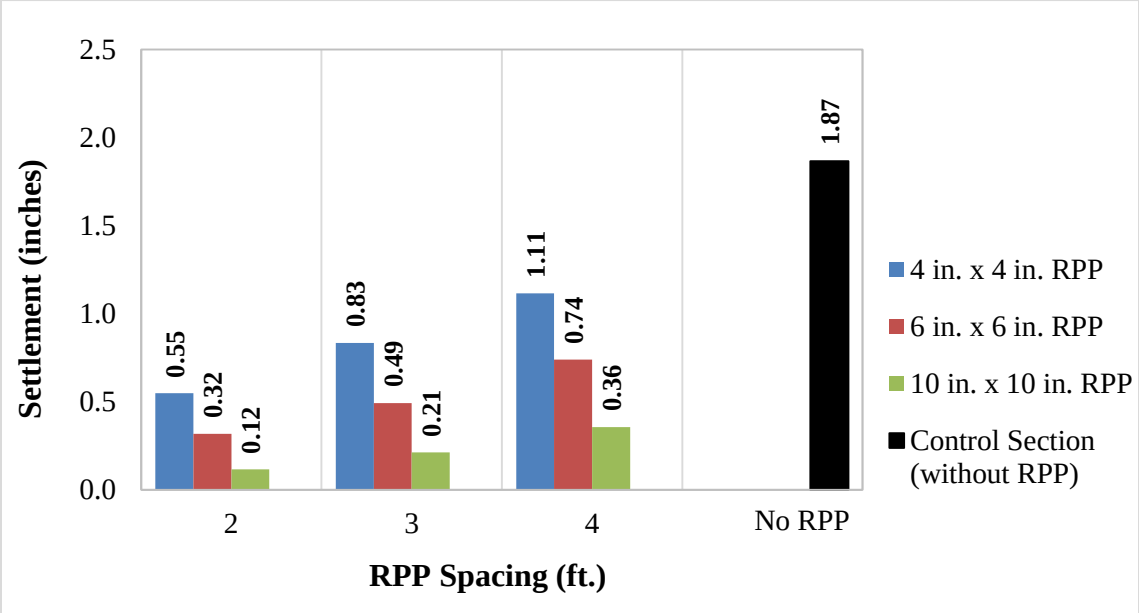

Figure 4. 1 Comparison of foundation settlement between control and RPP reinforced sections.

The calculated bearing capacity for the reinforced foundation (for 1 inch settlement) was plotted against RPP spacing and RPP size as presented in Figure 4.2 and Figure 4.3 respectively. From the plot it was observed that for same RPP size bearing capacity increases with decreasing RPP spacing. Also, for fixed spacing of RPP, bearing capacity increases with increasing size of RPP. It was observed that the rate of increase in bearing capacity increases with increasing RPP size which is due to the larger size has the benefit of replacing more void space in the soil matrix which better densifies the soil, improves the stiffness, has much higher load carrying capacity and thus improves the bearing capacity of the foundation soil.

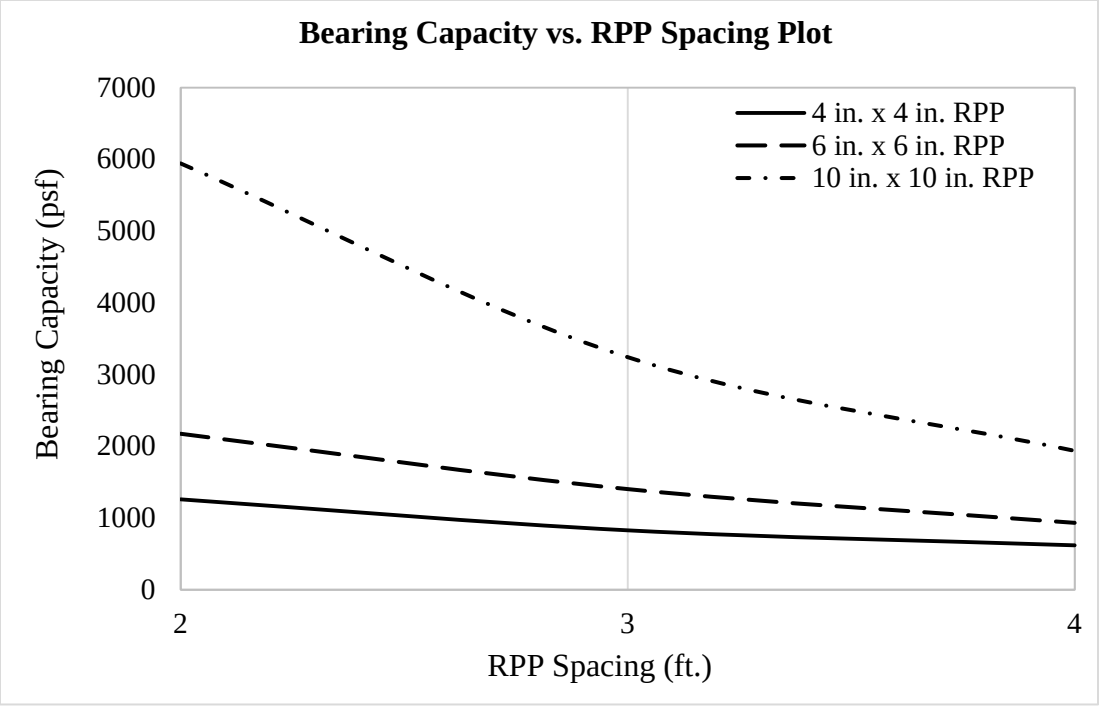

Figure 4. 2 Relation between bearing capacity and RPP spacing for different sizes of RPPs based on analytical study.

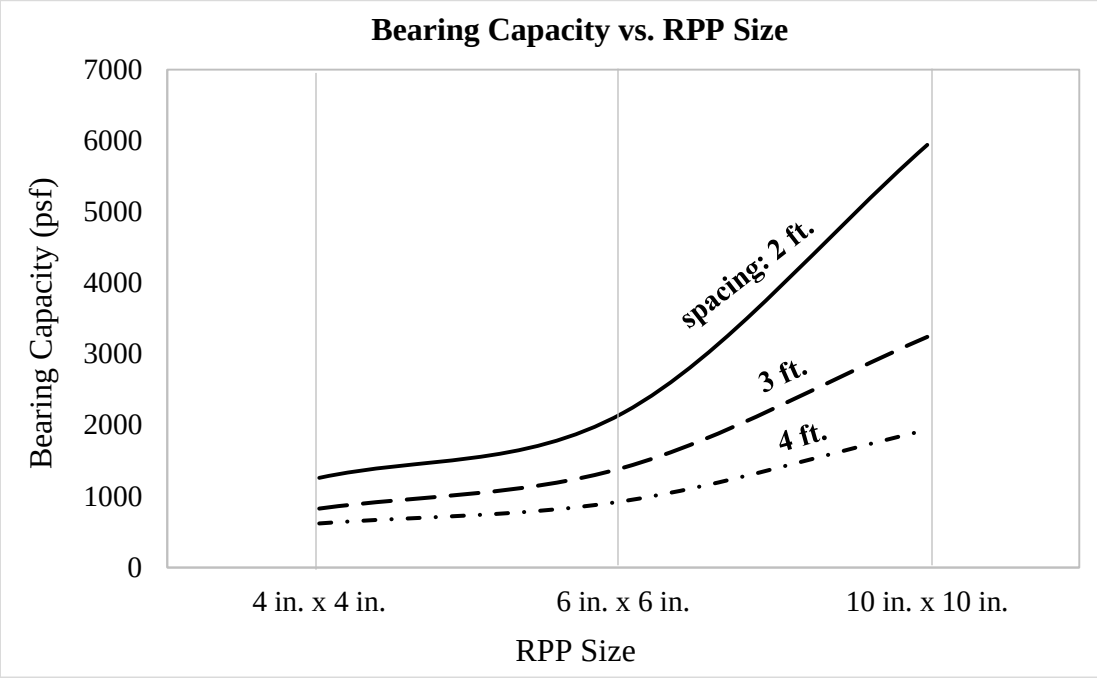

Figure 4. 3 Relation between bearing capacity and size of RPP for fixed spacing based on analytical study.

Elastic settlement was calculated for the foundation soil reinforced with RPP of different sizes and spacing under different bearing pressure. Figure 4.4 presents settlement vs bearing pressure plot. From the plot it was observed that for each configuration of RPP reinforcement, bearing pressure increases considerably compared to the control section (without any RPP reinforcement). It was also noticed that, in some cases performance of the test section reinforced with larger size of RPP with wider spacing could be relatively better compared to the smaller sized RPP with narrower spacing.

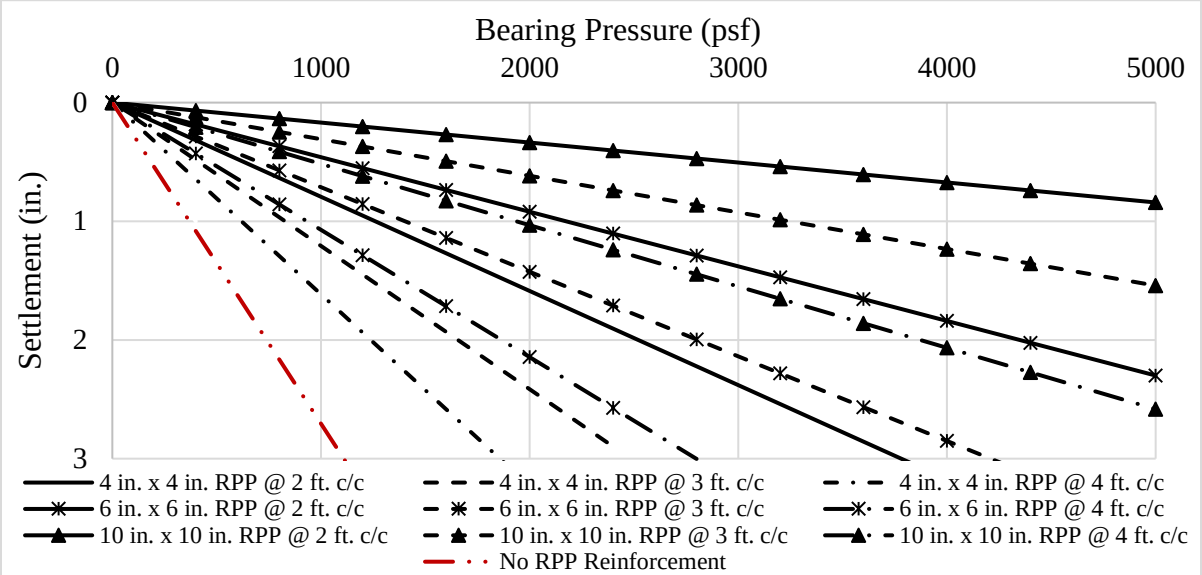

Figure 4. 4 Comparison of bearing capacity between control section and different RPP reinforced section based on analytical calculation.

4.1.2 Performance Monitoring Results: Phase – I

To understand the field performance of recycled plastic pins in improving the weak foundation soil, three different test sections were constructed in this phase. One of the test sections served as a control section without any RPP reinforcement for the foundation soil; foundation of the other two were reinforced with RPP (4 in. x 4 in. and 6 in. x 6 in. respectively). For all three test sections, a thin layer of high strength bi-axial geogrid was placed on the surface to facilitate load transfer from fill material to the RPP. Horizontal inclinometers were utilized to monitor the performance of the test sections. The inclinometers were monitored on weekly basis. Vertical deformation of the control section and the reinforced sections based on the instrumentation data are presented in the current study.

4.1.2.1 Control Test Section

The field monitoring results from the inclinometer at the control section is presented in Figure 4.5. Based on the field observations, the maximum vertical deformation/settlement was

found to be 2.01 inches for an embankment fill height of 6 ft. A significant differential settlement was observed due to load application. Two days after the construction of the test section, the settlement was observed to be 1.1 inches, which increased to about 1.9 inches after two weeks. This represents that, a significant amount of settlement took place within the first few weeks after the load application. With time the settlement of the control section was found to be increasing gradually. During the monitoring period, no significant immediate change in settlement was found due to the precipitation events; however, settlement increased by a little followed by the precipitation. This might be due to the embankment fill material being clayey soil, restricts immediate drainage and tends to store/absorb water, which slightly increases the unit weight of the fill material. Figure 4.6 shows the rainfall data during the monitoring period. Based on the plot, settlement was observed to be increasing steadily with time. After a major rainfall event, a slight increase in the settlement was observed.

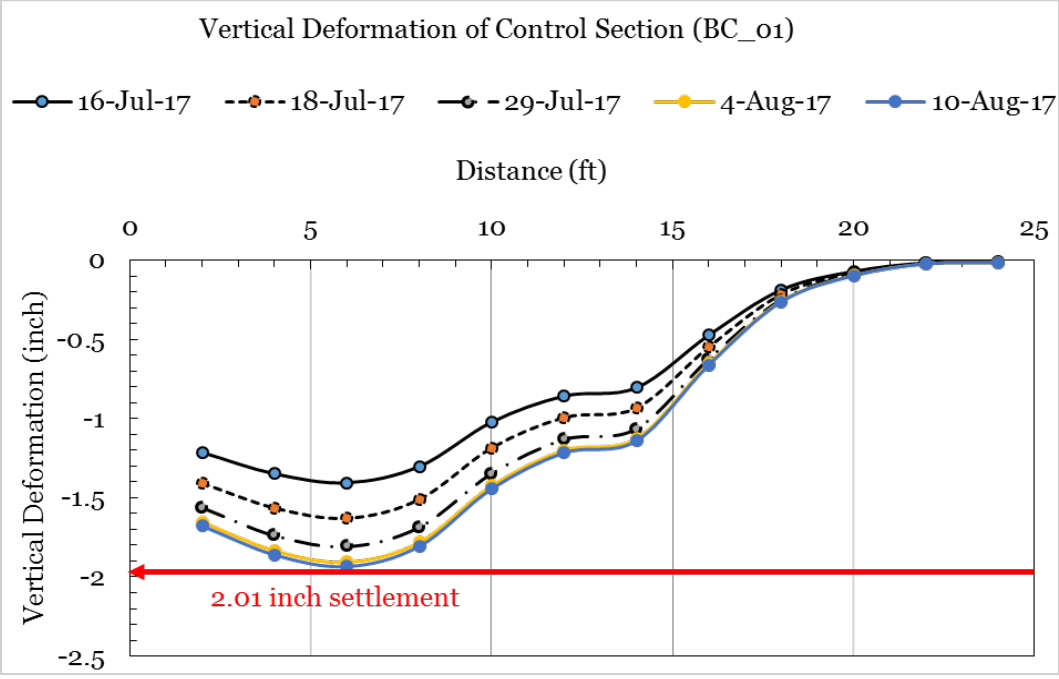

Figure 4. 5 Vertical deformation of control section.

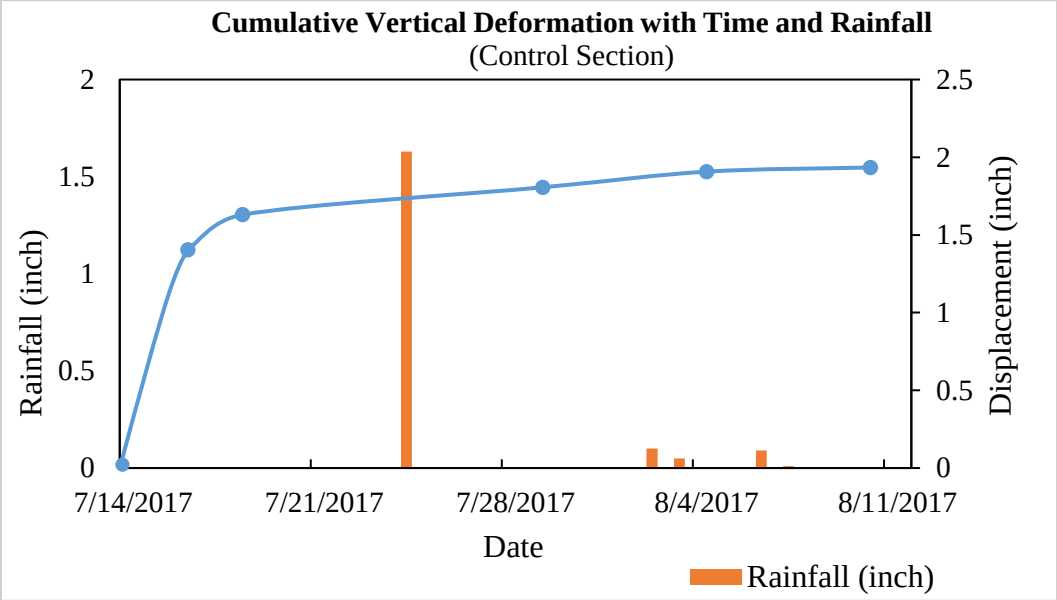

Figure 4. 6 Vertical deformation of the control section with time and rainfall event.

4.1.2.2 Reinforced Test Section 1 (4 in. x 4 in. RPP)

The field monitoring results from the inclinometer at the 4 in. x 4 in. RPP reinforced test section is presented in Figure 4.7. Based on the field observations, the maximum vertical deformation/settlement was found to be 0.8 inches. Unlike control section, almost uniform settlement was observed for this test section. This might be due to the arching effect of geogrid that is carrying load from the soil and uniformly transferring it to the RPP. Chen et al. (2009) concluded that, a major part of the soil pressure is transferred to the pile through arching effect of the geogrid, which also reduces the pressure on soil between the piles. According to Han and Gabr (2002), a significant portion of differential settlement can be restricted by using geogrid reinforced pile supported embankment. For this test section, a settlement of about 0.39 inches was observed two days after the construction of the test section, which increased to 0.7 inches after two weeks. Figure 4.8 presents settlement of the test section with time and in relation to precipitation events. No significant change was observed followed by precipitation

event. After the first month almost no change in settlement was observed and the total vertical deformation became almost constant.

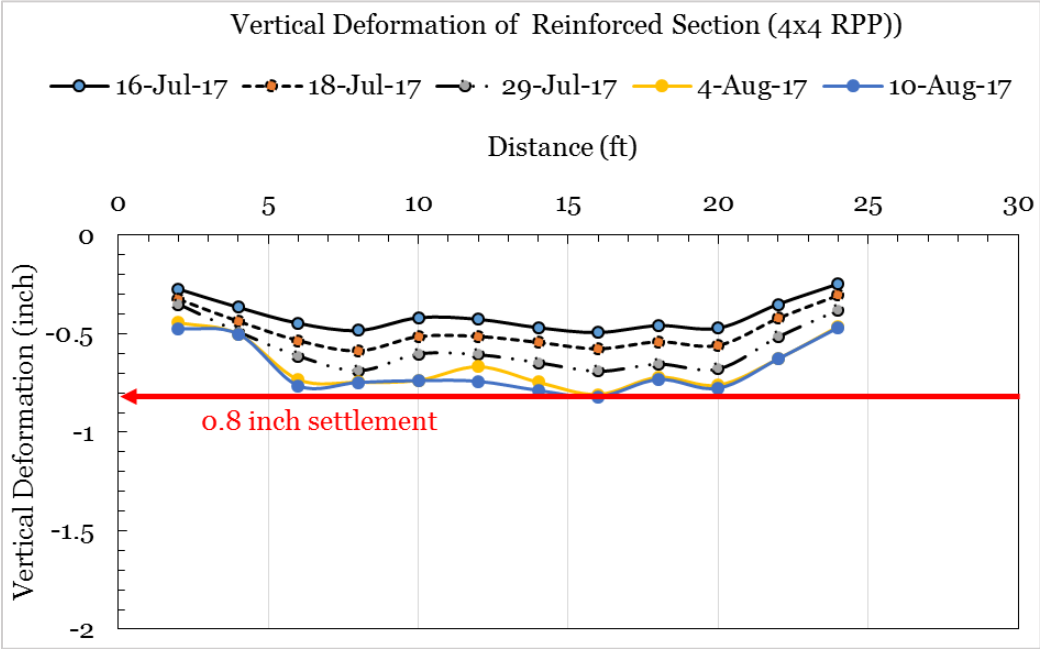

Figure 4. 7 Vertical deformation of 4 in. x 4 in. RPP reinforced test section.

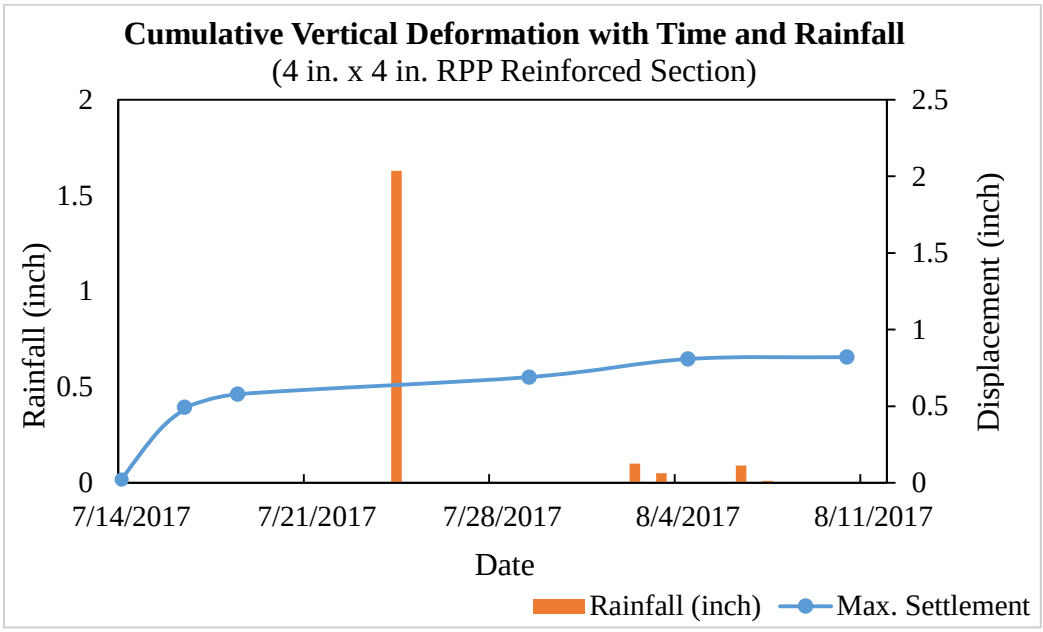

Figure 4. 8 Vertical deformation of the 4 in. x 4 in. RPP reinforced test section with time and rainfall event.

4.1.2.3 Reinforced Test Section 2 (6 in. x 6 in. RPP)

The field monitoring results from the inclinometer at the reinforced section having 6 in. x 6 in. RPP is presented in Figure 4.9. Based on the field observations, the maximum vertical deformation/settlement was found to be 0.64 inches. Relatively uniform settlement was observed for this test section. This might be due to the arching effect of geogrid that is carrying load from the soil and transferring it to the RPP. Compared to the 4 in. x 4 in. RPP reinforced section, there were minor differential settlement observed for this test section. The variation might be due to the poor installation of geogrid or the geogrid in some places might have been damaged during loading. A settlement of about 0.25 inches was observed immediately after the construction of the test section.

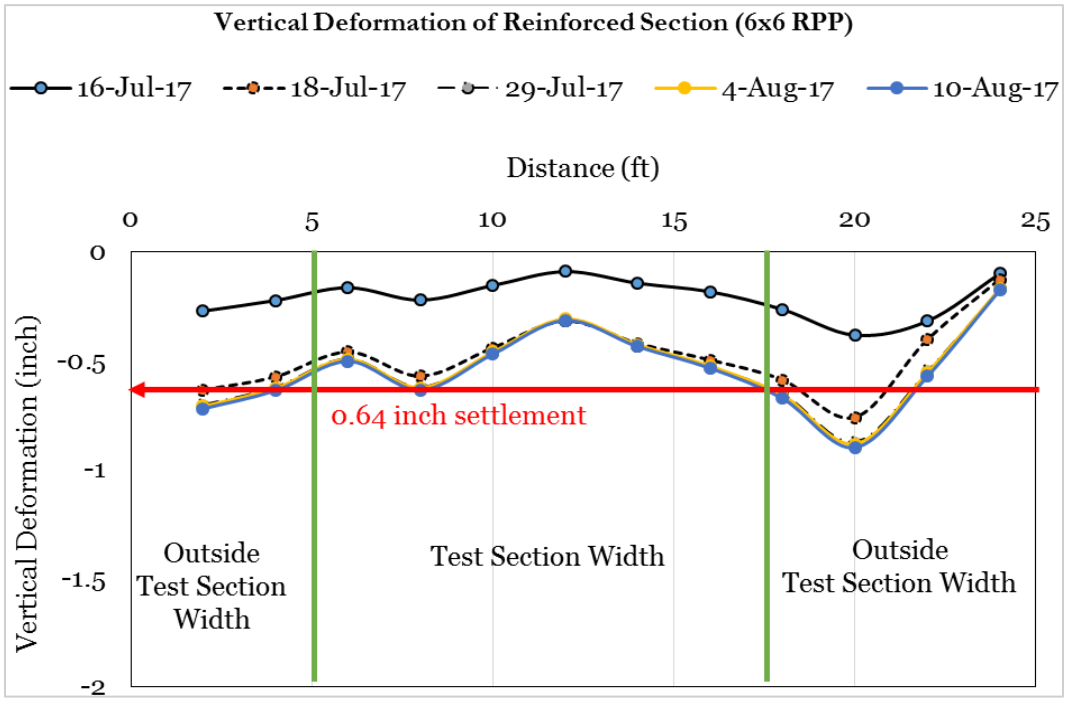

Figure 4. 9 Vertical deformation of 6 in. x 6 in. RPP reinforced section.

Figure 4.10 presents settlement of the test section with time and in relation to precipitation events. Based on the plot, the major part of the settlement took place during the

first few days after the construction. No significant change was observed followed by precipitation event or over the observation period after the initial settlement. After the first month of construction, almost no change in settlement was found and the total vertical deformation became almost constant.

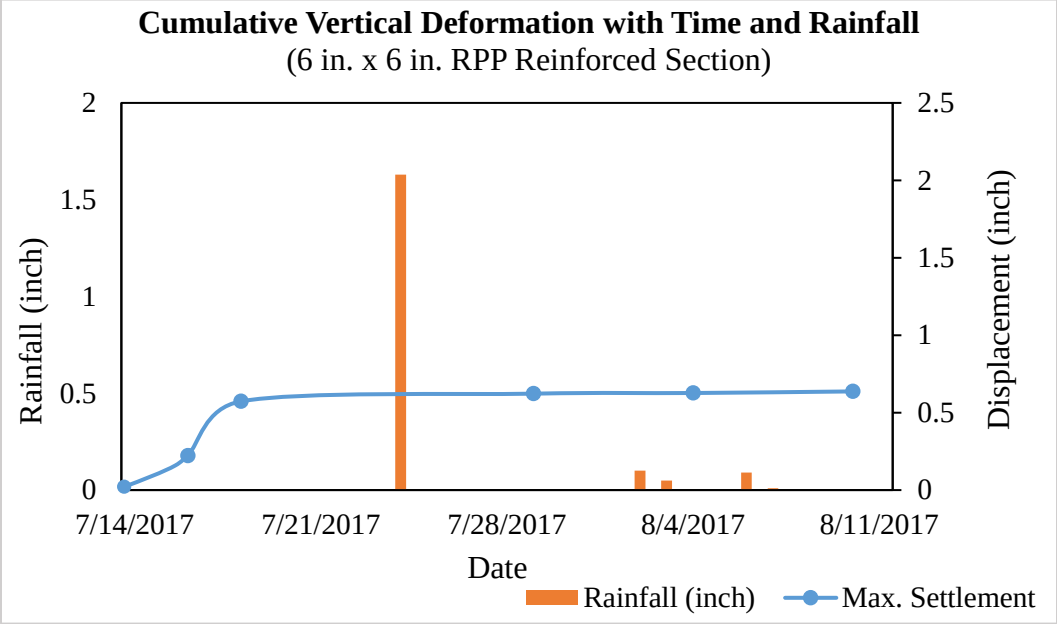

Figure 4. 10 Vertical deformation of the 6 in. x 6 in. RPP reinforced test section with time and rainfall event.

4.1.2.4 Comparison between Control and Reinforced Test Sections

Comparison between the control test section and the reinforced test sections is presented in this sub-section. From the performance monitoring data it was found that, under the similar load, the maximum vertical deformation for the control section was 2.01 inches, while for the reinforced section – 1 (reinforced with 4 in. x 4 in. RPP) maximum settlement was 0.8 inches and for the third section reinforced with 6 in. x 6 in RPP, the maximum settlement was found to be 0.64 inches (Figure 4.11). Due to the application of 4 in. x 4 in. and

6 in. x 6 in. RPP, a reduction in settlement of about 60% and 70 % was observed respectively compared to the control section. Also, application of geosynthetic in combination to RPP reduced the differential settlement for the reinforced sections compared to the control section.

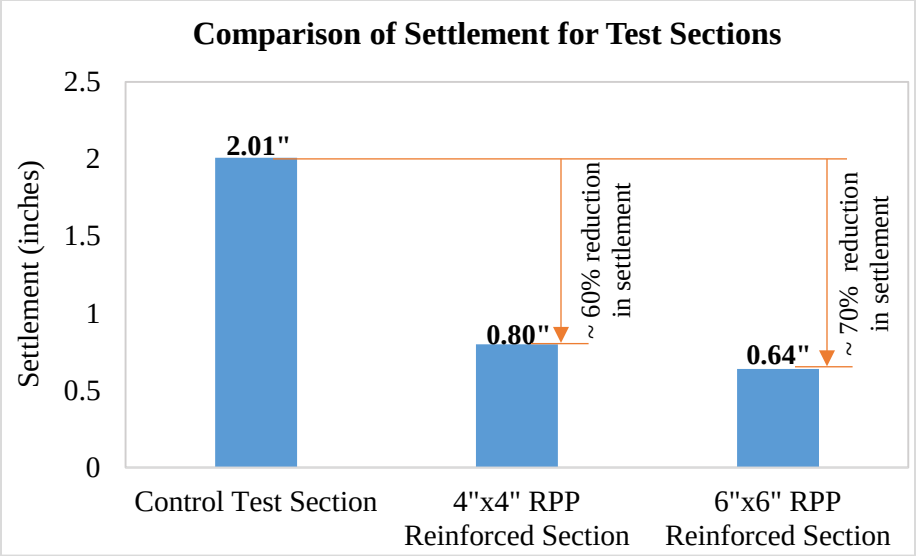

Figure 4. 11 Comparison of Settlement between control and reinforced test sections.

Figure 4.12 presents comparison of vertical movement between control section and the reinforced sections. A total settlement of more than twice was observed for the control section in comparison to reinforced section. This shows that the use of RPP at 3 ft. c/c spacing in the reinforced section in combination with geosynthetic helped to improve the bearing capacity of soil and reduced vertical deformation. In addition, similar to the pile supported embankment, RPP acts as pile and geogrid as platform which transfers the load to a deeper and stiff layer of soil through RPP. The arching effect of the geogrid in between two RPPs help mobilizing the load from fill material to the RPPs supporting the geogrid platform. However, in control section, the arching effect is not present nor any reinforcement in the foundation soil; therefore, observed total as well as differential settlement was more than twice for the control test section compared to the reinforced sections.

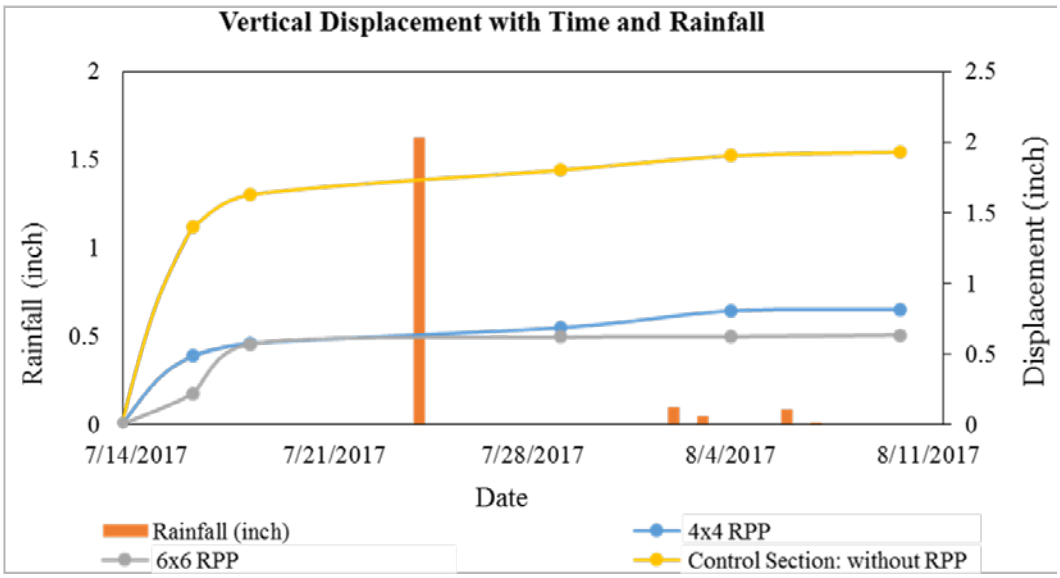

Figure 4. 12 Comparison between control and reinforced test sections with time and rainfall.

A study was conducted by Briancon and Simon (2011) to improve the support capacity of soft soil layer using piles in combination to geosynthetic. The authors concluded that a pile supported embankment in combination with a geosynthetic platform improves the performance of the foundation significantly. As shown in the Figure 4.13, the control section (1R) was found to have settled more than twice as much as the reinforced one (2R). The authors also pointed out that the total settlement depends on the thickness of the soft layer, not just geosynthetic type. However, better platform ensures higher load mobilization to the piles and reduces the settlement. Figure 4.13 presents the settlement profile with time and similar to current study it was observed that the maximum settlement took place during the first few days followed by the application of the load; after that the increase in settlement becomes almost constant. This suggests that RPP performs similar to the piles in improving the performance of foundation soil.

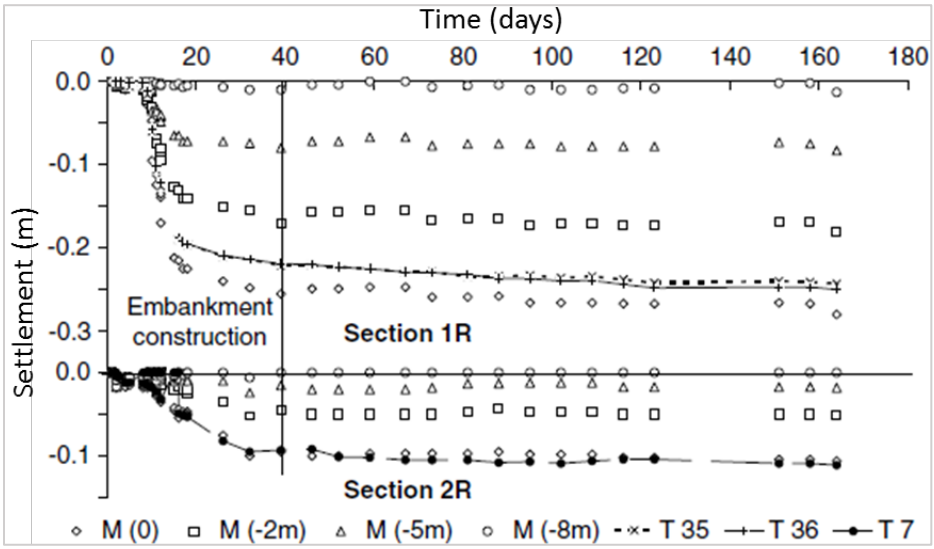

Figure 4. 13 Settlement with time for sections 1R (unreinforced) and 2R (reinforced) (Briancon and Simon, 2011).

Moreover, the settlement observed for all three test sections for the current study was mostly elastic or immediate settlement and the field results are in good agreement with the results obtained from analytical study. During soil boring, no water table was found up to the boring depth (20 ft.); therefore, no consolidation settlement took place.

From the performance monitoring data of phase – I, it can be concluded that the reinforced sections were performing satisfactorily compared to the unreinforced test section. A significant reduction in the settlement was observed due to RPP reinforcement in comparison to the control section. Between the reinforced test sections, the settlement was observed to be close to each other, although for 6 in. x 6 in. RPP test section, settlement was comparatively lower. It was decided to verify and further evaluate the effectiveness of RPP in phase – II.

4.1.3 Performance Monitoring Results: Phase – II

Purpose of the phase –II construction and monitoring was to validate the results observed from phase – I and to further evaluate the effectiveness of RPP in improving the

performance of weak foundation soil. In this phase, the soil used for the application of vertical loading was silty sand which allows water to infiltrate and reach the foundation soil. Unlike phase – I, a barrier wall was constructed to ensure application of uniform load of 5 ft. soil over the test sections. Identical boxed loading was applied to the test sections for better comparison. In phase – II, two sections were constructed, one as control and the other was reinforced with 4 in. x 4 in. RPP. Horizontal inclinometers were used to monitor the vertical movement of the foundation. However, data observed for the pressure plates was not in good agreement with the loading; therefore, it is not presented here. Monitoring results for the test section constructed in phase –II is presented in this section.

4.1.3.1 Control Test Section

The field monitoring results from the inclinometer at the control section is presented in Figure 4.14. Total maximum settlement for the control section was found to be about 1.06 inches. Variation of vertical deformation with time is presented in Figure 4.15 which shows a significant variation in the vertical deformation with time.

Rainfall data during the monitoring period is also presented in Figure 4.15. After the construction of the test section, an immediate settlement of 0.39 inches was observed. After each precipitation event, a sharp rise in settlement was observed, which might be due to increased saturated weight of the soil. However, shortly after the precipitation event followed by settlement, a reduction in the settlement was found. This might be due to the heaving of foundation soil. Foundation soil in this test location was found to be expansive clay. Soil used for the test section as fill material was silty sand which allows water to infiltrate through the soil into the foundation. This might have resulted in expansion of foundation soil resulted in

reduction of settlement. However, after extended dry period settlement was found to be increasing with drying out or expulsion of water.

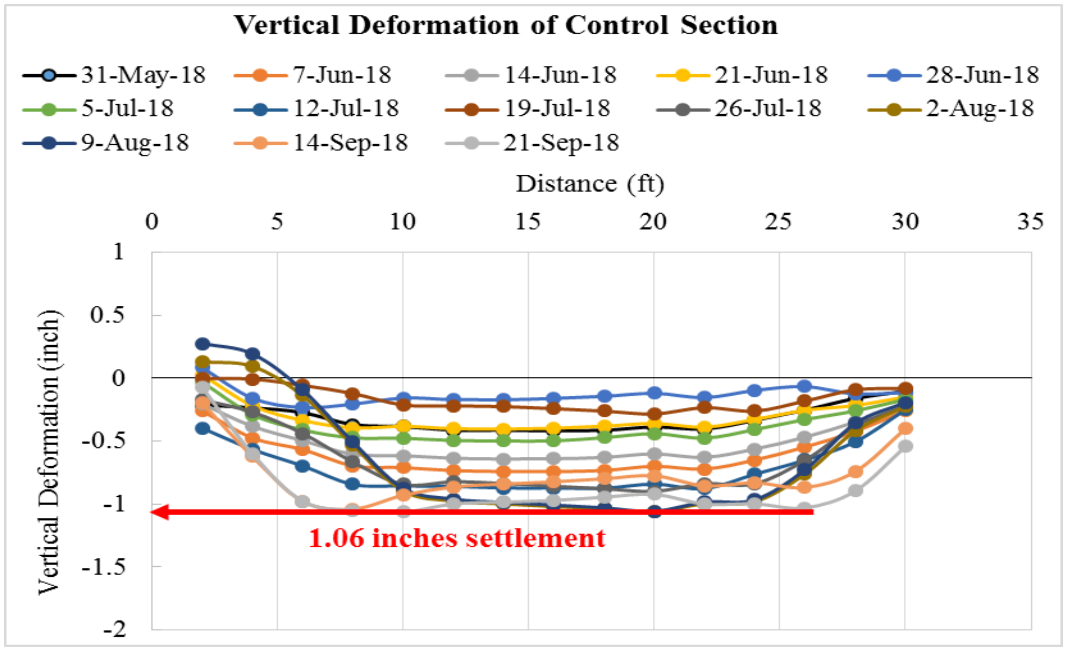

Figure 4. 14 Vertical deformation of control section (Phase - II).

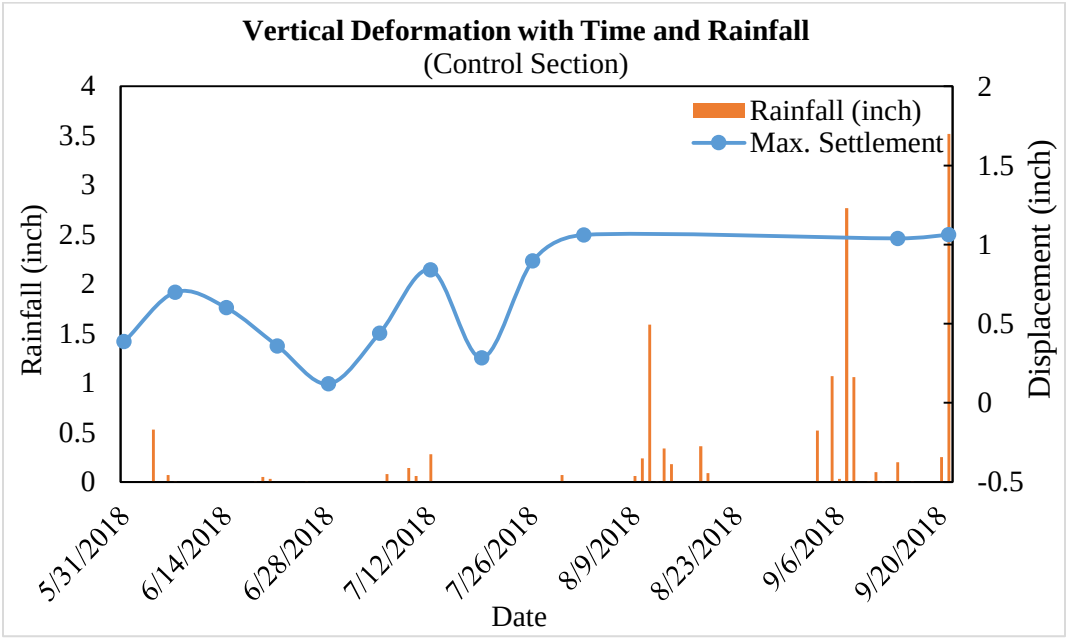

Figure 4. 15 Vertical deformation of the control section with time and rainfall event (phase – II).

4.1.3.2 Reinforced Test Section (4 in. x 4 in. RPP)

The field monitoring results from the inclinometer at the 4 in. x 4 in. RPP reinforced test section is presented in Figure 4.16. Based on the field monitoring result, maximum settlement for the reinforced section was observed to be about 0.45 inches. Variation of vertical deformation with time is presented in Figure 4.17. Unlike control section, the variation in settlement was very little and gradual. No significant change was observed during the monitoring period.

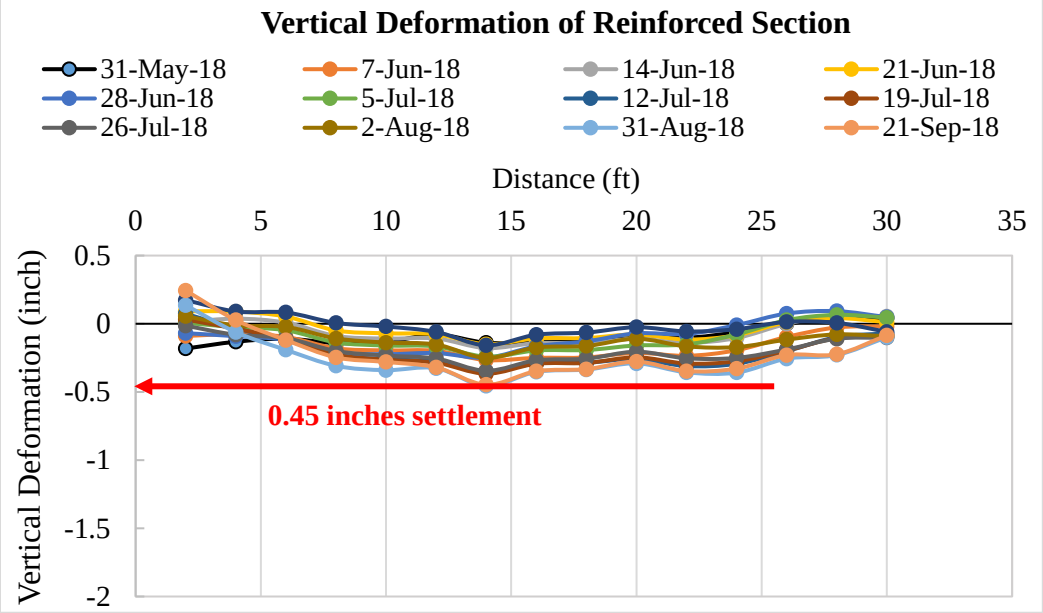

Figure 4. 16 Vertical deformation of reinforced section (Phase - II).

Rainfall data during the monitoring period is also presented in Figure 4.17. After the construction of test section an immediate settlement 0.14 inches was observed. After each precipitation event, due to increased saturated weight of the soil, there is an increase in settlement; however, unlike control section the change is very minor which might be because RPP is carrying a significant portion of the load, minimizing the foundation settlement. Shortly after the precipitation event followed by settlement, a slight reduction in the settlement was

observed similar to control section. This might be due to the heaving of foundation soil which was also very little. Due to fill material being silty sand, it allows water to infiltrate through the soil into the foundation soil. The foundation soil being expansive clay has the tendency to expand when in contact with water.

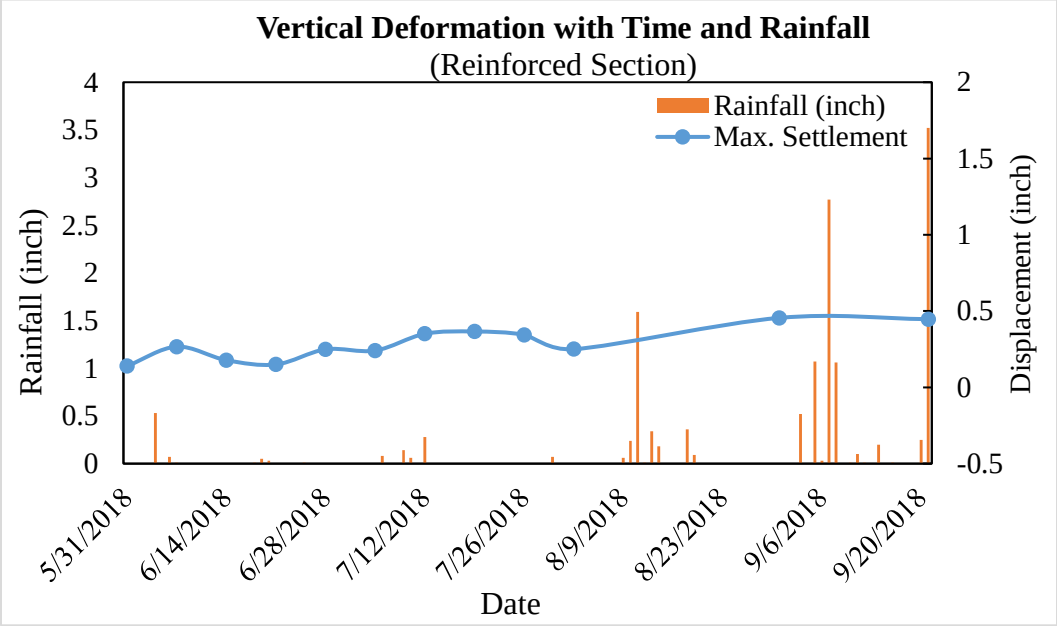

Figure 4. 17 Vertical deformation of the reinforced test section with time and rainfall event (phase – II).

4.1.3.3 Comparison between Control and Reinforced Test Section

Comparison between the control section and the reinforced section constructed in phase – II is presented in this sub-section. Based on the field monitoring data the control section experienced significant higher settlement (1.06 inches) compared to the reinforced test section (0.46 inches). The bar chart in Figure 4.18 shows a relative comparison. Use of RPP had a positive effect on settlement. A reduction in settlement of almost 57% was observed in the reinforced section. Also with time the change in settlement was negligible for the reinforced section compared to the control section. The observation data suggests that, the reinforcement

using RPP is providing noticeable load support capacity improvement for the weak foundation soil.

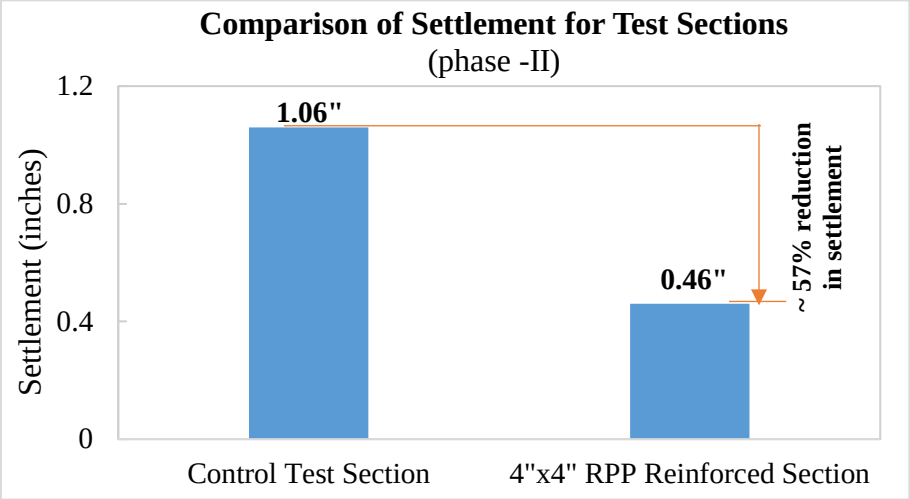

Figure 4. 18 Comparison of Settlement between control and reinforced test section.

4.1.4 Summary

RPP has sufficient capacity to carry significant amount of vertical load. Based on the phase – I monitoring data it was observed that both 4 in. x 4 in. and 6 in. x 6 in. RPP reinforced test sections performed significantly well compared to the control test section. A reduction in settlement of about 60% compared to control section was observed for foundation reinforced with 4 in. x 4 in. RPP, while for 6 in. x 6 in. RPP reinforced test section settlement reduction was found to be 70%. Use of geosynthetic in combination to RPP improved the load transfer efficiency of the test section and considerably reduced the differential and total settlement.

The field result for phase – II showed similar conclusion. A settlement reduction of approximately 56% was observed due to the use of 4 in. x 4 in. RPP compared to the control section, which is in good agreement with phase – I result. The slight difference might be due to the type and strength of the foundation soil.

Finally, based on phase – I and phase – II monitoring results, it can be concluded that the RPP in combination to geosynthetics improves the foundation soil to carry higher load and minimizes settlement compared to the unreinforced section.

4.2 Performance of Lateral Loaded Test Sections

The purpose of the lateral loading test sections was to determine the efficiency of RPP to take the lateral load from backfill as well as from surcharge and resist sliding of base of the wall. The following sub-sections present the analytical study on increasing shear resistance against sliding by RPP reinforcement for the MSE wall test sections and field performance monitoring of the test sections for both phase – I and phase – II.

4.2.1 Analytic Study on Lateral Loaded Test Sections

Recycled plastic pin had been proven to be an effective and sustainable alternative to restrict sliding soil mass in shallow slope failure by numerous researchers. Which proved the capability of RPP in resisting lateral force; therefore, it might also be effective in providing considerable resistance against lateral force from the backfill of MSE wall and improve the sliding resistance of the wall. When 10 ft. long RPP is driven into the base of the wall keeping 2 ft. above ground followed by the construction of MSE wall, it creates a composite structure. Hence, RPP becomes a part of the structure and tend to act similar to a shear key. Incorporating RPP as a shear key may increase the sliding resistance of MSE retaining wall by generating additional passive resistance and improves the factor of safety against sliding. As discussed in article 3.5.2, the factor of safety can be determined using equation 3.11 for unreinforced section, and equation 3.14 for reinforced section.

Let's assume a scenario with geotextile wrapped MSE wall, with foundation soil having friction angle, φ_2 = 20°, cohesion, c_2 = 300 psf. Internal friction angle between geotextile and foundation soil may be taken as δ' = 0.9 x 20° = 18° and adhesion between the geotextile and foundation soil may be taken as $c'_a = \frac{2}{3} \times c_2 = \frac{2}{3} \times 300 = 200$ psf. The active earth pressure coefficient,

$K_a = \tan^2 (45 - \varphi_2/2) = \tan^2 (45 - 20/2) = 0.49$

The factor of safety against sliding can be determined using equation 3.11. For a 5 ft. wall with backfill soil having unit weight of 116 pcf. and width of the foundation as 4 ft.,

$(\Sigma V) \tan \delta' = (116 \times 5) \times \tan (18) = 118.45$ lb/ft.

$Bc'_a = 4 \times 200 = 800$ lb/ft.

$Pa = \frac{1}{2} \times 116 \times 0.49 \times 5^2 = 710.5$ lb/ft.

Therefore, according to equation 3.11,

FS (sliding) $= \frac{(\sum V) tan\delta' + Bc'_a}{P_a} = (188.45 + 800) / 710.5 = 1.39 < 3.0$

Typically, the factor of safety against the base sliding of a conventional retaining wall system is recommended as 1.5. However, for MSE wall having flexible facing and foundation, the allowable factor of safety is considered to be higher, FS_{allow} = 3.0, than conventional retaining structures. The factor of safety found from the calculation for the current case is 1.39 which is far below the allowable factor of safety. Therefore, RPP may be introduced to find out the effectiveness in increasing the base sliding resistance of the MSE retaining wall. The RPP when used in the composite system, works similar to a shear key for the structure and generates additional passive force, P_{RPP}.

If RPP is installed at the base of the retaining wall system, base resistance is expected to increase as the pressure from lateral load acting on the wall will be transferred to the RPP thus reducing the effective pressure at the back of the wall. Based on the laboratory test conducted by Khan (2014), flexural modulus of the RPP is about 171 ksi and a flexural strength of 2.5 ksi. For the lateral loaded test sections, RPP was proposed to be installed in such a way that 8 ft. will be driven into the ground and 2 ft. will be kept extended from the ground to act as a cantilever beam to carry the lateral loads. Total tip deflection of RPP acting as a cantilever beam under uniformly distributed load and rectangular cross section can be determined using equation 3.13. Let's assume, the 4 in. x 4 in. x 10 ft. RPP will be used, for which the length of extended portion of the pin, L = 24 in., modulus of elasticity of RPP, E = 162,000 psi., moment of inertia, I = 21.33 in^4, equivalent diameter of the pin, D = 4.51 in. If the maximum deflection is limited to 0.5 inch, maximum allowable load can be calculated using equation 3.13 as follows,

$$\Delta = \frac{pL^4}{8EI}\left[1 + \frac{E}{2G}\left(\frac{D}{L}\right)^2\right]$$

$$0.5 = \frac{p\ x\ 24^4}{8\ x\ 162{,}000\ x\ 21.33}\left[1 + 5\ x\ (0.188)^2\right] \qquad \text{or, } p = 35.4 \text{ psi} \approx 5098 \text{ psf.}$$

where, the additional deflection due to shear deformations is given by the second term in the brackets. The effect of shear deformations increases with increasing E/G ratios and decreasing slenderness ratios (L/D). For RPP acting as shear key described above, the slenderness ratio (L/D) is about 5.3 (considering only the length of the pile where lateral deflections are significant), and the E/2G ratio is estimated to be about 5 for the plastic pile.

If the RPPs are installed at 3 ft. spacing, resisting force per unit length of the combined system will be,

P_{RPP} = (5098/3) = 1699.33 psf./ft.

With the addition of RPP, factor of safety against sliding based on equation 3.14 becomes,

$$FS\ (sliding) = \frac{(\sum V)tan\delta' + Bc'_a + P_{RPP}}{P_a}$$

$$= (188.45 + 800 + 1699.33)/710.5 = 3.78 > 3.0$$

Use of 4 in. x 4 in. RPP at 3 ft. spacing increases the factor of safety against sliding by more than 3 times. Using the same analytical process, factor of safety against sliding for MSE wall base reinforced with different size and spacing of RPP can be determined. Table 4.3 shows calculated factor of safety against sliding of the base of MSE wall reinforced with 4 in. x 4 in., 6 in. x 6 in. and 10 in. x 10 in. RPP at 2 ft., 3 ft. and 4 ft. spacing.

Table 4. 3 Calculated factor of safety against sliding for RPP reinforced MSE wall section.

Factor of Safety Chart (inches)			
RPP size / **Spacing (ft.)**	**4 in. x 4 in. RPP**	**6 in. x 6 in. RPP**	**10 in. x 10 in. RPP**
2	4.98	16.67	79.69
3	3.78	11.58	53.59
4	3.18	9.03	40.54

The calculated factor of safety against sliding for the RPP reinforced MSE retaining wall in question was plotted against RPP spacing and RPP size as presented in Figure 4.19 and Figure 4.20 respectively. From the plot it was observed that for same RPP size factor of safety against sliding increases with decreasing RPP spacing. Also, for fixed spacing of RPP, factor of safety increases with increasing size of RPP. From the plot it was observed that the rate of increase in factor of safety depends on load resistance capacity of the RPP. Higher size of RPP can resist more load compared to that of smaller size.

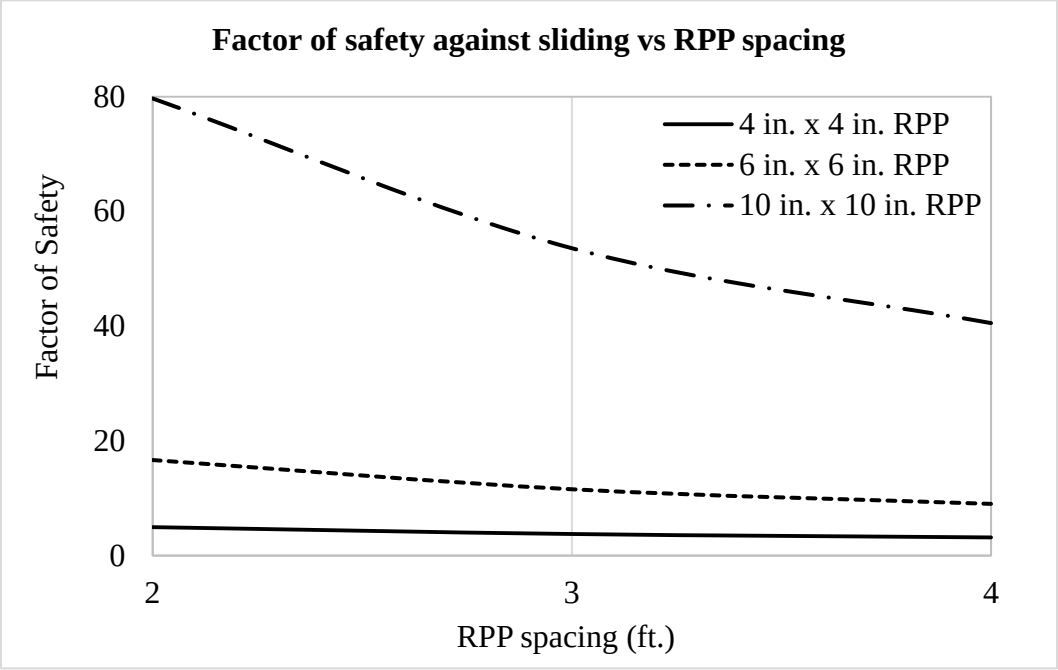

Figure 4. 19 Relation between factor of safety against sliding of MSE wall base and RPP spacing for different sizes of RPPs based on analytical study.

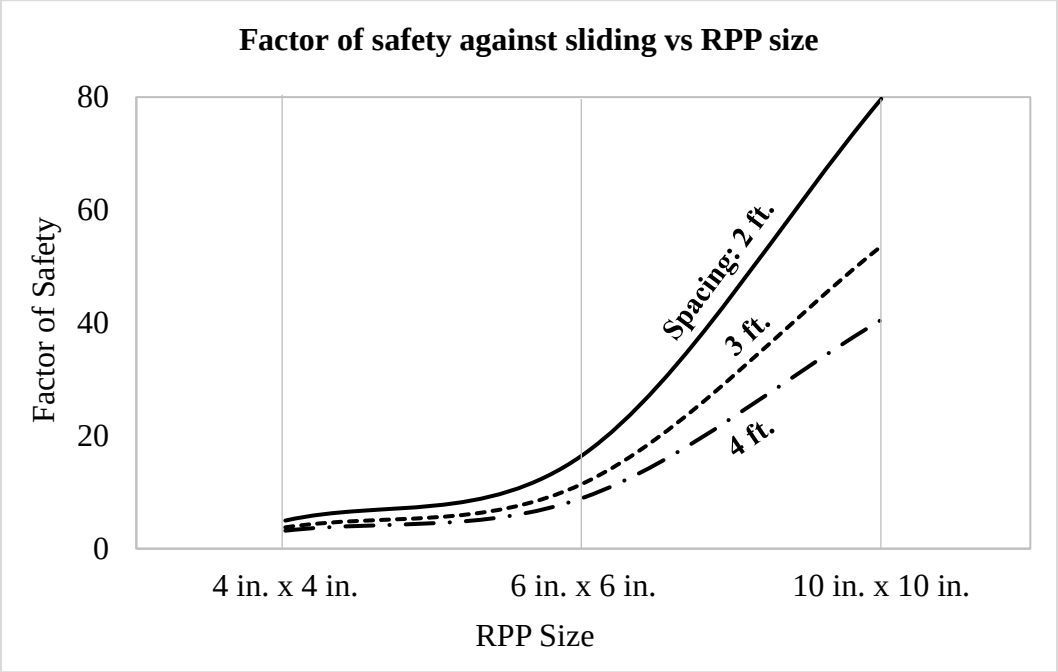

Figure 4. 20 Relation between factor of safety against sliding of MSE wall base with size of RPP for fixed RPP spacing based on analytical study.

4.2.2 Performance Monitoring Results: Phase – I

In the current study, RPP has been used at the base of the MSE retaining structure to serve the purpose of a shear key to provide additional resistance against sliding. As part of phase – I construction, two field scale MSE wall test sections were constructed to replicate the actual field scenario; one as a reinforced section with 4 in. x 4 in. RPP as reinforcement for the base of the structure and the other as a control section without any reinforcement. The height of loading backfill applied for this phase was about 4 ft. followed by a slope which generates the lateral force responsible for sliding of the wall. The prime instrumentation for this phase was vertical inclinometers. Two inclinometers, one for each test section, were installed at the beginning of the wall construction. The inclinometers were monitored on a weekly basis. Based on the monitoring data from the inclinometers, the performance of the test sections are presented in the current study.

4.2.2.1 Control Test Section

The field monitoring results from the inclinometer 1 (I – 1) at the control section is presented in Figure 4.21. The maximum lateral movement of the inclinometer was observed at the ground level which was at the same level as the base of the wall. The maximum lateral movement was found to be about 3.8 inches. With incremental depth of the inclinometer, the lateral movement had dropped and at a depth of 18 ft. almost no movement had taken place. Variation of lateral movement with time and rainfall is presented in Figure 4.22. It was observed that, there was a sharp increase in lateral movement during the first two weeks after construction, which turned out to be a major part of the total lateral displacement during the monitoring period. According to AASHTO (2007), the major part of wall movement occurs during the construction. A wall movement of about 2 inches was observed just after the construction of the wall. After the first two weeks change in the lateral movement was not significant.

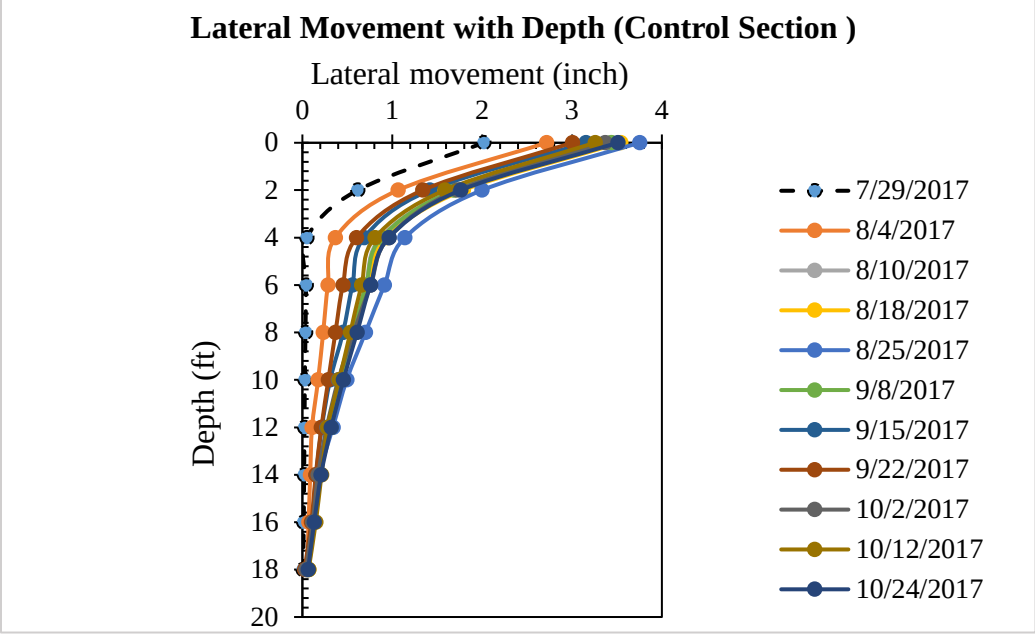

Figure 4. 21 Lateral movement of control section with depth.

However, after each precipitation incident a rise in the lateral movement was observed; also, followed by an extended period of dry weather, a reduction in the lateral movement was observed. This might be due to the shrinkage and swelling behavior of clayey soil which is releasing and applying pressure on the back of the wall facing respectively.

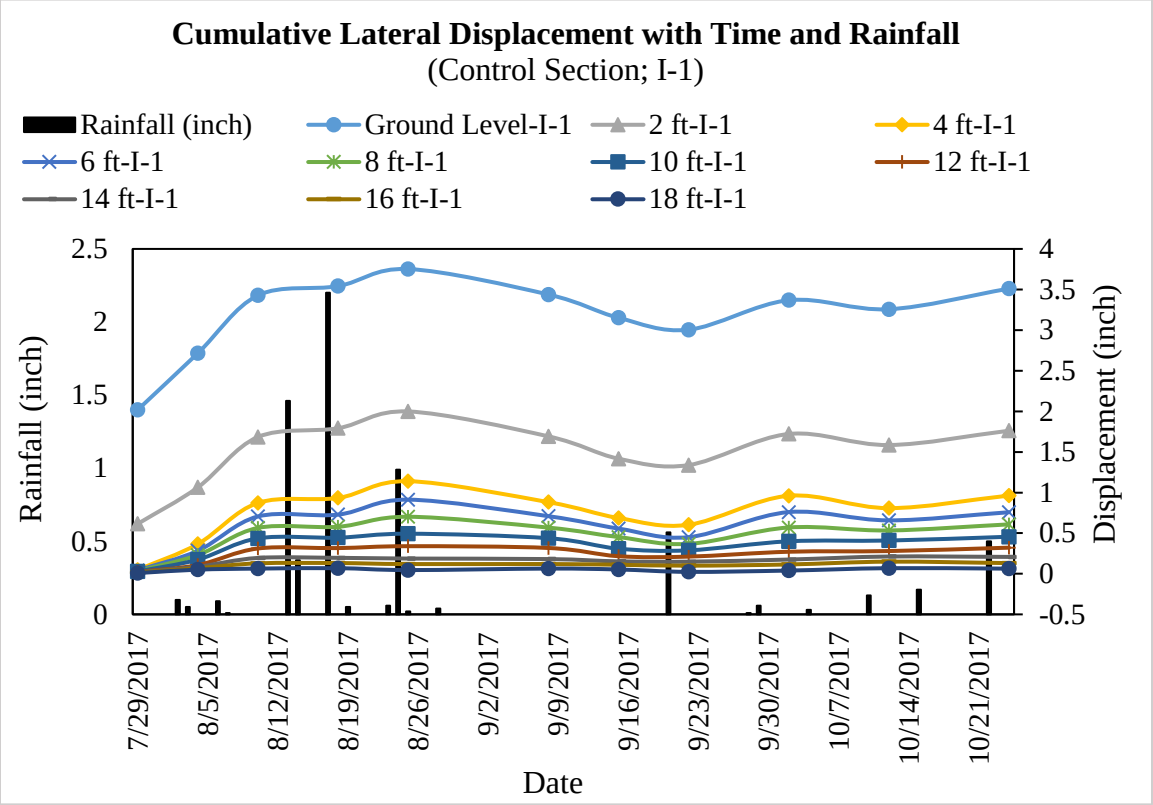

Figure 4. 22 Cumulative Lateral displacement with time for the Inclinometer-1 at the control section.

4.2.2.2 Reinforced Test Section

The field monitoring results from the inclinometer (I – 2) at the reinforced section is presented in Figure 4.23. For the reinforced section, the inclinometer movement was found to be almost negligible. Base of the wall showed maximum lateral displacement similar to the control section. Based on the monitoring results, the maximum lateral movement was found to

be about 0.055 inches. With incremental depth of the inclinometer, the lateral movement had dropped and at a depth of 18 ft., almost no movement was observed. Variation of lateral movement with time and rainfall is presented in Figure 4.24. The field monitoring results presented an incremental lateral displacement of the wall facing of the reinforced section.

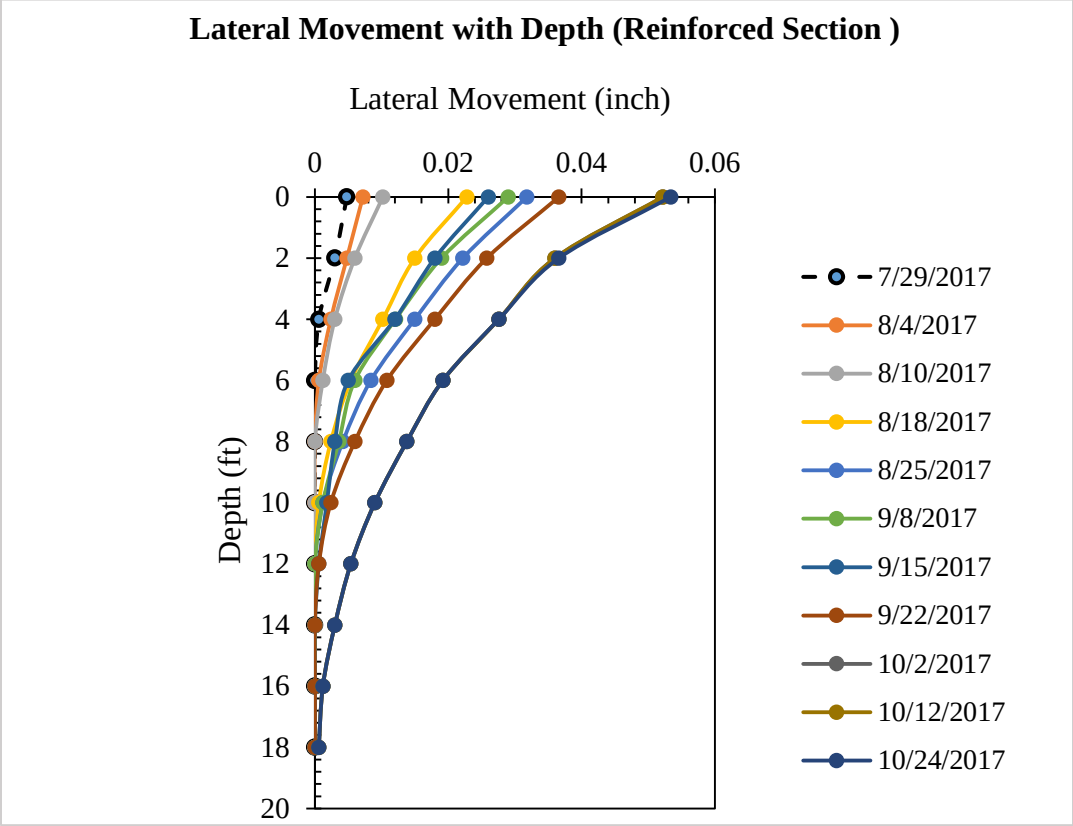

Figure 4. 23 Lateral movement of reinforced section with depth.

According to Loehr et al. (2007), incremental deformation is the result of load mobilization of RPP which occurs followed by a precipitation event. From the results similar trend was observed; after each rainfall event, due to the load mobilization, an increase in lateral displacement was observed. However, during the dry period, almost no noticeable movement was observed. A study conducted by Khan (2014) on RPP in slope for restricting sliding soil

mass showed that followed by the load mobilization no significant increment in deformation was observed for the reinforced slope.

For the current study, an increment in displacement was observed during the first two months after construction; however, after October, 2017, total lateral displacement became almost constant and no significant change was observed.

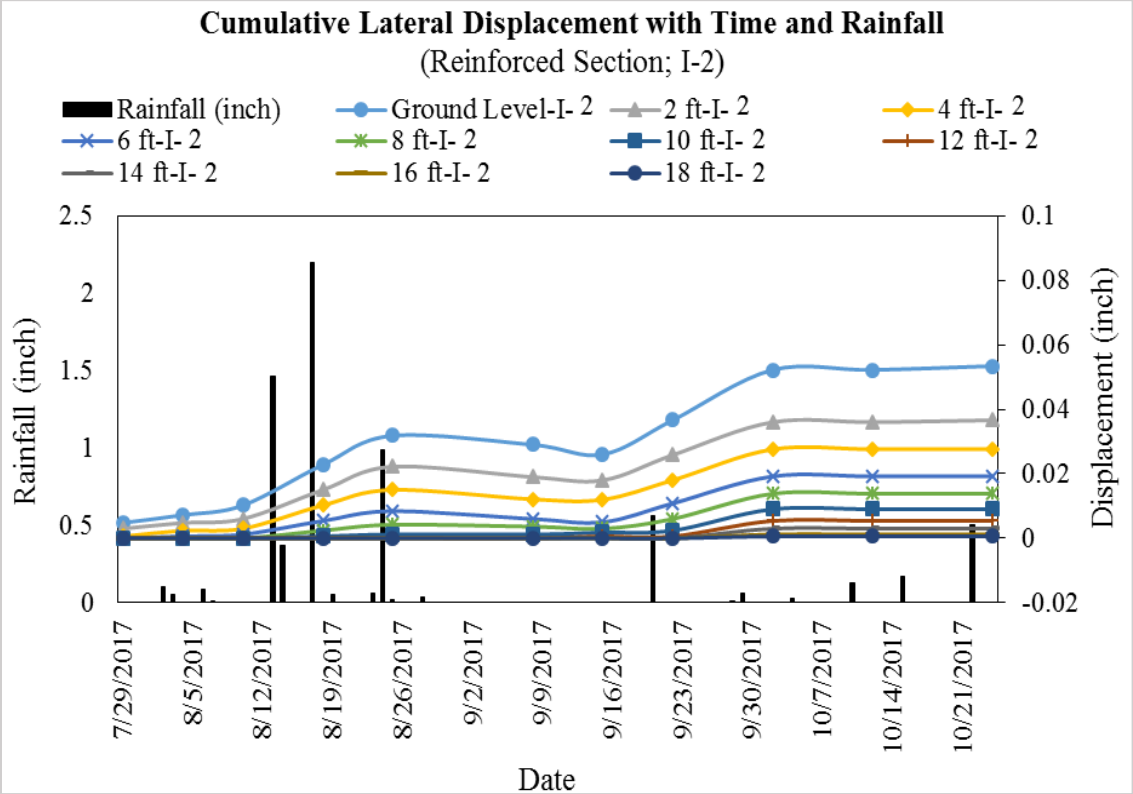

Figure 4. 24 Cumulative lateral displacement with time for I - 2 at the reinforced section.

4.2.2.3 Comparison between Control and Reinforced Test Sections

Comparison between lateral movement of the base of the wall at the control section and at the reinforced section is presented in this sub section. The base of the control section experienced a maximum lateral movement of almost 3.8 inches, while for the RPP reinforced section, a maximum movement of 0.055 inches was observed. Compared to the control section,

lateral movement for the reinforced section was almost negligible. Figure 4.25 represents the lateral movement for both test sections at same scale.

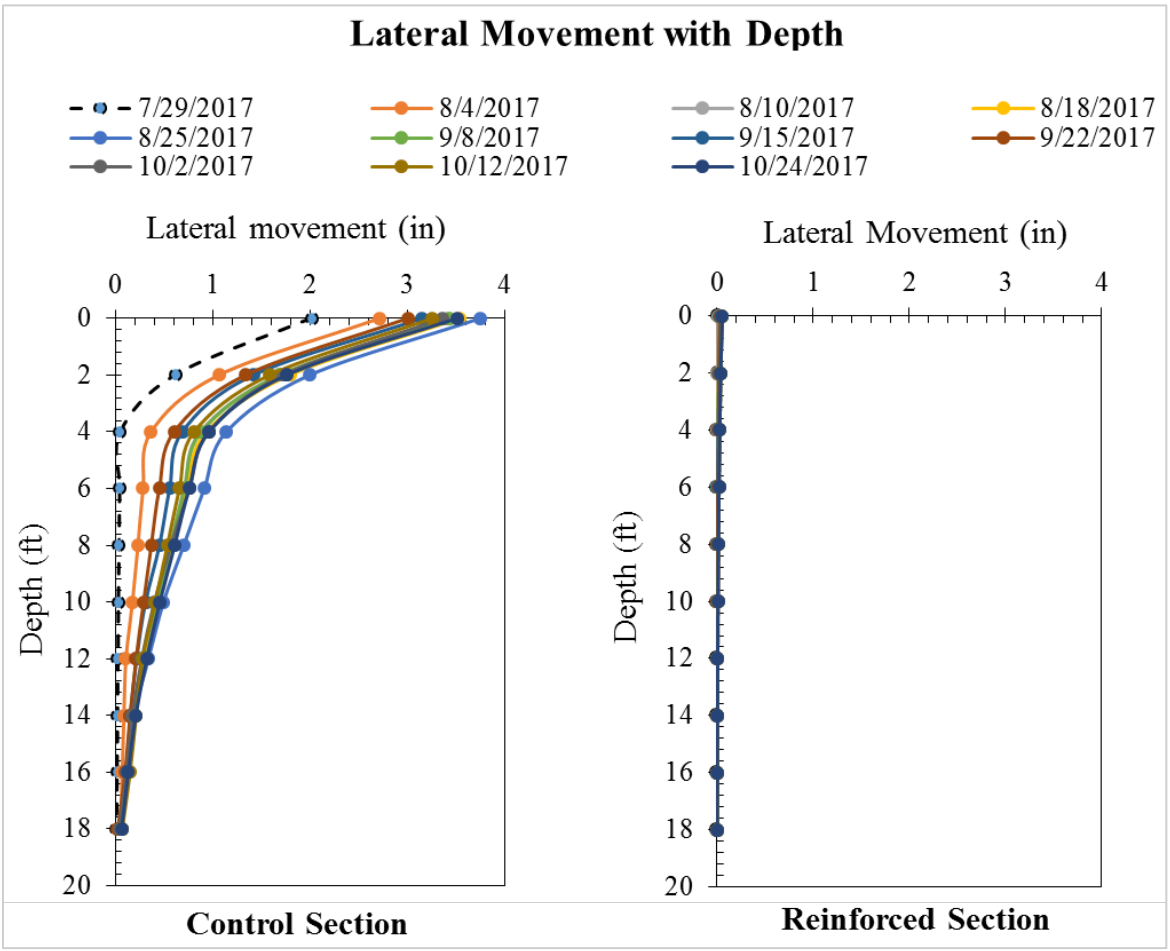

Figure 4. 25 Comparison of lateral movement with depth between control and reinforced section.

According to Loehr et al. (2007) and Khan (2014), RPP reinforcement is effective against sliding of soil body in slope stabilization. Similar mechanism was implemented and the result found is in good agreement with the concept. As part of performance monitoring, visual inspections were also conducted on a regular basis and a noticeable opening of wall facing of the control section was observed at the top of the wall. From the visual monitoring it seemed like the wall movement was much higher at the top of the wall; however, a study

conducted by Horpibulsuk et al. (2011) showed that, the wall movement at the top is the resultant movement of the wall panels from base to top. From the relative plot (Figure 4.26b) the authors showed that, the maximum lateral movement occurs at the base of the wall. The visual monitoring of the reinforced section in the current study showed no noticeable change.

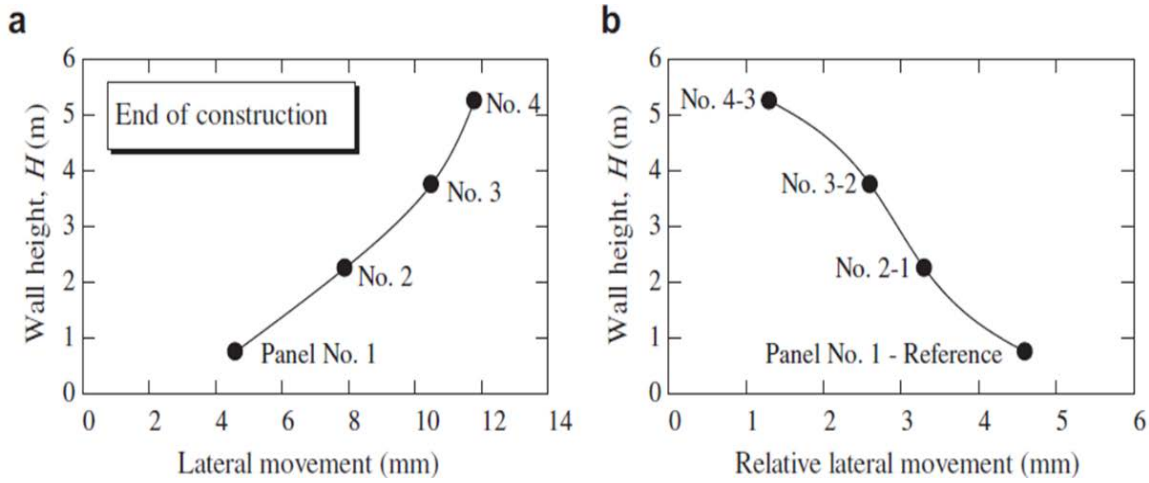

Figure 4. 26 (a) Cumulative and (b) Relative lateral movement of wall at the end of construction (Horpibulsuk et al., 2011).

Figure 4.27 and 4.28 presents the comparison of lateral movement between inclinometers I-1 and I-2 at different depths (ground level, 2 ft., 4 ft. and 10 ft.). It was observed that I-1 had significantly higher lateral movement compared to I-2 at all the depths. This is because, I-2 was installed in front of the reinforced section where RPP was used as reinforcement at 3 ft. c/c spacing which provided additional resistance against sliding of base of the wall.

From the performance monitoring data of phase-I, it can be concluded that the reinforced section was performing significantly well compared to the control sections. However, it was decided to improve the facing of the wall to apply higher load and further monitor the performance of the test sections in phase-II.

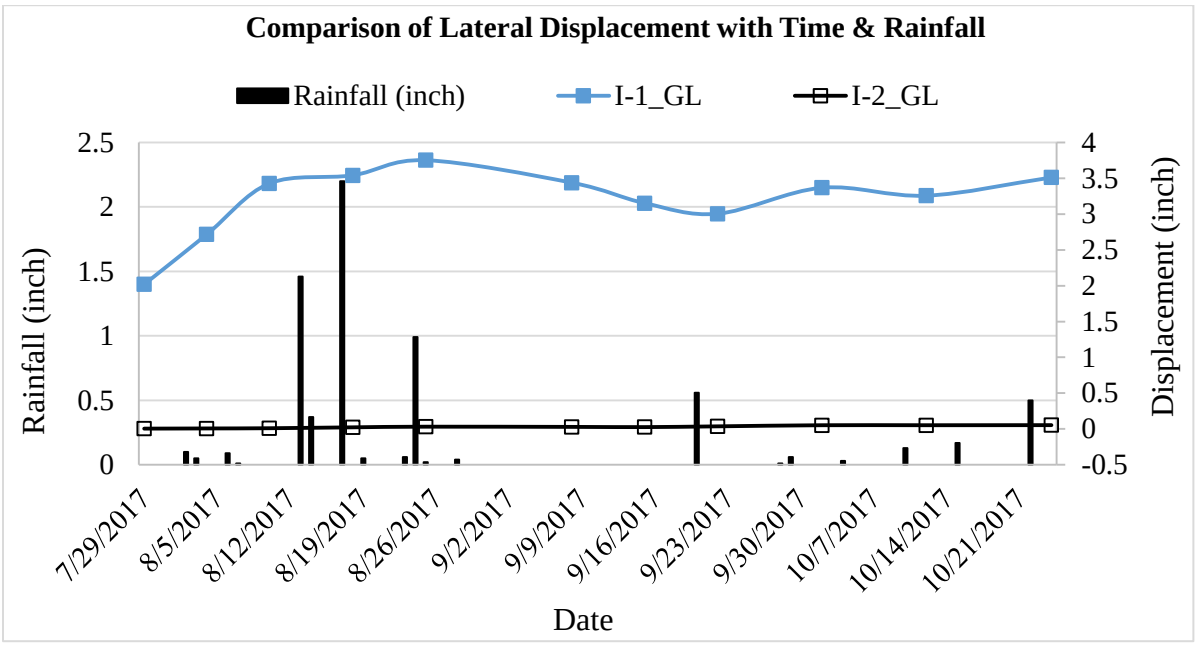

(a)

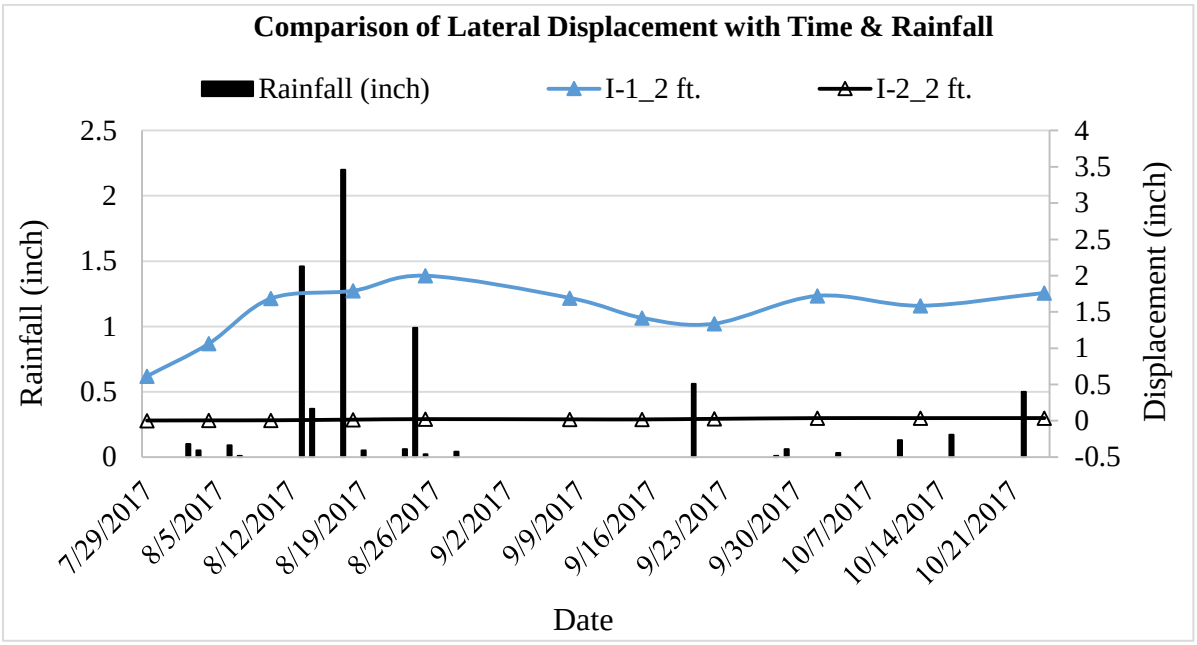

(b)

Figure 4. 27 Comparison of Lateral Displacement between Inclinometer 1 (control section) and Inclinometer 2 (reinforced section); (a) at ground level (GL), (b) at 2 ft.

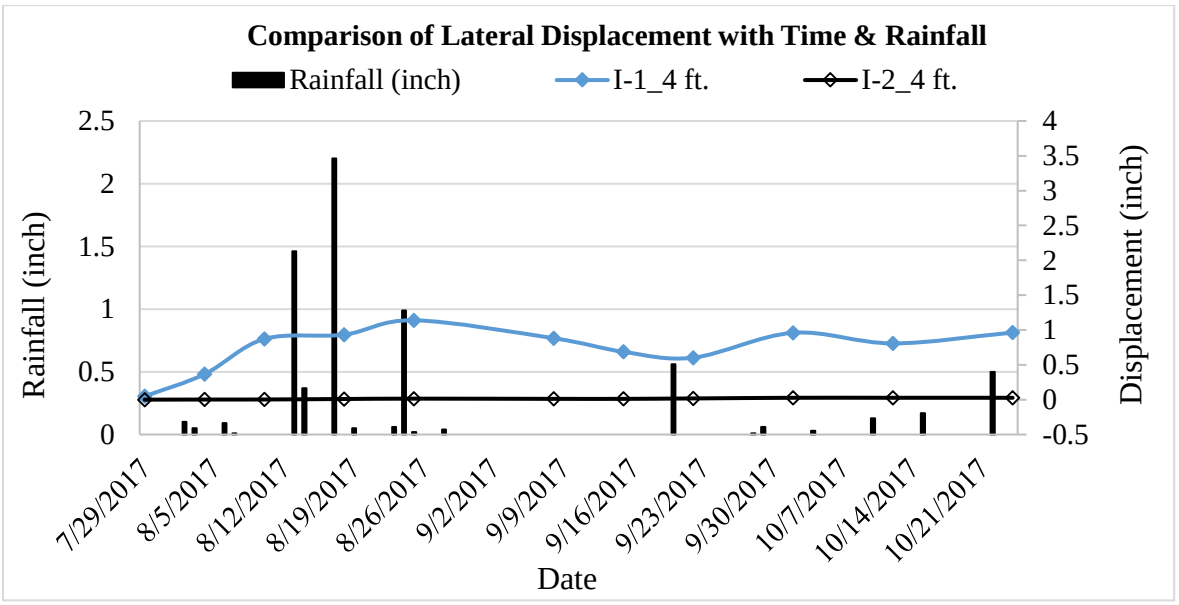

(a)

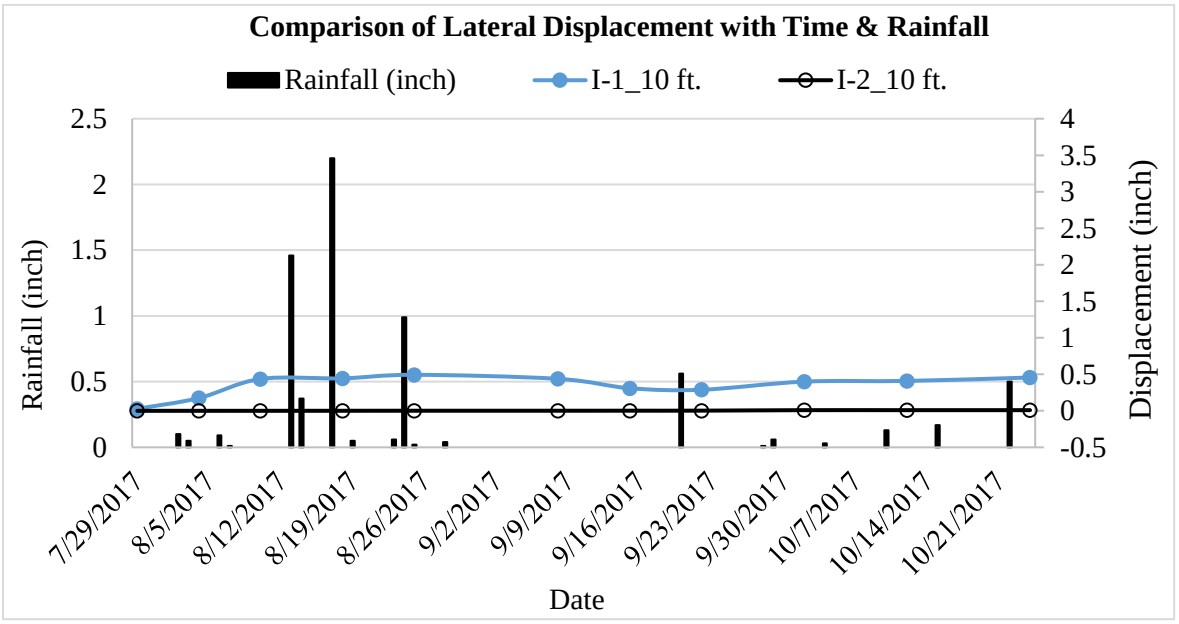

(b)

Figure 4. 28 Comparison of Lateral Displacement between Inclinometer 1 (control section) and Inclinometer 2 (reinforced section); (a) at 4 ft., (b) at 10 ft.

4.2.3 Performance Monitoring Results: Phase – II

Followed by the excessive movement of control section and almost negligible movement of the RPP reinforced section, it was decided to test the sections further to assess

the effect of RPP for higher loading. However, the initial wall facing was not strong enough for the application of a larger/higher backfill loading height. Therefore, new wall facing was constructed identically for both sections and a load equivalent to 5 ft. backfill soil was applied to the test sections. A new set of vertical inclinometers were used to monitor the lateral movement of the wall and pressure plates were installed to monitor the change in applied pressure at the back of the wall facing from backfill soil.

4.2.3.1 Inclinometer

Two new inclinometers, one for each test section, were installed close to the outside face of the wall (less than 10 inch from the facing) at the beginning of the wall construction. The inclinometers were monitored on a weekly basis. The horizontal movement of the inclinometer 3 (I-3) for control section and inclinometer 4 (I-4) for reinforced section is presented in the current study.

4.2.3.1.1 Inclinometer 3 (I-3): Control Test Section

The field monitoring results from the inclinometer 3 (I-3) at the control section is presented in Figure 4.29. The maximum lateral movement from the monitoring data was found to be about 1.76 inches which was at the ground surface. With incremental depth of the inclinometer, the lateral movement had dropped at a depth of 18 ft. and very little movement had taken place which is negligible compared to the base movement at the surface. Variation of lateral movement with time and rainfall is presented in Figure 4.30. A wall movement of about 0.25 inches was observed just after the construction of the wall. An increase in lateral movement was observed for wall base during the first three weeks after the construction. After that the total movement was found to be more or less constant.

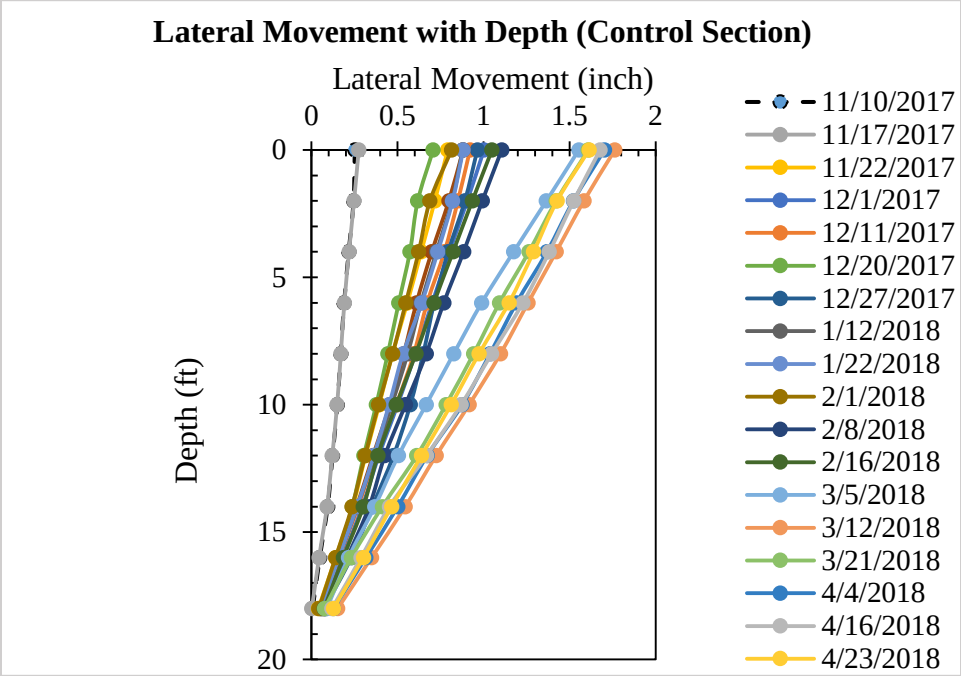

Figure 4. 29 Lateral movement of control section with depth (Inclinometer -3).

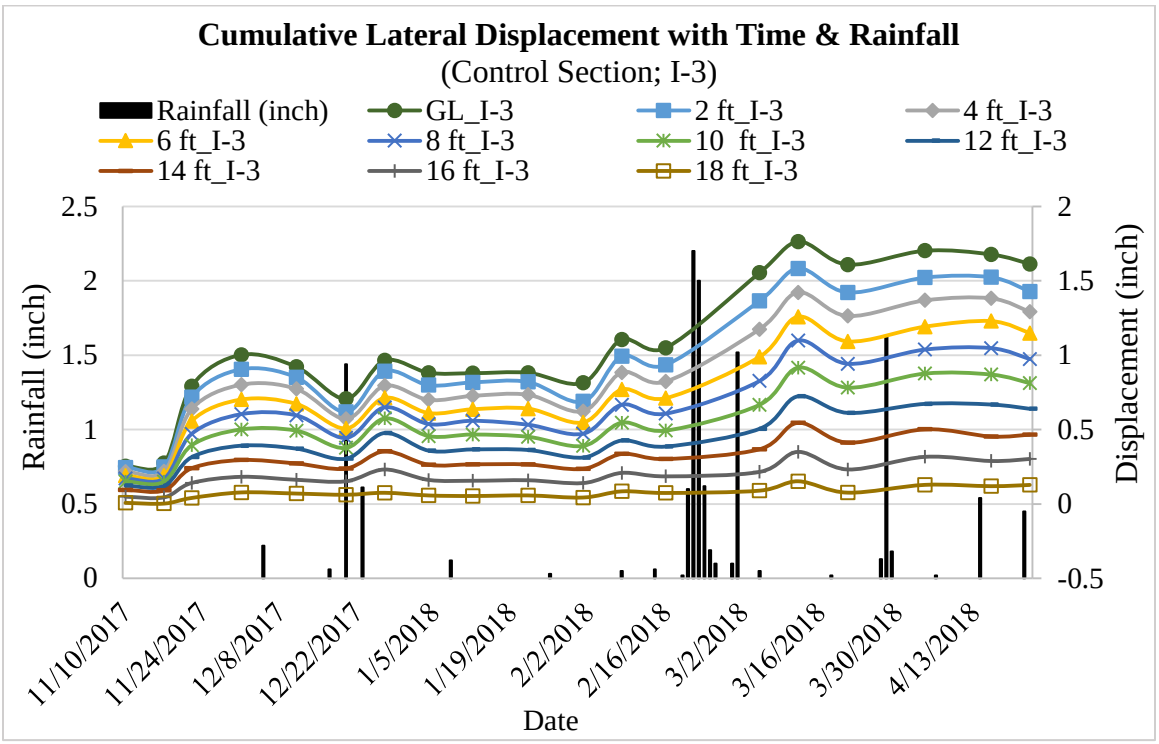

Figure 4. 30 Lateral displacement with time & rainfall for the Inclinometer-3 at control section.

However, throughout the monitoring period, an increase in lateral movement was observed followed by a precipitation event. A significant increase in lateral movement of about 0.8 inches was observed between mid of February 2018 and mid of March 2018 followed by a heavy and continuous precipitation event. After that no significant change was observed. This might be due to the expansive behavior of the backfill soil, which was applying additional pressure at the back of the wall.

4.2.3.1.2 Inclinometer 4 (I-4): Reinforced Test Section

The field monitoring results from inclinometer 4 (I – 4) at the reinforced section is presented in Figure 4.31. A maximum movement of about 0.29 inches was observed during the performance monitoring period. Similar to I-3, the maximum movement was observed at the base of the wall which decreased gradually with the increasing depth of 18 ft. and almost no movement had taken place at that depth. Figure 4.32 presents the variation of lateral movement with time and precipitation events. Increase in lateral movement was observed followed by every precipitation event. The change in lateral displacement was observed to be almost constant from the beginning. A relatively major increase in lateral movement was observed between mid of February 2018 and mid of March 2018 followed by a heavy and continuous precipitation event. The sudden change might be due to the swelling behavior of clayey soil (Khan, 2014) and the increased lateral force from the saturated clay at the backfill and slope. The cumulative movement dropped slightly and remained almost the same after March 2018.

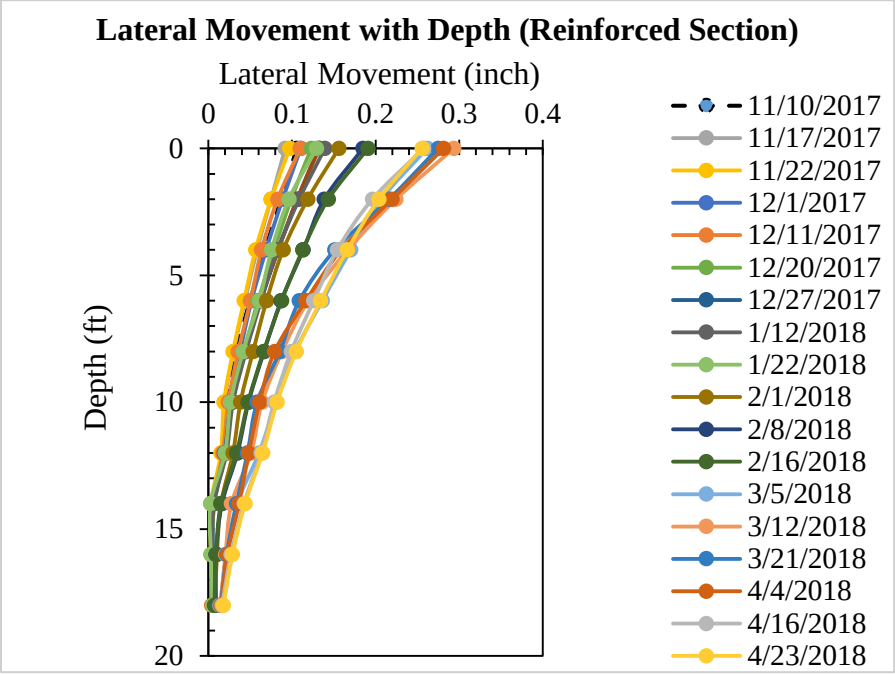

Figure 4. 31 Lateral movement of reinforced section with depth (Inclinometer - 4).

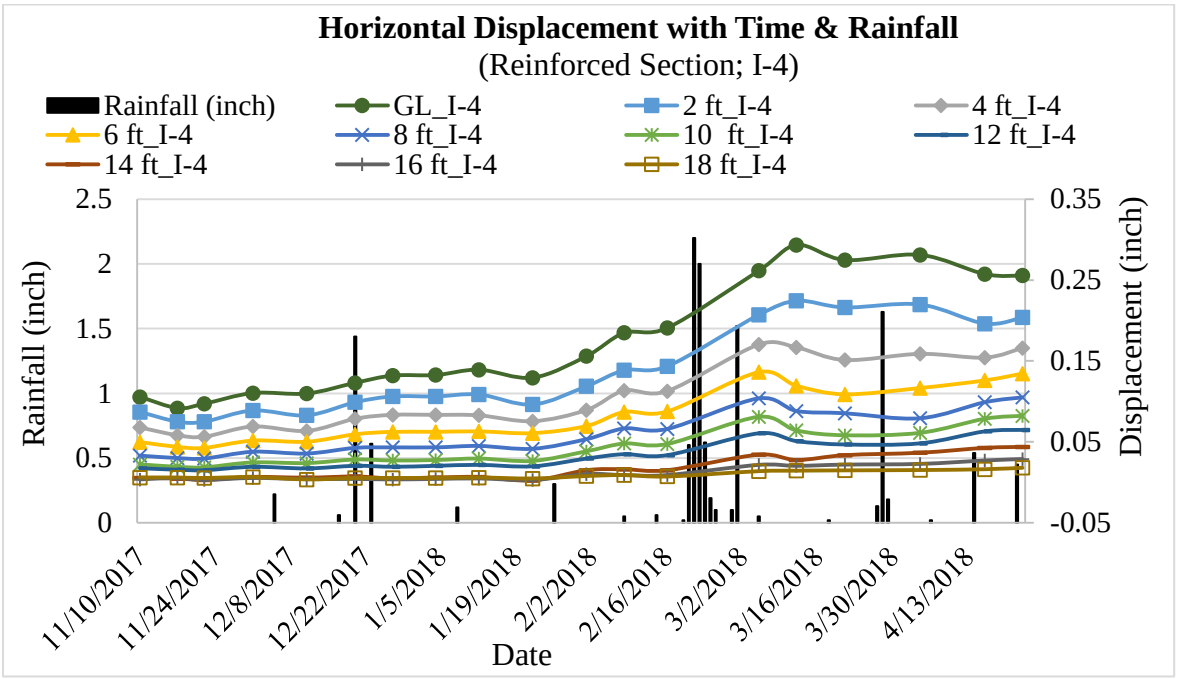

Figure 4. 32 Lateral displacement with time for the Inclinometer - 4 at the reinforced section.

Benjamim et al. (2007) conducted a study to monitor field performance of geotextile-reinforced soil-retaining walls. The authors constructed eight prototype geotextile-

reinforced soil structures for comprehensive study. From the field monitoring results they concluded that the lateral displacement had an increasing trend over time which is particularly associated with precipitation events as presented in Figure 4.33.

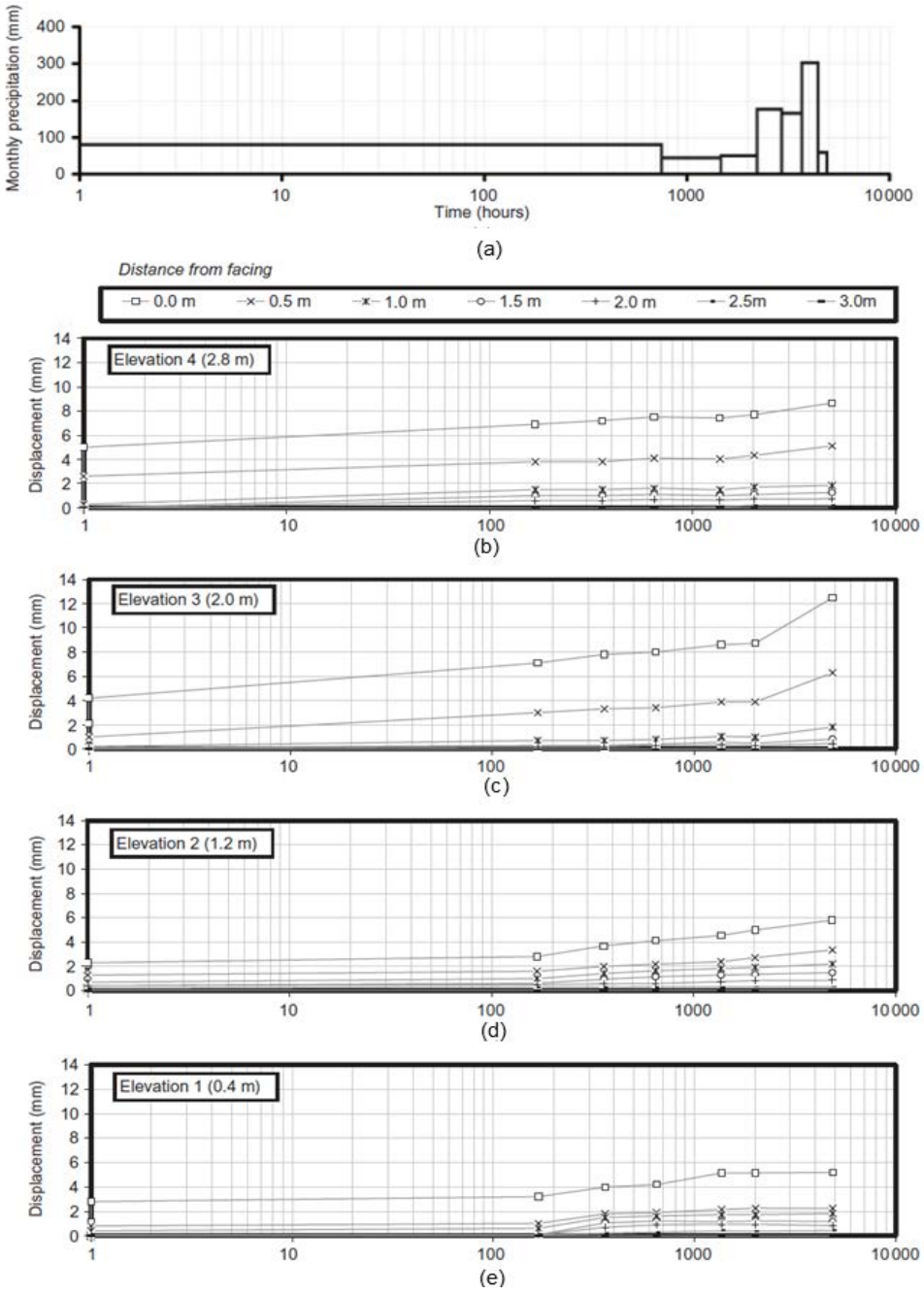

Figure 4. 33 Horizontal deformation in relation to precipitation with time: (a) precipitation; (b) elevation 4; (c) elevation 3; (d) elevation 2; (e) elevation 1 (Benjamim et al., 2007)

4.2.3.1.3 Comparison between Control and Reinforced Sections

Comparison between lateral movements results obtained based on inclinometer 3 at the control section and inclinometer 4 at the reinforced section is presented in this sub section. From the performance monitoring data it was observed that the base of the control section experienced a maximum lateral movement of almost 1.76 inches, while for the RPP reinforced section a maximum of 0.29 inches of movement was observed. This indicates that use of RPP reduced the lateral movement by almost 80 percent. For graphical comparison and better understanding, the lateral movements for both test sections are presented in Figure 4.34 keeping the scale same for both plots.

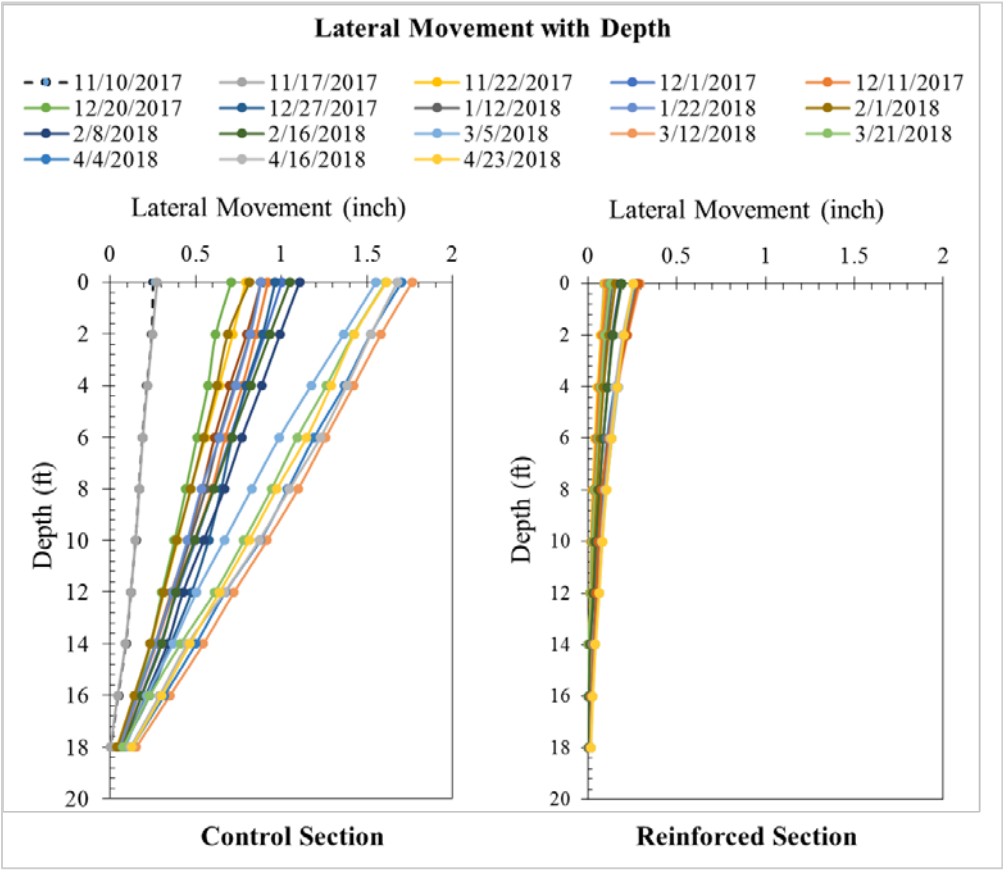

Figure 4. 34 Comparison of lateral movement with depth between control and reinforced test section (Phase-II monitoring data).

Based on the depth wise monitoring results, it is evident that at every depth the lateral movement for the reinforced section was found to significantly lower compared to the control section. Figure 4.35 and 4.36 presents the comparison of lateral movement between I-3 (control section) and I-4 (reinforced sections) for different depths (ground level, 2 ft., 4 ft. and 10 ft.) with time and rainfall events. From the comparison plot, it is evident that though for both cases there is an increasing trend of lateral movement; the quantitative value of the lateral movement differ quite a lot. Significantly higher lateral movement was observed for the inclinometer (I-3) at the control section compared to that of reinforced section (I-4) at all the depths similar to phase-I results. This is because in the reinforced test section, 4 in. x 4 in. RPP was used as reinforcement at 3 ft. c/c spacing to provide additional resistance against sliding of base of the wall.

As part of performance monitoring, visual inspections were also conducted on a regular basis. However, unlike phase-I no noticeable change in the wall facing was observed. This might be because of the use of better and systematic construction procedure of the phase – II wall facing, which was more stable, yet flexible and allows movement under lateral force from the backfill soil.

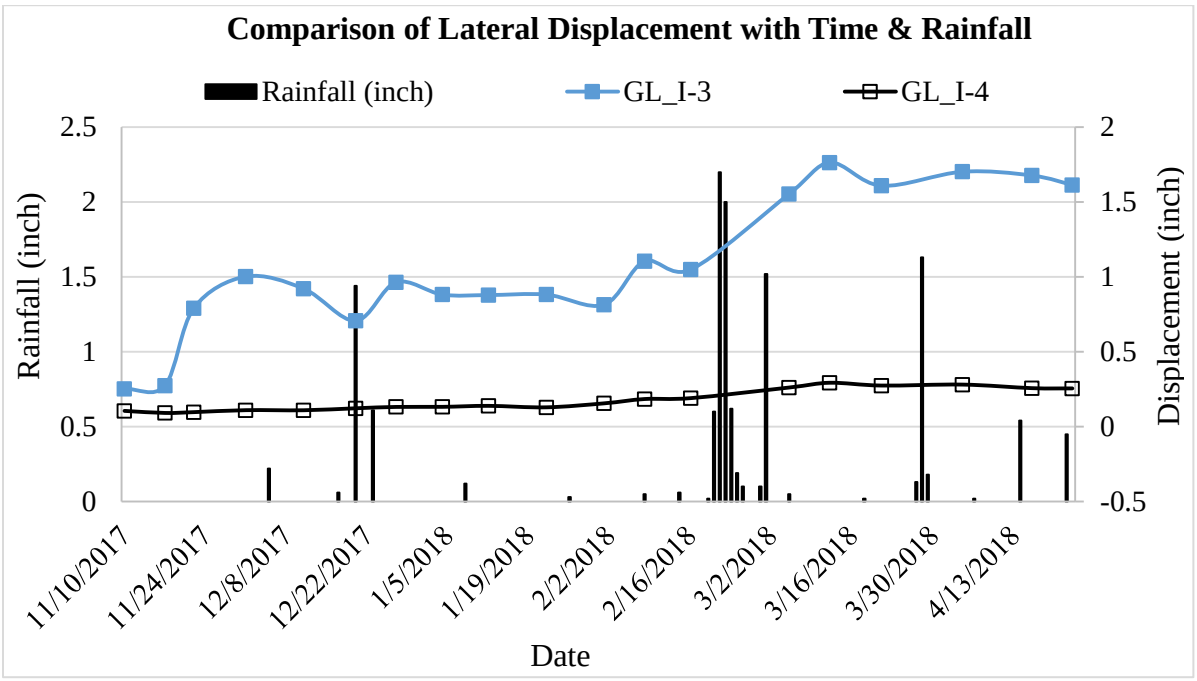

(a)

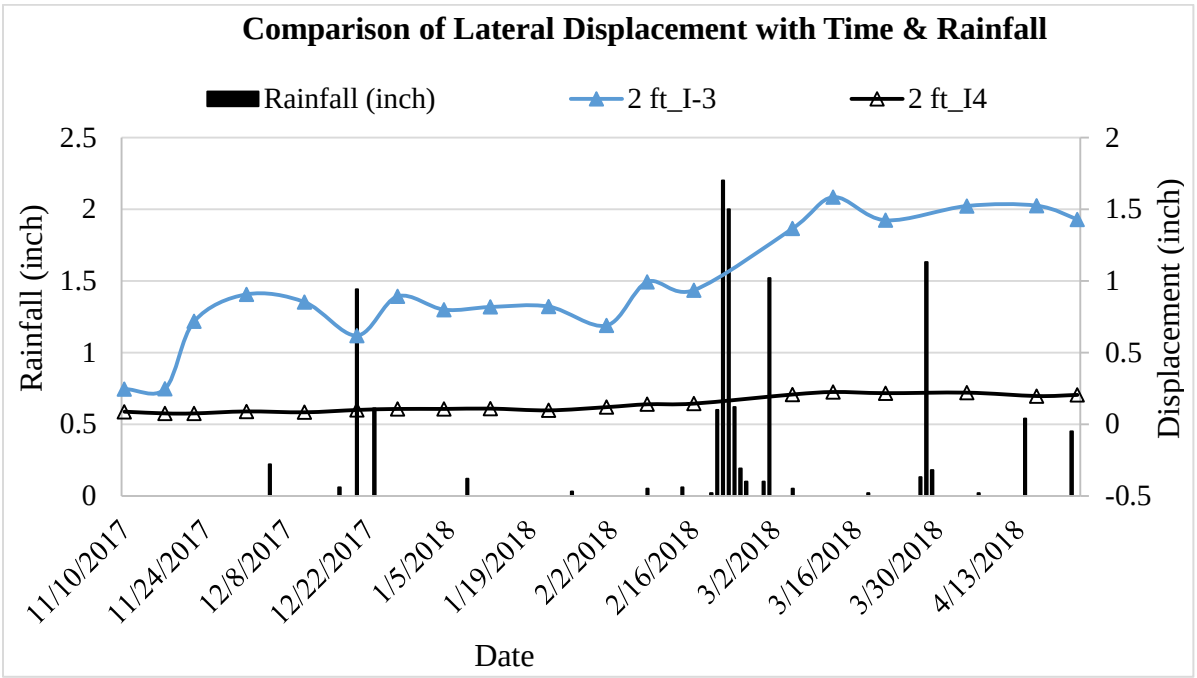

(b)

Figure 4. 35 Comparison of Lateral Displacement between Inclinometer 3 (control section) and Inclinometer 4 (reinforced section); (a) at ground level (GL), (b) at 2 ft.

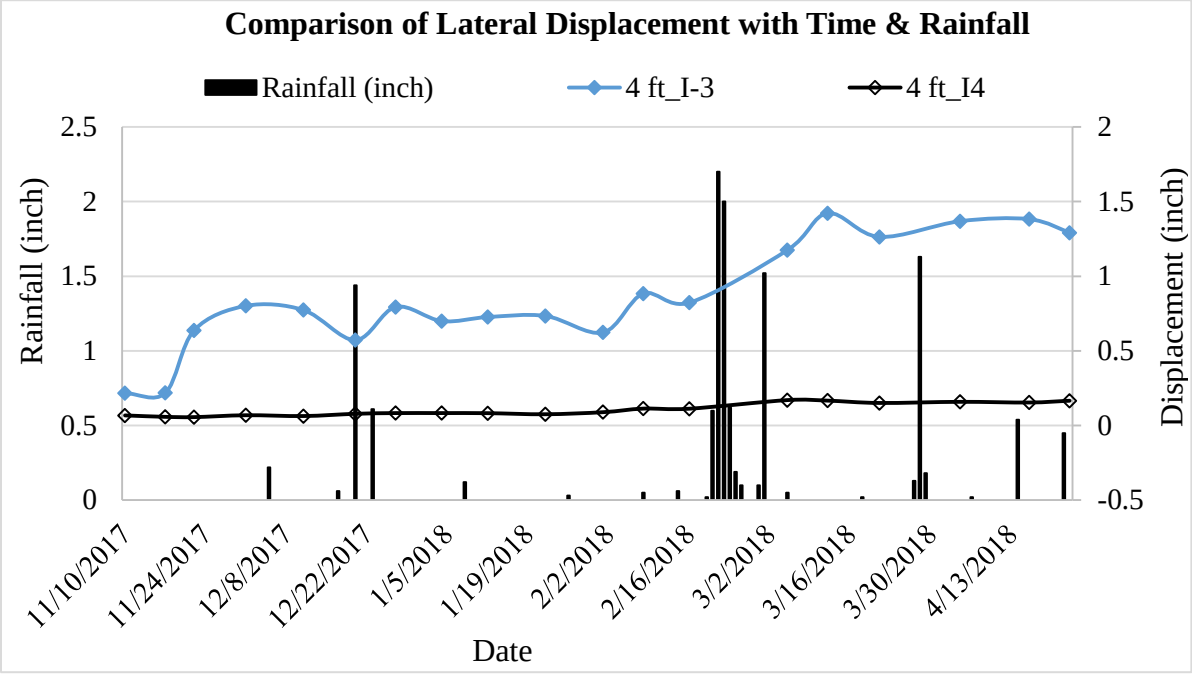

(a)

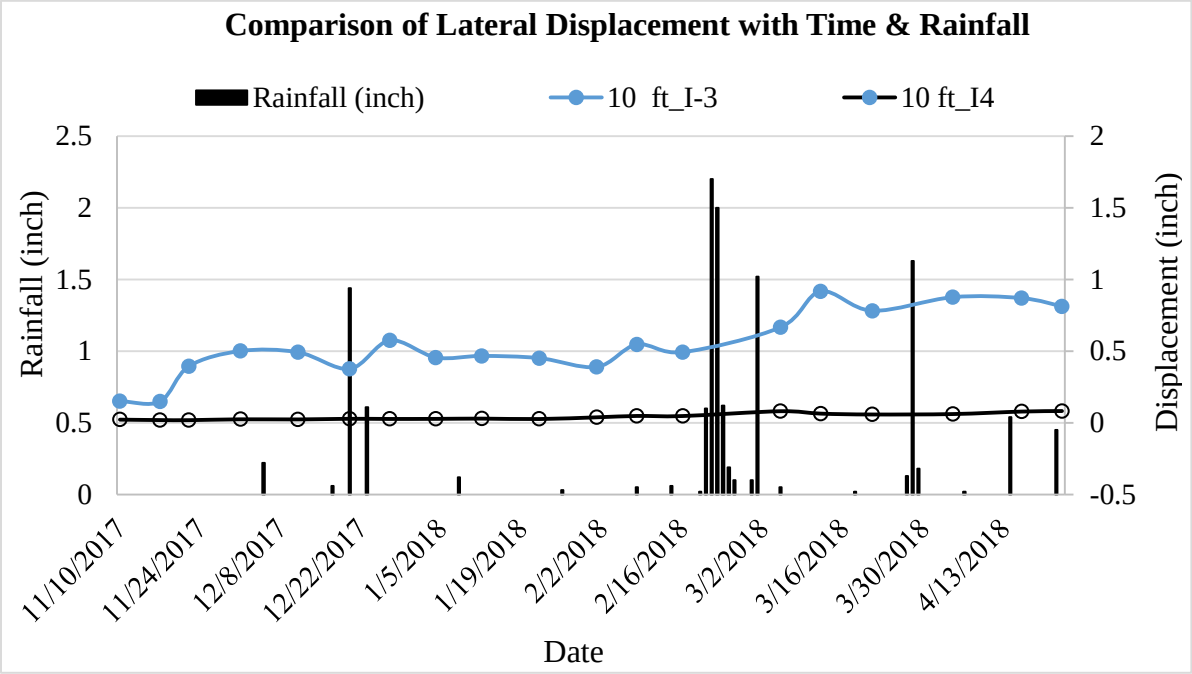

(b)

Figure 4. 36 Comparison of Lateral Displacement between Inclinometer 3 (control section) and Inclinometer 4 (reinforced section); (a) at 4 ft., (b) at 10 ft.

4.2.3.2 Pressure Plates

Pressure plates were installed at the inside face of the MSE wall; one close to the base and another close to the top, for both control and reinforced test sections to monitor the earth pressure acting on the wall. The sensors were connected to a data logging system which was programmed to record pressure data every hour. Pressure data from the bottom plates (P-1 for control section and P-2 for reinforced section) are presented in the current study. The data observed from the top plates were not in good agreement and therefore, is not presented here.

4.2.3.2.1 Change in Pressure (P – 1): Control Section

The pressure plate P-1 was installed on the inside face of wall at the control section, 1.5 ft. up from the wall base. From the hourly data points weekly average was determined. Change in pressure was plotted against time and presented in Figure 4.37. It was observed that the pressure change had an increasing trend during the first two weeks after the construction, which is due to the buildup/transfer of soil pressure at the back of the wall. When plotted against rainfall data as presented in the Figure 4.37, it was observed that, after each rainfall event there is a sharp rise in pressure and drop if there is extended period of dry weather. This might be due to swelling and shrinkage of soil which exerts and releases pressure at the back of the wall. During January 2018, almost no lateral movement was observed, however the pressure dropped significantly. This might be due to the extended dry period resulted in shrinkage of the backfill soil as shown in Figure 4.37.

However, the pressure changing trend shows a drop after each increasing scenario. When plotted with lateral displacement of the wall (Figure 4.38), it was observed that the change in pressure trend is inversely related to the lateral displacement of the wall. The wall

facing being flexible, it moves with excess pressure development at the back of the wall. The lateral movement of the facing away from the backfill, releases some pressure which might be the reason for the inverse trend in pressure change with displacement.

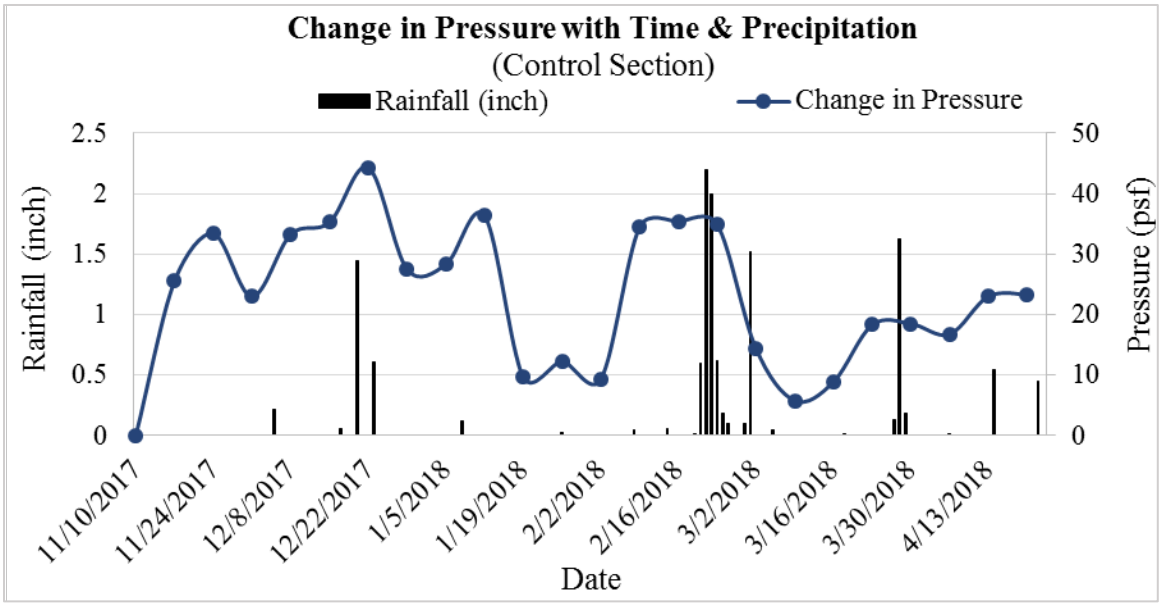

Figure 4. 37 Pressure variation in relation to rainfall and time for the control section.

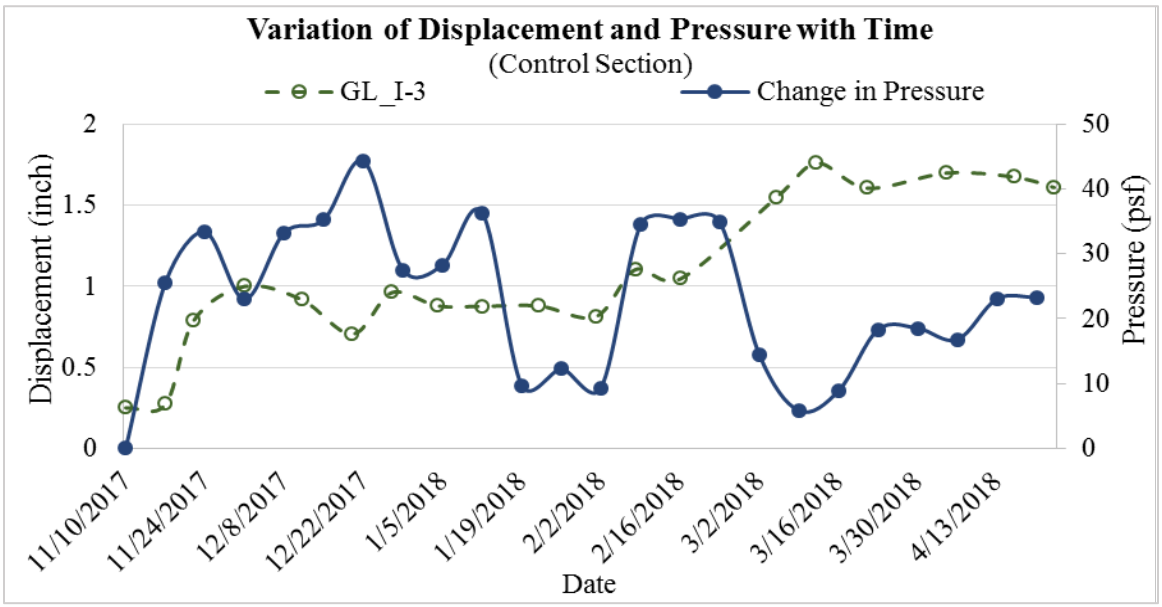

Figure 4. 38 Relation between change in pressure and displacement of wall facing (control section).

Fang et al. (1986) conducted a study on various wall movement due to earth pressure and developed a typical relationship between normalized earth pressure and the amount of lateral movement of the wall (Figure 4.39). The authors showed that earth pressure at the back of the wall decreases rapidly with increasing wall displacement. Similar result was observed in the current study.

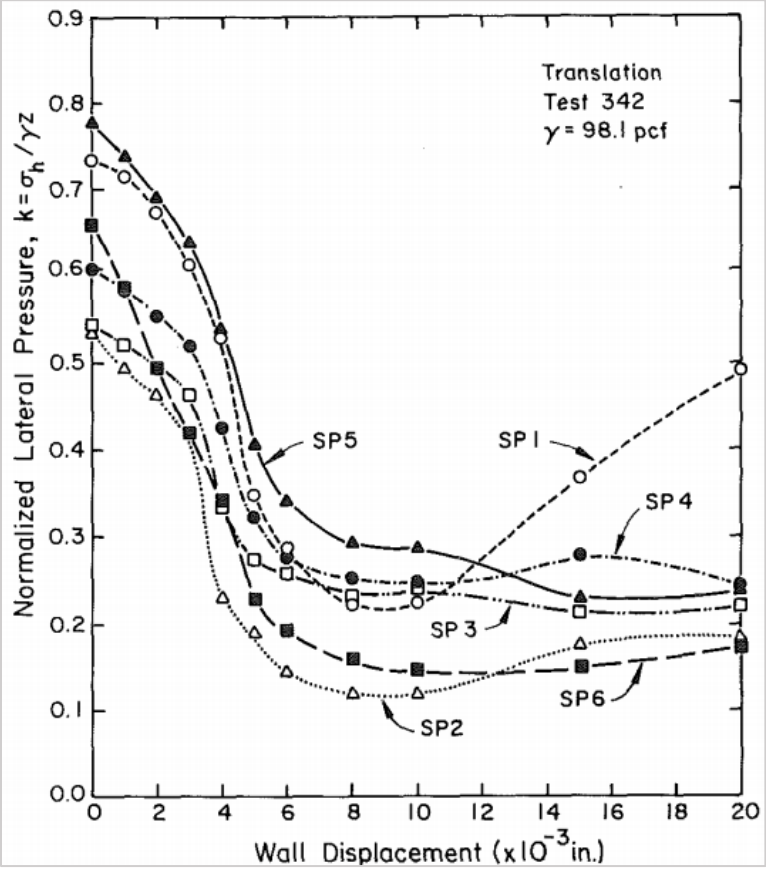

Figure 4. 39 Changes in Normalized Lateral pressure with lateral displacement of wall (Fang et al., 1986).

4.2.3.2.2 Change in Pressure (P – 2): Reinforced Section

The pressure plate P-2 was installed in the reinforced test section, identical to the P-1. From the field monitoring data, weekly average was determined and the change in pressure with time plot is presented in Figure 4.40. An increasing trend was observed followed by the

end of construction, during the next two weeks of observation. When plotted against rainfall (Figure 4.40), similar trend in pressure change as control section was observed, a rise in pressure after each precipitation event and drop during extended dry period.

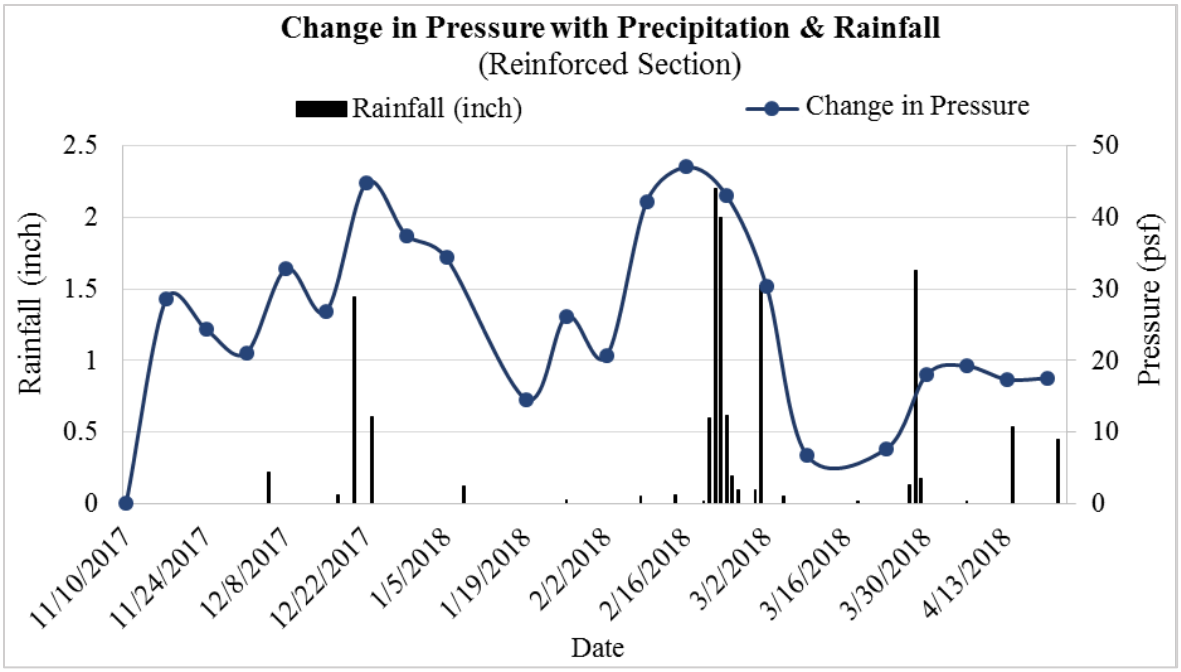

Figure 4. 40 Pressure variation in relation to rainfall for the reinforced section.

Figure 4.41 presents the change in pressure trend with lateral displacement of the wall facing. With increase in lateral displacement pressure release occurs similar to the control section. However, the lateral movement for the reinforced section wall is much less compared to the control section. So, based on the field monitoring data it can be mentioned that pressure change trend follows the opposite trend of the displacement; a decrease in pressure while lateral movement takes place away from the backfill. Also, rainfall causes pressure to rise due to the swelling behavior of soil and induce an increase in lateral displacement.

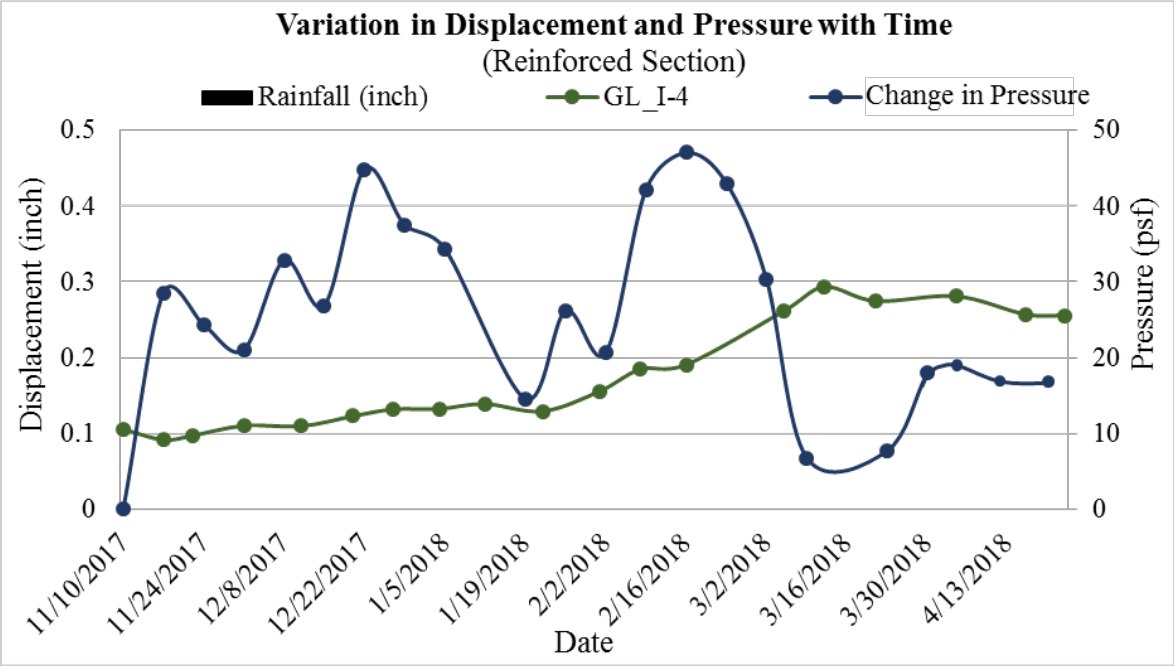

Figure 4. 41 Relation between change in pressure and displacement of wall facing (reinforced section).

Simac et al. (1990) constructed a 19.5 ft. (6 m) MSE wall and installed pressure cell to monitor the earth pressure. Abu-Hejleh et al. (2001) conducted a study on a new full-height facing system for MSE wall where 19 pressure gauges were installed at back of wall facing. The authors recorded the average earth pressure developed on the facing using the gages. The authors used adjustable nuts to allow lateral movement which reduces the earth pressure developed on the wall facing.

4.2.4 Summary

RPP has sufficient flexural strength to carry/resist significant amount of lateral force. Previous field application to stabilize slope failure proved RPP to be effective in providing additional resistance against sliding soil mass. Therefore, a concept was developed and applied in the current study to utilize RPP as shear key for the MSE wall base to resist lateral movement

of the wall base. RPP of 4 in. x 4 in. was used at 3 ft. c/c as reinforcement for the improved test section. Based on the phase – I field monitoring data it was observed that the RPP reinforced test section performed significantly well compared to the control test section. Negligible amount (0.0055 inches) of lateral movement was noted for the reinforced section, while control section wall moved quite a bit (3.8 inches). The test sections were further evaluated for higher backfill/loading height and a new facing to sustain the loading was constructed as part of phase – II construction and monitoring.

The field result for phase – II presented convincing conclusion to support results obtained in phase – I. Approximately 80% reduction in the lateral displacement was observed due to the utilization of 4 in. x 4 in. RPP as reinforcement/shear key, compared to the control section. The control section experienced a total lateral displacement of about 1.76 inches, while for the reinforced section the amount was found to be 0.29 inches.

Finally, based on phase – I and phase – II monitoring results, it can be concluded that the RPP, if used properly, might become an excellent solution to the problem associated with the lateral movement of the MSE wall base. RPP creates a composite structure when incorporated within the MSE wall base and acts as a shear key to provide additional resistance against sliding.

CHAPTER 5

NUMERICAL STUDY

5.1 Introduction

The objective of the current study is to develop a sustainable ground improvement method using Recycled Plastic Pin, i.e. improving bearing capacity of soft foundation soil and increasing shear resistance against base sliding of MSE retaining structure. A field scale study was conducted to evaluate the effectiveness of RPP in improving the condition of unsuitable soil. As a part of the study, five field scale test sections were constructed.

The field scale study was divided in to two major parts. The first part included construction of three vertical loaded test sections, one as control section and the other two served as reinforced section. The reinforced sections include reinforcement of the foundation soil with 4 in. x 4 in. and 6 in. x 6 in. RPP respectively, to evaluate the effectiveness of RPP in improving the foundation soil to carry higher load with reduced settlement condition. In the second part of the study, two lateral loaded MSE wall test sections were constructed, one as control section and the other reinforced with 4 in. x 4 in. RPP, to assess the effectiveness of RPP in increasing the sliding resistance of the MSE wall base.

Based on the monitoring results, it was evident that RPP provided additional support in improving the weak foundation soil (reducing settlement) subjected to vertical loading, as well as, served effectively as shear key by providing additional shear resistance against base sliding of MSE wall. Numerical study was conducted to recalibrate the performance of the

RPP reinforced test sections and the calibrated model was used to further assess the effect of increasing loading and different RPP length, size and spacing.

5.2 Finite Element Model

Deformation analysis were performed using PLAXIS 2D, a two dimensional finite element program, developed for the purpose of analyzing deformation, stability and groundwater flow in geotechnical engineering applications (PLAXIS 2D reference manual, 2017). PLAXIS has several soil models which are Linear Elastic model (LE), Mohr-Coulomb model (MC), Hardening Soil model (HS), Soft Soil model (SS), Soft Soil Creep model (SSC), Jointed Rock model (JR), Modified Cam-Clay model (MCC), NGI-ADP model, Hoek-Brown model, Sekiguchi-Ohta model, and User-Defined model (UD). However, Mohr-Coulomb model is considered to be the first order approximation of real soil behavior among all these models. Five basic soil input parameters are required for this elastic perfectly plastic model, namely unit weight (γ), young's modulus (E), poisons ratio (υ), cohesion (c) and friction angle (φ). If the soil parameters are not known with great certainty, Mohr-Coulomb model is highly recommended.

Finite element analysis using PLAXIS is carried out by creating finite element mesh and specifying the material properties and boundary conditions during pre-processing of data. Finite element model is developed as a 2D geometry model created in the XY-plane. Generation of properties, boundary conditions and appropriate mesh generation is automatically performed by the PLAXIS mesh generator depending on the input of the geometry model. At the end it is required to generate water pressure and to set the initial state of the initial effective stresses.

Plain strain model is used in the analysis using PLAXIS 2D. A plain strain model is usually used for geometries with a (more or less) uniform cross section and corresponding stress state and loading scheme over a certain length perpendicular to the cross section (z direction). In the z-direction, all displacements and strains are assumed to be zero; however, normal stresses in z-direction are fully taken into account. The analysis is conducted using 15-node triangle element in this study. Figure 5.1 shows the units, model and element used for the analysis.

The model is generated to simulate the vertical loading test section constructed for the field scale study for both control as well as reinforced section. Field results are used to calibrate the model to represent field scenario. The calibrated model is used to better predict the outcome in the field for varying parameters.

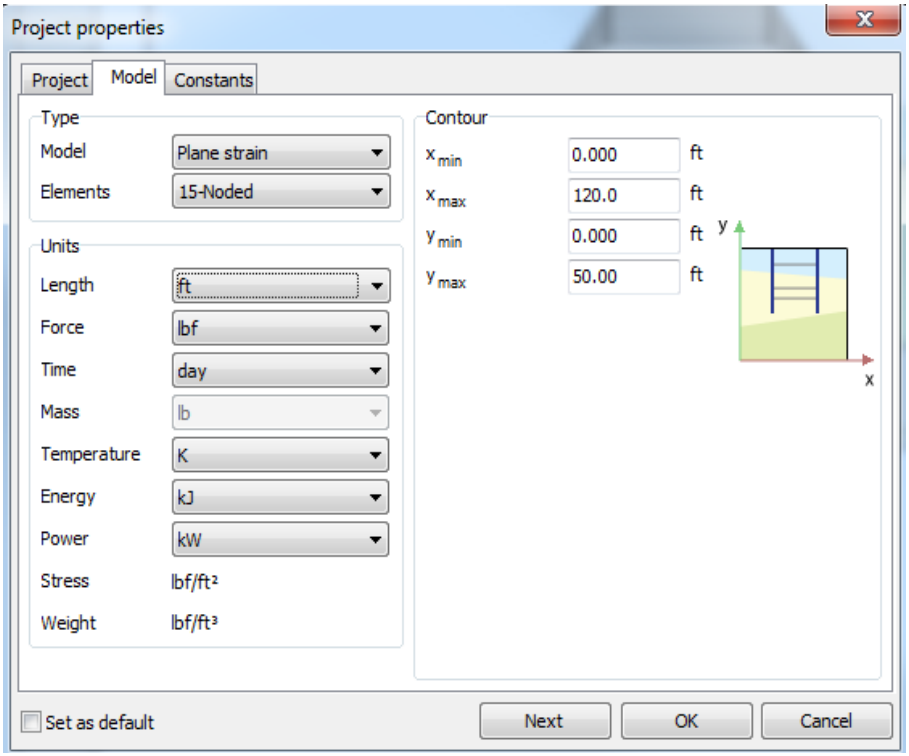

Figure 5. 1 Units, model and elements used in PLAXIS 2D.

5.3 Numerical Study for Vertical Loaded Test Sections

The field scale study for the vertical loading included a control section with no RPP and two sections reinforced with 4 in. x 4 in. and 6 in. x 6 in. RPP respectively, having a uniform RPP spacing of 3 ft. c/c in a staggered pattern. All the test sections were identically loaded with a soil height of 6 ft. The effective size of the test sections were 15 ft. x 15 ft. In the reinforced section, RPP was installed in such a way that top of the RPP is flushed with the ground surface. A single layer of bi-axial geogrid was placed above the ground surface to provide a flexible platform to transfer the load on the RPP through arching effect which also minimizes differential settlement of the foundation soil. Based on the performance monitoring results, it was evident that RPP reinforced foundation has the added advantage of providing support to minimize settlement of the foundation soil; hence, improved the bearing capacity.

The field monitoring results were used to develop calibrated model as part of the numerical study. The numerical modeling was conducted for two different considerations. First, a comparison between control and reinforced section for increasing loading height was conducted. The numerical study was further conducted to study the effect of RPP size, length and spacing. Details of finite element modelling (FEM) is presented in the following sub-sections.

5.3.1 Model Calibration

Development of a mathematical model is necessary which is capable of simulating the response to the prescribed actions such that predicted results is in an acceptable agreement with the physical observations (Meyer, 1987; Rao, 2006). Standardizing, modifying, and verifying process of a mathematical model can take several forms. Constructing a mathematical model

to predict from its output is one of the common engineering practice. A satisfactory agreement between predicted outputs and physical experiments confirms accuracy of both mathematical model and the physical test. Therefore, calibration of model is mandatory for numerical analysis.

The elastic perfectly plastic Mohr-Coulomb soil model was utilized for deformation analyses, using 15 node triangle elements. The FEM analysis using a 15 node triangular element which has 9 stress points, is a very accurate method and produces high quality stress results for different problems (PLAXIS 2D Reference Manual, 2017). Standard fixities were applied as boundary condition.

The finite element is simulated with 3 layers of native soil profile along with applied load from fill soil. Native soil consists of: 9 ft. of very stiff clay (soil layer 1) as the bottom layer of the soil profile, overlain by 16 ft. of stiff clay layer (soil layer 2). Finally, the top layer consists of 5 ft. of soft clay layer (soil layer 3). As loading material in the model, properties of onsite clay soil was considered which was used as embankment loading of 6 ft. height for the test sections. Bi-axial geogrid used for the test sections were modeled by linear elastic sheet elements. All the soil layers were modeled as linear elastic perfectly plastic materials that obey Mohr-Coulomb failure criteria. Undrained behavior was considered for all soil layers for short-term or rapid construction, in which effective properties define the stiffness and strength of the soil layers.

To evaluate the soil parameters for the control section, back analysis were performed using PLAXIS 2D. The soil profile is presented in the Figure 5.2. The baseline of the calibration started by using soil unit weights, permeability and strength properties (cohesion,

c and friction angle, φ) of soil found from laboratory test results, using typical value of Poisson's ratio and elastic modulus, E determined using equations that depends on SPT number. The back analysis was performed using the anticipated deformation that was found from the field monitoring results.

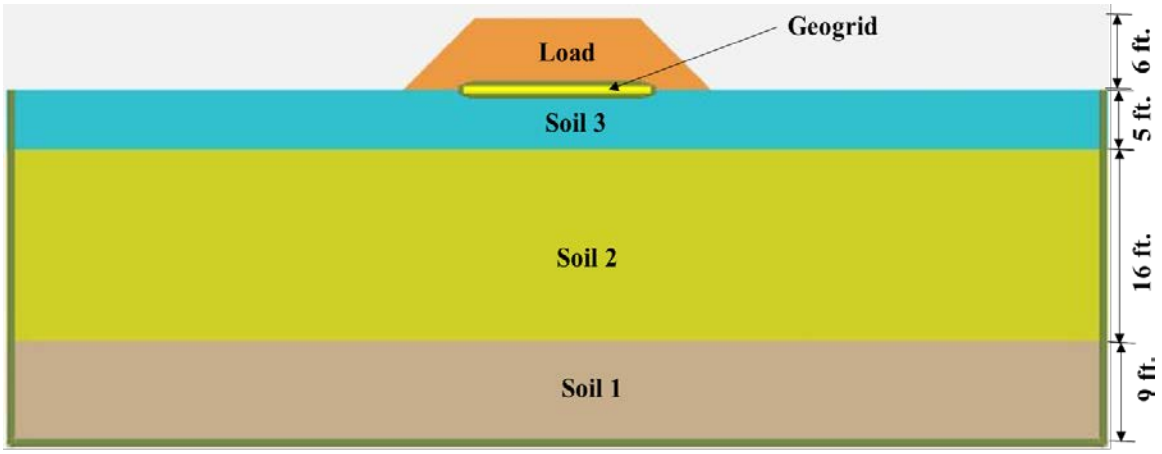

Figure 5. 2 Soil model for control section.

Numerous iteration was performed during numerical analysis to evaluate soil parameters. The parameters used for native soil layers and embankment fill materials at which the calibrated model showed lateral deformation close to the field result are presented in the Table 5.1.

Table 5. 1 Soil parameters from FEM analysis.

Soil Type -	Friction angle Φ °	Cohesion c psf	Unit Weight, γ pcf	Elastic Modulus, E psf	Poisson Ratio, υ -
1	25	3,500	120	240,000	0.25
2	20	2,000	120	160,000	0.25
3	0	125	115	12,000	0.3
Load	15	800	115	150,000	0.25

The bi-axial geogrids used in the field are considered as slender structure having only normal stiffness and without any bending stiffness. It is a tensile element that has zero compression sustainability. “Geogrid” element has been used for geogrid that act as isotropic element at each nodes and unable to work under compression. Table 5.2 presents the material properties of modeled geogrid.

Table 5. 2 Geogrid parameters used in the model.

Identification	EA (lb/ft.)	υ
Bi-axial Geogrid	1,500	0

The calibrated model was developed for deformation analysis of the control section. Based on the calibrated model for the soil parameters presented in Table 5.1, the vertical deformation was found to be 2.03 inches which is close to the field observation (2.01 inches).

The slight variation between predicted result and field observation might be due to the non-uniformity of the soil load placement in the field, shape of the embankment and also the level of compactness of soil body. Figure 5.3 shows the displacement contour and shading for the control section generated using the calibrated model.

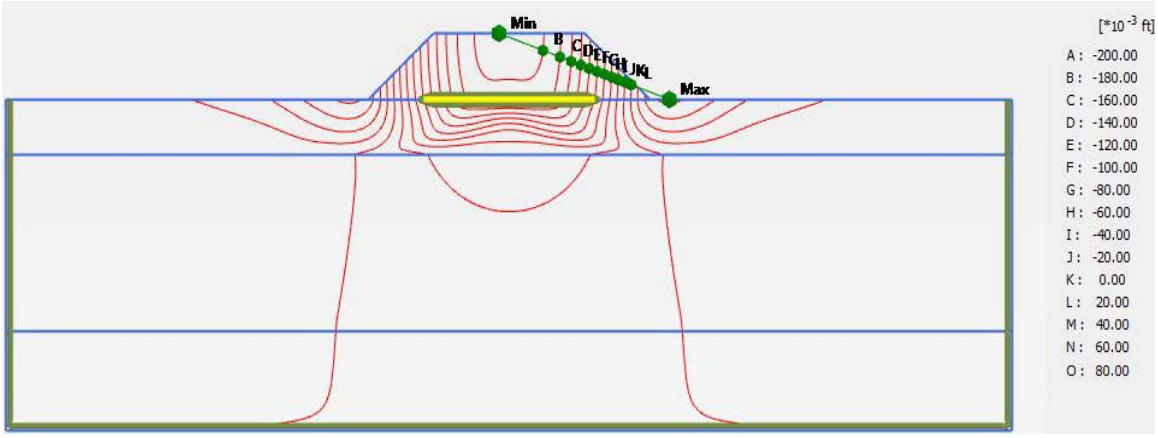

(a)

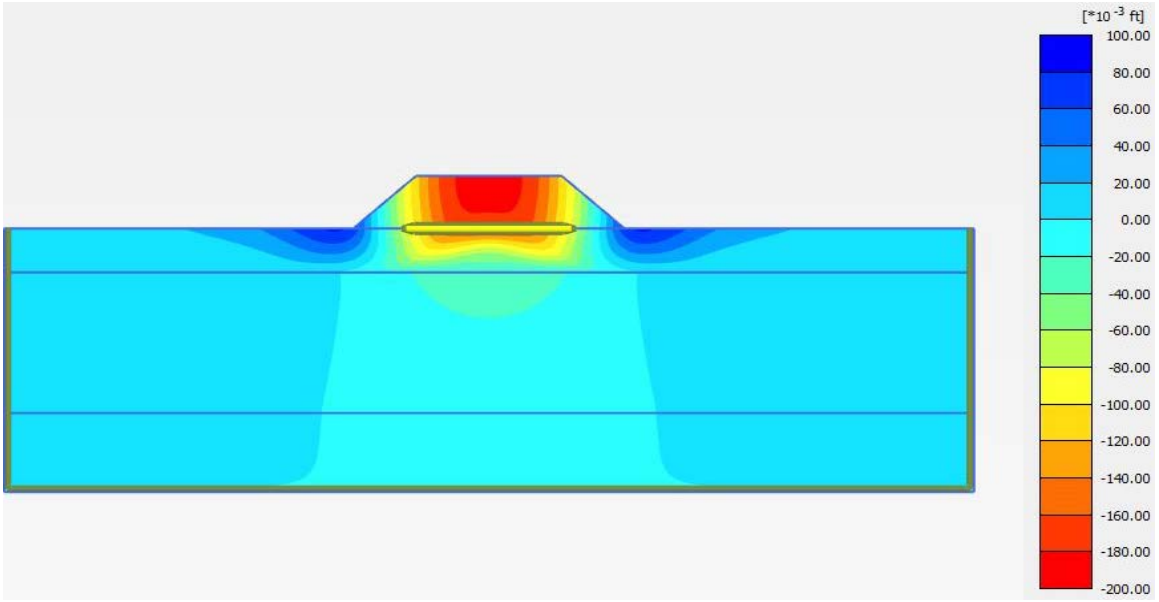

(b)

Figure 5. 3 FEM Vertical deformation plot of control section, 2.03 inches of settlement; (a) Contour lines, (b) Shading.

Among different types of embankment loading failure, the one in relation to the soft/weak foundation soil is the bearing capacity failure in the form of excessive settlement. The deformed shape of the modeled test section (Figure 5.4) in PLAXIS shows similar output which supports the field observation and verifies the theory.

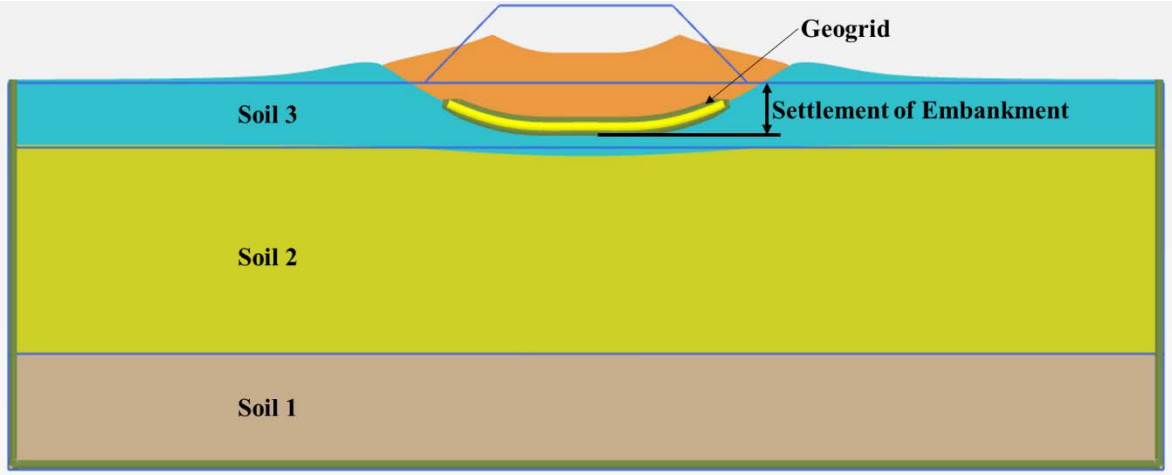

Figure 5. 4 Deformed shape of the control test section.

5.3.2 Performance Evaluation of 4 in. x 4 in. RPP Reinforced Section

The identical soil parameters used in the calibrated control test section model were utilized to perform the deformation analysis for the reinforced test section. The model details for the reinforced section is presented in Figure 5.5.

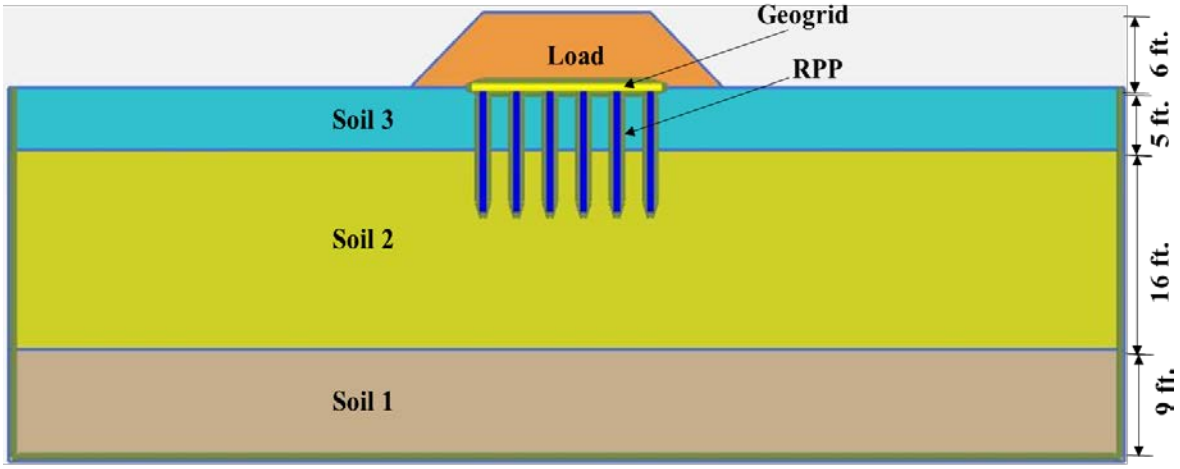

Figure 5. 5 FEM model for 4" x 4" RPP reinforced section.

According to the deformation analysis performed, the predicted vertical deformation/settlement was found to be about 0.75 inches. It should be noted that the maximum settlement of the test section, reinforced with 4 in. x 4 in. RPP, predicted using the calibrated model is in good agreement with the settlement observed at the field for the same reinforced section (0.8 inches). The slight variation from field result might be due to the non-uniform placement of the soil for the load application and there are possibilities of poor installation of geogrid resulted from human errors. Also, temporary live loads from excavators, backhoe etc., while loading the sections with native soil was not considered in the model which might have induced some additional settlement in the field.

Vertical deformation diagrams (displacement contour and shading) of the 4 in. x 4 in. RPP reinforced section is presented in Figure 5.6. Properties of 4 in. x 4 in. RPP used in the numerical analysis is presented in table 5.3.

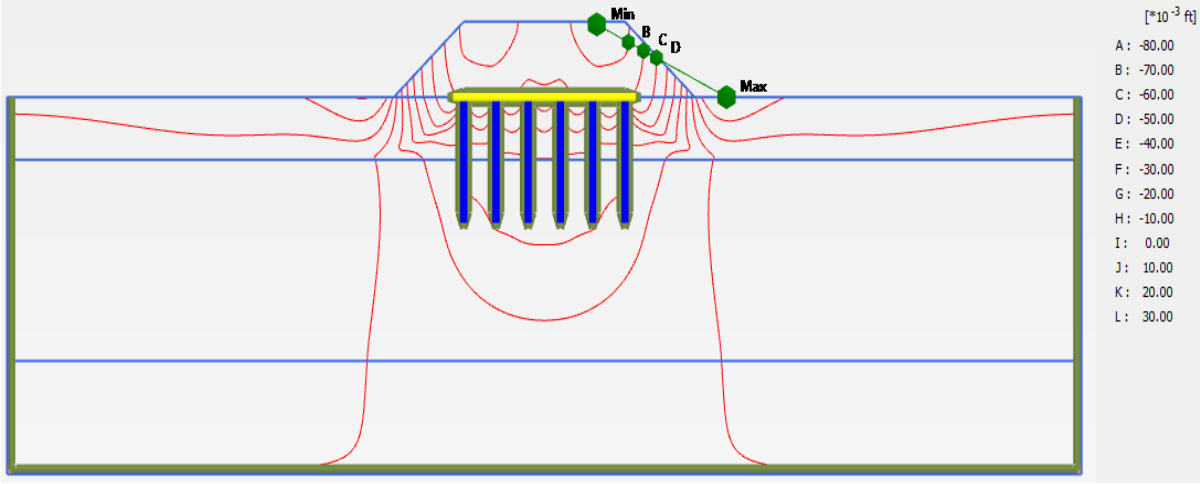

(a)

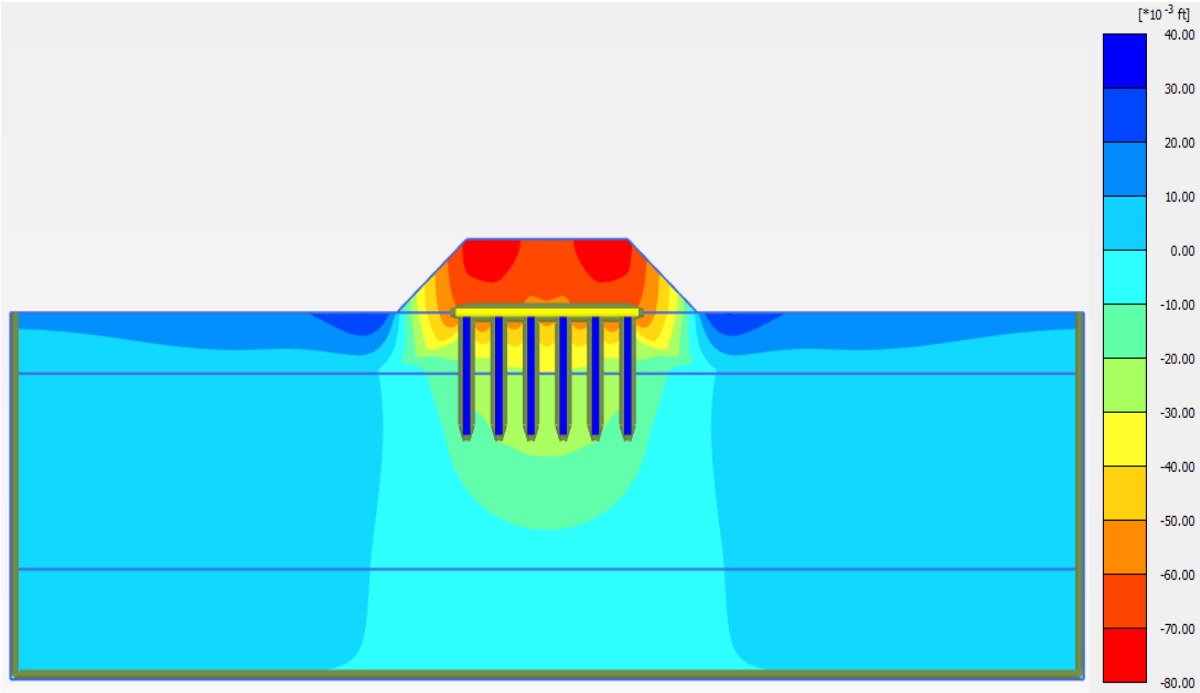

(b)

Figure 5. 6 FEM Vertical deformation plot of reinforced section, 0.75 inches foundation settlement; (a) Contour lines, (b) Shading.

Table 5. 3 RPP (4” x 4”) parameters used for FE analysis.

RPP Properties	Units	Parameters
EA	lb./ft.	3,200,000
EI	$lbft^2/ft.$	29,630
d	ft.	0.333
w	lb./ft./ft.	1.85
υ (nu)		0.30

From the deformation diagram presented in Figure 5.7, it is evident that the RPP is supporting the loads from the embankment and the load from soil is being transferred to the RPP by arching effect of geogrid. Also, underneath the foundation the soil is trying to move laterally to accommodate the settling structure, which is also restricted by the RPP. Thus keeping the soil in place, RPP helps to provide additional support and minimizes the settlement.

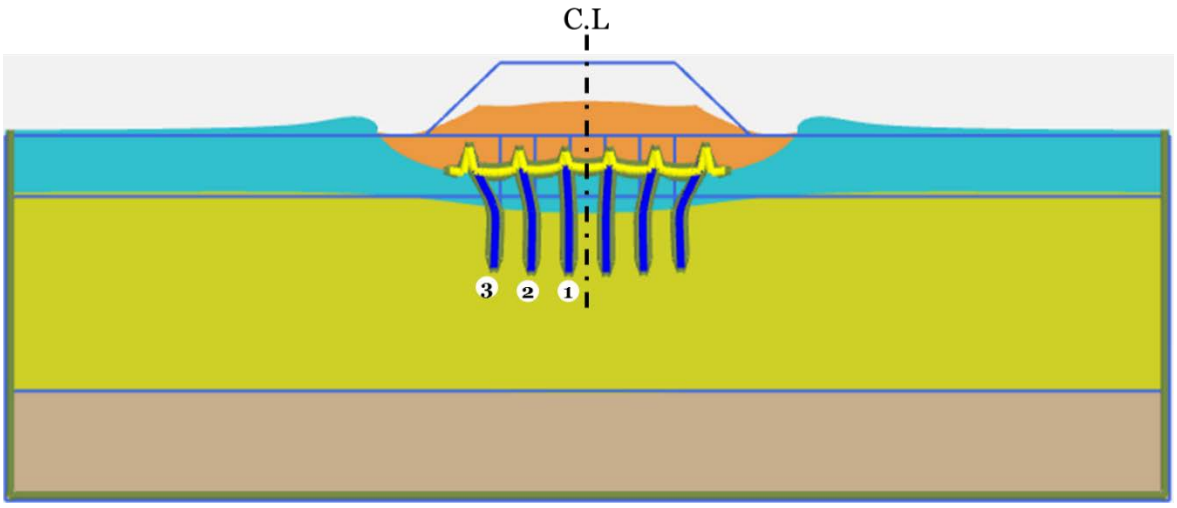

Figure 5. 7 Deformed shape of the soil body from FEM due to load application for 4 in. x 4 in. Reinforced test section.

The embankment considered in the current study was a symmetric structure, therefore, the forces experienced by the RPP of the two sides of center line should be of same values (mirror image). Due to the tendency of the foundation soil to move laterally under vertical loading, there is lateral force acting on the RPP. Moment is generated due to the lateral force from soil. Portion of piles in the foundation soil is considered as free end as the soil has minimum resistance to the force acting on it. In this study, Top 5 ft. of the piles reside in the soft soil layer and bottom 5 ft. is anchored within the stiff soil layer; therefore, the lateral load generated within the soft soil has the tendency to move laterally which is restricted by the anchorage and the stiffness of the RPP. Bending moment along the length of left 3 rows of RPPs is presented in Figure 5.8. Using the equation 5.1, percentage of moment transfer for RPP can be calculated.

$$\%\, Moment\ Transfer\ = \frac{Bending\ Moment\ M\ of\ RPP}{Maximum\ Moment\ Capacity\ of\ RPP, M_{max}} \qquad (5.1)$$

From the bending moment plot (Figure 5.8a) along the depth of RPP it was observed that the maximum moment took place at the 3rd row of RPP. The maximum bending moment was found to be about 209 lb-ft. The maximum moment was observed near the interface between soft soil and the stiff underlying layer which is providing support or anchorage against the lateral shift. Figure 5.8b presents the percentage of moment transfer in the RPP. From the plot it is evident that maximum percentage of moment transfer is about 9% which signifies that a total of 9% of the moment capacity of the RPP has been utilized. Based on a study done by Chen et al. (2007), a life prediction model for RPP was developed depending on the % of moment transfer and showed that a design life of 100 years can be expected for a moment transfer up to 35%. From the current model observation, the maximum moment transfer for

the 3rd row of RPP was found to be about 9% which might result in a design life for the RPP more than 100 years.

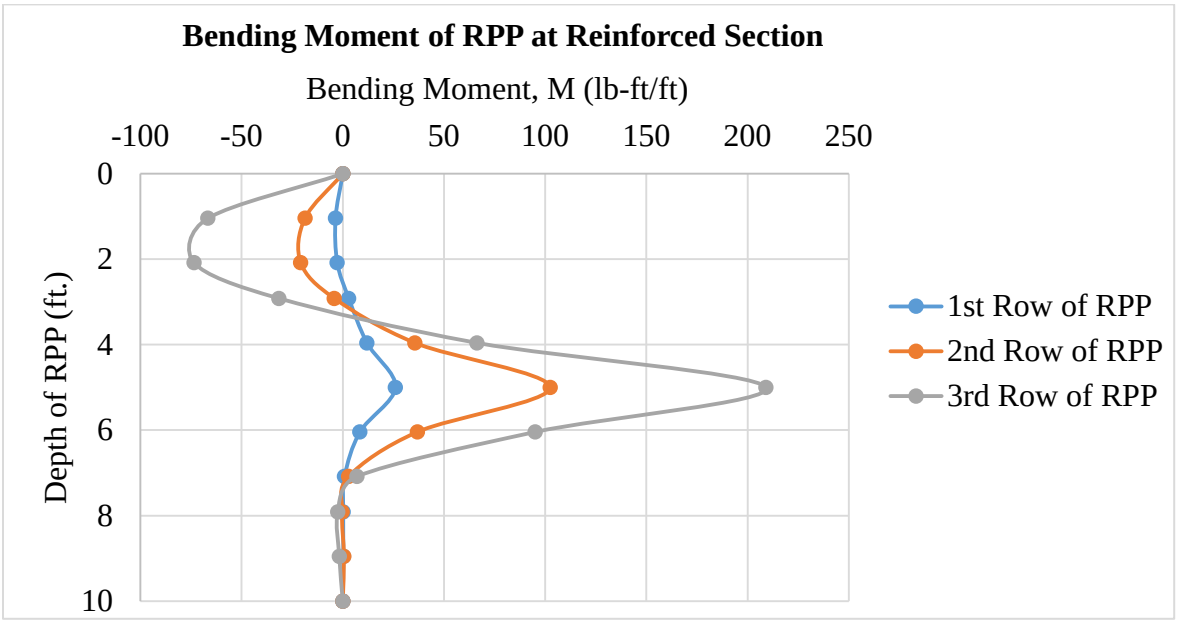

(a)

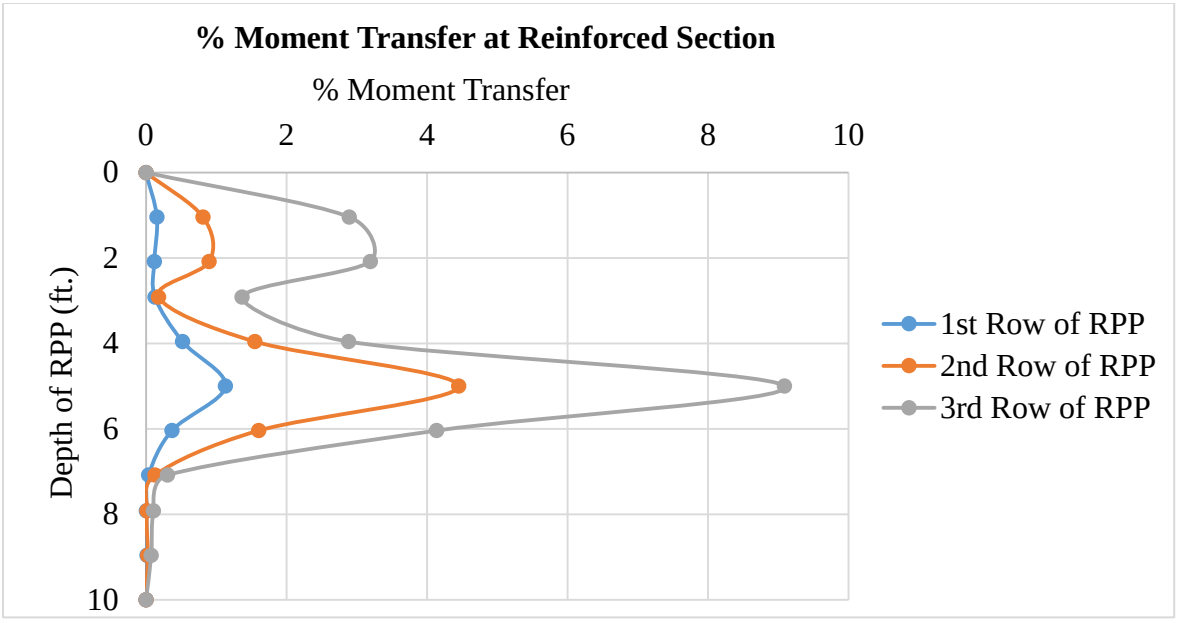

(b)

Figure 5. 8 Moment along the length of 4 in. x 4 in. RPP; (a) Bending moment, (b) % of moment transfer.

For the vertically loaded test section, the RPP carries the load from the structure by arching effect of geogrid and transfer it to a deeper layer, resulting in less pressure on the surface of soft foundation soil. At the same time, RPP, when inserted in to the ground, helps densifying the soil. Therefore, the total and differential settlement of the foundation is reduced considerably. From the model it was found that maximum axial force for the 4 in. x 4 in. RPP was 1,065 lb. in the form of compressive strength and stress acting on the RPP was calculated to be about 66 psi. According to Chen et al. (2007), typical minimum compressive stress for RPP is about 100 psi. Figure 5.9 shows the axial force diagram of the RPP from FEM.

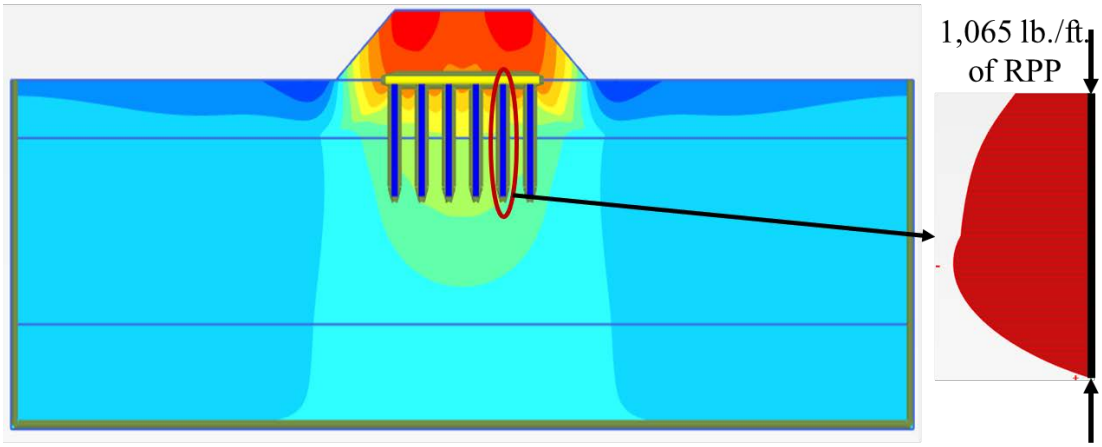

Figure 5. 9 Maximum axial force acting on the 4 in. x 4 in. RPP (from FEM).

5.3.3 Performance Evaluation of 6 in. x 6 in. RPP Reinforced Section

The identical soil parameters of the control section and 4 in. x 4 in. RPP reinforced section were utilized to perform the deformation analysis for the 6 in. x 6 in. RPP reinforced section. The model of the 6 in. x 6 in. RPP reinforced test section is identical to the 4 in. x 4 in. RPP reinforced test section as shown in Figure 5.5.

According to the deformation analysis performed, the predicted vertical deformation/settlement was found to be 0.53 inches which slightly less than that observed in

the field for the 6 in. x 6 in. reinforced section (0.64 inches). This might be due to the non-uniform loading and settlement due to temporary load from excavator during the construction etc. Vertical deformation diagram of the 6 in. x 6 in. RPP reinforced section is presented in Figure 5.10. Properties of 6 in. x 6 in. RPP used in the numerical analysis is presented in table 5.4.

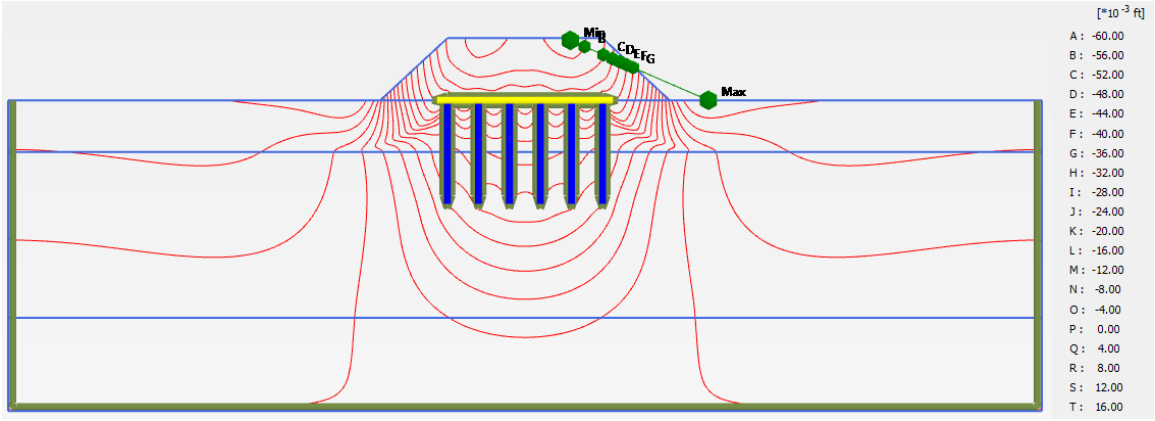

(a)

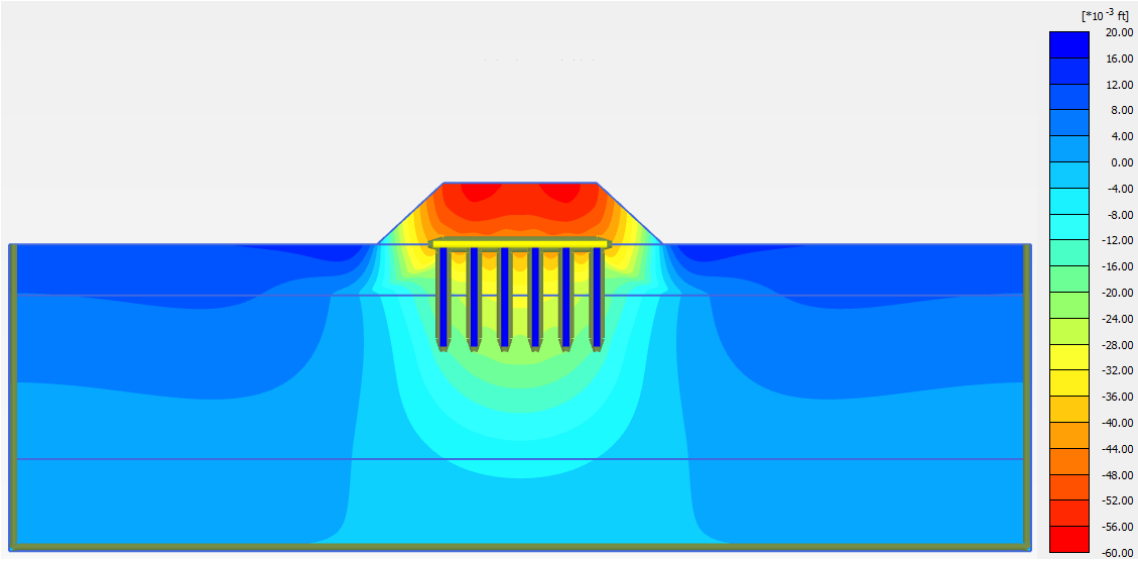

(b)

Figure 5. 10 FEM Vertical deformation plot of 6 in. x 6 in. RPP reinforced section, 0.53 inches foundation settlement; (a) Contour lines, (b) Shading.

Table 5. 4 RPP (6” x 6”) parameters used for FE analysis.

RPP Properties	Units	Parameters
EA	lb./ft.	7,200,000
EI	$lbft^2/ft.$	150,000
d	ft.	0.5
w	lb./ft./ft.	4.167
υ (nu)		0.40

The deformation diagram of the 6 in. x 6 in. RPP reinforced test section is presented in Figure 5.11. The deformed shape is similar to the 4 in. x 4 in. RPP reinforced test section which shows the same concept that the RPP is supporting the loads from the embankment and the load from soil is being transferred to the RPP by soil arching effect because of using geogrid. Also, the RPPs are providing additional support to restrict the lateral movement of the soil mass underneath the foundation and minimizes the settlement.

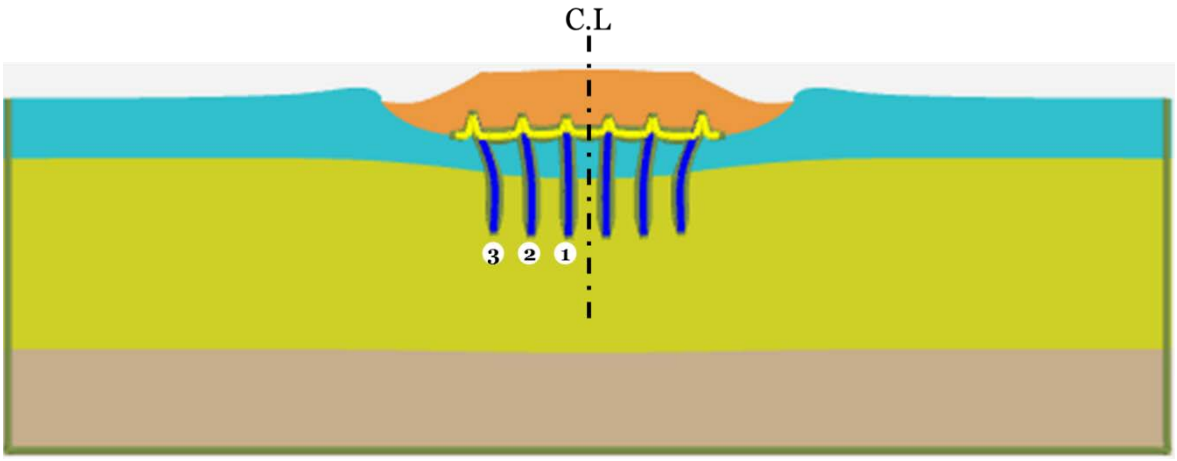

Figure 5. 11 Deformed shape of the soil body from FEM due to load application.

From the deformed shape diagram it is evident that moment is generated due to the lateral force from settling soil on the relatively free end of RPP which is resisted by the anchorage and the stiffness of the RPP. Bending moment along the length of left 3 rows of RPP is presented in Figure 5.12. Using the equation 5.1, percentage of moment transfer for RPP can be calculated.

From the bending moment plot (Figure 5.12a) along the depth of RPP it was observed that the maximum moment was resisted by the 3rd row of RPP. The maximum bending moment was found to be about 306 lb-ft. Similar to the reinforced section 1, the maximum moment was observed near the interface between soft soil and the stiff underlying layer (5 ft. from ground surface). The stiff layer is providing support as well as anchorage against the lateral shift. Total Moment resisted by the 6 in. x 6 in. RPP is higher comparative to the 4 in. x 4 in. RPP for the same loading condition which might be because of the surface area of the 6 in. x 6 in. RPP being higher, it was subjected to higher load and being stiffer it can resist greater force from the soil. Figure 5.12b presents the percentage of moment transfer in the RPP. From the plot it is evident that maximum percentage of moment transfer was about 13.5% which signifies that 13.5% of the moment capacity of the RPP had been utilized; this might result in a design life for the RPP more than 100 years, (based on a study by Chen et al., 2007).

From the model it was found that the maximum axial load transferred through the 6 in. x 6 in. RPP was 1,120 lb and stress acting on the RPP was about 31 psi. According to Chen et al. (2007), typical minimum compressive stress for creep of RPP was found to be 100 psi. Which indicates only 31% of the RPP's compressive strength is utilized before it reaches the creep strength. Figure 5.13 shows the axial force diagram of the RPP from the FEM.

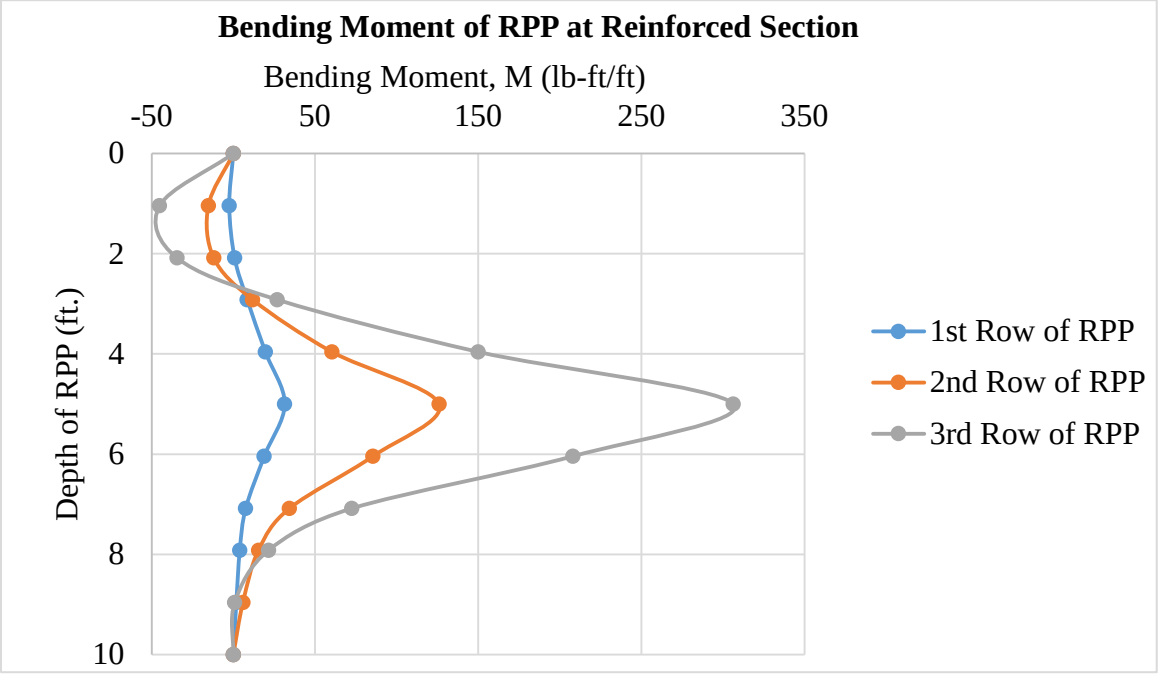

(a)

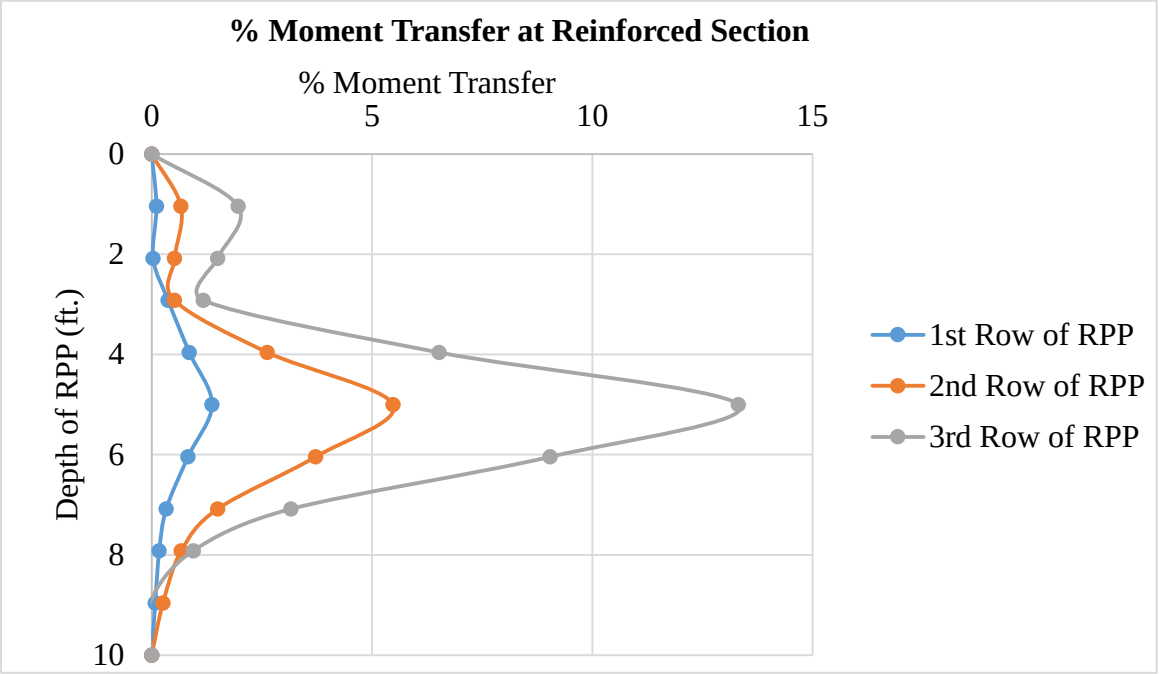

(b)

Figure 5. 12 Moment along the length of 6 in. x 6 in. RPP; (a) Bending moment, (b) % of moment transfer.

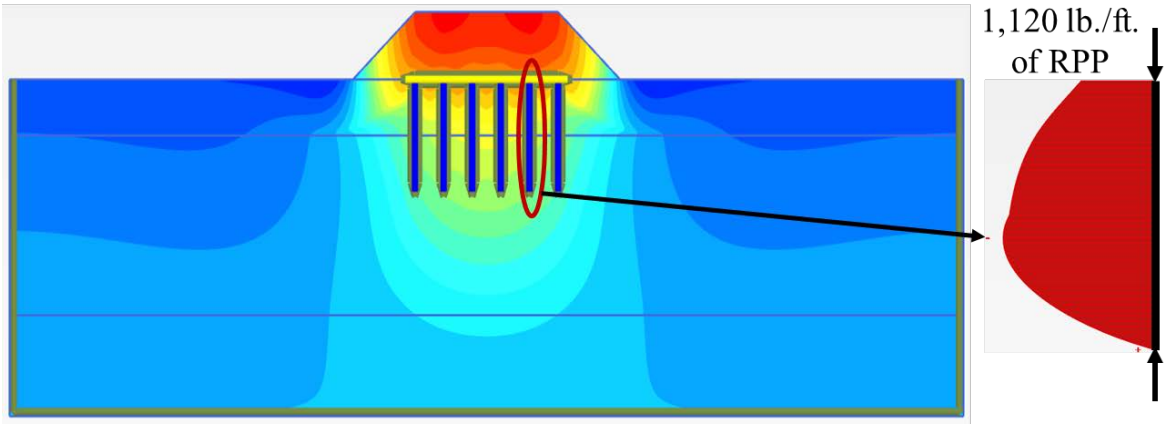

Figure 5. 13 Maximum axial force acting on the RPP (from FEM).

5.3.4 Comparison of Settlement between Control and Reinforced Section

A relative comparison plot of settlement between control and reinforced test sections (4 in. x 4 in. and 6 in. x 6 in. RPP) observed from the calibrated models are presented in Figure 5.14. The plot shows the comparative settlement of the test sections at different points of the embankment base from the edge to the center of the embankment. From the plot, it was observed that for the control section settlement increased with the distance to the center of the embankment, while for the reinforced sections settlement varies due to the geosynthetic and RPP reinforcement as well as soil arching effect. Between the RPP settlement is higher as the geogrid platform is flexible and at the point of RPP settlement is much less as the RPPs are comparatively stiff and has a relatively fixed support at their toe within the underlying stiffer soil layer. Jenck et al. (2009) observed similar results from a numerical study conducted for pile supported embankment, where the piles are considered to be completely rigid, therefore no settlement was observed at the point of piles (Figure 5.15). Also, at the edge of the embankment for the control section upward movement of the soil was observed, which is due to the insufficient bearing capacity of the soil; the soil is moving away from the underneath of the embankment. While for the reinforced section due to foundation improvement no such

thing was observed. Maximum settlement found for the 4 in. x 4 in. and 6 in. x 6 in. RPP reinforced sections are 0.75 inches and 0.53 inches respectively under the base of the embankment, which corresponds to a settlement reduction of about 60% and 70% respectively compared to the unreinforced section.

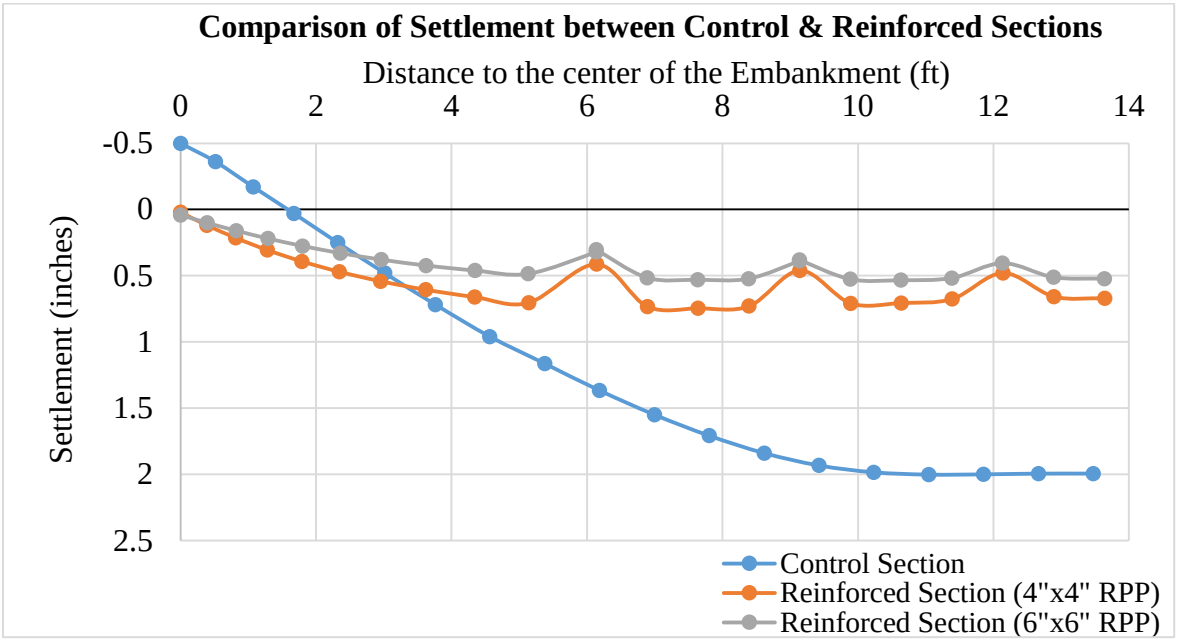

Figure 5. 14 Settlement comparison between the control and reinforced test sections from the toe to the center of the embankment.

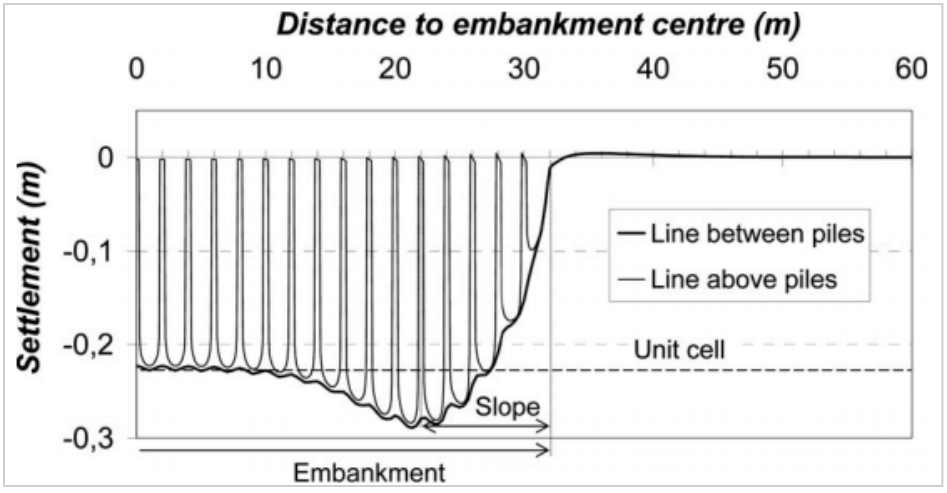

Figure 5. 15 Settlement profile for pile supported embankment (Jenck et al., 2009).

An embankment loading of 6 ft. height was tested in the field. For the further evaluation, embankment loading height up to 14 ft. was considered for the test sections and compared for settlement due to increasing loading height. Figure 5.16 shows a comparative bar chart plot of foundation settlement under increasing height of the embankment loading for the test sections.

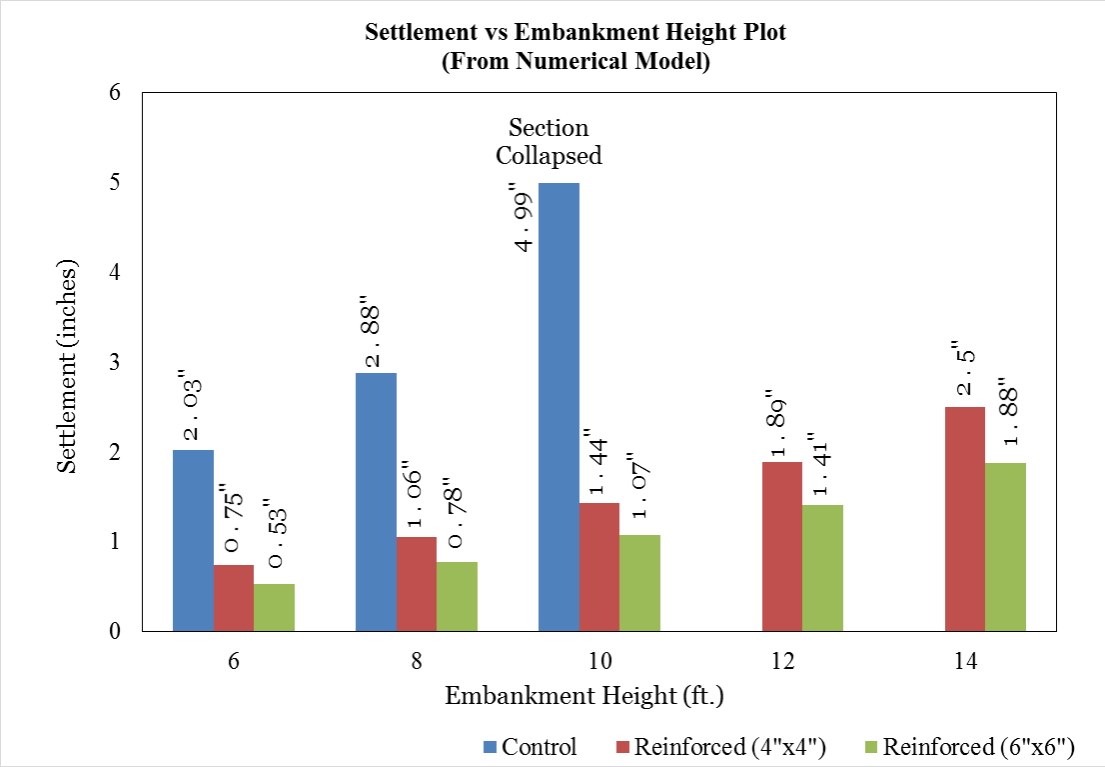

Figure 5. 16 Vertical deformation of foundation with increasing height of embankment.

Based on the model predicted results, control section might collapse for an embankment height of 10 ft. while the reinforced sections were analyzed up to a loading height of 14 ft. and was performing well; however the settlement increases with increasing height of the embankment. A significant difference in settlement was found between control section and reinforced sections. Also, between the reinforced sections, difference in settlement was found to be increasing gradually with increasing loading height.

Han and Gabr (2002) conducted a numerical study to evaluate the performance of geosynthetic reinforced pile supported embankment for different fill height. The result obtained by the authors based on the numerical model is presented in Figure 5.17 which shows the impact of fill height on the maximum settlement of the pile supported embankment. It was found that the unreinforced embankment experienced larger settlement compared to the reinforced embankment. Geogrid was used as the load transfer element which ensures load mobilization to the piles. Similar conclusive result was observed (Figure 5.18) from the current numerical modeling. RPP reinforced section showed considerably lower settlement compared to the unreinforced section. Also, with increasing RPP size the settlement found to be reducing as shown in Figure 5.18.

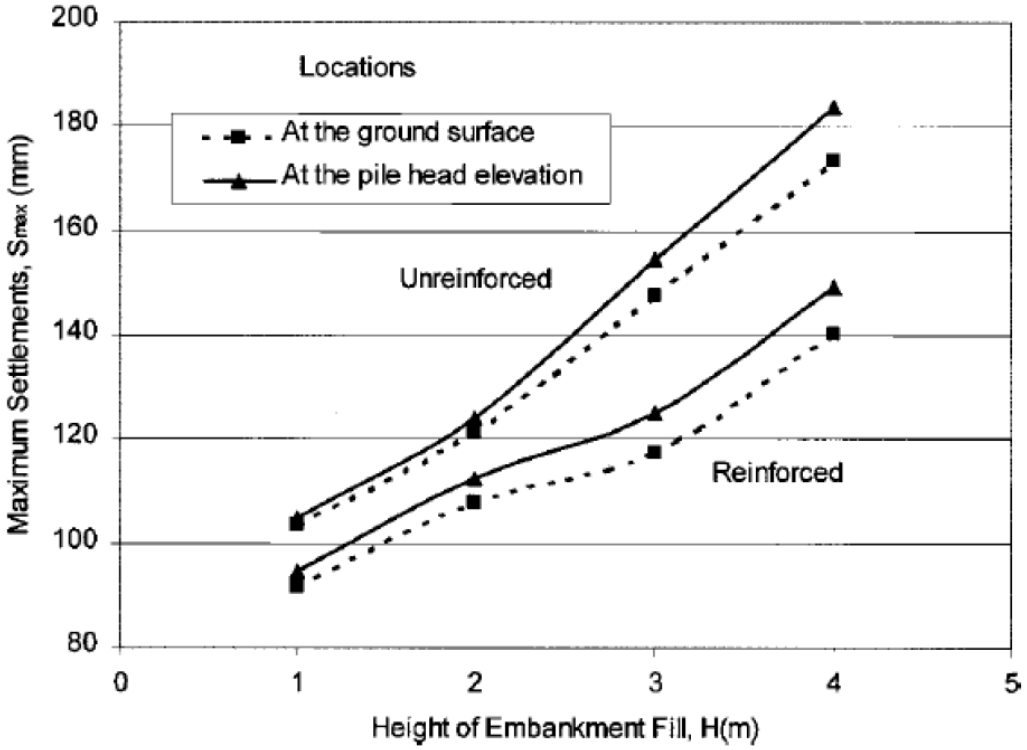

Figure 5. 17 Effect of embankment height on maximum settlement of pile supported embankment on soft foundation soil (Han and Gabr, 2002).

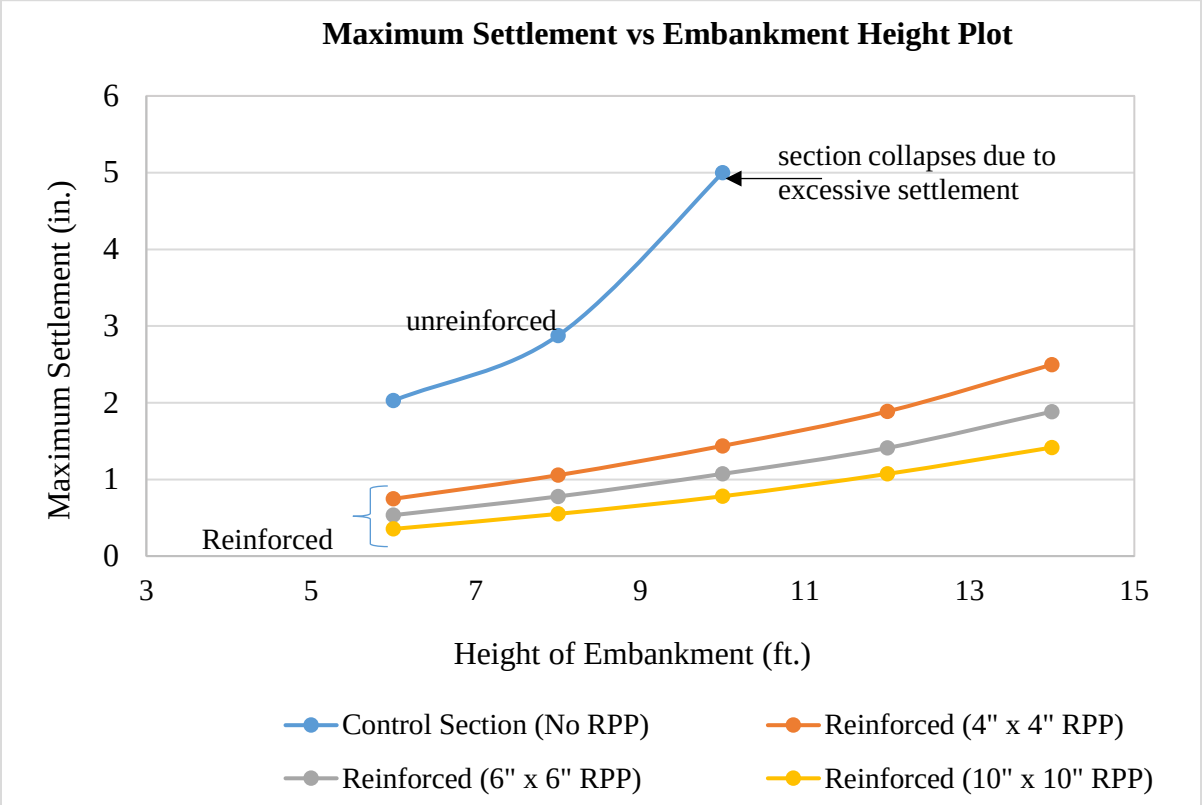

Figure 5. 18 Effect of embankment height on maximum settlement of RPP supported embankment.

5.3.5 Parametric Study

The numerical study of the reinforced section was further evaluated using parametric study. The parametric analysis was conducted to evaluate the effect of loading height for the existing reinforced section, effect of different size, length and spacing of RPP on the settlement of the foundation soil. During the current field scale study, 4 in. x 4 in. and 6 in. x 6 in. RPPs of 10 ft. length had been utilized as a load transfer device as well as improving the condition of weak foundation soil and minimizing the possible foundation settlement. In addition, depending on the depth of stiff soil strata and economy, 8 ft. and 12 ft. long RPP may be utilized. Therefore, 8 ft., 10 ft. and 12 ft. long RPPs are selected for parametric study. Also, effect of 10 in. x 10 in. RPP is included in the parametric study. The field study included

spacing of RPP at 3 ft. c/c. Spacing plays a major role for any and all types of pile supported structures. Therefore, in the current parametric study, different spacing of RPP that ranged from 2 ft. c/c to 4 ft. c/c, with 1 ft. c/c increments are also included.

The numerical modeling matrix for parametric study is presented in Table 5.5. The parametric study was performed using the calibrated model developed based on the field behavior of the test sections. The RPP was modeled as plate element with 0.7 interface element strength for all models.

Table 5. 5 Numerical model matrix for parametric study of vertical loaded test section.

Size of RPP	Length of RPP	Spacing of RPP	Type of Analysis
4 in. x 4 in.	8 ft.	2 ft., 3 ft. and 4 ft.	Plastic Deformation (settlement analysis)
	10 ft.	2 ft., 3 ft. and 4 ft.	
	12 ft.	2 ft., 3 ft. and 4 ft.	
6 in. x 6 in.	8 ft.	2 ft., 3 ft. and 4 ft.	Plastic Deformation (settlement analysis)
	10 ft.	2 ft., 3 ft. and 4 ft.	
	12 ft.	2 ft., 3 ft. and 4 ft.	
10 in. x 10 in.	8 ft.	2 ft., 3 ft. and 4 ft.	Plastic Deformation (settlement analysis)
	10 ft.	2 ft., 3 ft. and 4 ft.	
	12 ft.	2 ft., 3 ft. and 4 ft.	

Plastic calculation was performed in PLAXIS 2D for deformation analysis. Soil parameters found from the calibrated model through back analysis for the control section was used for the whole set of parametric matrix. Based on the FEM analysis, the vertical

deformation (settlement) of the foundation soil was plotted with varying length (fixed spacing) as presented in Figure 5.19, Figure 5.20 and Figure 5.21 and with changing spacing (fixed length) of RPP is plotted in Figure 5.22, Figure 5.23 and Figure 5.24 for different sizes of RPP. Based on the plot, it was observed that increasing the length has very small effect on the settlement; however, for larger RPP size, effect of length on settlement is relatively higher compared to the smaller sizes of RPP.

Spacing between RPP has significant effect on settlement. With reduced spacing, a noticeable reduction in settlement was observed as shown in Figure 5.22 through Figure 5.24 for all sizes of RPPs.

Size of RPP also showed significant effect on settlement. Increasing RPP size reduces settlement by providing additional support. Figure 5.25, Figure 5.26 and Figure 5.27 presents settlement plots to show the effect of RPP size for different length and spacing of RPP.

Comparison between the results from analytical study and numerical model results showed similar trend and it was observed that larger the pile size lesser is the settlement and a reduction in spacing results in much reduced settlement. For comparison with analytical results, settlements observed in numerical modeling due to 6 ft. high embankment loading on different RPP reinforced sections is presented in Table 5.6. The trend was found to be in good agreement with the results found from analytical calculation.

Table 5. 6 Settlement found from the numerical modelling for the RPP reinforced sections (for 6 ft. loading height)

Settlement (inches)			
RPP size / **Spacing (ft.)**	**4 in. x 4 in. RPP**	**6 in. x 6 in. RPP**	**10 in. x 10 in. RPP**
2	0.60	0.42	0.23
3	0.75	0.53	0.35
4	0.97	0.74	0.45

Settlement for Different RPP Length with Fixed Spacing (4 in. x4 in. RPP)

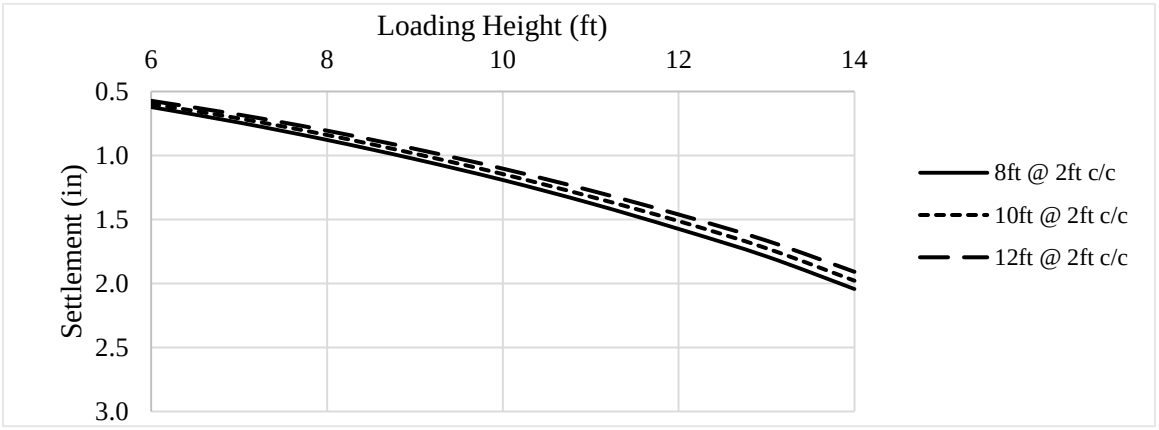

(a)

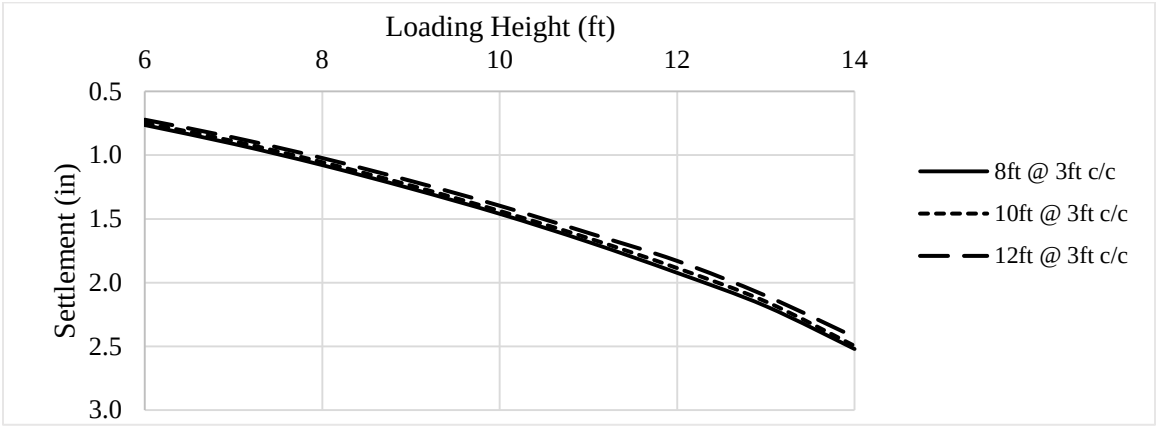

(b)

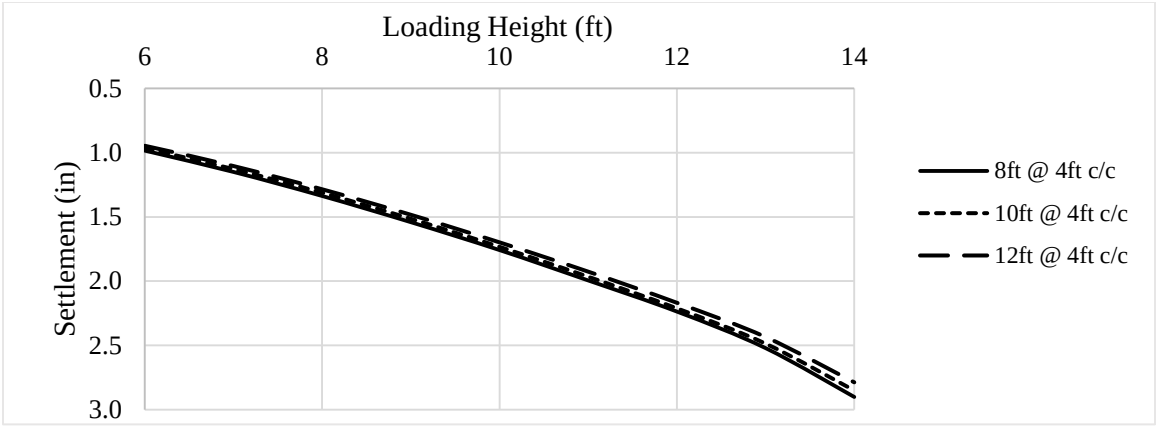

(c)

Figure 5. 19 Settlement for different length of 4 in x 4 in. RPP with spacing of (a) 2 ft. c/c; (b) 3 ft. c/c; (c) 4 ft. c/c.

Settlement for Different RPP Length for Fixed Spacing (6 in. x 6 in. RPP)

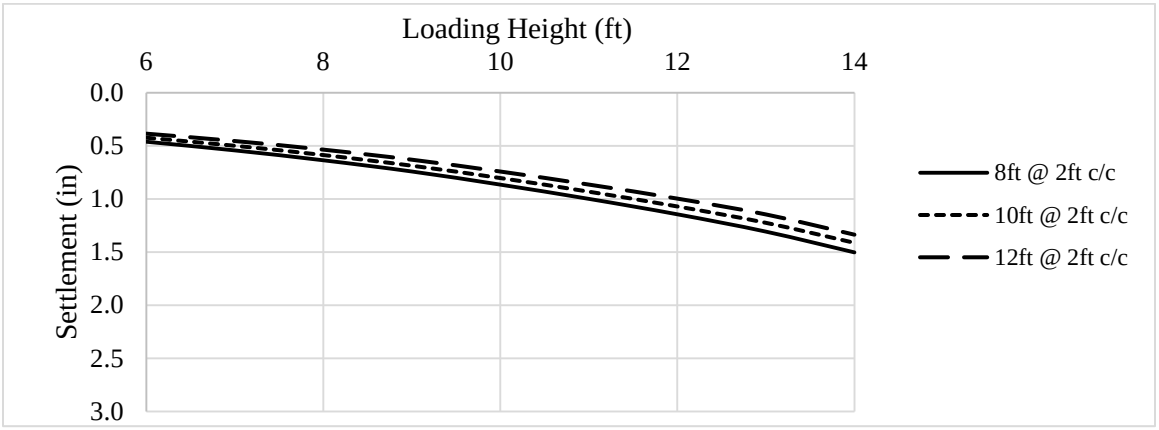

(a)

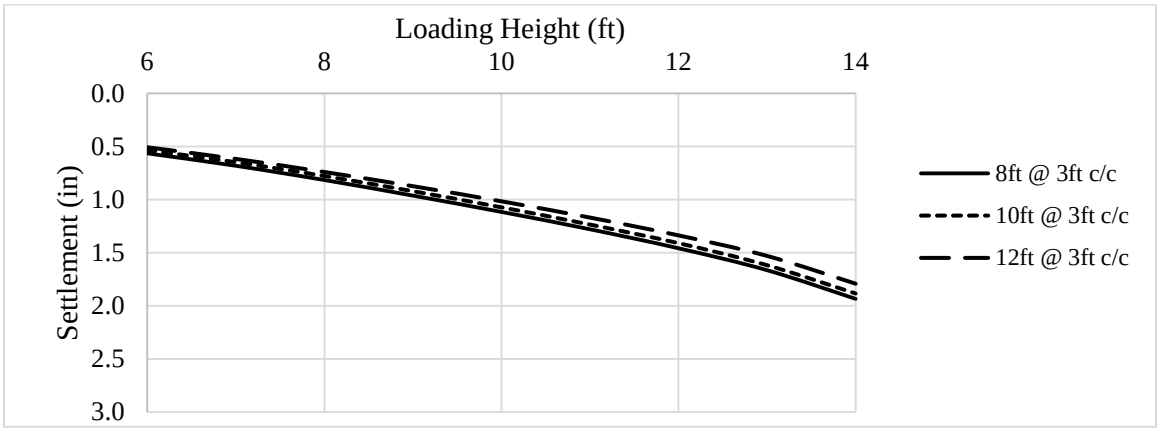

(b)

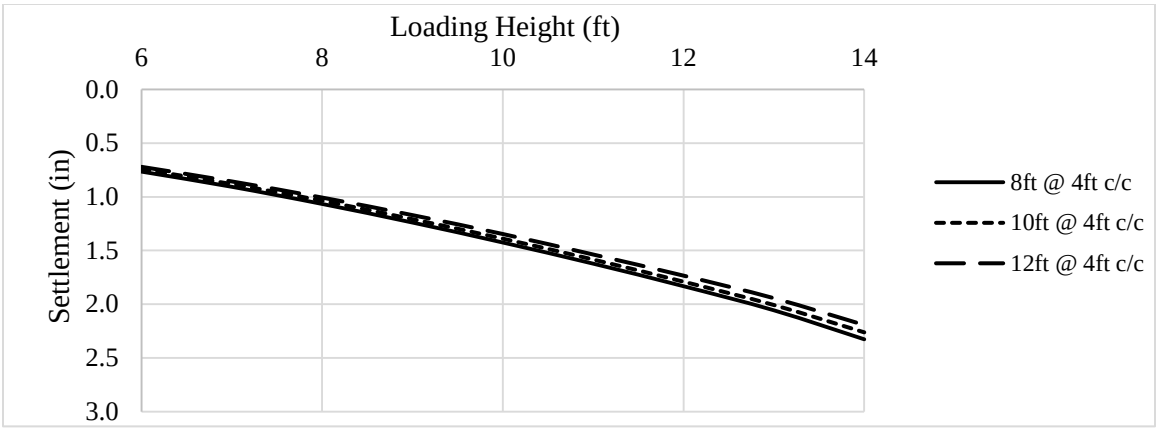

(c)

Figure 5. 20 Settlement for different length of 6 in. x 6 in. RPP with spacing of (a) 2 ft. c/c; (b) 3 ft. c/c; (c) 4 ft. c/c.

Settlement for Different RPP Length with Fixed Spacing (10 in. x 10 in. RPP)

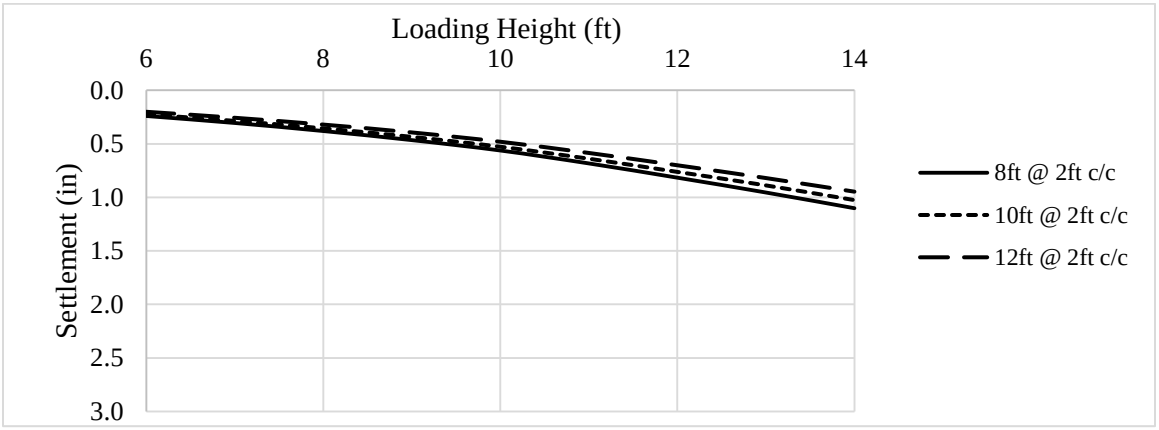

(a)

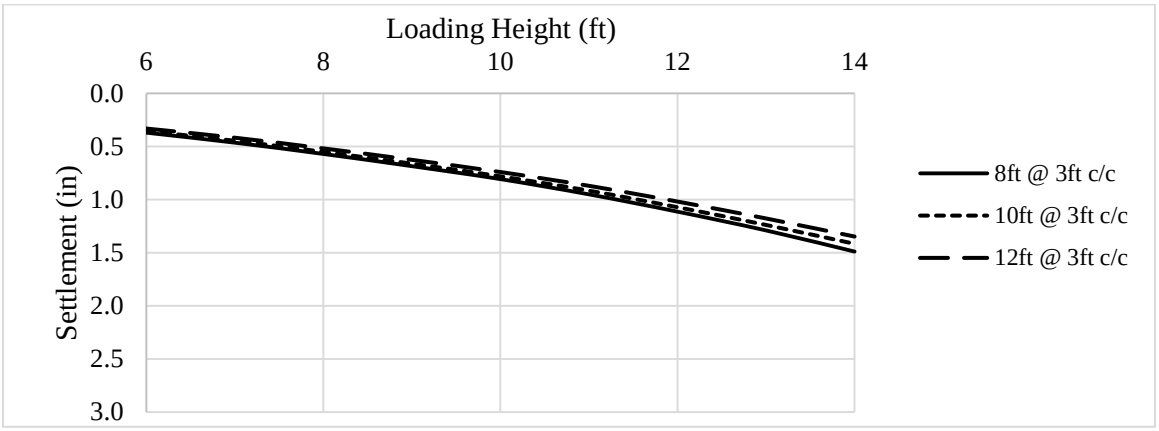

(b)

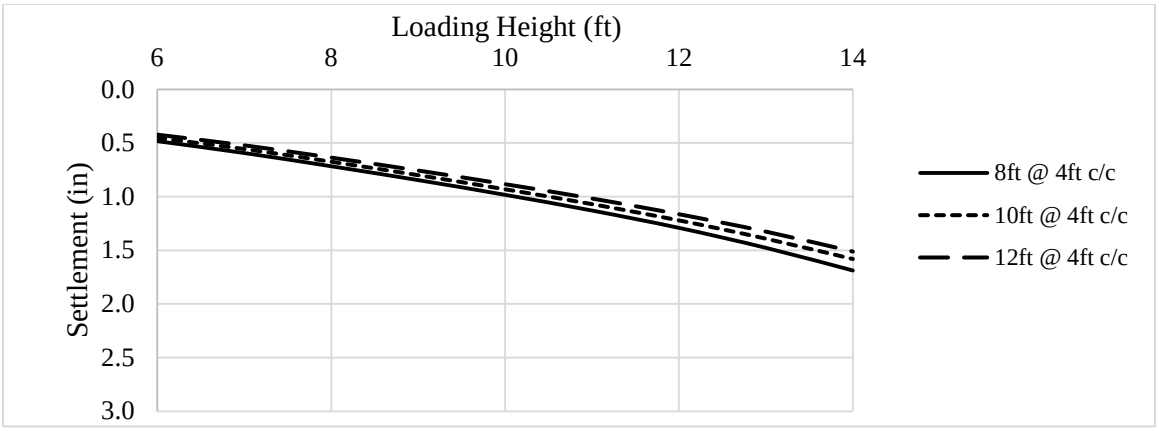

(c)

Figure 5. 21 Settlement for different length of 10 in. x 10 in. RPP with spacing of (a) 2 ft. c/c; (b) 3 ft. c/c; (c) 4 ft. c/c.

Settlement for Different Spacing for Fixed Length of RPP (4 in. x 4 in. RPP)

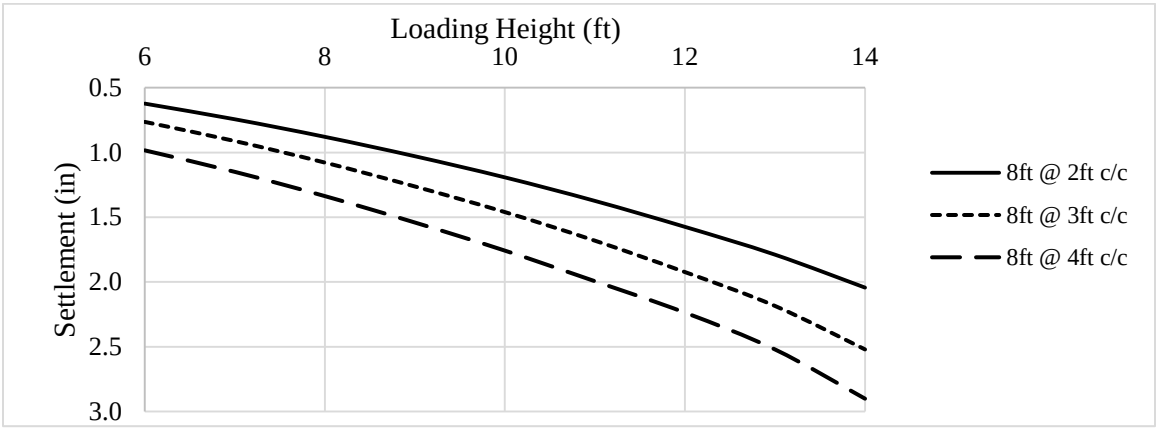

(a)

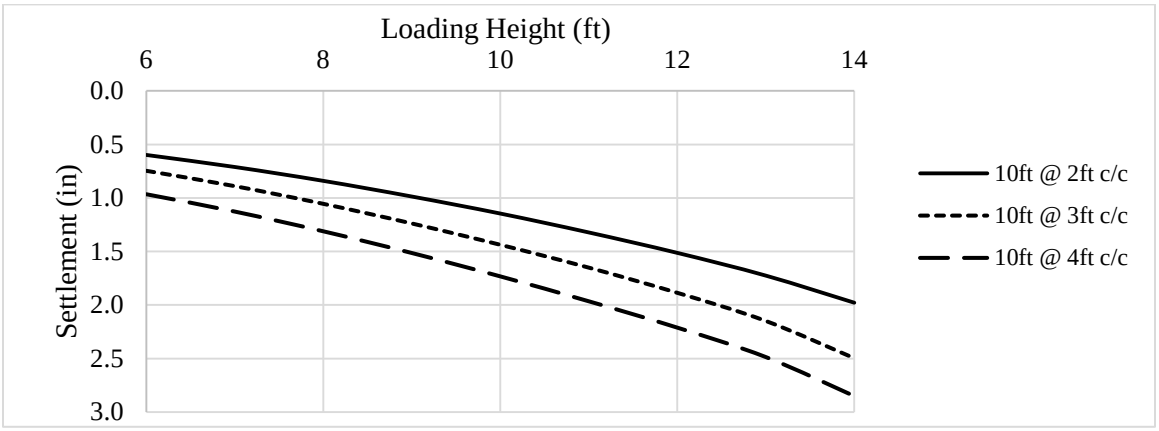

(b)

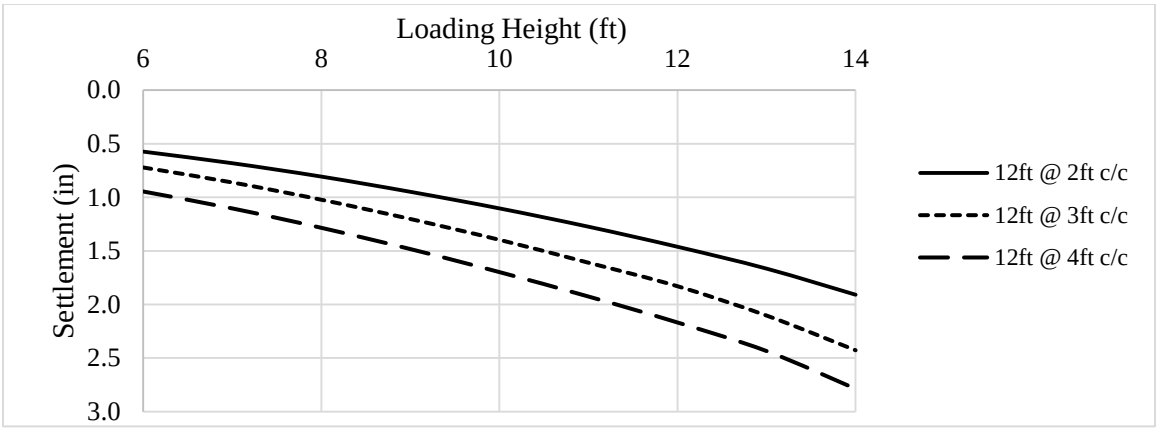

(c)

Figure 5. 22 Settlement for different spacing of 4 in. x 4 in. RPP having length of (a) 8 ft.; (b) 10 ft.; (c) 12 ft.

Settlement for Different Spacing for Fixed Length of RPP (6 in. x 6 in. RPP)

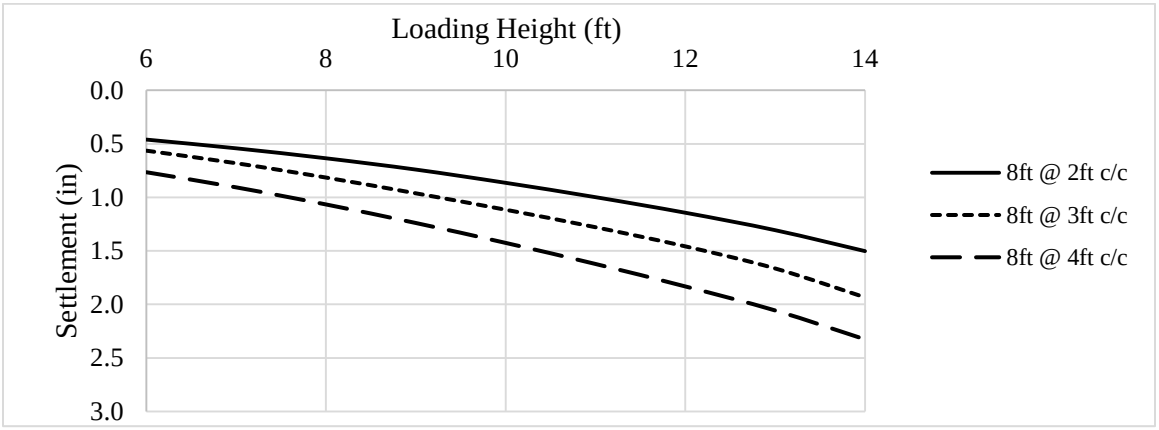

(a)

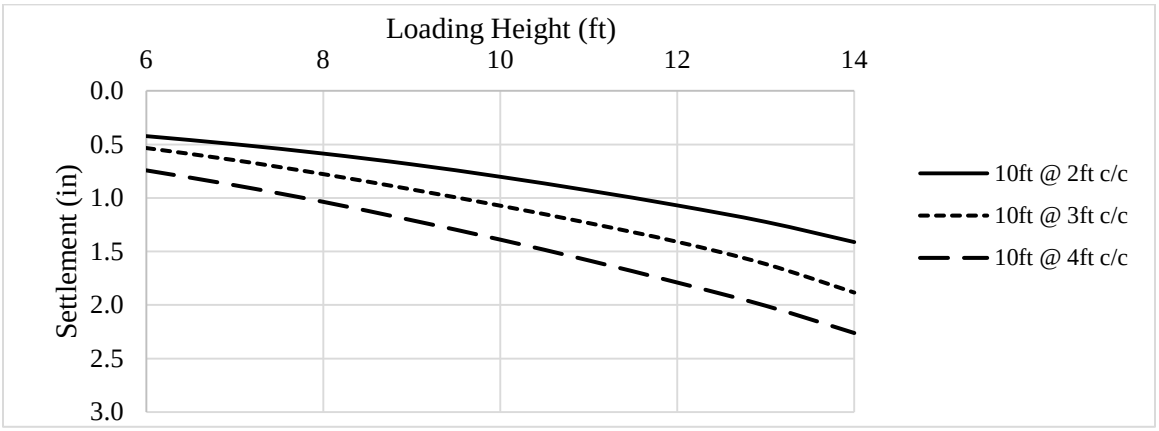

(b)

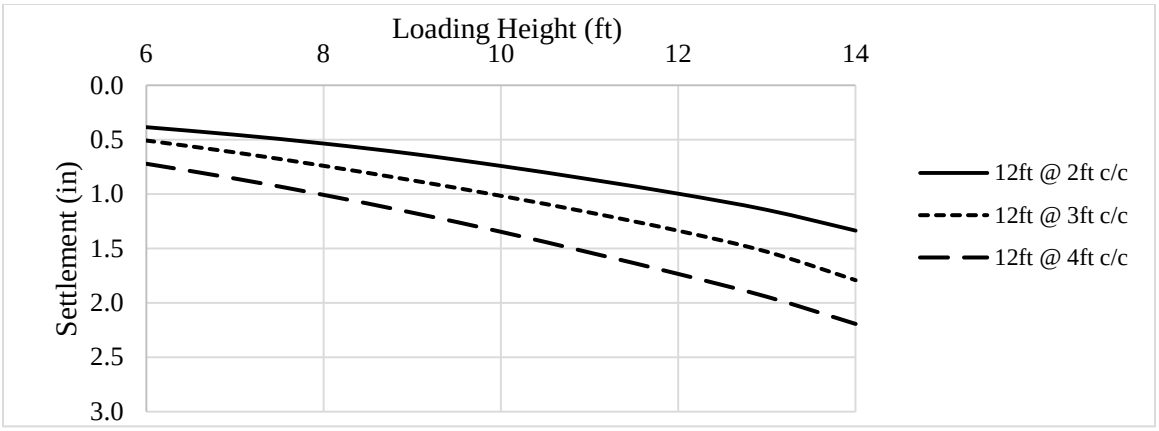

(c)

Figure 5. 23 Settlement for different spacing of 6 in. x 6 in. RPP having length of (a) 8 ft.; (b) 10 ft.; (c) 12 ft.

Settlement for Different Spacing for Fixed Length of RPP (10 in. x 10 in. RPP)

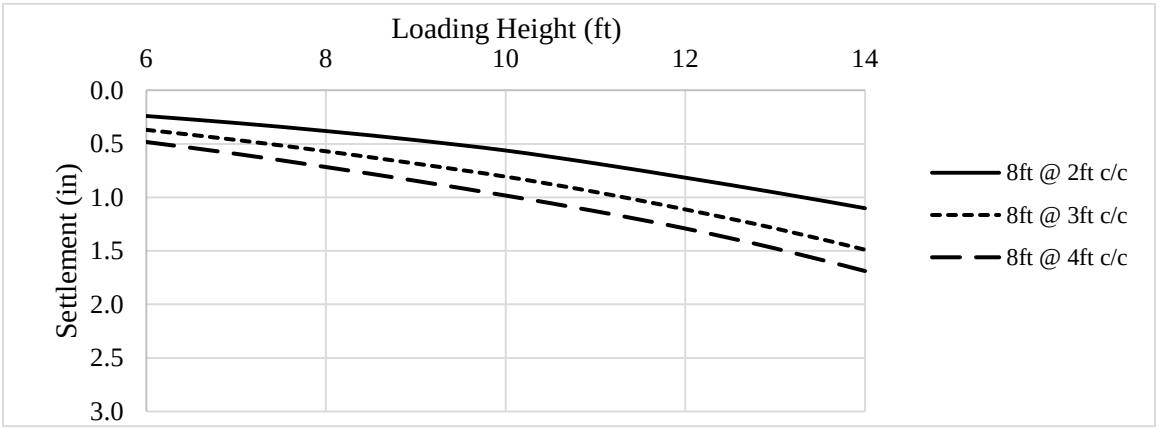

(a)

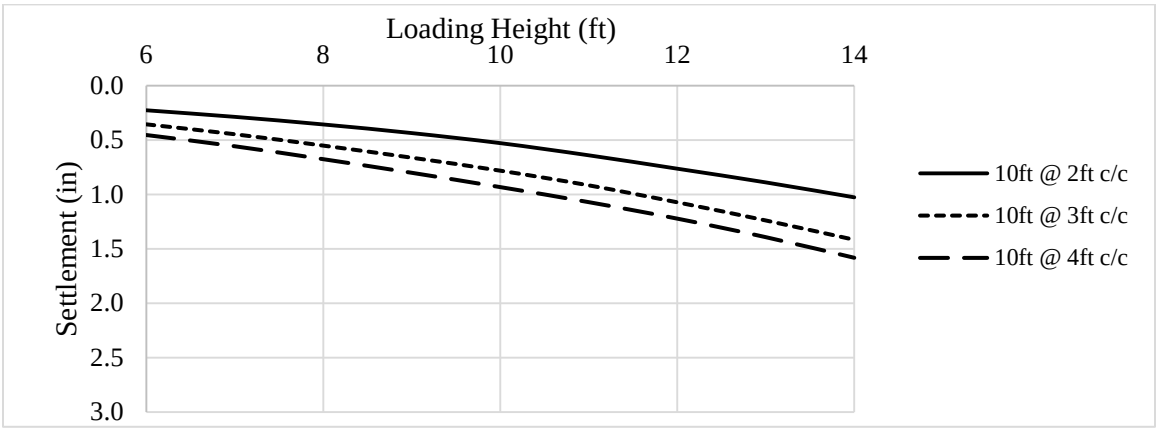

(b)

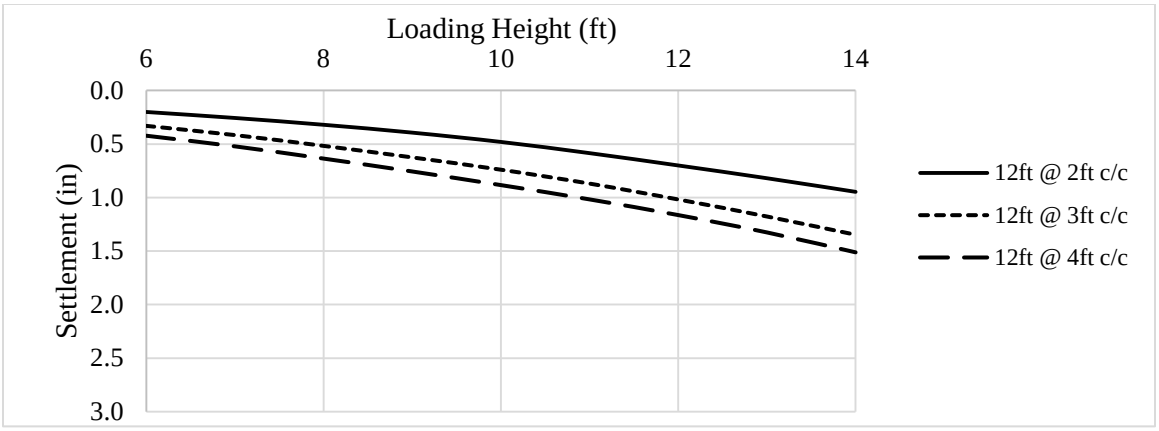

(c)

Figure 5. 24 Settlement for different spacing of 10 in. x 10 in. RPP having length of (a) 8 ft.; (b) 10 ft.; (c) 12 ft.

Settlement due to Different Size of RPP for Fixed Spacing (8 ft. long RPP)

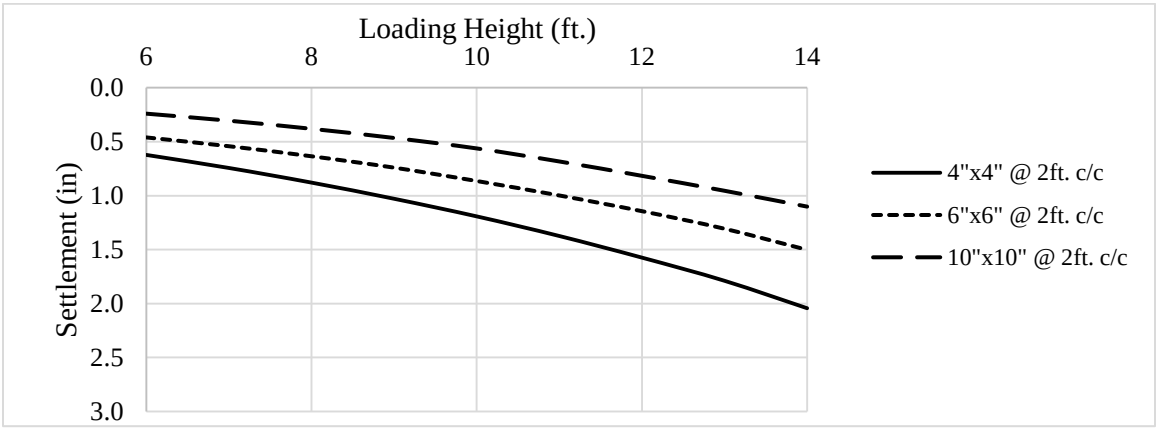

(a)

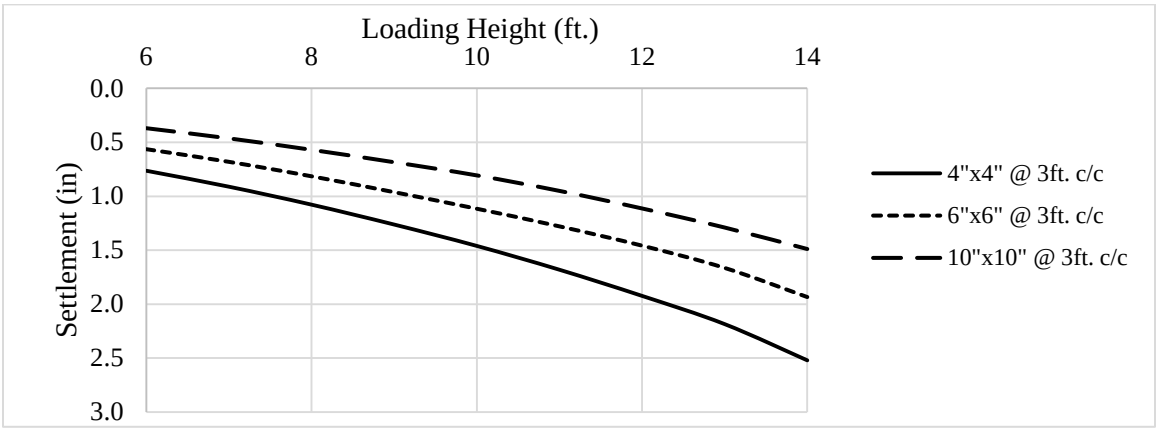

(b)

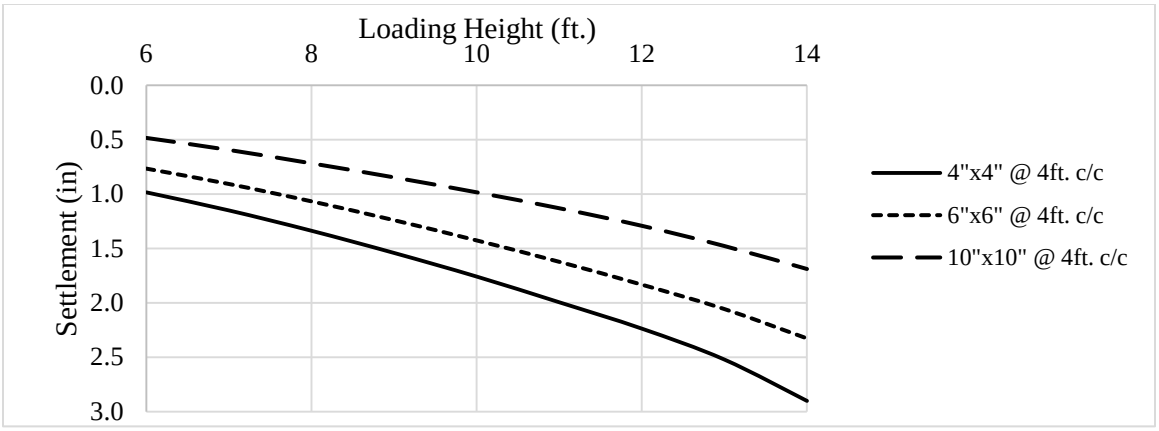

(c)

Figure 5. 25 Effect of 8 ft. long RPP size on settlement for spacing of (a) 2 ft. c/c; (b) 3 ft. c/c; (c) 4 ft. c/c.

Settlement due to Different Size of RPP for Fixed Spacing (10 ft. long RPP)

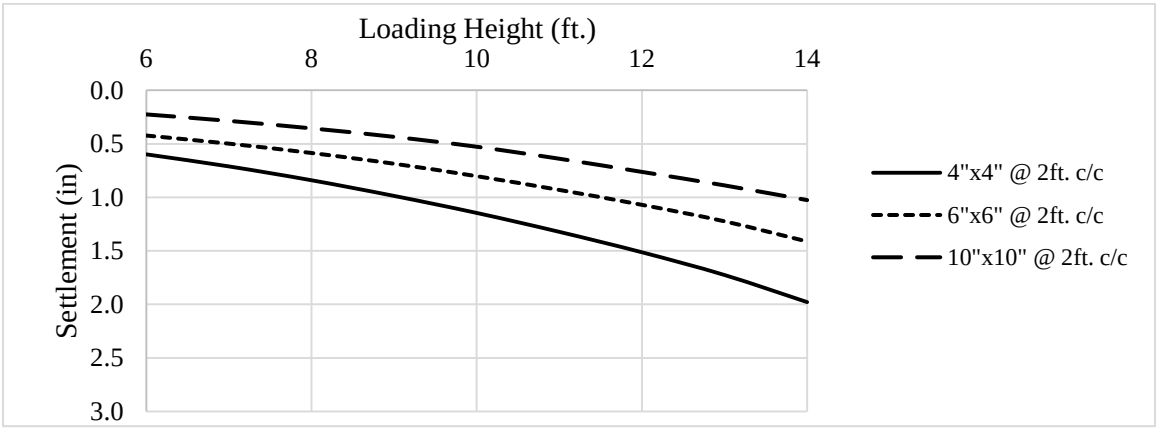

(a)

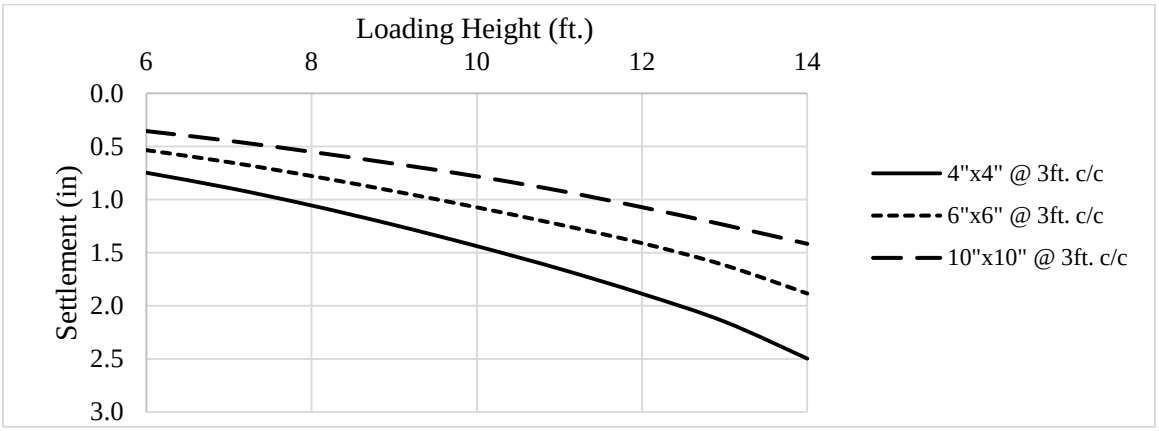

(b)

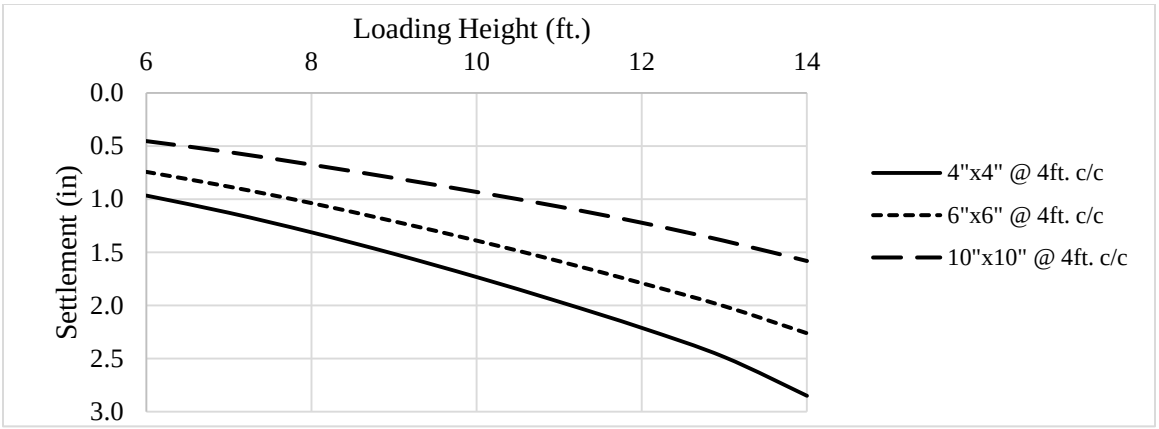

(c)

Figure 5. 26 Effect of 10 ft. long RPP size on settlement for spacing of (a) 2 ft. c/c; (b) 3 ft. c/c; (c) 4 ft. c/c.

Settlement due to Different Size of RPP for Fixed Spacing (12 ft. long RPP)

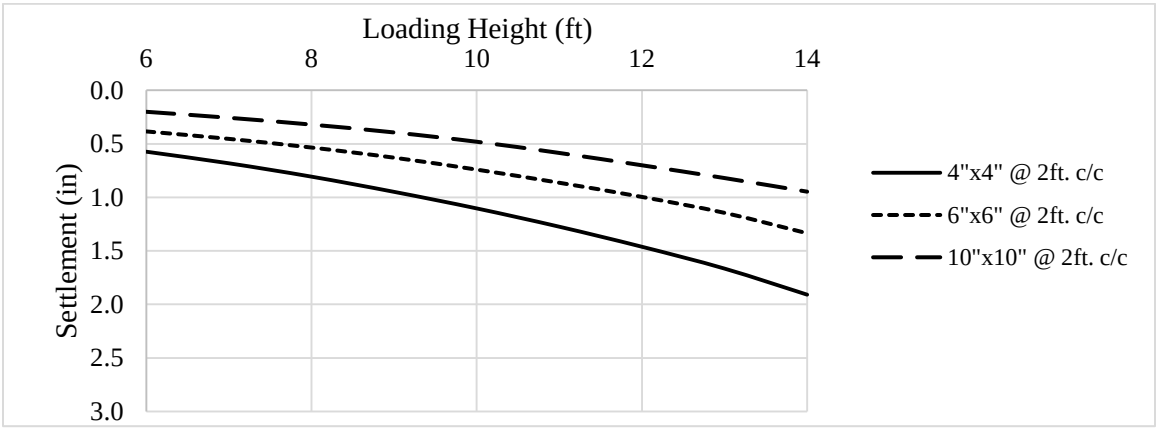

(a)

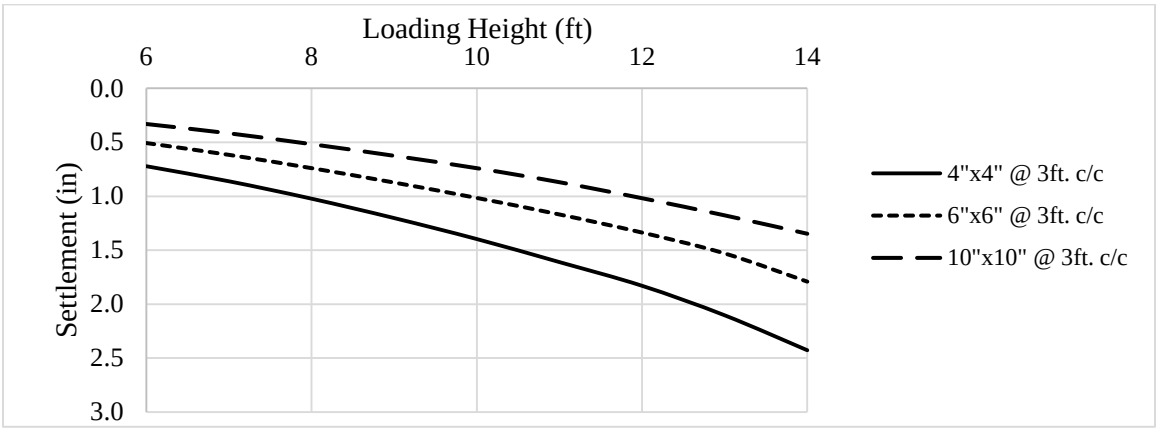

(b)

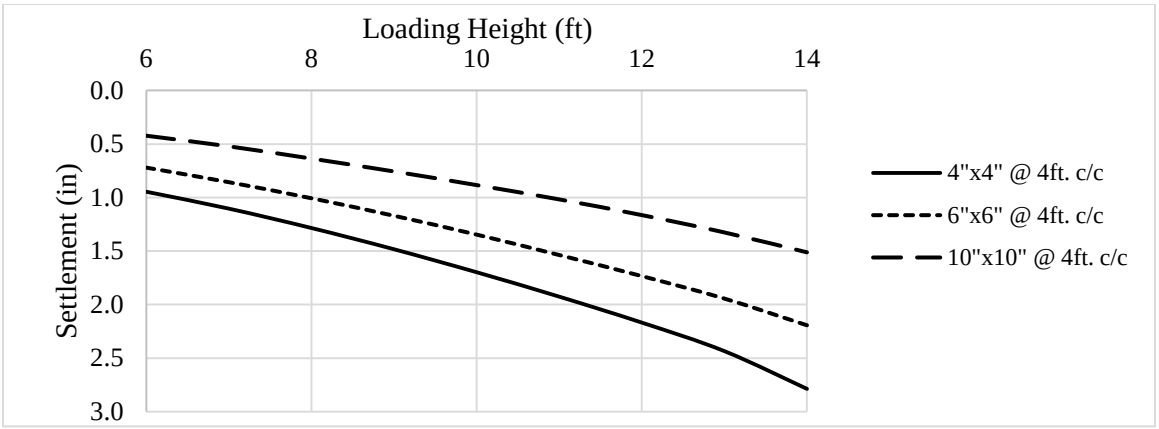

(c)

Figure 5. 27 Effect of 12 ft. long RPP size on settlement for spacing of (a) 2 ft. c/c; (b) 3 ft. c/c; (c) 4 ft. c/c.

5.4 Numerical Study for Lateral Loaded Test Sections

The field scale study for the lateral loading included a control section with no RPP and a 4 in. x 4 in. RPP reinforced section having a uniform spacing of 3 ft. c/c in a staggered pattern. Both the retaining structure test sections had a wall facing made of raw pressure treated wood of 2 in. x 6 in. in size, supported by galvanized schedule 40 post of 2.375 in. diameter. The reinforced test section had RPP installed in such a way that 2 ft. of the pin was kept above ground and 8 ft. was embedded in to the foundation soil. The purpose was to create a composite structure where RPP might act similar to a shear key. Based on the performance monitoring results, it was evident that RPP at the base of MSE retaining structure provided additional shear resistance against lateral movement/sliding of the base.

A calibrated model was developed as a part of the numerical study based on the field monitoring results. Similar to the vertical loading analysis, numerical modeling for this segment was also conducted for two different considerations. First, a comparison between control and reinforced section for increasing wall height or loading height at the back of the wall was conducted. Numerical study was further conducted to study the effect of different RPP size, length and spacing. Details of finite element modelling (FEM) is presented in the following sub-sections.

5.4.1 Model Calibration

Development of a mathematical model capable of simulating field condition and predicting results similar to the outputs from physical experiment is necessary to predict the possible outcome without further field test. Therefore, a calibrated model was developed for this study.

The elastic perfectly plastic Mohr-Coulomb soil model was utilized for deformation analyses, using 15 node triangle elements. The FEM analysis using a 15 node triangular element which has 9 stress points, is a very accurate method and produces high quality stress results for different problems (PLAXIS 2D Reference Manual, 2017). Standard fixities were applied as boundary condition.

The finite element is simulated with 4 layers of native soil profile along with a drainage layer and backfill soil. Native soil consisted of: 15 ft. of very stiff clay at the bottom (soil 1), overlain by 6 ft. of stiff clay layer (soil 2). The soils in the slope was divided in two parts according to soil test results; soil 3 was medium stiff clay of 7 ft. thickness overlain by 5 ft. of soft silty clay (soil 4). Geotextile used in the MSE wall was modeled by linear elastic sheet elements. Facing of the wall was modeled as plate material with stiffness properties of the materials used. All the soil layers were modeled as linear elastic perfectly plastic materials that obey Mohr-Coulomb failure criteria. Apart from the drainage layer, all the soil layers were considered having undrained behavior for short-term or rapid construction in which stiffness and strength are defined in terms of effective properties. Drainage layer was considered having drained behavior; no excess pore water pressure was generated. It is a long-term behavior where stiffness and strength are defined in terms of effective properties.

To evaluate the soil parameters for the control section, back analysis were performed using PLAXIS 2D. The soil profile is presented in the Figure 5.28. The baseline of the calibration started by using soil unit weights, permeability and strength properties of soil layers found from laboratory test results, corresponding typical value of Poisson’s ratio and elastic

modulus, E (using empirical equations that depends on SPT number). The back analysis was performed using the anticipated deformation that was observed in the field.

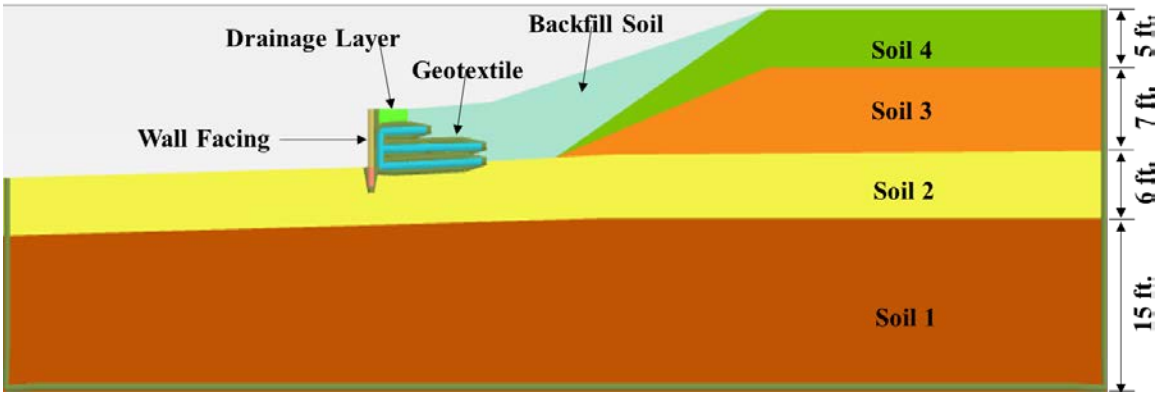

Figure 5. 28 Soil profile model for control section.

Numerous iteration was performed during numerical analysis to evaluate the soil parameters. The soil parameters used for native soil, drainage material and backfill soil at which the model showed lateral deformation close to the field result are presented in Table 5.7.

Table 5. 7 Soil parameters from FEM analysis.

Soil Layer	**Friction angle, Φ**	**Cohesion, c**	**Unit Weight, γ**	**Elastic Modulus, E**	**Poisson Ratio, ν**
-	◦	**psf**	**pcf**	**psf**	**-**
Soil 1	5	3,000	120	350,000	0.25
Soil 2	20	1,500	116	50,000	0.30
Soil 3	5	1,200	116	30,000	0.25
Soil 4	10	200	110	6,000	0.30
Drainage Material	20	60	102	15,000	0.30
Backfill Material	5	600	120	2,500	0.40

Geotextile were used as horizontal reinforcement for the soil at the back of the MSE wall. Geotextile were considered as slender structures having only normal stiffness and without any bending stiffness. It is a tensile element that has zero compression sustainability. Geotextiles was modeled using “geogrid” elements which acts as isotropic element at each nodes and unable to work under compression. Table 5.8 presents the material properties of geotextile.

Table 5. 8 Geotextile parameters used in the model.

Identification	**EA (lb/ft)**	**υ**
Geotextile	2,500	0

Facing system of the MSE wall was modeled as plate elements which are slender structures in the ground having a significant flexural rigidity (or bending stiffness) and a normal stiffness. The facing units are divided and modeled in two parts: footing and facing elements.

The footing was made of concrete which was embedded 2 ft. into the ground and the facing consisted of 2 in. x 6 in. raw pressure treated wooden planks supported by galvanized steel pipes. A composite material properties were provided for the wall facing while modelling. The material properties of footing and wall facing elements are presented in Table 5.9. The total height of the facing was kept 5 ft., similar to that in the field.

Table 5. 9 Parameters used for Wall Facing.

Identification	EA (lb/ft)	EI (lb/ft)	W (lb/ft/ft)	υ
Wall facing	1.43E+8	3.31E+5	5.00	0.20
Footing	1.109E+8	1.751E+6	1.20	0.20

The calibrated model was developed for deformation analysis of the control section. Based on the calibrated model using the soil parameters presented in Table 5.7, the lateral deformation was found to be 1.68 inches which is close to the field result (1.76 inches). The slight variation between predicted result and field observation might be due to the non-uniformity of the slope in the field, non-uniformity of loading and also the level of compactness of soil body. In addition, there was also temporary live load while filling the back of the wall, load from backhoe, excavator etc. which might also have incorporated some additional displacement. In finite element modelling, displacement due to the temporary loads was not taken into consideration. Figure 5.29 shows the displacement contour and shading for the control section generated using the calibrated model.

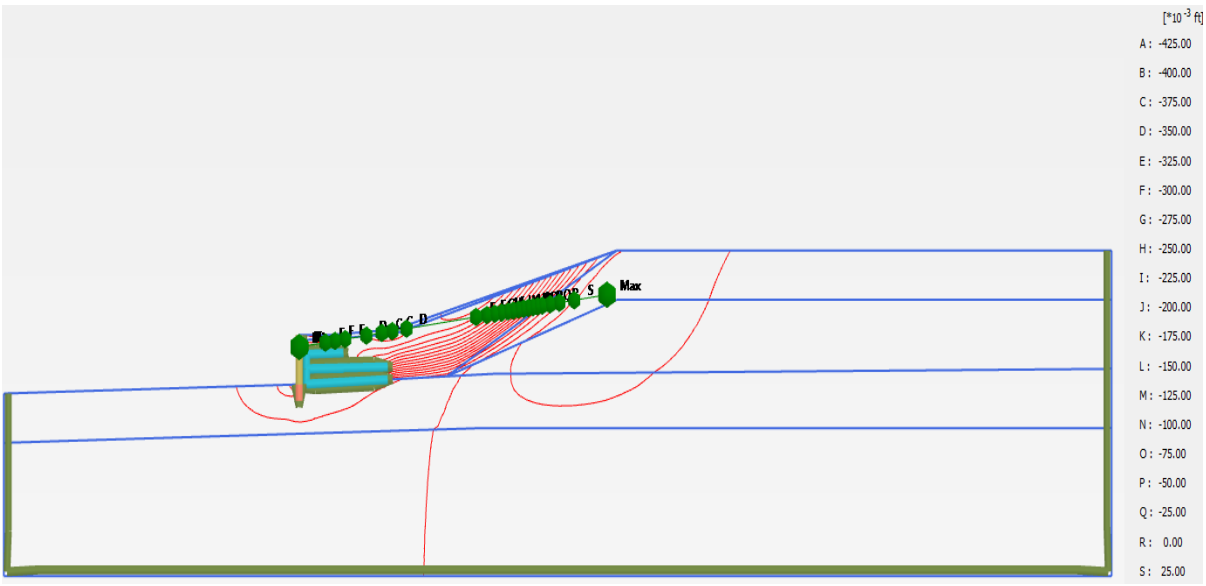

(a)

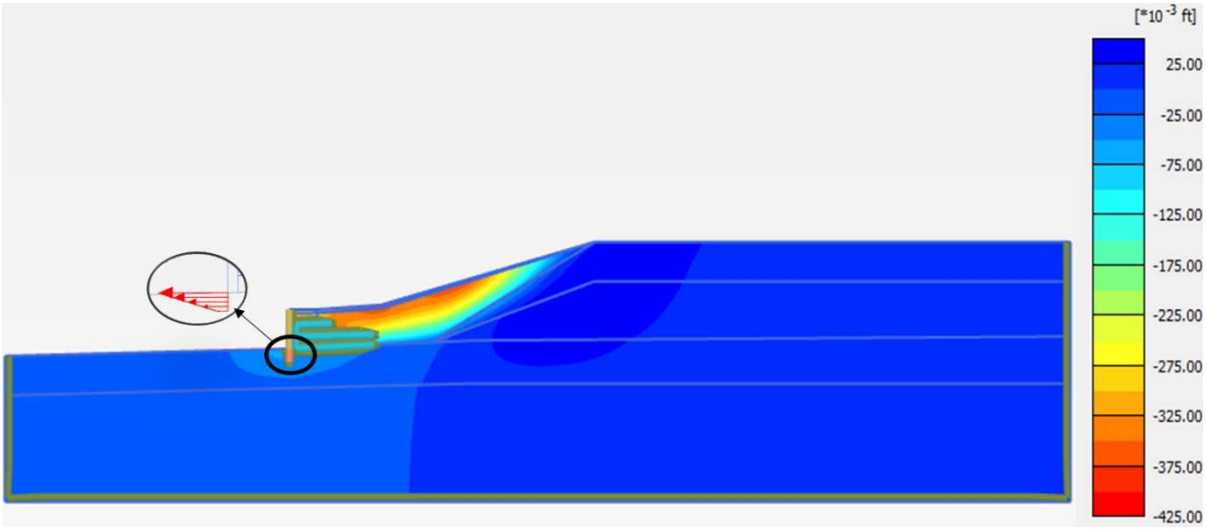

(b)

Figure 5. 29 FEM Lateral displacement plot of control section, 1.68 inches of base movement; (a) Contour lines, (b) Shading.

5.4.2 Performance Evaluation of Reinforced Section

The identical soil parameters for the control section were utilized to perform the deformation analysis of the reinforced section. The model of the reinforced section is presented in Figure 5.30.

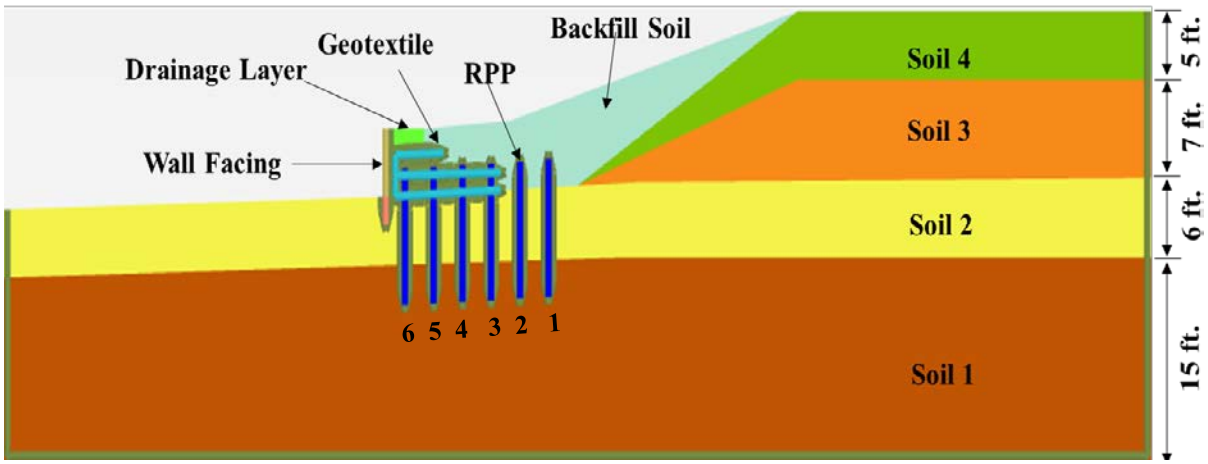

Figure 5. 30 FEM model for reinforced section.

According to the initial deformation analysis performed, the predicted lateral movement of the base of the wall was observed to be relatively higher compared to the field observation. This might be because driving RPP in the soil replaces the voids and increases the stiffness of soil which cannot be simulated in the model. To consider such effect a pragmatic method was adopted based on a study done by Chai and Lu (2018). This was done by identifying the layer where the effect of RPP driving is significant; which is soil layer 2 shown in Figure 5.30 for the current study. The RPP passes through the entire thickness of the layer. Changing the value of E for layer 2 to about 2.5 times of the corresponding initial value provided much better prediction of the model.

Based on the final prediction model the lateral movement was found to be 0.32 inches which is in good agreement with the lateral movement observed in the field (0.29 inches). This slight variation from field result might be due to the non-uniform placement of backfill soil and also the slope of the section was not uniform throughout the section. Another reason might be because in field the geotextile was anchored to the RPP which was not considered in the PLAXIS simulation. The lateral displacement diagram for the reinforced section is presented

in Figure 5.31. Properties of RPP used in the numerical analysis is presented in Table 5.10. Due to the 4 in. x 4 in. RPP reinforcement, factor of safety was found to be 3.84 from the numerical model which is in good agreement with the analytical result (FS = 3.78).

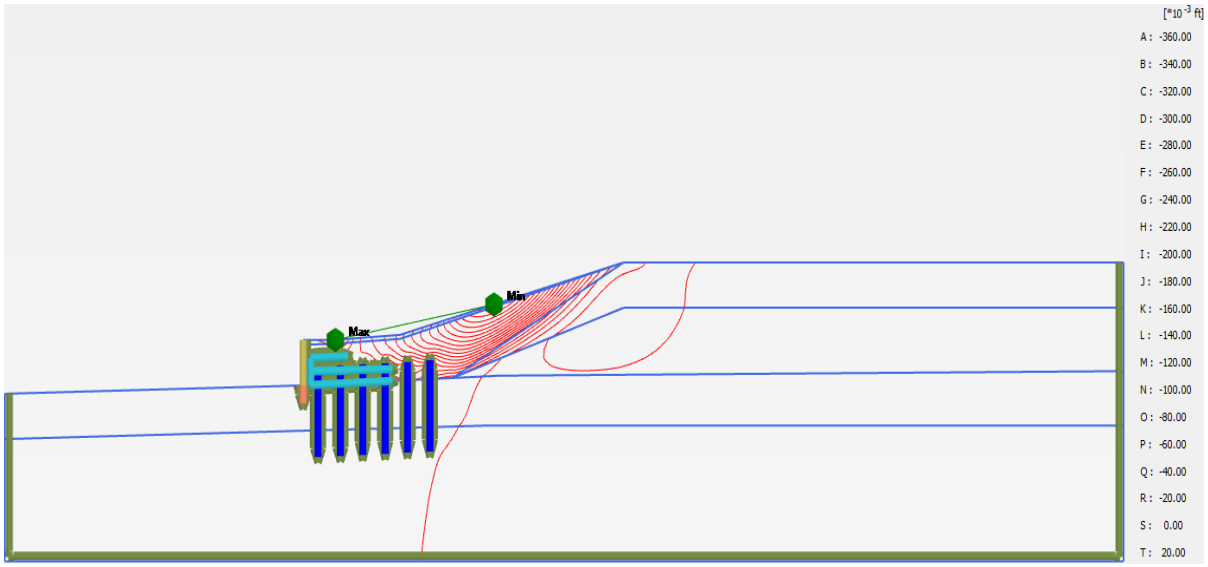

(a)

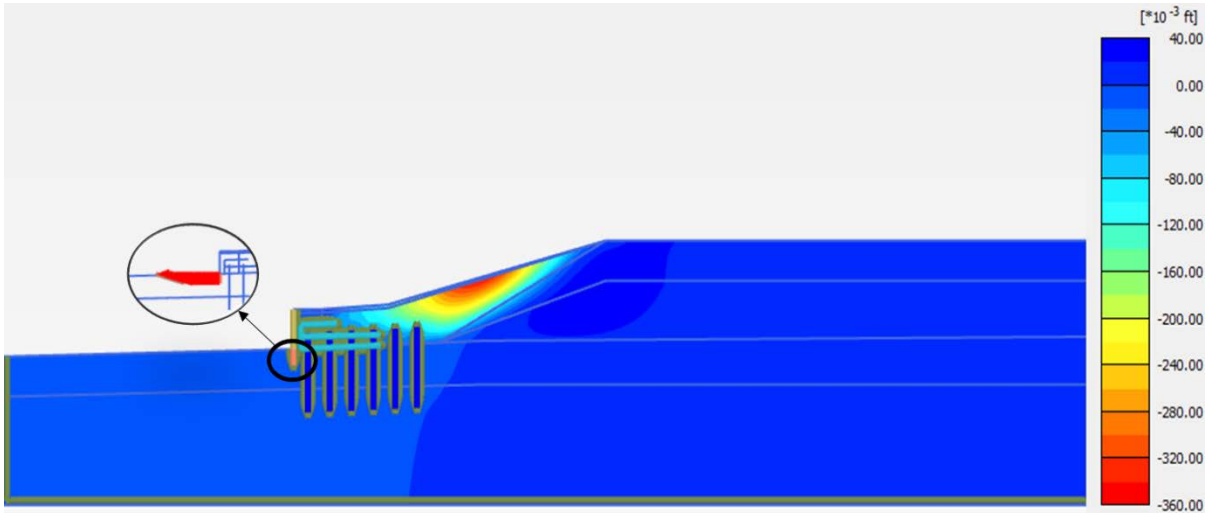

(b)

Figure 5. 31 FEM Lateral displacement plot of reinforced section, 0.32 inches of base movement; (a) Contour lines, (b) Shading.

Table 5. 10 RPP (4” x 4”) parameters used for FE analysis

RPP Properties	Units	Parameters
EA	lb./ft.	3,200,000
EI	$lbft^2/ft.$	29,630
d	ft.	0.333
w	lb./ft./ft.	1.85
υ (nu)		0.40

From the model analysis it was evident that the lateral force is resisted by the RPP before reaching the back of the wall facing; therefore, each row of RPP experienced some lateral movement while resisting the force from the sliding soil mass. The horizontal movement of the 6 row of RPP is presented in Figure 5.32. The horizontal displacement plot presented a plastic hinge movement of the top two (2) ft. similar to long pile. Long pile action takes place when the pile has sufficient anchorage from the stiff foundation soil. The RPP had approximately 8 ft. of anchorage from the foundation soil, thus resulted in long pile action. The maximum horizontal deformation of almost 0.8 inches was observed for 1st row of RPP and after that the displacement tend to reduce gradually with each rows.

Bending moment along the length of RPP for each row and the percent of moment transfer in each row of RPP is presented in Figure 5.33. Percentage of moment transfer for RPP was calculated using the equation 5.1.

From the bending moment plot (Figure 5.33a) along the depth of RPP it was observed that the maximum moment took place at the 1st row of RPP as the major force is resisted by

this layer of RPP before reaching other rows. The maximum bending moment was found to be 394 lb-ft; this moment was observed near the interface between backfill material and the stiff foundation soil. The maximum moment in this interface proves that the RPP had sufficient anchorage from the foundation soil. Figure 5.33b presents the percentage of moment transfer in the RPP. From the plot it is evident that maximum percentage of moment transfer is about 17% which signifies that a total of 17% of the moment capacity of the RPP has been utilized. Based on a study carried out by Chen et al. (2007), a life prediction model for RPP was developed depending on the % of moment transfer and showed that a design life of 100 years can be expected for a moment transfer up to 35%. From the current model observation, the maximum moment transfer for the 1st row of RPP was found to be about 17% which might result in a design life for the RPP more than 100 years.

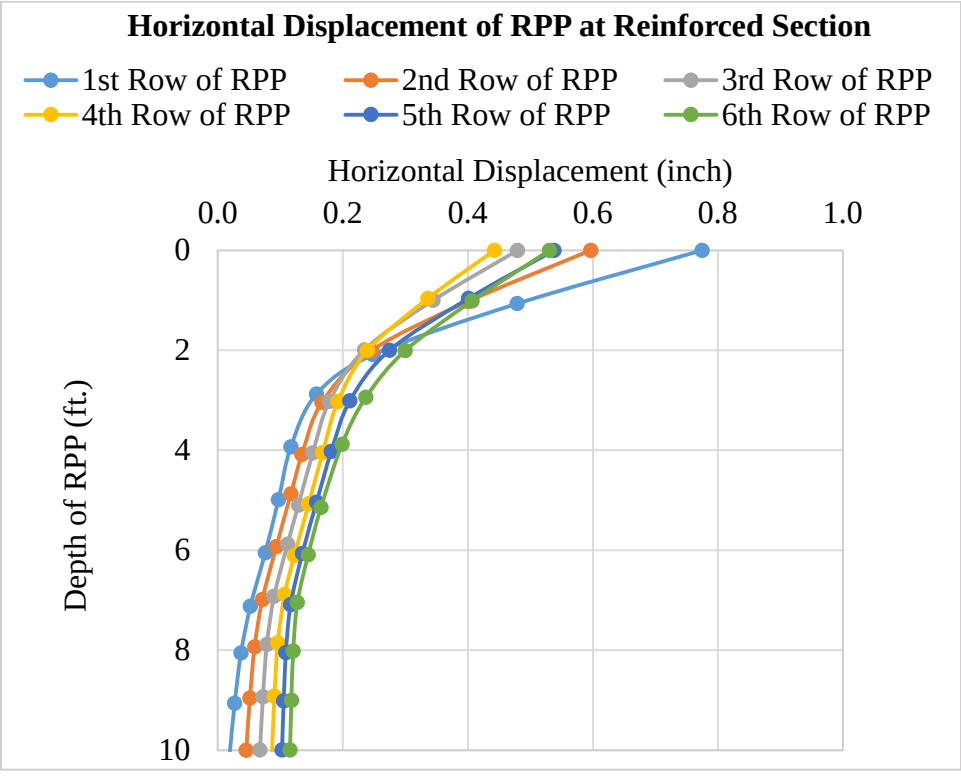

Figure 5. 32 Horizontal displacement of each row of RPP at the reinforced section.

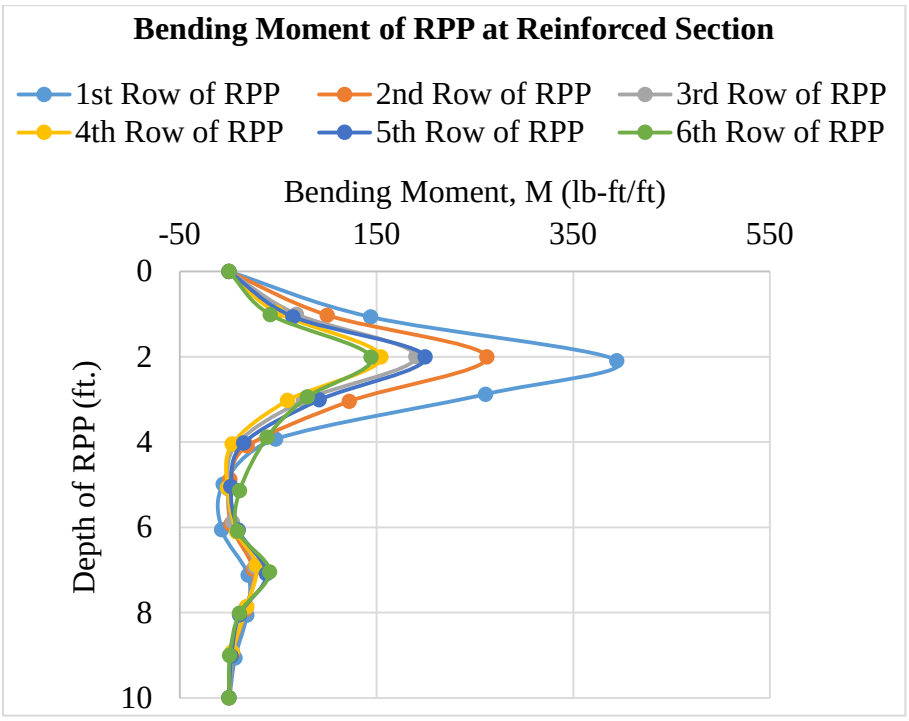

(a)

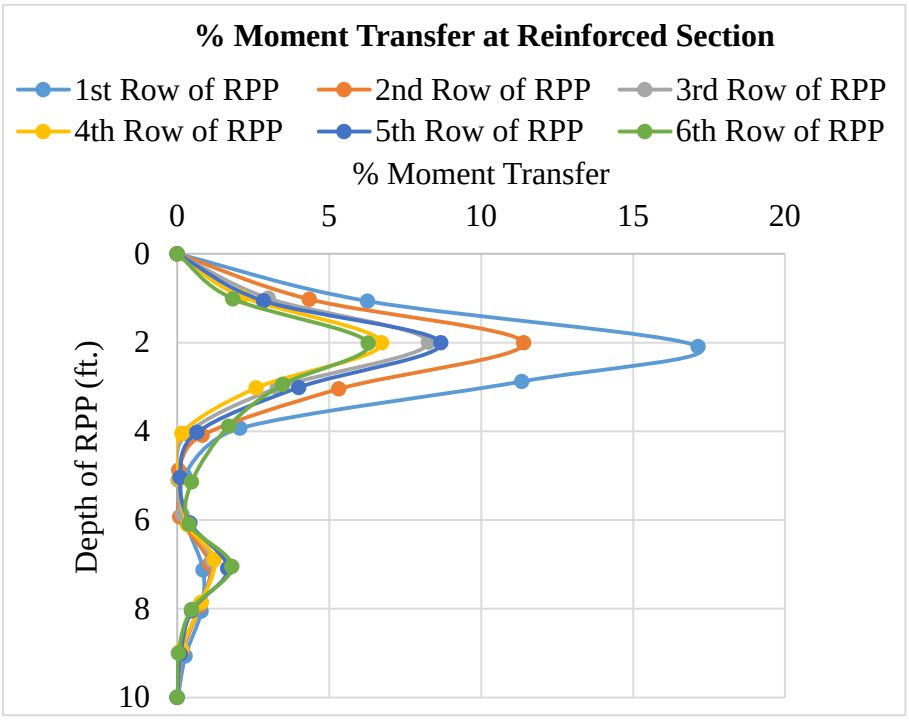

(b)

Figure 5. 33 Moment along the RPP length; (a) Bending moment, (b) % of moment transfer.

The results indicate that the RPPs are resisting significant amount of lateral force starting from the 1st row and reducing the pressure before reaching the wall facing; the pressure decrease at the back of the wall resulted in less lateral displacement of the wall facing. If RPP reinforced MSE wall base is considered as a composite structure, then it can be said that the RPP is providing significant shear resistance against base sliding of the wall; therefore, it is acting similar to a shear key for the MSE wall base.

5.4.3 Comparison between Field Result and Model Prediction

A relative comparison plot between field result and model prediction is presented in Figure 5.34.

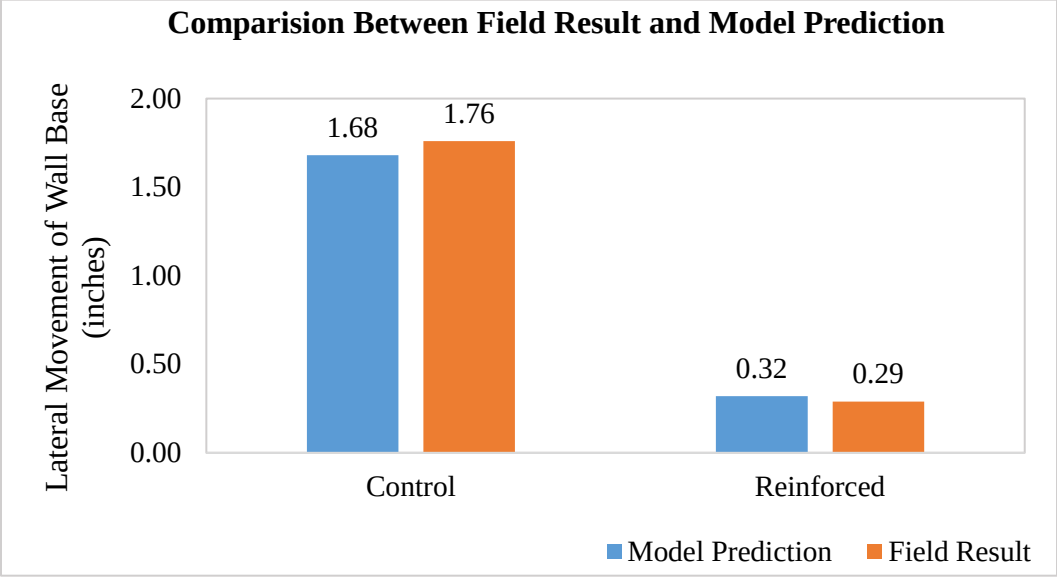

Figure 5. 34 Comparison between field result and model prediction.

The plot shows that for control section, the calibrated model relatively under predicts from what is found in the field which might be due to non-uniformity of the slope and also there is some initial lateral plastic deformation in the field while loading with backfill material due to temporary load from instruments which cannot be simulated in the model. However, in

case of reinforced section the calibrated model slightly over predicts the lateral deformation from the value observed in the field. This might be the due to the anchorage of geotextile with RPP resulting in additional resistance for soil body movement, which cannot be simulated in the FEM analysis thus making the model more conservative.

5.4.4 Effect of Backfill Loading Height on the Base Movement of MSE Wall

An extended study was conducted using the calibrated model for both control and reinforced section to further evaluate the effect of increasing MSE wall height on the lateral deformation. Plastic deformation calculation was performed using PLAXIS 2D. Height of the slope and the backfill was increased and analyzed using the calibrated model for a wall height up to 9.5 ft. Figure 5.35 presents comparison plot of the lateral deformation found for both control and reinforced section for increasing backfill height. From the plot it is evident that for each loading height, control section experiences significantly larger lateral deformation compared to the reinforced section.

It should be noted that the inclinometer data showed the deformation to be in relatively good agreement with the model prediction. The visual observation of the wall suggested that the wall if fails, it will fail due to overturning from excessive load addition not because of sliding of the base, which is also in good agreement with the model prediction. This might be because the RPPs are holding the base and providing additional shear resistance against sliding failure which increases the factor of safety against sliding significantly.

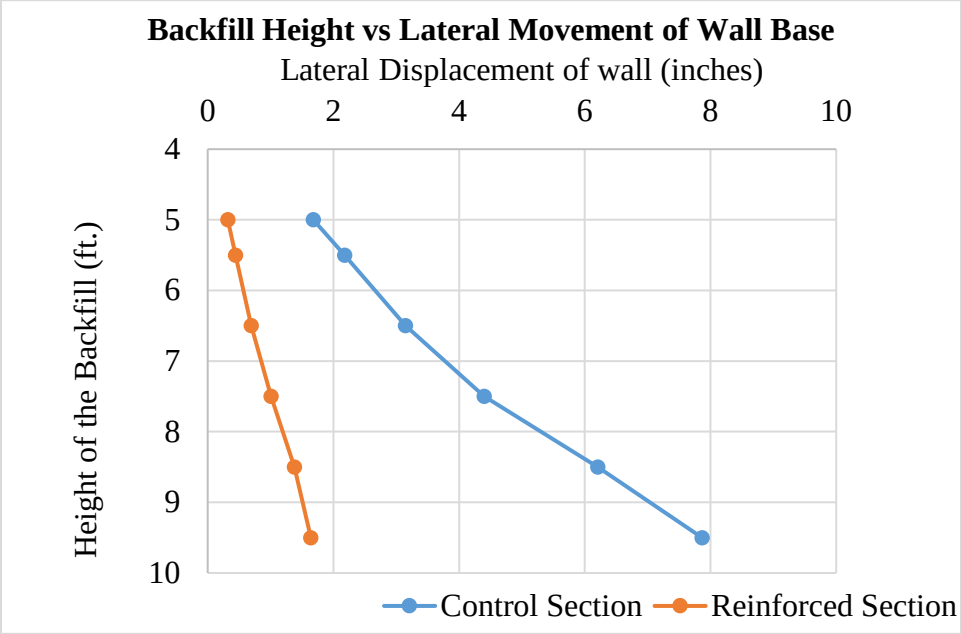

Figure 5. 35 Model predicted data for increasing height of backfill: Comparison between Control and reinforced section).

A study conducted by Stuedlein et al. (2010) on a MSE wall constructed in 4 tier with a total height of 150 ft. (exposed height 137.5 ft.) showed that with increasing height of the wall, lateral displacement increases. The authors recorded lateral displacement after each tier of construction and reported that at the end of each tier of construction as the wall reaches a new height the lateral displacement increases (Figure 5.36). Based on the monitoring results, it was reported that, the maximum horizontal movement took place at the base of the MSE wall. After the completion of tier 4 construction the lateral movement was recorded to be about 3.5 inches (90 mm). Similar conclusion was drawn from the numerical analysis in the current study; with increasing backfill/wall height lateral displacement was found to be increasing.

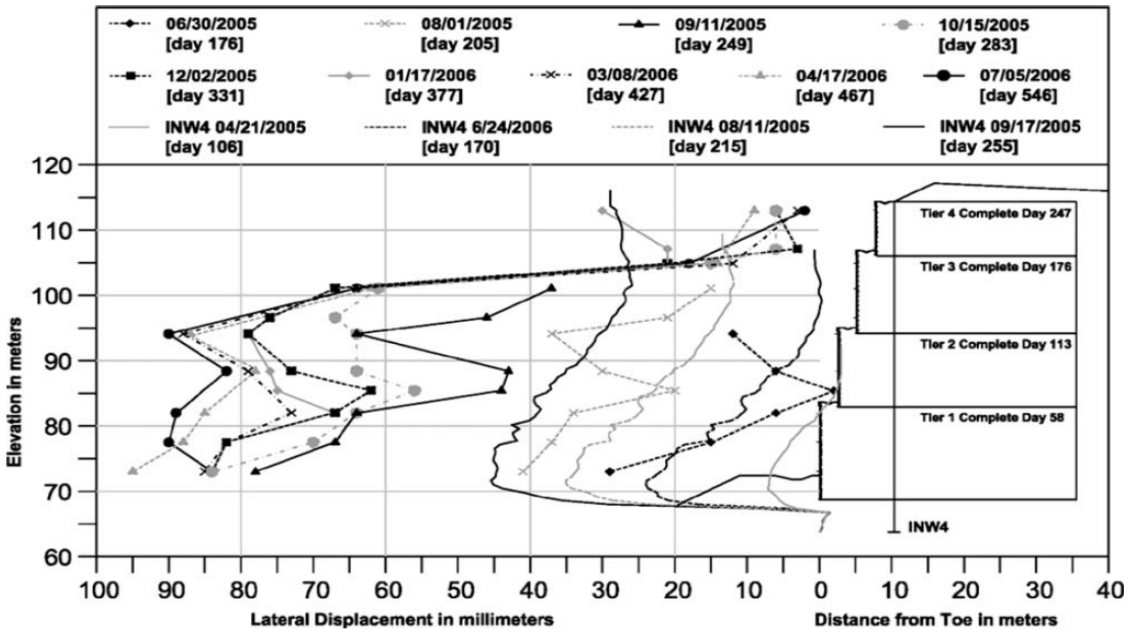

Figure 5. 36 Lateral displacement of the facing of the MSE wall after each stage of construction (Stuedlein et al., 2010).

Based on the FEM analysis, the first three rows of RPP show relatively higher horizontal deformation compared to the other rows. Figure 5.37 presented the deformation of first three rows of RPP for increasing backfill height. The highest horizontal displacement is observed for the 1st row of RPP. The increasing height of the backfill / wall induces higher force. The RPPs carry most of the lateral force generated by the backfill soil, resulting in higher resistance from the RPP which reduces the lateral movement of the MSE wall base.

Similarly, depth wise bending moment is plotted for the first three rows of RPPs for different backfill height. For different loading, the maximum moment resistance was observed for the 1st row of RPP. With increasing loading height, bending moment increases up to a maximum of 804 lb-ft for a wall height of 9.5 ft., which is about 34% of the maximum capacity of RPP. Bending moment plot and % bending moment transfer is presented in Figure 5.38 & 5.39.

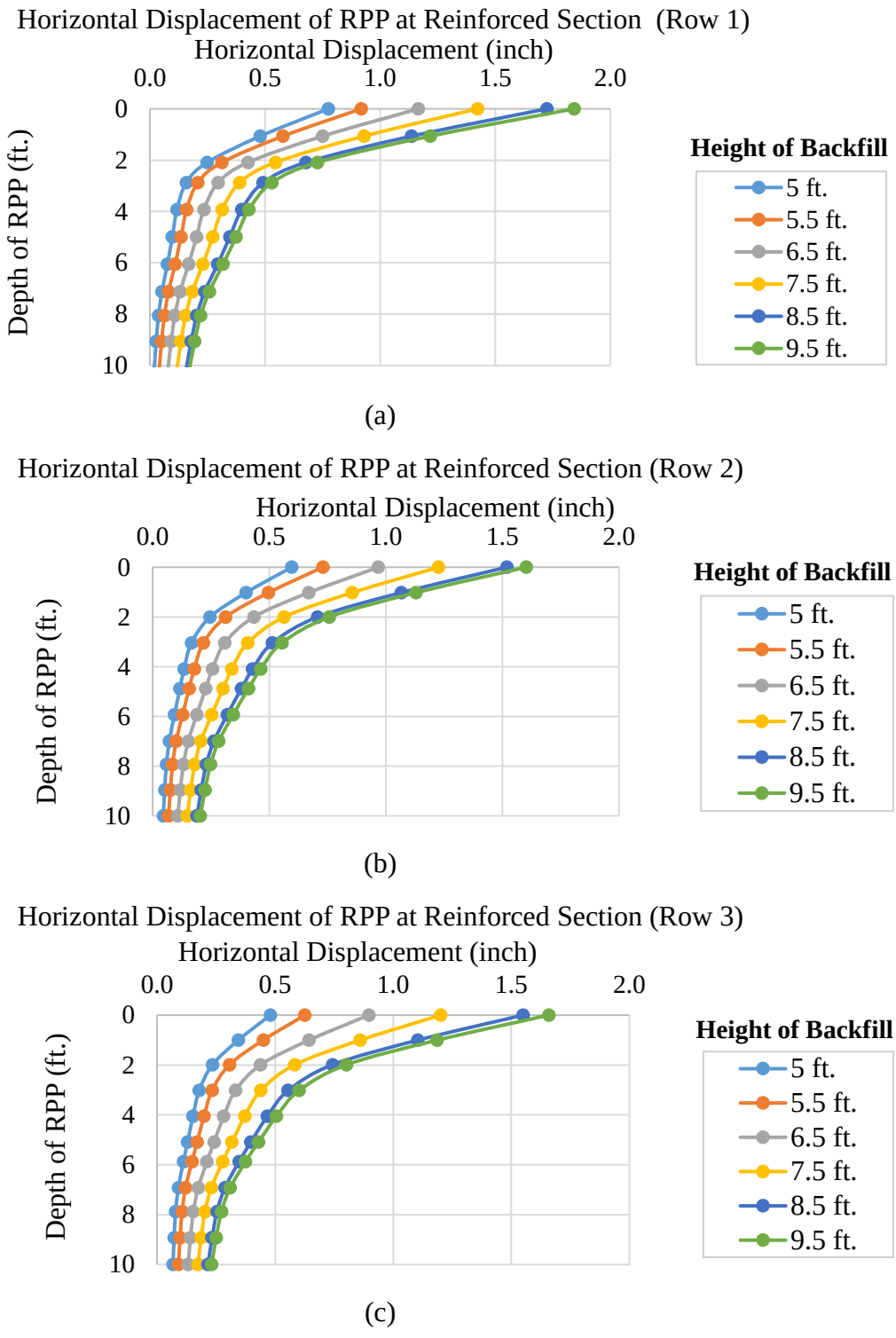

Figure 5. 37 Horizontal displacement profile of RPP for different wall height; (a) 1st row of RPP, (b) 2nd row of RPP, (c) 3rd row of RPP.

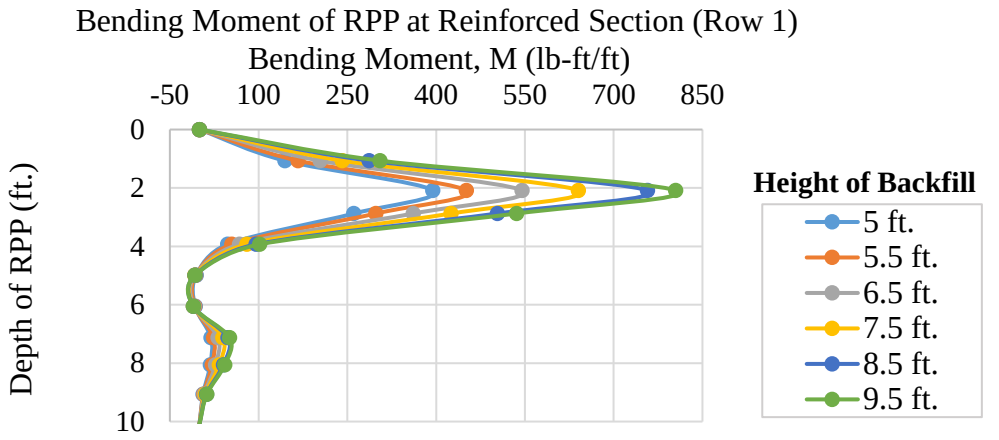

(a)

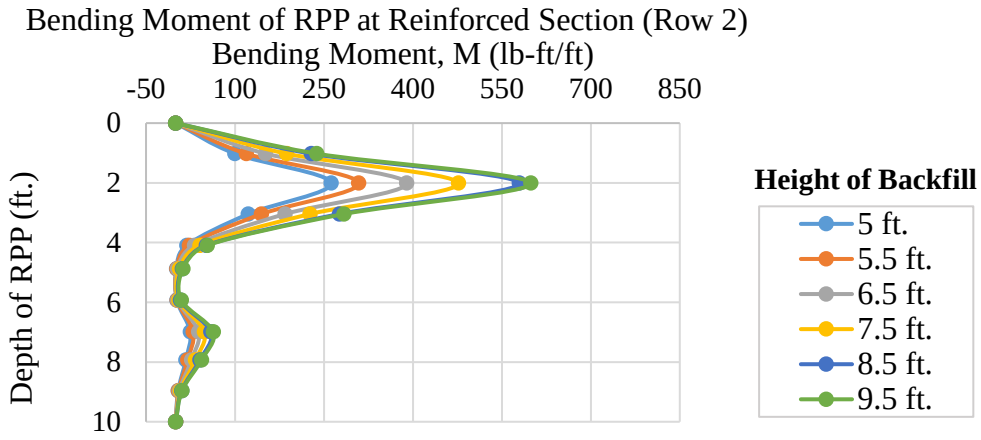

(b)

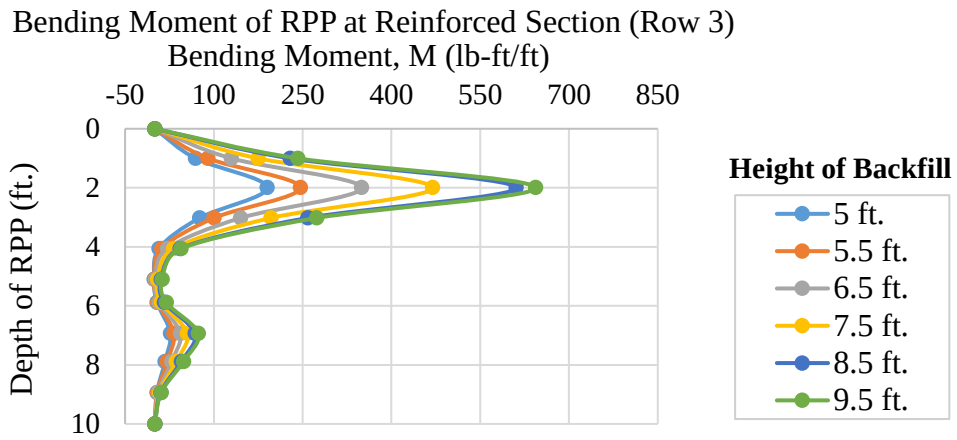

(c)

Figure 5. 38 Bending Moment along the length of RPP; (a) 1st row of RPP, (b) 2nd row of RPP, (c) 3rd row of RPP.

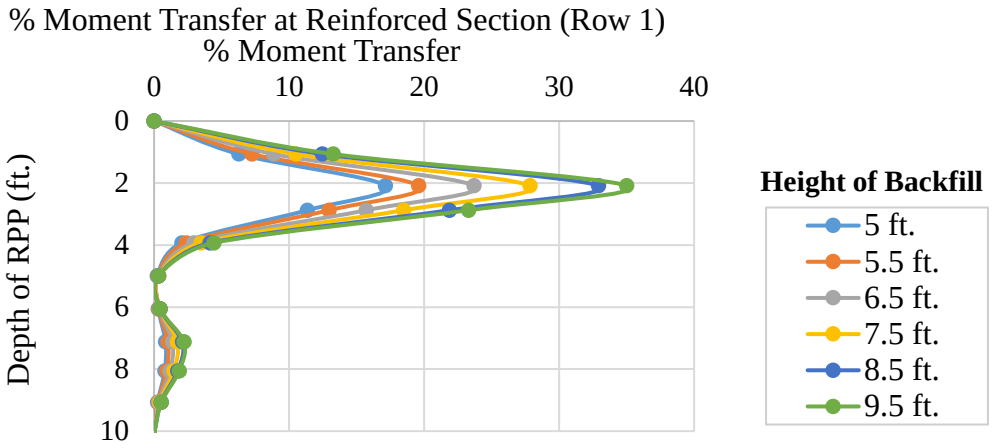

(a)

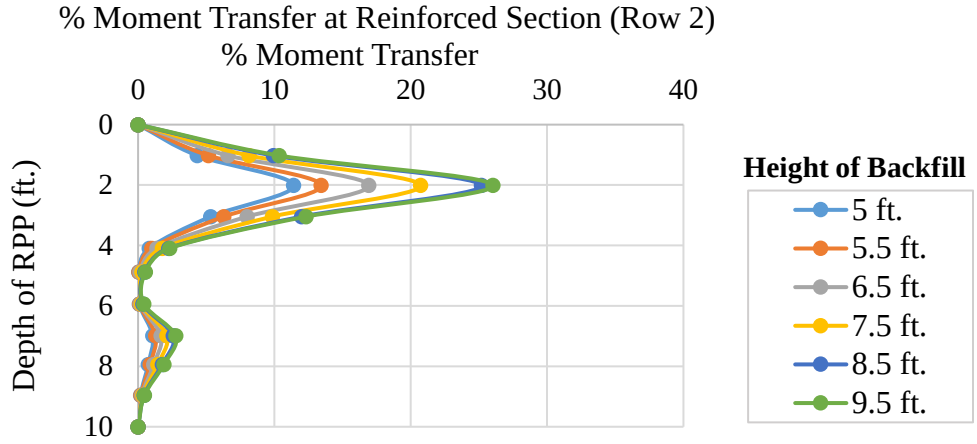

(b)

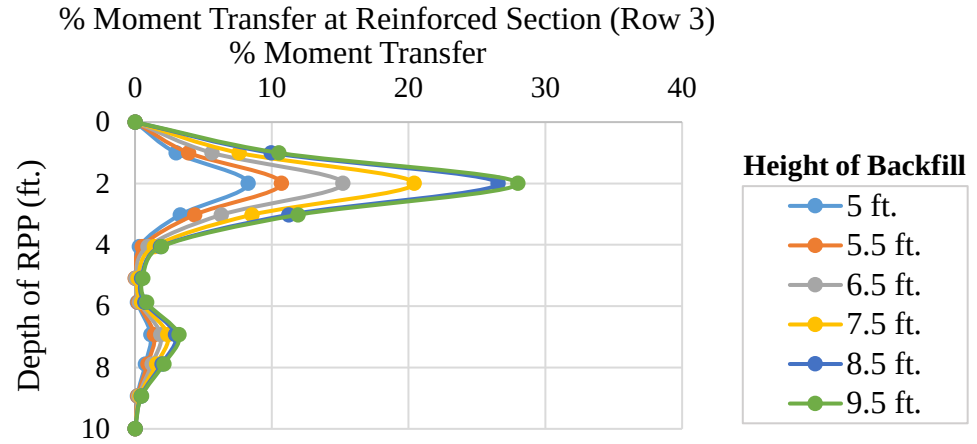

(c)

Figure 5. 39 Percent moment transfer along the length of (a) 1st row of RPP, (b) 2nd row of RPP, (c) 3rd row of RPP.

It is to be noted that the first row of RPP takes on major part of the lateral force transferred from the soil body and the subsequent rows also take part in resisting the lateral movement by restricting/limiting transfer of lateral pressure from reaching the back of the wall. Therefore, the group effect of RPP minimizes deformation or sliding of the base of the wall by providing additional shear resistance similar to the shear key.

5.4.5 Parametric Study

A parametric study was conducted as a part of numerical study to further assess the effectiveness of RPP in improving the shear resistance of the MSE wall base against sliding. The parameters considered for this study included different size, length and spacing of RPP for increasing backfill height for the existing soil condition and geometry of the test sections. Current field scale study included stabilization of MSE wall base using 4 in. x 4 in. RPPs of 10 ft. in length at 3 ft. c/c to increase sliding resistance of the wall. Based on the effectiveness and economy, RPPs of 6 in. x 6 in. and 10 in. x 10 in. in size and of different length e.g. 8 ft. and 12 ft. may also be utilized. Therefore, these different sizes and lengths have been selected for the parametric study. In addition, three different spacing (2 ft., 3 ft. and 4 ft. c/c) for each configuration of RPP was also included in the study.

The numerical modeling matrix for the parametric study is presented in Table 5.11. The parametric study was performed using the calibrated model developed based on the field behavior of the test sections. The RPP was modeled as plate element with 0.8 interface element strength for all models.

Table 5. 11 Numerical model matrix for parametric study of lateral loaded test section.

Size of RPP	Length of RPP	Spacing of RPP	Type of Analysis
4 in. x 4 in.	8 ft.	2 ft., 3 ft. and 4 ft.	Plastic Deformation (horizontal displacement analysis)
	10 ft.	2 ft., 3 ft. and 4 ft.	
	12 ft.	2 ft., 3 ft. and 4 ft.	
6 in. x 6 in.	8 ft.	2 ft., 3 ft. and 4 ft.	Plastic Deformation (horizontal displacement analysis)
	10 ft.	2 ft., 3 ft. and 4 ft.	
	12 ft.	2 ft., 3 ft. and 4 ft.	
10 in. x 10 in.	8 ft.	2 ft., 3 ft. and 4 ft.	Plastic Deformation (horizontal displacement analysis)
	10 ft.	2 ft., 3 ft. and 4 ft.	
	12 ft.	2 ft., 3 ft. and 4 ft.	

Plastic calculation was performed in PLAXIS 2D for deformation analysis. Soil parameters found from the calibrated model through back analysis for the control section was used for the whole set of parametric matrix. Based on the FEM analysis it was found that the length has almost no effect on the improvement of lateral movement. This might be because other than the extended 2 ft. above ground, the rest of the portion of RPP is embedded into the ground which ensures sufficient anchorage and resistance from foundation soil for 8 or 10 ft. long RPP. Increasing the length further does not change the scenario. However, if the foundation was composed of soft soil, the scenario might have been different. Spacing has significant effect on the horizontal movement of the wall base. Figure 5.40 presents lateral deformation plot for different RPP spacing for 4 in. x 4 in., 6 in. x 6 in. and 10 in. x 10 in. 10 ft. long RPPs for increasing backfill loading height. The graphical representation shows that

lateral deformation has a direct relationship with spacing; deformation increases with increasing RPP spacing.

Size of RPP also plays considerable role in controlling the lateral deformation of the MSE wall base. As shown in Figure 5.41, for fixed spacing the lateral deformation decreases with increasing RPP size. This might be because the greater coverage area and higher stiffness of the larger size of RPPs are able to resist much more lateral force from the backfill compared to the smaller sections of RPPs.

Horizontal Displacement of MSE Wall Base for Different Spacing (10 ft. long RPP)

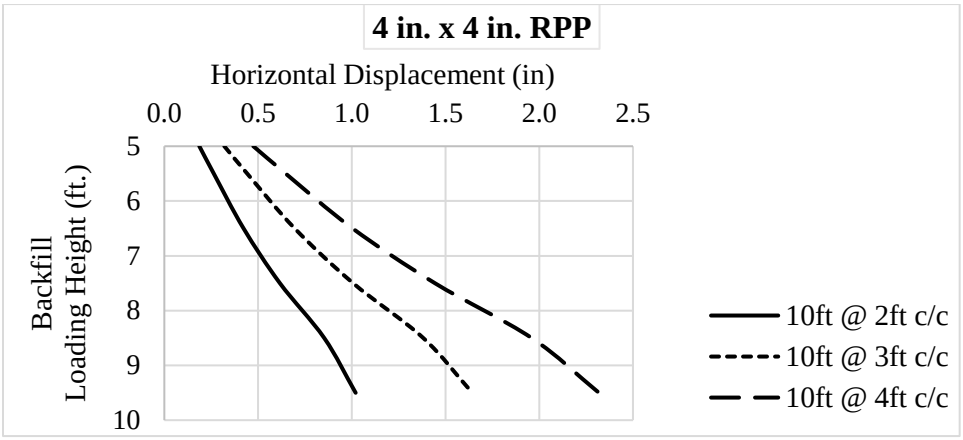

(a)

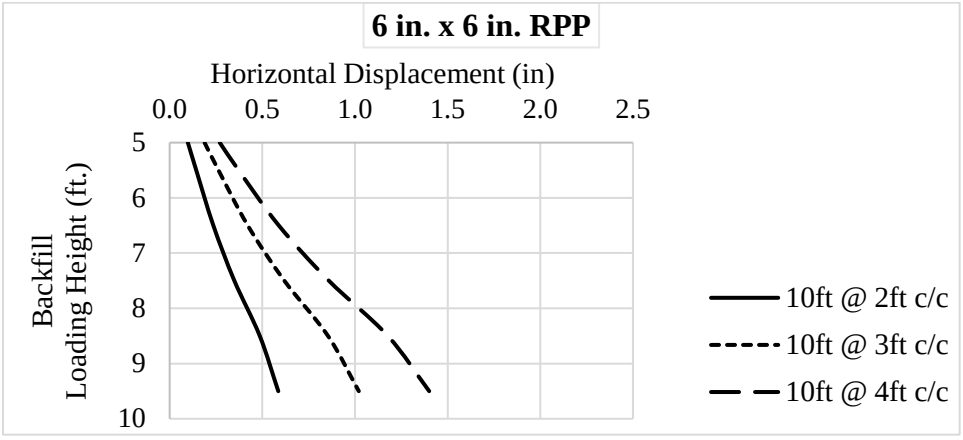

(b)

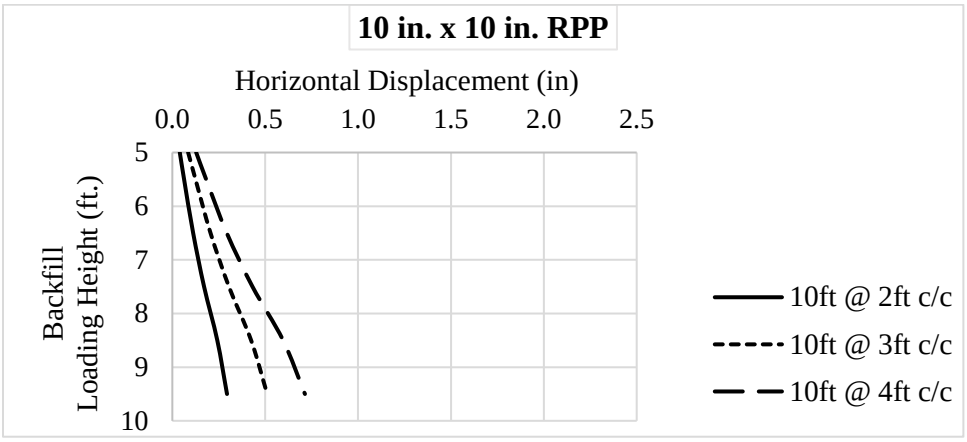

(c)

Figure 5. 40 Horizontal displacement for varying spacing of 2 ft., 3 ft. & 4 ft. for RPP sizes of (a) 4 in. x 4 in.; (b) 6 in. x 6 in.; (c) 10 in. x 10 in.

Horizontal Displacement of MSE Wall Base for Different RPP Sizes (10 ft. long)

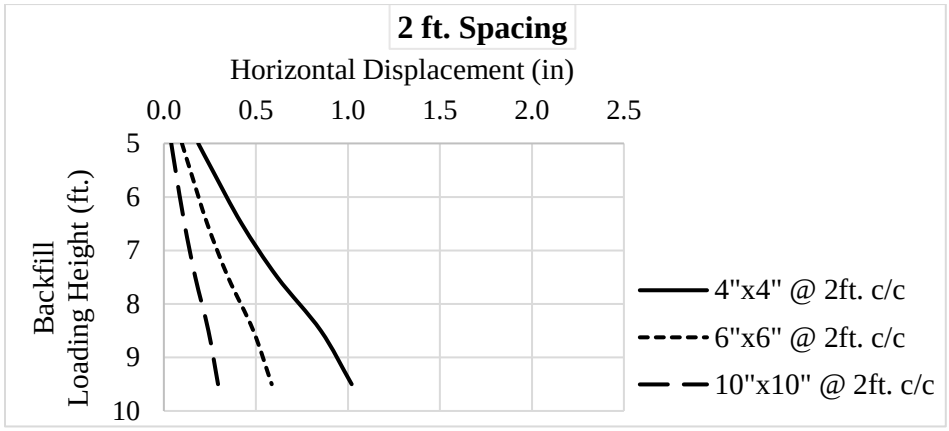

(a)

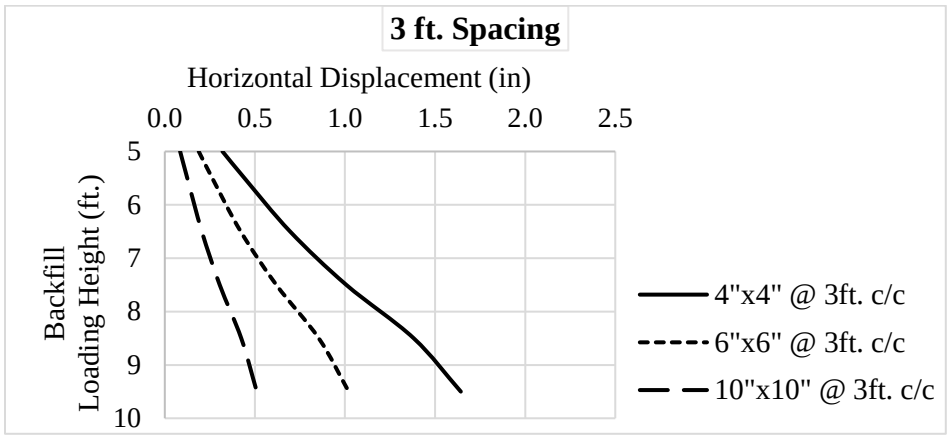

(b)

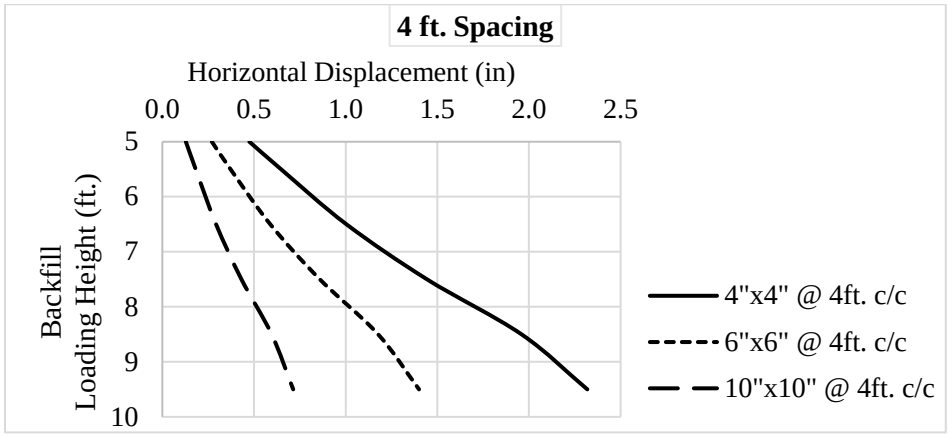

(c)

Figure 5. 41 Horizontal displacement for varying RPP sizes (4 in. 4 in., 6 in. x 6 in. and 10 in. x 10 in.) having fixed spacing of (a) 2 ft.; (b) 3 ft.; (c) 4 ft.

CHAPTER 6

CONCLUSIONS AND RECOMMENDATIONS

6.1 Introduction

Bearing and shearing capacity failure is a common phenomenon for the structures constructed on unsuitable foundation soil, which leads to spending a significant portion of the budget for repair and maintenance for the related agencies. Structures (e.g. embankments, roadways, highways etc.) constructed on weak/soft foundation soil tend to experience excessive total and differential settlement due to not having sufficient support; on the other hand, MSE retaining structure constructed on stiff foundation soil, subjected to excessive lateral load is prone to sliding failure due to lack of shear resistance of the base. In order to improve the performance of such structures, it is imperative to develop a sustainable ground improvement technique which is suitable and efficient, yet cost effective. For this reason, the current research focused on developing a sustainable ground improvement solution using recycled plastic pin (RPP). This chapter presents the summarized findings of the research and recommendation for future studies.

6.2 Summary and Conclusions

The current study summarized an innovative, economic and sustainable remediation to the excessive settlement scenario of weak foundation soil and inadequate shear resistance of MSE wall base against sliding, using recycled plastic pin.

Improving Weak foundation soil:

A field scale study has been conducted by replicating the scenario of embankment type structures constructed on weak foundation soil. Identical test sections has been constructed, each having an effective test area of 15 ft. x 15 ft. The construction and monitoring has been carried out in two phases. For each phase, one section served as control section and the foundation soil of the other sections were reinforced with RPP to compare and evaluate the effectiveness of RPP. The purpose of second phase was to validate and further evaluate the effectiveness of RPP to minimize the settlement of the structure by improving the foundation soil. The field performance monitoring was carried out using horizontal inclinometers installed at the base of the test section. Summarized findings are presented as follows:

- The site investigation indicated that the foundation soil at the test location of phase – I was relatively soft with low SPT N-value and the location had sufficient flat ground for the construction of the test sections. The soil of the top 5 ft. was found to be extremely soft having unconfined compressive strength of only 120 psf. underlain by a considerably stiff soil to provide sufficient support for the RPPs.
- Analytical study on the improvement of weak foundation soil showed that with increasing RPP size settlement decreases due to improved bearing capacity and with increasing spacing of RPP bearing capacity of the foundation soil decreases. However, all configuration of RPP reinforcement considerably improves the weak foundation soil.
- Phase – I had two reinforced section using 4 in. x 4 in. and 6 in. x 6 in. RPPs of 10 ft. long as reinforcement respectively, installed in a staggered pattern at 3 ft. c/c spacing.

To validate the results of phase – I and to further evaluate the performance of RPP one reinforced section (4 in. x 4 in. RPP at 3 ft. c/c) was included in phase – II. For the purpose of comparison, one control section was constructed for each phase.

- From the field installation program of phase – I, it was evident that an excavator with hydraulic breaker hammer worked effectively while installing RPPs. The factors involving the driving rate of RPP includes soil type (stiffness), driving length of RPP and expertise of installation team. The observation showed that the overall driving rate for the 4 in. x 4 in. RPP was 2.87 ft./min, which signifies that to drive a single 4 in. x 4 in. RPP into the ground it takes about 3.5 minutes and a total of 115 to 135 RPPs can be installed each day. On the other hand, comparatively more time was needed to install 6 in. x 6 in. RPP due to its larger size and greater driving resistance. The overall driving rate for 6 in. x 6 in. RPP was found to be about 1.5 ft./min, i.e., it takes 6.7 minutes to install a single RPP into the ground and a total of 50 to 70 RPPs can be installed each day.
- Performance monitoring results from phase – I indicated that a total settlement of 2.01 inches took place for the foundation of the control section; while for the reinforced section the settlement reduced considerably. Use of 4 in. x 4 in. RPP as foundation reinforcement reduced the settlement by 60%, while for 6 in. x 6 in. RPP, the reduction in settlement was found to be about 70%.
- The performance monitoring results from phase – II presented similar conclusion. A reduction in settlement of about 56% was observed due to the use of 4 in. x 4 in. RPP compared to the control section. The settlement reduction/ improvement depends on

the strength of existing foundation soil. From the field investigation result it was found that the soil condition of the site for phase – II was slightly better than phase – I.

- The results showed that wet and dry period has slight influence on the settlement. If the embankment soil is clay, an extended rainfall event might induce slight increase in settlement due to saturated weight and an extended dry period results in shrinkage of soil and release of some load resulting in decrease in cumulative settlement. If embankment has permeable soil, it might result in initial increase in settlement; however, in case of foundation with expansive clay, the water infiltration might result in slight expansion of foundation soil as observed for the control section (phase – II) which was not significant for the reinforced section.
- It should be noted that, geogrid has a significant role as efficiency of the load transfer from the embankment fill soil to the RPP relies on the soil arching effect of the geogrid in between the RPP. Higher the geogrid strength, higher the load transfer will be. In addition, geogrid also minimizes the possible differential settlement.
- Finite element modeling software PLAXIS 2D was used to develop a calibrated model for the control section which is able to predict the performance similar to the field observations. The FEM model was found to be in good agreement with the field results. The calibrated model was used for the reinforced sections and it was found that the predicted outputs are in good agreement with the field results.
- From the FEM model it was observed that when the embankment tries to sink in to the foundation soil, the soil tries to accommodate the embankment fill material by moving laterally; RPP restricts this lateral moment of foundation soil making it capable of supporting the load from the embankment.

- FEM model was used to evaluate the effectiveness of RPP for increased loading height and compared with the control section. The result showed, with increasing loading height, foundation settlement of the control section increases significantly while for reinforced section the settlement was found to be significantly low compared to the control section.
- The calibrated FEM model was further utilized and a parametric study was performed to investigate the effect of RPP size, spacing and length on the vertical deformation of the foundation. The parametric study indicated that, the vertical deformation is low for larger RPP size for fixed length and spacing. It was also observed that the vertical deformation decreases with decreasing RPP spacing. However, it was noticed that the length of RPP does not have any significant effect on the settlement. Though, the effect of length is relatively higher for larger RPP size and at increased loading height.
- Based on the field investigation and FEM analysis it can be concluded that RPP can be utilized to improve the weak foundation soil and provide additional support to carry loads from structures with minimum total and differential settlement of the foundation soil.

Increasing Shear Resistance of MSE Wall Base against Sliding:

The field scale study for this part included replicating the practical sliding scenario of MSE wall. Two identical MSE wall test sections were constructed, each having a wall facing of 24 ft. long. One section served as a control section and the other was reinforced with 4 in x 4 in. RPP to compare and evaluate the effectiveness of RPP against base sliding. The construction was carried out in two phases, where the purpose of the second phase was to further assess the

effectiveness of RPP for higher backfill loading height. The field performance of the test sections were monitored using inclinometers and pressure plates installed in front and the back of the wall respectively. Results and conclusions obtained from the study are summarized as follows:

- The site investigation indicated that the foundation soil near the toe of the slope in the site was very stiff with high SPT N-value which was suitable for the construction of field scale MSE wall test sections. The soil at the top of the slope was found to be relatively soft and had the tendency to slide which was expected to incorporate additional lateral force at the back of the wall.
- The reinforced section had 10 ft. long RPPs having 8 ft. driven into the ground, keeping 2 ft. above. Similar to the vertical test sections, an excavator with hydraulic breaker hammer was used for RPP installation. The observation showed that the overall driving rate for the whole section was 1.58 ft./min, which signifies that, to drive 8 ft. of a single 4 in. x 4 in. RPP into the ground, it takes about 5 minutes and a total of 75 to 95 RPPs can be installed each day.
- Performance monitoring result from Phase – I indicated that the base of the control section experienced significant lateral movement (as much as 3.8 inches) during the monitoring period, while almost no movement was observed for the reinforced section.
- The performance monitoring results observed in the Phase – II presented similar outcome as observed in Phase – I. The control section experienced a lateral movement of 1.76 inches while horizontal movement of the reinforced section was much less (as low as 0.29 inches) compared to the control section. From the inclinometer data it was

observed that the maximum horizontal movement was observed at the base level of the wall which reduces with depth under the ground level.

- The results showed that, precipitation events influence the base movement of the wall. The higher intensity of rainfall resulted in higher lateral deformation and an extended dry period is followed by slight decrease in movement.
- The backfill soil was low plastic soil having a swelling and shrinkage behavior. The laboratory test results showed that the soil has low permeability which tend to store water after each rainfall event, resulting in additional lateral pressure at the back of the wall causing the wall to move further. An extended dry period results in shrinkage of the soil releasing some pressure from the back of the wall.
- Monitoring result from the pressure plate shows an increase in pressure followed by backfilling of the wall, resulted in the initial lateral movement of the wall base, which was significant for control section compared to RPP reinforced section. In addition, after each rainfall event an increase in pressure was observed followed by a drop when the lateral movement takes place due to the generation of excess pressure. This is because the pressure readings are generated from the resistance of the wall facing due to pressure form the soil. The wall facing being flexible, releases some pressure when it moves away from the backfill as a result of excess lateral pressure.
- It should be noted that the RPP requires proper grip with the soil to perform well. The initial movement of the wall is due to load mobilization during first four months after that the change in movement became almost negligible.
- Finite element modeling software PLAXIS 2D was used to develop and calibrate a model for control section which is able to predict the performance similar to the field

observations. Further deformation analysis was conducted for the reinforced section. Deformation prediction obtained from the FEM analysis for the reinforced section was found to be in good agreement with the field results. The deformation analysis presented that only 17% of the load transfer had taken place compared to the ultimate capacity of the RPP.

- The calibrated FEM model was further utilized to evaluate the effectiveness of RPP for higher backfill height compared to the control section. The result showed, with increasing wall height and backfill loading the base of the control section experiences significant increase in horizontal movement while for reinforced section the movement was significantly less.
- A parametric study was performed to investigate the effect of different RPP size, length and spacing. Based on the analysis, it was observed that changing length has almost no effect as the RPPs have sufficient anchorage to resist the lateral movement. Spacing has a significant influence on the lateral movement of the wall; lower lateral movement was observed for closer spacing. Size of RPP also plays a major role in increasing the shear resistance of the wall. Smaller the RPP size, greater is the base movement; as larger RPP has higher stiffness, therefore, can resist more lateral load.
- Based on the field investigation and FEM analysis it can be concluded that RPP can be effectively utilized to act as a shear key at the base of MSE retaining structures to provide additional shear resistance against base sliding; hence, it might result in prevention of failure to the structures supported by the MSE wall.

6.3 Recommendation for Future Studies

Based on the current study, the following recommendations are proposed for future studies:

- The study presented a field scale demonstration for both vertical and lateral loading scenarios of few test sections. However, no large scale actual ground improvement were performed. Therefore, it is highly recommended to conduct a study on actual embankment or MSE retaining structure constructed on unsuitable soil reinforced with RPP.
- Laboratory scale study should be conducted to have a better understanding of the reinforcing mechanism of RPP.
- The field investigation showed absence of a ground water table. Hence, it can be said that no consolidation settlement took place and was unable to investigate the effect of ground water table. It is recommended to perform a study in a location having ground water table close to the ground surface. In addition, effect of RPP in very soft soil scenario needs to be evaluated.
- The current study conducted for the MSE wall had a mild slope at the back. A steeper slope has a tendency to slide which might generate significant lateral force and therefore, a study should be performed to investigate efficiency of RPP in such case.
- The current study was performed for MSE wall constructed on a stiff soil considering only sliding scenario. However, if the foundation soil is relatively weak or height of MSE wall exceeds the natural bearing capacity of the foundation soil, chances of global failure is also present. A field investigation is recommended to evaluate the effectiveness of RPP in such cases.

- The current study results are based on a short term performance monitoring period. It is advised to perform or continue the monitoring to evaluate the effect for long term, seasonal variation etc. on the performance of the improved soil, especially for the cases related to MSE retaining structures.
- During the current study, RPP of only rectangular cross sections was utilized. There are other shapes (e.g. circular, H-pile etc.) that are commercially available which can be used to perform another study to determine effect of different shapes of RPP.
- During the current study, two-dimensional numerical modelling was conducted using finite element software PLAXIS 2D. Especially for the MSE retaining test sections, 2D analysis cannot perfectly model field scenario; therefore, to have a better understanding, it is suggested to conduct 3D numerical analysis for the test sections.
- Based on the performance monitoring data, extensive modelling should be performed to develop a design method for ground improvement using RPP.

REFERENCES

AASHTO (2007). *AASHTO LRFD Bridge Design Specifications: SI Units (4th Edition).* American Association of State Highway and Transportation Officials.

Abu-Hejleh, N., McMullen, M., Hearn, G., & Zornberg, J. G. (2001). *Design and Construction Guidelines for MSE Walls with Independent Full-height Facing Panels* (Vol. 5). Report No. CDOT-DTD-R-2001.

Adams, M., Nicks, J., Stabile, T., Wu, J., Schlatter, W., and Hartmann, J. (2011). "Geosynthetic Reinforced Soil Integrated Bridge System, FHWA Synthesis Report." 68.

Ahmed, F. S. (2013). Engineering Characteristics of Recycled Plastic Pin, Lumber and Bamboo for Soil Slope Stabilization.

Alzamora, D. E., Wayne, M. H., & Han, J. (2000). Performance of a segmental Retaining wall supported by a geosynthetic reinforced load transfer platform. In *Submitted for Geo-Institute Specialty Conference on Performance Verification of Constructed Geotechnical Facilities*.

Alzamora, D., and Barrows, R. J. (2007). "Research Pays Off: Mechanically Stabilized Earth Walls on the Interstate Highway System: Thirty Years of Experience." *TR News* (249).

Arenicz, R. M. (1992). Effect of reinforcement layout on soil strength. *Geotechnical Testing Journal*, *15*(2), 158-165.

Ariema, F., and Butler, B.E. (1990). Embankment Foundations - Guide to Earthwork Construction. *Transportation Research Board, National Research Council, Washington, D.C. pp. 59-73.*

Aubeny, C., Biscontin, G., Huang, J., Bin-Shafique, S., Dantal, V. S., & Sadat, R. (2014). *Design Parameters and Methodology for Mechanically Stabilized Earth (MSE) Walls* (No. FHWA/TX-14/0-6716-1). Texas A & M Transportation Institute.

Babu, G. S., Raja, J., Basha, B. M., & Srivastava, A. (2016). Forensic analysis of failure of retaining wall. In *Forensic Geotechnical Engineering* (pp. 451-465). Springer, New Delhi.

Barchard, J., (1999). Centrifuge Modeling of Piled Embankments on Soft Soils. *Thesis presented to University of New Brunswick, Canada, in partial fulfillment of the requirement of degree of Master of Engineering*.

Basore, C. E., & Boitano, J. D. (1969). Sand densification by piles and vibroflotation. *Journal of the Soil Mechanics and Foundations Division*, *95*(6), 1303-1324.

Benjamim, C. V. S., Bueno, B. S., & Zornberg, J. G. (2007). Field monitoring evaluation of geotextile-reinforced soil-retaining walls. *Geosynthetics International*, *14*(2), 100-118.

Berg, R. R., Christopher, B. R., & Samtani, N. C. (2009). *Design of mechanically stabilized earth walls and reinforced soil slopes–Volume I* (No. FHWA-NHI-10-024).

Berg, R. R., Christopher, B. R., and Samtani, N. C. (2009). *Design of Mechanically Stabilized Earth Walls and Reinforced Soil Slopes–Volume II.*

Bowders, J., Loehr, J., Salim, H., & Chen, C. W. (2003). Engineering properties of recycled plastic pins for slope stabilization. *Transportation Research Record: Journal of the Transportation Research Board*, (1849), 39-46.

Bowles, J. E. (1988). *Foundation analysis and design*. McGraw-hill.

Breslin, V. T., Senturk, U., & Berndt, C. C. (1998). Long-term engineering properties of recycled plastic lumber used in pier construction. *Resources, Conservation and Recycling*, *23*(4), 243-258.

Briançon, L., & Simon, B. (2011). Performance of pile-supported embankment over soft soil: full-scale experiment. *Journal of Geotechnical and Geoenvironmental Engineering*, *138*(4), 551-561.

Brinkgreve, R. B. J., Kumarswamy, S., & Swolfs, W. M. (2017). PLAXIS 2D Reference Manual 2017. *Delft, Netherlands*.

Chai, J. C., & Lu, Y. (2018). Behavior of an Embankment on Column-Slab Improved Clay Deposit – A Case Study. *Computers and Geotechnics, Manuscript number: COGE-18-00634.*

Chalermyanont, T., and Benson, C. H. (2005). "Reliability-Based Design for External Stability of Mechanically Stabilized Earth Walls." *International Journal of Geomechanics*, 5(3), 196–205.

Chen, C. W., Salim, H., Bowders, J. J., Loehr, J. E., & Owen, J. (2007). Creep behavior of recycled plastic lumber in slope stabilization applications. *Journal of materials in civil engineering*, *19*(2), 130-138.

Chen, R. P., Xu, Z. Z., Chen, Y. M., Ling, D. S., & Zhu, B. (2009). Field tests on pile-supported embankments over soft ground. *Journal of Geotechnical and Geoenvironmental Engineering*, *136*(6), 777-785.

Chow, Y. K., Yong, D. M., Yong, K. Y., & Lee, S. L. (1992). Dynamic compaction analysis. *Journal of Geotechnical engineering*, *118*(8), 1141-1157.

Christopher, B. R., Gill, S., Giroud, J. P., Juran, I., Mitchell, J. K., Schlosser, F., & Dunnicliff, J. (1990). *Reinforced soil structures. Volume I, Design and construction guidelines* (No. FHWA-RD-89-043). United States. Federal Highway Administration.

Christopher, B. R., Leshchinsky, D., and Stulgis, R. (2005). "Geosynthetic-Reinforced Soil Walls and Slopes: U.S. Perspective." *Proc., Geo-Frontiers Congress 2005*, Austin, TX, ASCE, 12.

Das, B. M. (2011). *Principles of geotechnical engineering, 7th Edition*. Cengage learning.

Das, B. M. (2015). *Principles of foundation engineering*. Cengage learning.

Delphia, J. G. (2011). Presentation titled "MSE Wall Case Studies." <https://static.tti.tamu.edu/conferences/tsc12/presentations/structhydraulics/delphia.pdf>. (2011).

Elias, V., Christopher, B. R., & Berg, R. R. (2001). *Mechanically stabilized earth walls and reinforced soil slopes design and construction guidelines.* (No. FHWA-NHI-00-043).

Esmaeili, M., Nik, M. G., & Khayyer, F. (2012). Experimental and numerical study of micropiles to reinforce high railway embankments. *International Journal of Geomechanics*, *13*(6), 729-744.

Fang, Y. S., & Ishibashi, I. (1986). Static earth pressures with various wall movements. *Journal of Geotechnical Engineering*, *112*(3), 317-333.

Fatani, M. N., Bauer, G. E., & Al-Joulani, N. (1991). Reinforcing soil with aligned and randomly oriented metallic fibers. *Geotechnical Testing Journal*, *14*(1), 78-87.

FHWA Publication (1995) - "Geosynthetic Design and Construction Guideline", *FHWA Publication Number: FHWA-HI-95-038, Publication Year: 1995, http://isddc.dot.gov/OLPFiles/FHWA/011431.pdf*

Freeby, G. A. TxDOT Memorandum (2013). *New and Revised Retaining Wall Standard Drawings.*

Giroud, J. P., & Noiray, L. (1981). Geotextile-reinforced unpaved road design. *Journal of Geotechnical and Geoenvironmental Engineering*, *107*(ASCE 16489).

Griffiths, D. V., & Lane, P. A. (1999). Slope stability analysis by finite elements. *Geotechnique*, *49*(3), 387-403.

Guetif, Z., Bouassida, M., & Debats, J. M. (2007). Improved soft clay characteristics due to stone column installation. *Computers and Geotechnics*, *34*(2), 104-111.

Haliburton, T. A., Anglin, C. C., & Lawmaster, J. D. (1978). Testing of geotechnical fabric for use as reinforcement. *Geotechnical Testing Journal*, *1*(4), 203-212.

Han, J., & Collin, J. G. (2005). Geosynthetic support systems over pile foundations. In *Geosynthetics Research and Development in Progress* (pp. 1-5).

Han, J., & Gabr, M. A. (2002). Numerical analysis of geosynthetic-reinforced and pile-supported earth platforms over soft soil. *Journal of geotechnical and geoenvironmental engineering*, *128*(1), 44-53.

Han, J., & Wayne, M. H. (2000). Pile-soil-interactions in geosynthetic reinforced platform/piled embankments over soft soil. In *Rep. No. 000777, Presentation and CD-Print at 79th Annual Transportation Research Board Meeting*.

Han, J., Bhandari, A., & Wang, F. (2011). DEM analysis of stresses and deformations of geogrid-reinforced embankments over piles. *International Journal of Geomechanics*, *12*(4), 340-350.

Hewlett, W.J., and Randolh, M.F. (1988). Analysis of Piled Embankment. *Ground Engineering, Vol. 21, n 3.*

Horpibulsuk, S., Suksiripattanapong, C., Niramitkornburee, A., Chinkulkijniwat, A., & Tangsutthinon, T. (2011). Performance of an earth wall stabilized with bearing reinforcements. *Geotextiles and Geomembranes*, *29*(5), 514-524.

Hossain, M. S., Dharmateja, M., & Hossain, J. (2010). Assessment of geo-hazard potential and site investigations using Resistivity Imaging. *International Journal of Environmental Technology and Management*, *13*(2), 116-129.

Hossain, M. S., Lozano, N., Hossain, J., & Khan, S. (2011). Investigation of geohazard potential of highway embankment slopes on expansive clay by using geophysical method. In *Geotechnical Engineering For Disaster Mitigation And Rehabilitation And Highway Engineering 2011: Geotechnical and Highway Engineering—Practical Applications, Challenges and Opportunities (With CD-ROM)* (pp. 552-557).

Hossain, S., & Rao, K. N. (2006). Performance evaluation and numerical modeling of embankment over soft clayey soil improved with chemico-pile. *Transportation research record*, *1952*(1), 80-89.

Hossain, S., Khan, S., & Kibria, G. (2017). *Sustainable slope stabilization using recycled plastic pins.* The Netherlands: CRC Press/Balkema.

Jenck, O., Dias, D., & Kastner, R. (2009). Three-dimensional numerical modeling of a piled embankment. *International Journal of Geomechanics*, *9*(3), 102-112.

Jenck, O., Dias, D., & Kastner, R. (2009). Three-dimensional numerical modeling of a piled embankment. *International Journal of Geomechanics*, *9*(3), 102-112.

Khan, M. S. (2014). Sustainable Slope Stabilization Using Recycled Plastic Pin In Texas.

Khan, M. S., Hossain, M. S., Lozano, N., & Kibria, G. (2014). Temporary Lateral Support of a Concrete Retaining Wall Footing using Recycled Plastic Pin. In *Geo-Congress 2014: Geo-characterization and Modeling for Sustainability* (pp. 3851-3860).

Khan, M. S., Hossain, S., & Kibria, G. (2015). Slope stabilization using recycled plastic pins. *Journal of Performance of Constructed Facilities*, *30*(3), 04015054.

Kim, H. S., & Bilgin, Ö. (2007). Studying the effect of concrete key size on mechanically stabilized earth wall deformations using finite element method. In *Computer Applications in Geotechnical Engineering* (pp. 1-8).

Krishnaswamy, P., and Francini, R. (2000). Long-term durability of recycled plastic lumber in structural applications. *http://www.environmental-expert.com/Files/0/articles/2183/2183.pdf* Accessed September 19, 2018

Lai, H. J., Zheng, J. J., Zhang, J., Zhang, R. J., & Cui, L. (2014). DEM analysis of "soil"-arching within geogrid-reinforced and unreinforced pile-supported embankments. *Computers and Geotechnics*, *61*, 13-23.

Lampo, R., & Nosker, T. J. (1997). Development and testing of plastic lumber materials for construction applications. US Army Corps of Engineers, Construction Engineering Research Laboratories, USACERL Technical Report 97/95.

Leonards, G. A., Cutter, W. A., & Holtz, R. D. (1980). DYNAMIC COMPACTION OF GRANULAR SOILS (ABRIDGMENT). *Transportation Research Record*, (749).

Leshchinsky, D., & Han, J. (2004). Geosynthetic reinforced multitiered walls. *Journal of Geotechnical and Geoenvironmental Engineering*, *130*(12), 1225-1235.

Liu, H. L., Ng, C. W., & Fei, K. (2007). Performance of a geogrid-reinforced and pile-supported highway embankment over soft clay: case study. *Journal of Geotechnical and Geoenvironmental Engineering*, *133*(12), 1483-1493.

Loehr, J. E., & Bowders, J. J. (2007). *Slope Stabilization Using Recycled Plastic Pins–Phase III* (No. OR07-006).

Loehr, J., Bowders, J., Owen, J., Sommers, L., & Liew, W. (2000). Slope stabilization with recycled plastic pins. *Transportation Research Record: Journal of the Transportation Research Board*, (1714), 1-8.

Mahmood, T. (2009). *Failure analysis of a mechanically stabilized earth (MSE) wall using finite element program plaxis* (Doctoral dissertation, The University of Texas at Arlington).

Malcolm, G. M. (1995). Recycled Plastic Lumber and shapes design and specifications. In *Proc. Structures congress* (Vol. 13, pp. 2-5).

Marto, A., & Kasim, F. (2002). Grid Mat Method to Increase the Bearing Capacity of Subgrade Soil.

McNulty, J. W. (1965). *An experimental study of arching in sand* (No. AEWES-TR-1-674). ARMY ENGINEER WATERWAYS EXPERIMENT STATION VICKSBURG MS.

Meyer, C. (1987). Finite Element Idealization for Linear Elastic, Static, and Dynamic Analysis of Structures in Engineering Practice. ASCE.

Min, Y., Leshchinsky, D., Ling, H. I., & Kaliakin, V. N. (1995). Effects of sustained and repeated tensile loads on geogrid embedded in sand. *Geotechnical Testing Journal*, *18*(2), 204-225.

Murugesan, S., & Rajagopal, K. (2009). Studies on the behavior of single and group of geosynthetic encased stone columns. *Journal of Geotechnical and Geoenvironmental Engineering*, *136*(1), 129-139.

National Academy of Sciences, National Academy of Engineering, and Institute of Medicine (2006). *Advanced Research Instrumentation and Facilities.* Washinton, DC: National Academies Press. https://doi.org/10.17226/11520.

Nazir, A. K., & Azzam, W. R. (2010). Improving the bearing capacity of footing on soft clay with sand pile with/without skirts. *Alexandria Engineering Journal*, *49*(4), 371-377.

Nosker, T. J., & Renfree, R. (2000, June). Recycled plastic lumber: from park benches to bridges. In *Approved for Proceedings of R'2000 5th World Congress, Toronto, Canada*.

Ozdemir, M. A. (2016). Improvement in Bearing Capacity of a Soft Soil by Addition of Fly Ash. *Procedia engineering*, *143*, 498-505.

Ozdemir, M. A. (2016). Improvement in Bearing Capacity of a Soft Soil by the Addition of Fly Ash. *Thesis presented to Middle East Technical University, Turkey, in partial fulfillment of the requirement for the degree of Master of Science in Civil Engineering*.

Parra, J., Loehr, J., Hagemeyer, D., & Bowders, J. (2003). Field performance of embankments stabilized with recycled plastic reinforcement. *Transportation Research Record: Journal of the Transportation Research Board*, (1849), 31-38.

Passe, P. D. (2000). *Mechanically Stabilized Earth Wall Inspector's Handbook*. State of Florida, Department of Transportation.

Rao, K. N. (2006). *Numerical modeling and analysis of pile supported embankments* (MS Thesis dissertation). University of Texas at Arlington, USA).

Rathmayer, H. (1975). *Piled embankment supported by single pile caps*.

Reid, W. M., & Buchanan, N. W. (1984). PAPER 21 Bridge approach support piling. In *Piling and ground treatment* (pp. 267-274). Thomas Telford Publishing.

Reinaldo, V. M., & Shao, Y. (2005). Geogrid-reinforced and pile-supported roadway embankment. *Proceedings of Contemporary Issues in Foundation Engineering. New York: ASCE Publications*, 26-28.

Robertson, J., & Gilchrist, A. J. T. (1987). Design and construction of a reinforced embankment across soft lakebed deposits. In *Ing. Conf. on Foundation and Tunels*.

Russell, D., & Pierpoint, N. (1997). An assessment of design methods for piled embankments. *Ground Engineering*, *30*(10).

Sarath, N., Shivashankar, R., & Shankar, A. R. (2011). Role of shear keys in cantilever retaining wall. *Proceedings of Indian Geotechnical Conference December 15-17, 2011, Kochi (Paper No. K-056).*

Schmidt, J. M., & Harpstead, D. L. (2011). MSE Wall Engineering–A New Look at Contracting, Design, and Construction.

Shin, E. C., Das, B. M., Puri, V. K., Yen, S. C., & Cook, E. E. (1993). Bearing capacity of strip foundation on geogrid-reinforced clay. *Geotechnical Testing Journal, 16*(4), 534-541.

Simac, M. R., Christopher, B. R., & Bonczkiewicz, C. (1990, June). Instrumented field performance of a 6 m geogrid soil wall. In *Proceedings of the 4'th Int. Conference on Geotextiles, Geomembranes and Related Products* (pp. 53-59).

Sommers, L., Loehr, J. E., & Bowders, J. J. (2000, May). Construction methods for slope stabilization with recycled plastic pins. In *Proceedings of the Mid-continent Transportation Symposium, Iowa State University, Ames, Iowa* (pp. 15-16).

Stuedlein, A. W., Bailey, M., Lindquist, D., Sankey, J., & Neely, W. J. (2010). Design and performance of a 46-m-high MSE wall. *Journal of Geotechnical and Geoenvironmental Engineering, 136*(6), 786-796.

Stuedlein, A. W., Mikkelsen, P. E., & Bailey, M. J. (2007). Instrumentation and performance of the third runway north MSE wall at Seattle-Tacoma International Airport. In *7th FMGM 2007: Field Measurements in Geomechanics* (pp. 1-14).

Suksiripattanapong, C., Chinkulkijniwat, A., Horpibulsuk, S., Rujikiatkamjorn, C., & Tanhsutthinon, T. (2012). Numerical analysis of bearing reinforcement earth (BRE) wall. *Geotextiles and Geomembranes, 32*, 28-37.

Tamrakar, S. (2015). *Slope Stabilization and Performance Monitoring of I-35 and SH-183 Slopes Using Recycled Plastic Pins* (Master's Thesis).

Tang, C., Shi, B., Gao, W., Chen, F., & Cai, Y. (2007). Strength and mechanical behavior of short polypropylene fiber reinforced and cement stabilized clayey soil. *Geotextiles and Geomembranes*, *25*(3), 194-202.

Tornaghi, R., & Cippo, A. P. (1985, March). Soil improvement by jet grouting for the solution of tunnelling problems. In *Proceedings of the 4th International Symposium Tunnelling*(Vol. 85, pp. 265-276).

Tsukada, Y., Isoda, T., & Yamanouchi, T. (1993). Geogrid subgrade reinforcement and deep foundation improvement, Yono City, Japan. *Geosynthetics Case Histories*.

Turner, A. K., and R. L. Schuster (eds.) (1996). Special Report 247: Landslides: Investigation and Mitigation. *TRB, National Research Council, Washington, D.C*.

Van Ness, K. E., Nosker, T. L., Renfree, R. W., and Killion, J. R., (1998). Long term creep of commercially produced plastic lumber. *SPEANTEC'98: Conference Proceedings, Brookfield, CN, 26 April, 1998. p. 2916–20.*

Verma, B. P., & Char, A. N. R. (1986). Bearing capacity tests on reinforced sand subgrades. *Journal of geotechnical engineering*, *112*(7), 701-706.

Zhang, J., Zheng, J. J., Chen, B. G., & Yin, J. H. (2013). Coupled mechanical and hydraulic modeling of a geosynthetic-reinforced and pile-supported embankment. *Computers and Geotechnics, 52*, 28-37.

Zheng, J. J., Chen, B. G., Lu, Y. E., Abusharar, S. W., & Yin, J. H. (2009). The performance of an embankment on soft ground reinforced with geosynthetics and pile walls. *Geosynthetics International, 16*(3), 173-182.

Zhou, C., Yin, J. H., & Ming, J. P. (2002). Bearing capacity and settlement of weak fly ash ground improved using lime fly ash or stone columns. *Canadian Geotechnical Journal, 39*(3), 585-596.

APPENDIX A

Borehole Log: Site Location 1

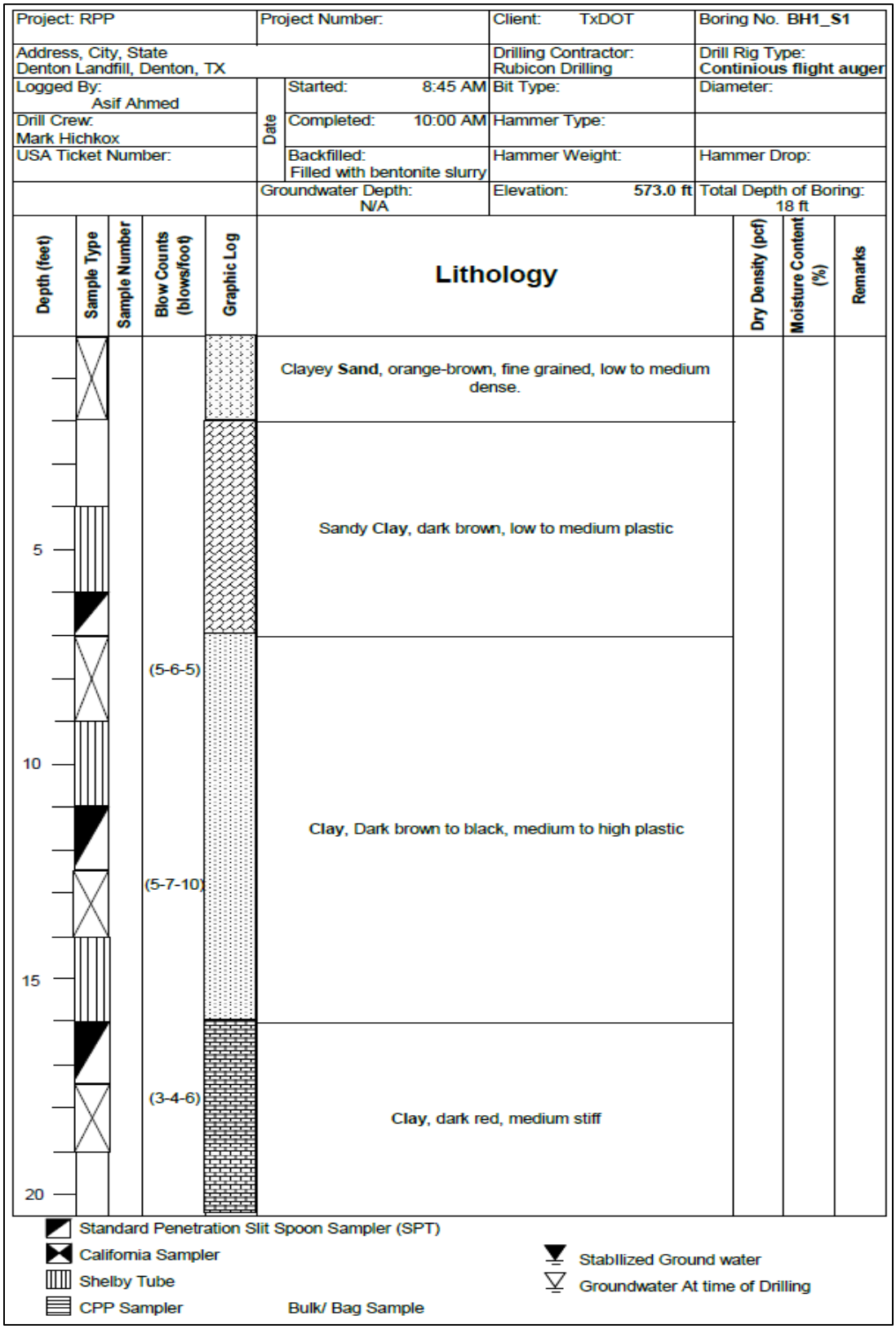

Figure A 1 Log of BH1_S1

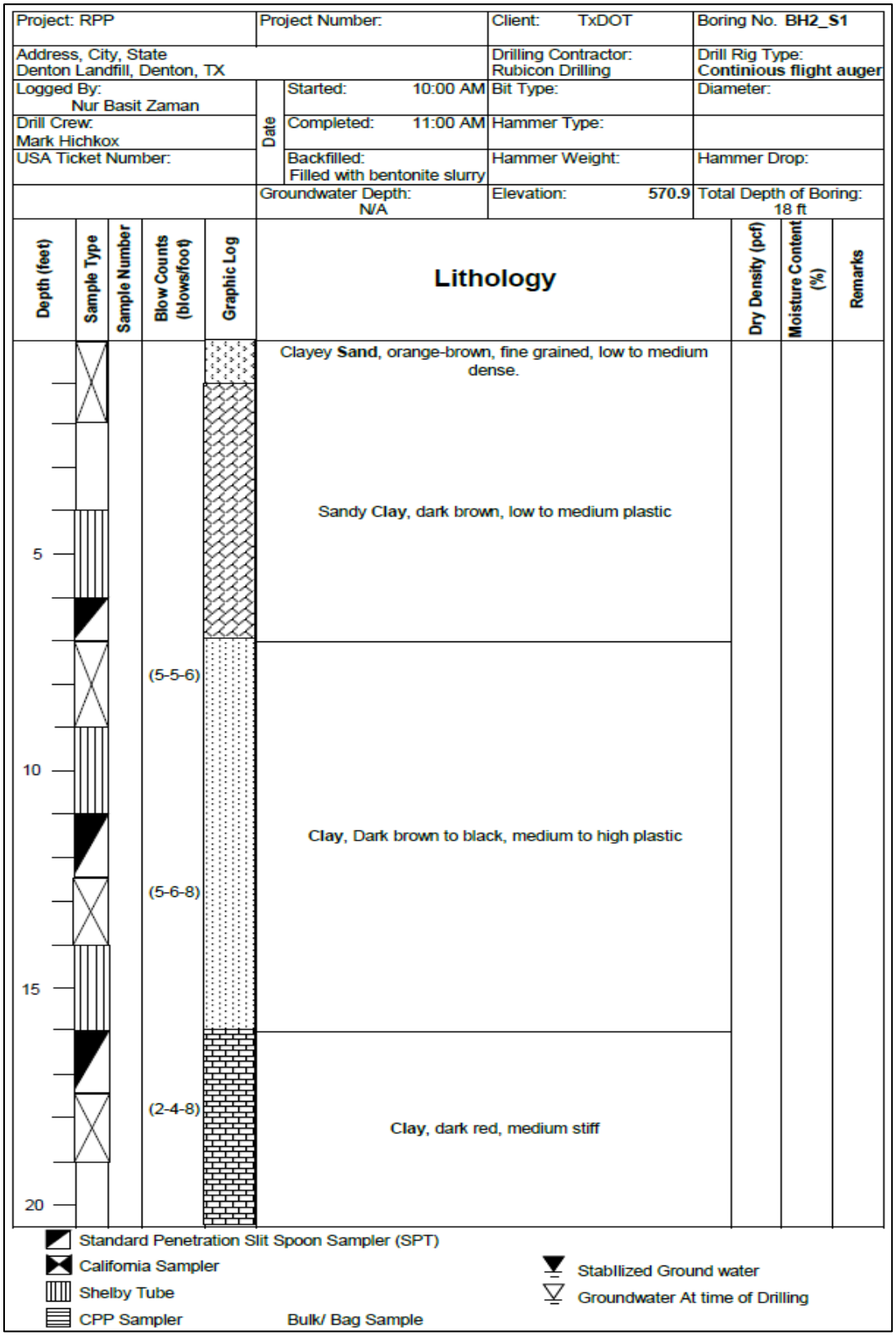

Figure A 2 Log of BH2_S1.

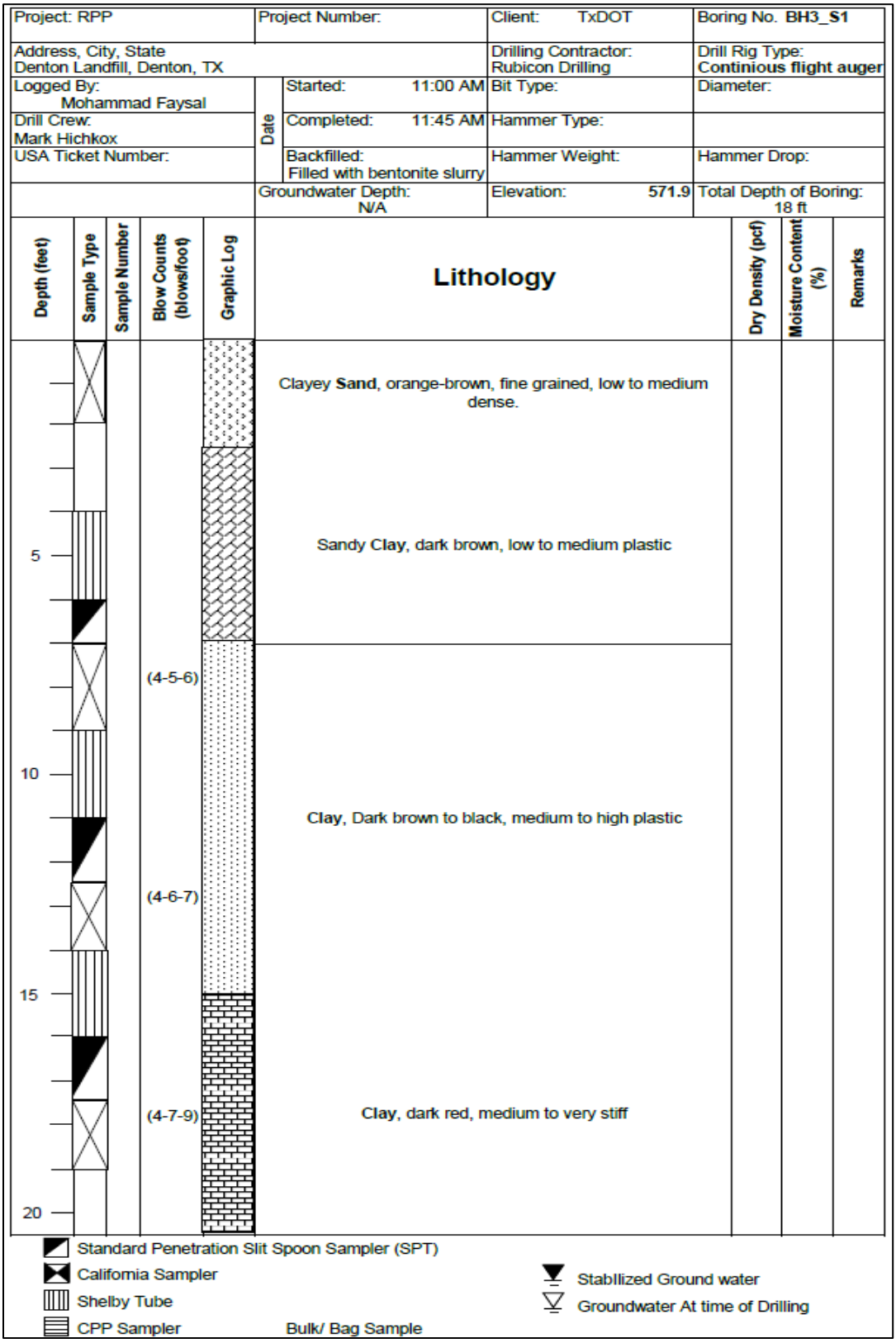

Figure A 3 Log of BH3_S1.

APPENDIX B

Borehole Log: Site Location 2

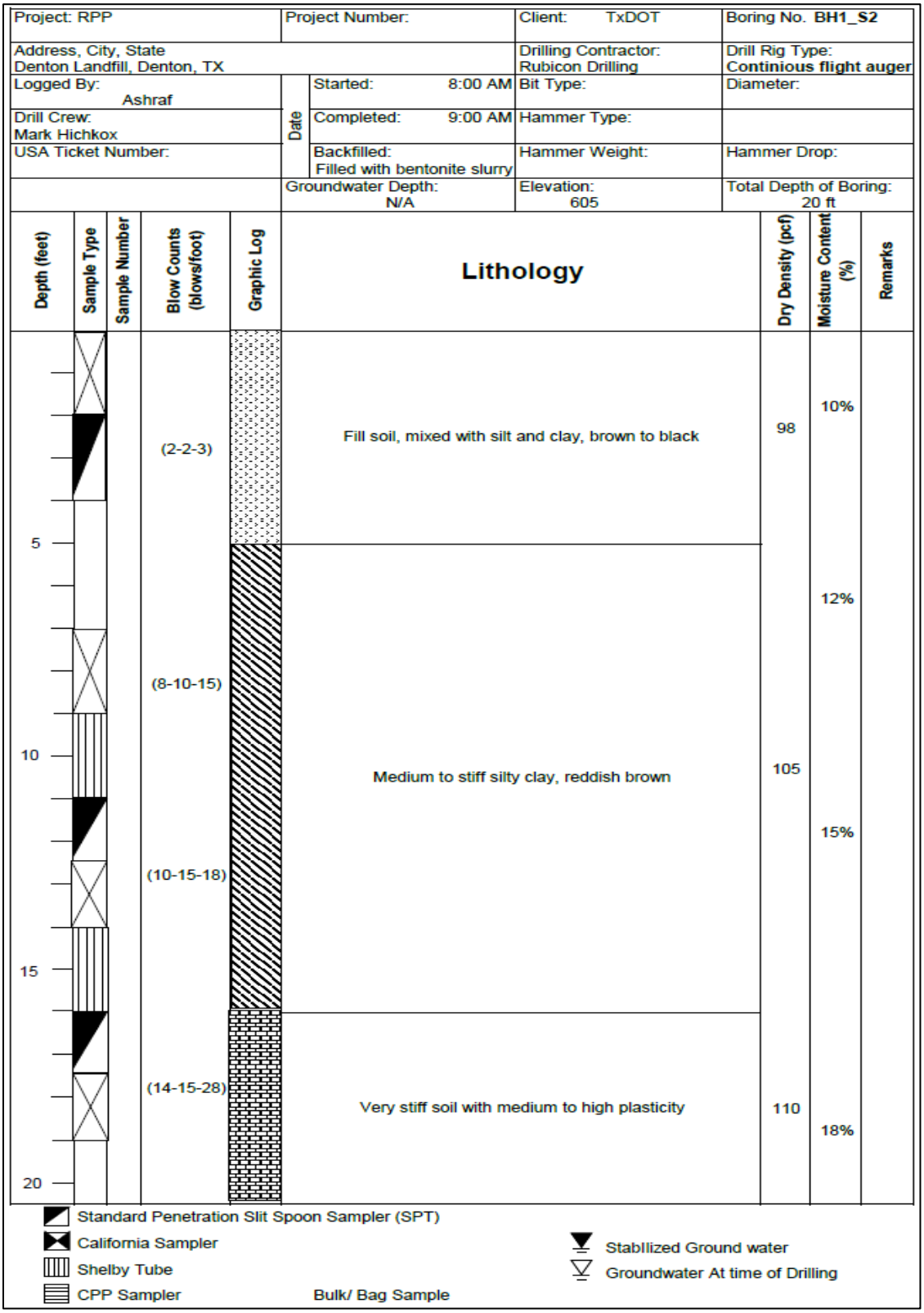

Figure B 1 Log of BH1_S2.

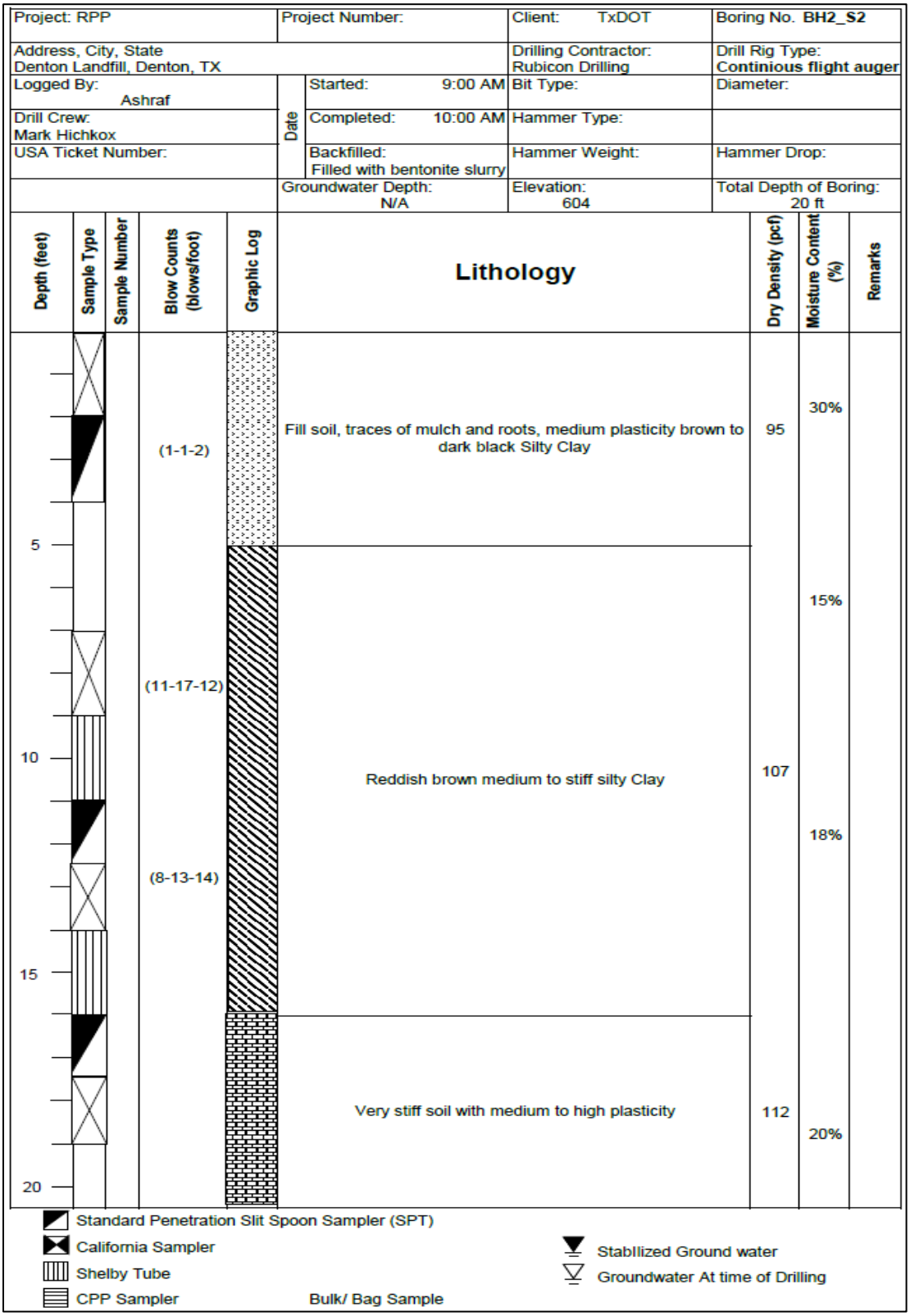

Figure B 2 Log of BH2_S2.

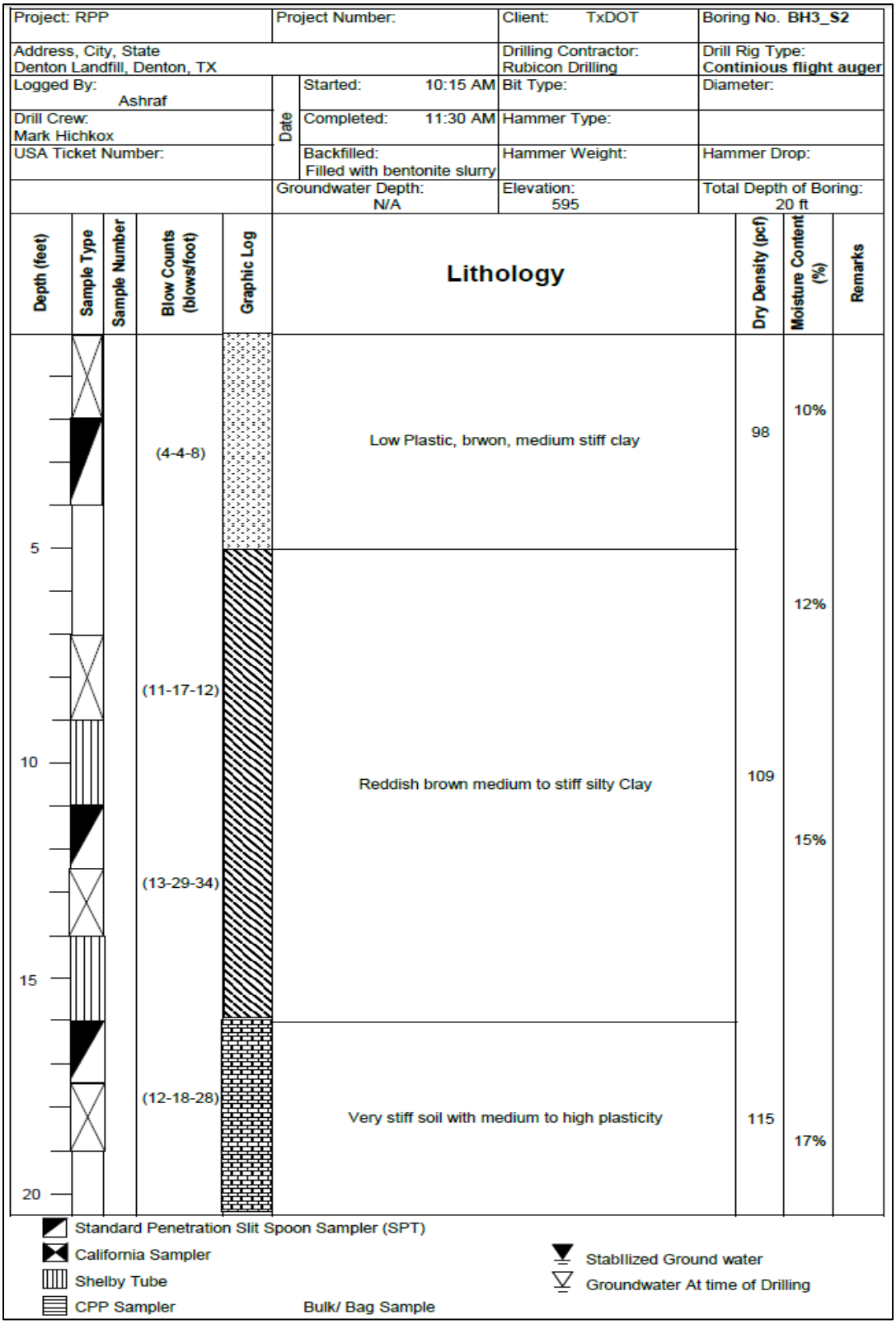

Figure B 3 Log of BH3_S2.

APPENDIX C

Borehole Log: Site Location 3

BORING NUMBER BH1_S3

DATE STARTED 2/9/18 COMPLETED 2/9/18 GROUND ELEVATION 482 ft

DRILLING CONTRACTOR

Time: 8:00AM to 11:00 AM

DRILLING METHOD Flight Auger

Hammer Type: Automatic Hammer (140 lbs, 30" drops)

LOGGED BY Md Nur Basit Zaman CHECKED BY

NOTES

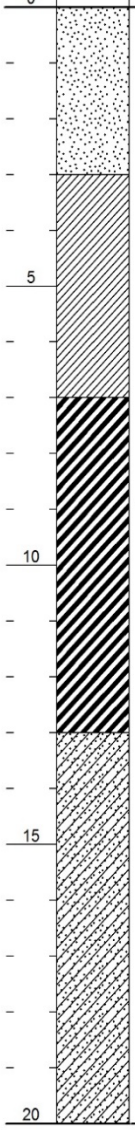

DEPTH (ft)	BLOW COUNTS (N VALUE)	Lithology	MOISTURE CONTENT (%)	PLASTICITY INDEX	Remarks
0		Clay, dark brown/gray, high plastic			
5	4-6-10 (16)	Clay, dark brown, high plastic			
10	4-10-12 (22)	Stiff Clay, dark brown to black, high plastic			
15	5-9-13 (22)	Stiff Clay, dark gray, high plastic			
20	3-6-10 (16)				

Bottom of borehole at 20.0 feet.

Figure C. 1 Log of BH1_S3.

BORING NUMBER BH2_S3

DATE STARTED 2/9/18 COMPLETED 2/9/18 GROUND ELEVATION 482 ft

DRILLING CONTRACTOR

Time: 8:00AM to 11:00 AM

DRILLING METHOD Flight Auger

Hammer Type: Automatic Hammer (140 lbs, 30" drops)

LOGGED BY Md Nur Basit Zaman CHECKED BY

NOTES

DEPTH (ft)	GRAPHIC LOG	BLOW COUNTS (N VALUE)	Lithology	MOISTURE CONTENT (%)	PLASTICITY INDEX	Remarks
0			Stiff Clay, brown, fine grained, medium to high plastic			
5		6-9-10 (19)	Clay, blackish gray, high plastic			
10		4-6-7 (13)	Clay, grayish black, high plastic			
15		5-9-10 (19)	Clay, dark brown, high plastic			
20		5-8-11 (19)				

Bottom of borehole at 20.0 feet.

Figure C. 2 Log of BH2_S3.

BORING NUMBER BH3_S3

DATE STARTED 2/9/18 COMPLETED 2/9/18 GROUND ELEVATION 482 ft

DRILLING CONTRACTOR

Time: 8:00AM to 11:00 AM

DRILLING METHOD Flight Auger

Hammer Type: Automatic Hammer (140 lbs, 30" drops)

LOGGED BY Md Nur Basit Zaman CHECKED BY

NOTES

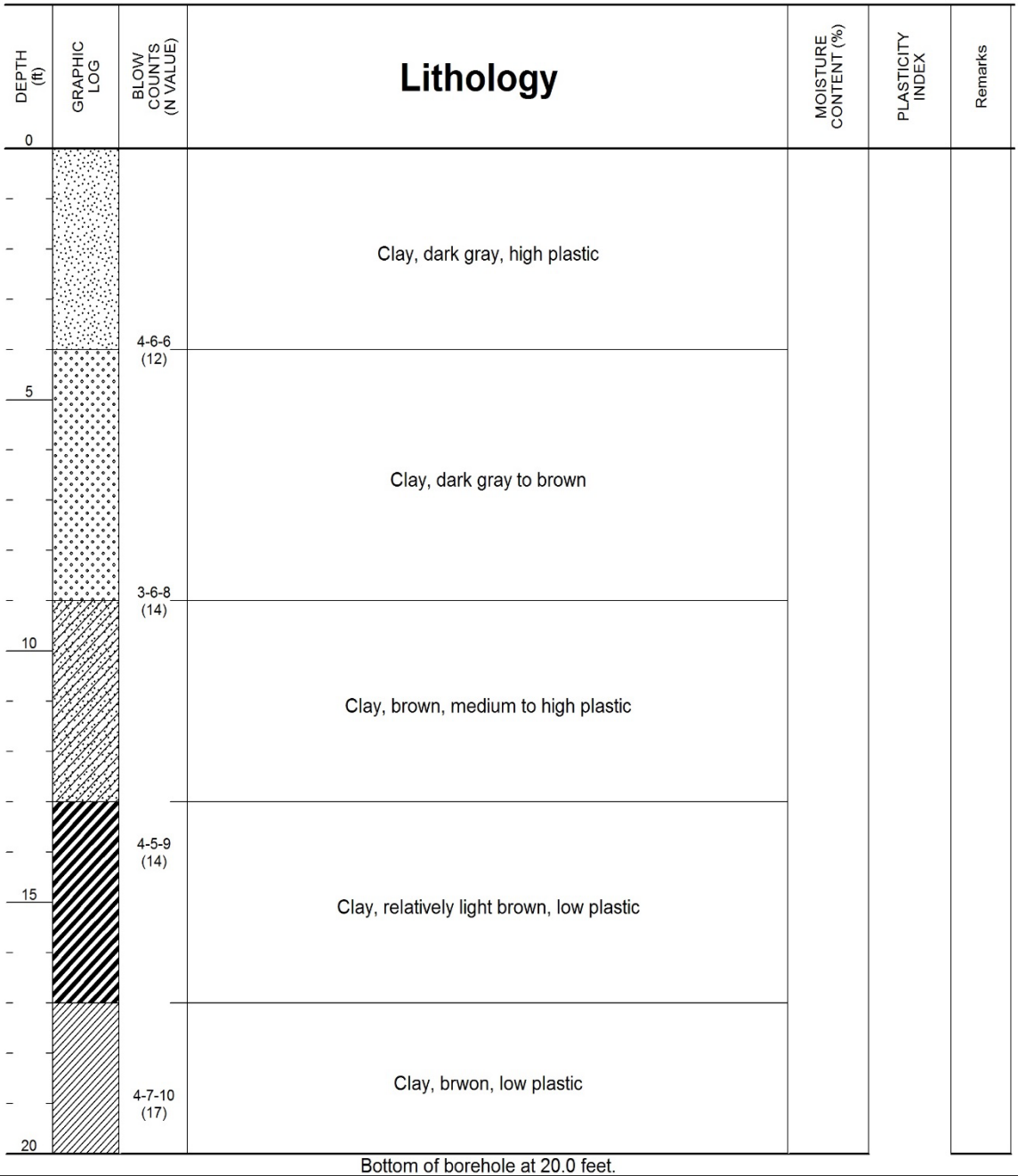

Figure C. 3 Log of BH3_S3.

APPENDIX D

Borehole Log: Site Location 4

BORING NUMBER BH1_S4

DATE STARTED 3/8/18 COMPLETED 3/8/18 GROUND ELEVATION 482 ft

DRILLING CONTRACTOR

Time: 8:00AM to 11:00 AM

DRILLING METHOD Auger Drilling

Hammer Type: Automatic Hammer (140 lbs, 30" drops)

LOGGED BY Md Nur Basit Zaman CHECKED BY

NOTES

DEPTH (ft)	GRAPHIC LOG	BLOW COUNTS (N VALUE)	Lithology	MOISTURE CONTENT (%)	PLASTICITY INDEX	Remarks
0		0-2-3 (5)	Clay, dark grey, high plastic			
5		4-6-9 (15)	Clay, dark gray, high plastic			
10		4-6-8 (14)	Clay, brown, medium to high plastic			
15		3-4-5 (9)	Clay, light brown, medium to high plastic			
20			Bottom of borehole at 20.0 feet.			

Figure D. 1 Log of BH1_S4.

BORING NUMBER BH2_S4

DATE STARTED 3/8/18 COMPLETED 3/8/18 GROUND ELEVATION 482 ft

DRILLING CONTRACTOR

Time: 8:00AM to 11:00 AM

DRILLING METHOD Auger Drilling

Hammer Type: Automatic Hammer (140 lbs, 30" drops)

LOGGED BY Md Nur Basit Zaman CHECKED BY

NOTES

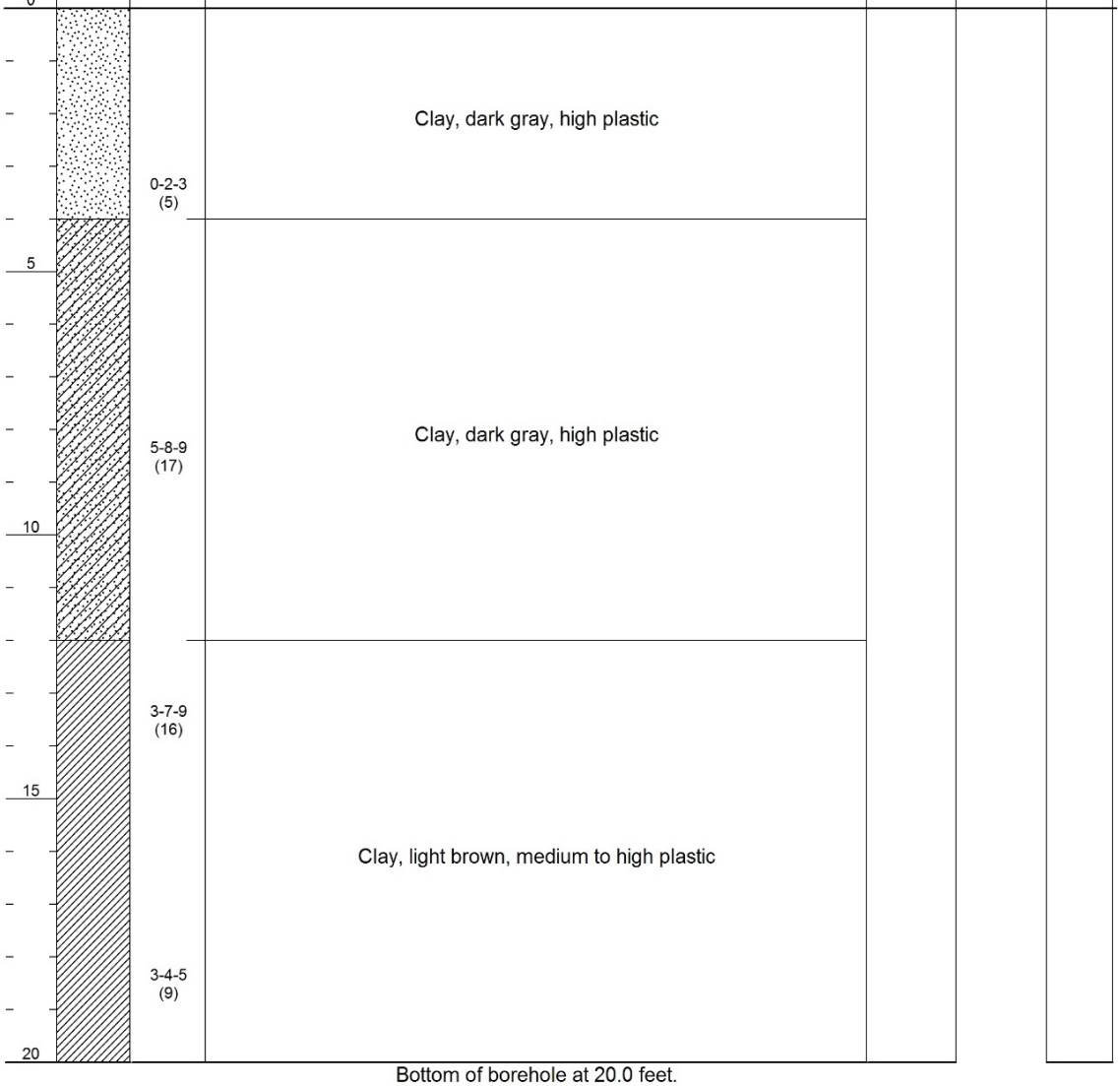

Bottom of borehole at 20.0 feet.

Figure D. 2 Log of BH2_S4

APPENDIX E

Construction Sequence: Vertical Loaded Test Section

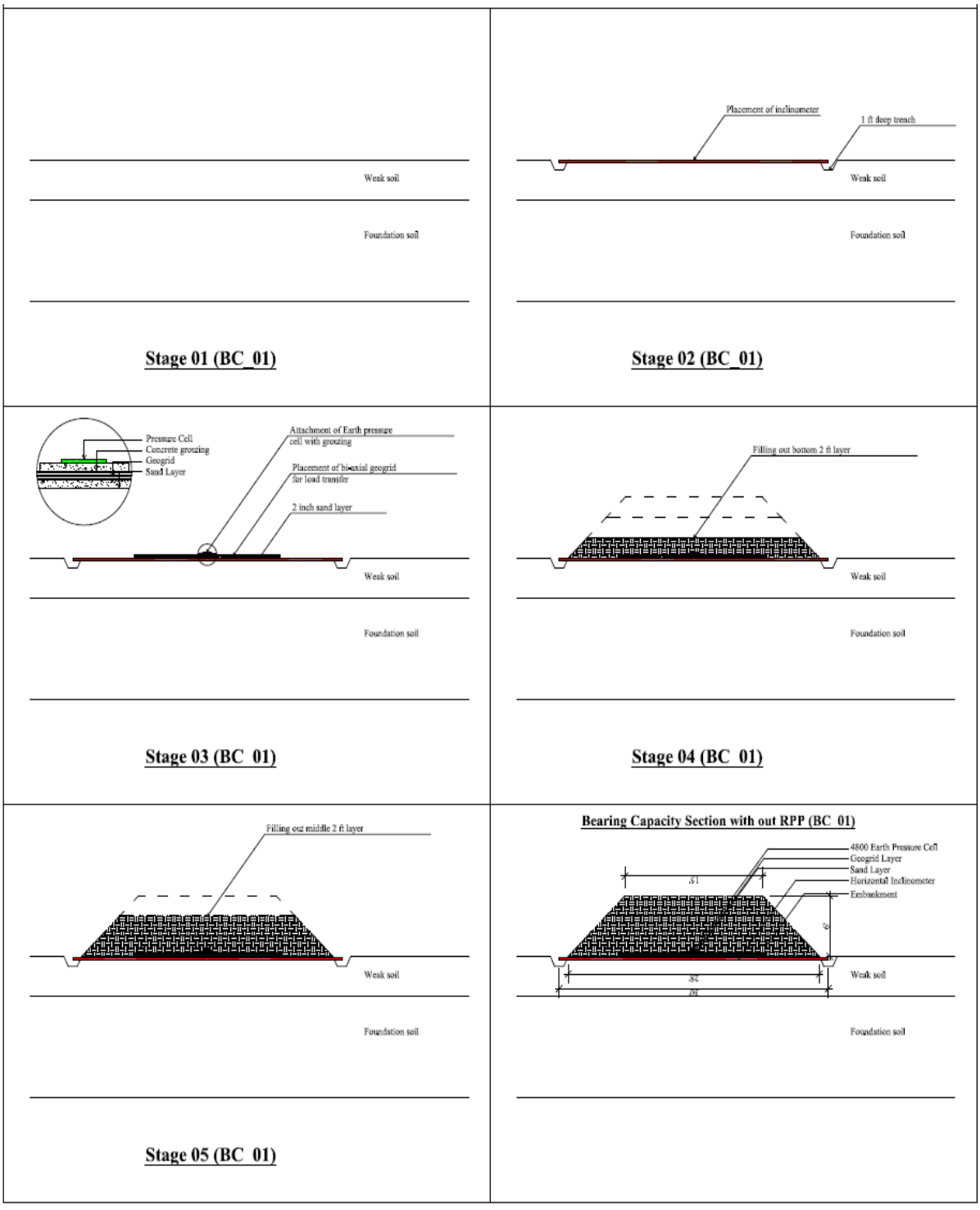

Figure E. 1 Construction sequence of control test section (BC_01) without RPP.

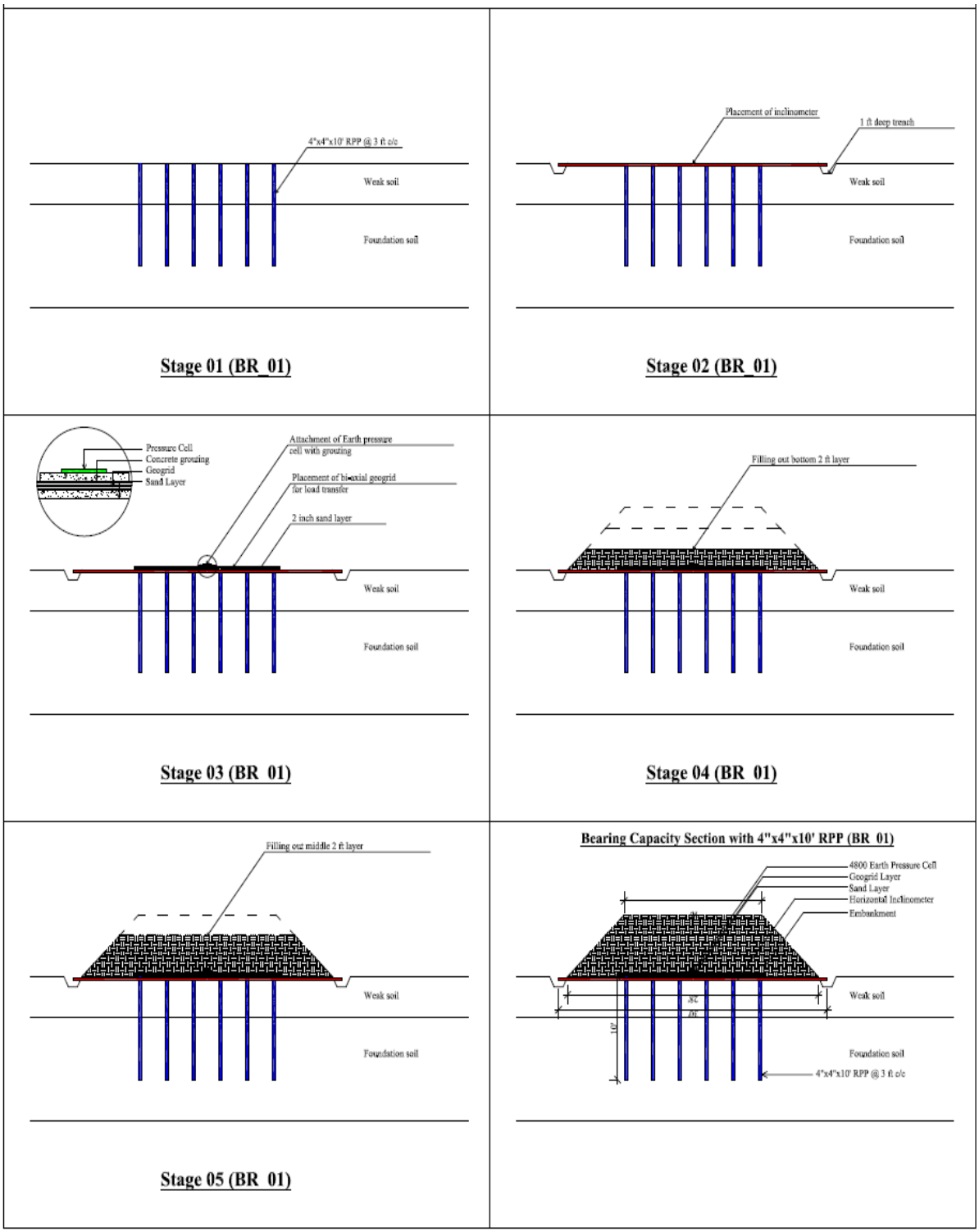

Figure E. 2 Construction sequence of reinforced test section (BR_01) with 4 in. x 4 in. x 10 ft. RPP.

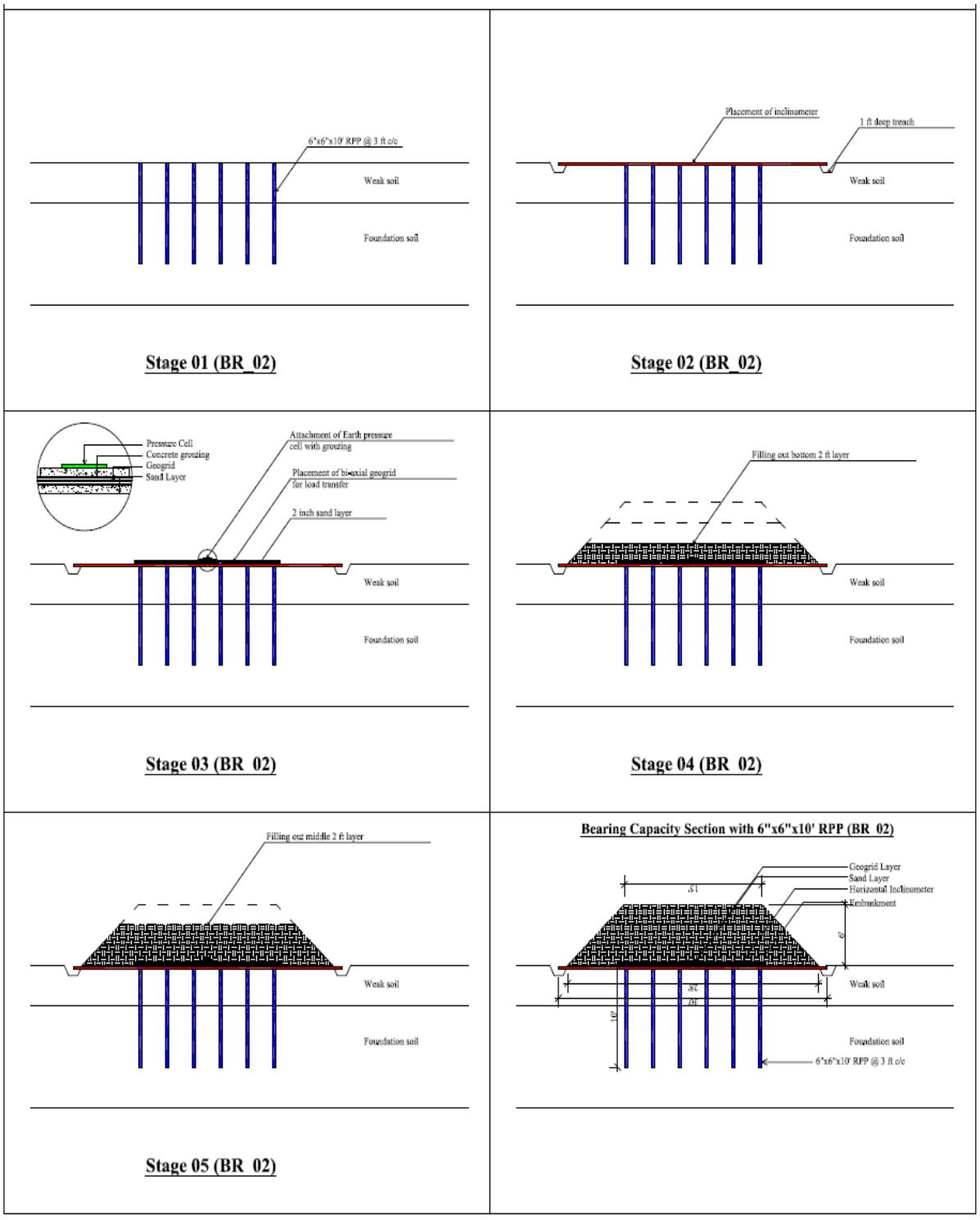

Figure E. 3 Construction sequence of reinforced test section (BR_01) with 6 in. x 6 in. x 10 ft. RPP.

APPENDIX F

Construction Sequence: Lateral Loaded Test Section

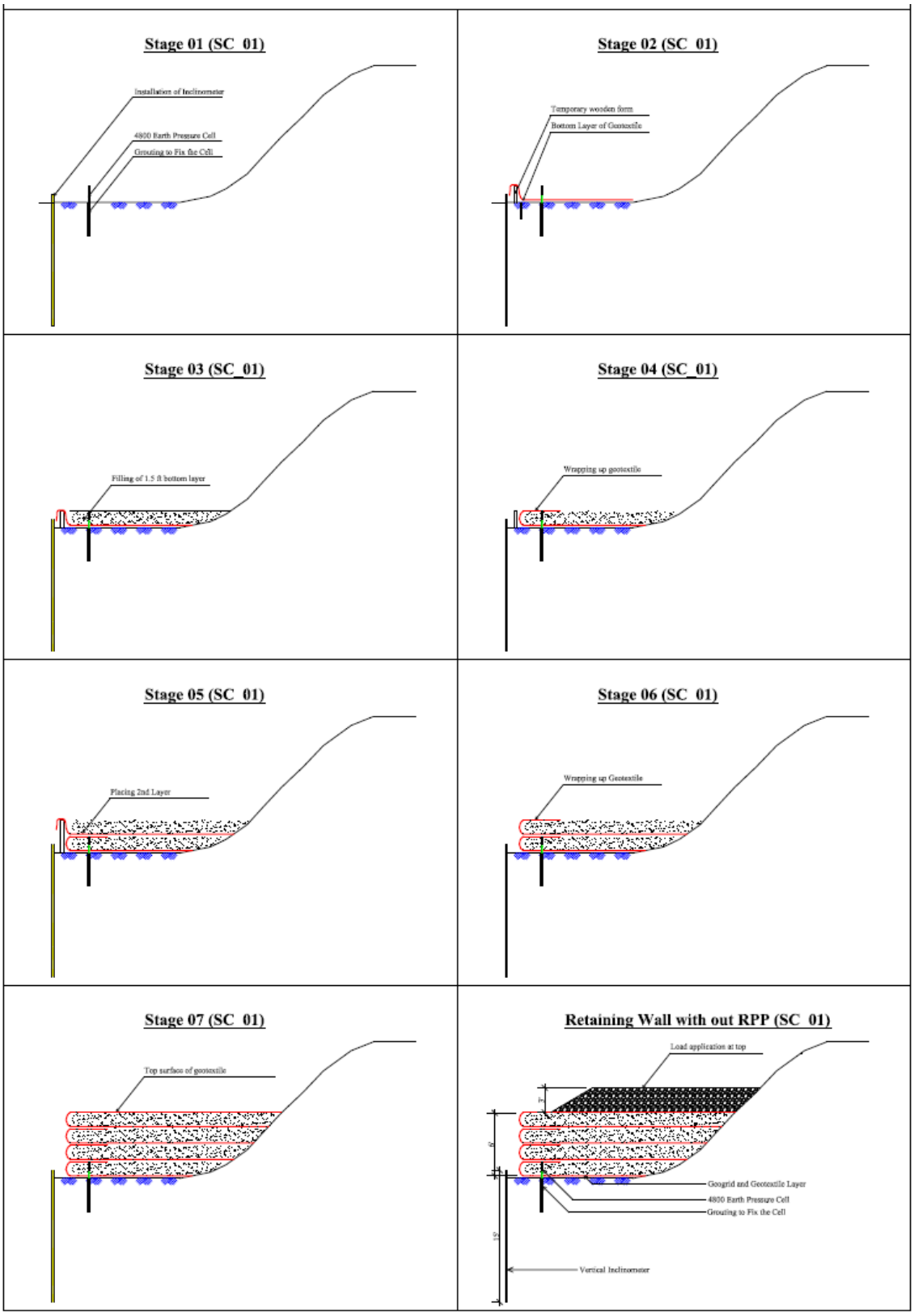

Figure F. 1 Construction sequence of control test section (SC_01).

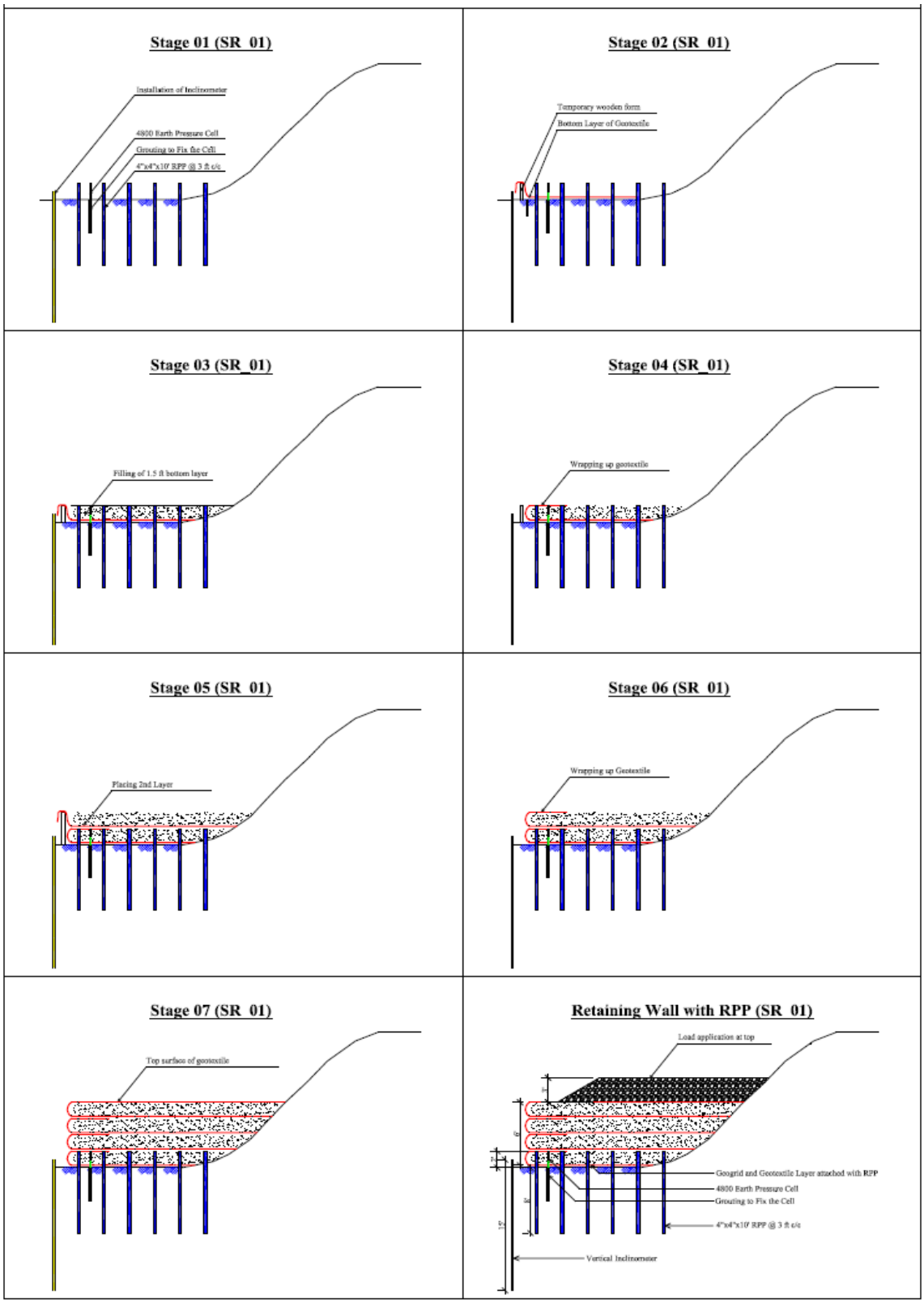

Figure F. 2 Construction sequence of reinforced test section (SR_01).

BIOGRAPHICAL INFORMATION

Md Nur Basit Zaman was born in Dhaka, Bangladesh. He completed his Bachelor's (B.Sc.) degree in Civil Engineering from Bangladesh University of Engineering and Technology (BUET), Dhaka, Bangladesh in February 2013. After completing his bachelor's degree, he joined as a faculty member in the department of Civil Engineering at the University of Information Technology and Sciences, Dhaka, Bangladesh. He also worked as a junior engineer in a multinational company named SMEC in Bangladesh on railway projects. During his professional carrier, Md Nur Basit encountered many problems associated with geotechnical issues like landslide, slope stability, and unsuitable ground condition for construction in his country, which motivated him to pursue his higher education in geotechnical engineering. He started his graduate studies at The University of Texas at Arlington (UTA) in Spring 2015 as a graduate research assistant under the supervision of Dr. Sahadat Hossain. During his graduate study life, he took part in the national Solid Waste Design Competition (SWDC) organized by Solid Waste Association of North America (SWANA) in WASTECON 2016 and secured first place. He received Outstanding Graduate Student Award in Civil Engineering at UTA in 2016 – 17 and 2017 – 18. His research interest includes but not limited to ground improvement, sustainable solutions to geotechnical problems, numerical modelling, retaining wall, slope stability, municipal solid waste (MSW), biocell landfill, landfill gas and landfill mining. He is a student member of American Society of Civil Engineers (ASCE) and SWANA, and is an engineer-in-training (E.I.T) in the State of Texas. He is passionate about working in a field where lies the prospect to surpass his latent potentials, creativity and adroitness in order to make significant contribution towards the research field by utilizing skills and ingenuity and also involving a steep learning curve.